NATO ADVANCED STUDY INSTITUTE

CONF-820853--Absts.

DE83 017399

* * * * * *

PHOTOPHYSICS AND PHOTOCHEMISTRY IN THE VACUUM-ULTRAVIOLET

* * * *

Lake Geneva, Wisconsin

August 15-28, 1982

DIRECTOR

S.P. McGlynn
Louisiana State University

ASSOCIATE DIRECTORS

G.L. Findley
New York University

R.H. Huebner
Argonne National Laboratory

DISCLAIMER

This report was prepared as an account of work sponsored by an agency of the United States Government. Neither the United States Government nor any agency thereof, nor any of their employees, makes any warranty, express or implied, or assumes any legal liability or responsibility for the accuracy, completeness, or usefulness of any information, apparatus, product, or process disclosed, or represents that its use would not infringe privately owned rights. Reference herein to any specific commercial product, process, or service by trade name, trademark, manufacturer, or otherwise does not necessarily constitute or imply its endorsement, recommendation, or favoring by the United States Government or any agency thereof. The views and opinions of authors expressed herein do not necessarily state or reflect those of the United States Government or any agency thereof.

NOTICE
PORTIONS OF THIS REPORT ARE ILLEGIBLE.
It has been reproduced from the best available copy to permit the broadest possible availability.

MASTER

DISTRIBUTION OF THIS DOCUMENT IS UNLIMITED

NATO-ASI

PHOTOPHYSICS AND PHOTOCHEMISTRY IN THE VACUUM ULTRAVIOLET

SCHEDULE OF LECTURES

Monday, 8/16

MORNING SESSION

9:00 - 10:30	R.H. Huebner, Argonne National Laboratory WELCOME
10:30 - 12:00	S.P. McGlynn, Louisiana State University GIANT ATOMS AND MOLECULES

AFTERNOON SESSION

2:00 - 3:30	G.L. Findley, New York University A LEXICON FOR VUV PHOTOPHYSICS
3:30 - 5:00	E.E. Koch, Deutsches Elektronen-Synchrotron METHODS FOR STUDYING HIGHER EXCITED STATES IN ATOMS, MOLECULES AND MOLECULAR CRYSTALS: SYNCHROTRON RADIATION

EVENING SESSION

7:00 - 8:30	S.C. Wallace, University of Toronto TUNABLE LASER SOURCES IN THE VACUUM ULTRAVIOLET
8:30 - 10:00	H.H. Brongersma, University of Leiden ELECTRON AND ION IMPACT SPECTROSCOPY OF MOLECULES. I. EXPERIMENTAL DETAILS

Tuesday, 8/17

MORNING SESSION

9:00 - 10:30	A.R.P. Rau, Louisiana State University ELEMENTS OF QUANTUM DEFECT THEORY. INTRODUCTION
10:30 - 12:00	J.L. Dehmer, Argonne National Laboratory SHAPE RESONANCES AND AUTOIONIZATION IN MOLECULAR PHOTOIONIZATION

EVENING SESSION

7:00 - 8:30	A.R.P. Rau, Louisiana State University ELEMENTS OF QUANTUM DEFECT THEORY. MULTICHANNEL AND OTHER GENERALIZATIONS
8:30 - 10:00	J.C. Miller, Oak Ridge National Laboratory MULTIPHOTON IONIZATION AND THIRD HARMONIC GENERATION IN ATOMS AND MOLECULES

Wednesday, 8/18

MORNING SESSION

9:00 - 10:30	K.T. Lu, Argonne National Laboratory ELEMENTS OF QUANTUM DEFECT THEORY. THE UNIFIED THEORY OF RYDBERG AND AUTOIONIZING STATES. I.
10:30 - 12:00	S.C. Wallace, University of Toronto LASER SPECTROSCOPY AND PHOTOPHYSICS IN THE VACUUM ULTRAVIOLET

EVENING SESSION

7:00 - 8:30	K.T. Lu, Argonne National Laboratory ELEMENTS OF QUANTUM DEFECT THEORY. THE UNIFIED THEORY OF RYDBERG AND AUTOIONIZING STATES. II.
8:30 - 10:00	continued

8:30 - 10:00 H.H. Brongersma, University of Leiden
ELECTRON AND ION IMPACT SPECTROSCOPY OF MOLECULES. II. APPLICATIONS TO MOLECULES.

Thursday, 8/19

MORNING SESSION

9:00 - 10:30 C.H. Greene, Louisiana State University
ELEMENTS OF QUANTUM DEFECT THEORY. MOLECULAR RYDBERG STATES.

10:30 - 12:00 M.B. Robin, Bell Telephone Laboratories
MULTIPHOTON IONIZATION SPECTROSCOPY AND PHOTOCHEMISTRY

AFTERNOON SESSION

2:00 - 3:30 C.H. Greene, Louisiana State University
ELEMENTS OF QUANTUM DEFECT THEORY. APPLICATIONS OF GENERALIZED QUANTUM DEFECT THEORY

3:30 - 5:00 P.M. Dehmer, Argonne National Laboratory
VUV STUDIES OF THE SYSTEMATICS OF ELECTRONIC STRUCTURE IN VAN DER WAALS MOLECULES

Friday, 8/20

MORNING SESSION

9:00 - 10:30 R.N. Compton, Oak Ridge National Laboratory
PRODUCTION AND REACTION OF NEGATIVE IONS

10:30 - 12:00 J. Jortner, Tel-Aviv University
EXCITATIONS AND ENERGY TRANSFER IN CONDENSED PHASES

EVENING SESSION

7:00 - 8:30 continued

7:00 - 8:30 E.E. Koch, Deutsches Elektronen-Synchrotron
ELECTRONIC STRUCTURE OF MOLECULAR CRYSTALS: BAND STRUCTURE AND RESONANCE EFFECTS

* * * * * *

Monday, 8/23

MORNING SESSION

9:00 - 10:30 J. Jortner, Tel-Aviv University
DYNAMICS OF HIGHLY EXCITED STATES OF LARGE ISOLATED MOLECULES. I.

10:30 - 12:00 M.N.R. Ashfold, University of Bristol
PHOTODISSOCIATION DYNAMICS OF SMALL GAS-PHASE MOLECULES. I.

EVENING SESSION

7:00 - 8:30 J. Jortner, Tel-Aviv University
DYNAMICS OF HIGHLY EXCITED STATES OF LARGE ISOLATED MOLECULES. II.

8:30 - 10:00 M.N.R. Ashfold, University of Bristol
PHOTODISSOCIATION DYNAMICS OF SMALL GAS-PHASE MOLECULES. II.

Tuesday, 8/24

MORNING SESSION

9:00 - 10:30 J.C. Gay, Laboratoire de Spectroscopie Hertzienne
THEORETICAL ASPECTS OF ATOMIC DIAMAGNETISM: THE ATOMIC SPECTRUM FROM BOHR TO LANDAU

10:30 - 12:00 J.D. Scott, University of Montana
MCD SPECTROSCOPY IN THE VACUUM ULTRAVIOLET

AFTERNOON SESSION

2:00 - 3:30 continued

2:00 - 3:30 J.C. Gay, Laboratoire de Spectroscopie Hertzienne
RYDBERG ATOMS IN MAGNETIC FIELDS: EXPERIMENTAL ADVANCES

3:30 - 5:00 A. Gedanken, Bar-Ilan University
CD AND MCD MEASUREMENTS IN THE VUV

Wednesday, 8/25

MORNING SESSION

9:00 - 10:30 A.R. Rossi, University of Connecticut
THEORETICAL CORRELATIONS OF ORGANIC PHOTOCHEMICAL REACTIONS IN THE FAR UV

10:30 - 12:00 C. von Sonntag, Max-Planck-Institut fur Strahlenchemie
PHOTOCHEMISTRY OF SATURATED ALCOHOLS AND OPEN-CHAIN ETHERS AT 185 nm IN THE LIQUID PHASE

AFTERNOON SESSION

2:00 - 3:30 C. Sandorfy, University of Montreal
VALENCE-SHELL AND RYDBERG TRANSITIONS IN ORGANIC MOLECULES

EVENING SESSION

7:00 - 8:30 A.R. Rossi, University of Connecticut
THEORETICAL ASPECTS OF NH_3 AND ITS POSITIVE IONS

8:30 - 10:00 C. von Sonntag, Max-Planck-Institut fur Strahlenchemie
PHOTOLYSIS OF CYCLIC ETHERS AND ACETALS AT 185 nm IN THE LIQUID PHASE

Thursday, 8/26

MORNING SESSION

9:00 - 10:30 J.D. Scott, University of Montana
PERTURBATION SPECTROSCOPY IN THE VACUUM ULTRAVIOLET

10:30 - 12:00 continued

10:30 - 12:00 B.R. Russell, North Texas State University
ELECTRIC FIELD STUDIES IN THE VACUUM ULTRAVIOLET

Friday, 8/27

MORNING SESSION

9:00 - 10:30 S. Leach, Laboratoire de Photophysique Moleculaire
SUPEREXCITED AND IONIC STATE RELAXATION PROCESSES IN VACUUM-ULTRAVIOLET EXCITED POLYATOMIC MOLECULES. I.

10:30 - 12:00 M. Robnick, University of Bonn
REGULAR AND IRREGULAR MOTION IN CLASSICAL AND QUANTUM SYSTEMS. I.

AFTERNOON SESSION

2:00 - 3:30 S. Leach, Laboratoire de Photophysique Moleculaire
SUPEREXCITED AND IONIC STATE RELAXATION PROCESSES IN VACUUM-ULTRAVIOLET EXCITED POLYATOMIC MOLECULES. II.

3:30 - 5:00 M. Robnick, University of Bonn
REGULAR AND IRREGULAR MOTION IN CLASSICAL AND QUANTUM SYSTEMS. II.

* * * * * *

EXTENDED ABSTRACTS/PRELIMINARY MANUSCRIPTS

(ARRANGED IN ORDER OF PRESENTATION)

Journal of Photochemistry, *17* (1981) 461–475

GIANT MOLECULE INTERACTIONS*

S.P. McGLYNN and G.L. FINDLEY

Choppin Chemical Laboratories, Louisiana State University, Baton Rouge, LA 70803 (U.S.A.)

Summary

Molecular Rydberg states are discussed from the point of view of atomic physics, the appropriate molecular extensions being provided where necessary. The interactions of Rydberg states with each other, with intravalence excitations and with their environment are elaborated. A further subdivision is made into channel interactions, strong perturbations and external field effects. By these means it is possible to discuss the molecular Rydberg regime, even at small n, in ways which are remarkably similar to those pertinent to the atom, and hence to generate a coherent picture of the interesting and important area of very large molecules.

1. Introduction

1.1. Pertinence

Giant atoms are currently of considerable concern. Little has been said, however, concerning giant molecules. Both are relevant to the development of future generations of weak field detectors and tunable microwave sensors. In addition, the study of electric and magnetic effects is often inhibited by the inability to generate high field strengths; however, such field effects may be simulated in giant species with relatively small field strengths. Field effect studies are obviously of great concern in astrophysics, plasma physics, photophysics and photochemistry. In photochemistry, for example, electrons are so readily removed from giant systems that novel chemistry must surely result: certain charge transfer to solvent (CTTS) reactions are presumably mediated by such giant states. These states are also of compelling theoretical interest because they demand better formulation of the core–peel separability problem. Finally, the resonance phenomenon, itself a facet of the Rydberg (R) structure, must surely stimulate new approaches both to rate problems and to questions concerning the ability of an N-electron system to support an additional electron (*i.e.* the negative ion problem).

1.2. Scope

The characterization of molecular R transitions is embroiled in decisions concerning the meaning of the term "Rydberg". In atomic physics an R transi-

* Paper presented at the Xth International Conference on Photochemistry, Iraklion, Crete, Greece, September 6 - 12, 1981.

0047-2670/81/0000-0000/$02.50

© Elsevier Sequoia/Printed in Switzerland

tion occurs whenever an electron is promoted from a ground state orbital to an upper state orbital possessing an *aufbau* quantum number greater than that of the valence shell. In molecular physics this intuitive clarity is lost in the inability to assign a "principal" quantum number to the valence shell, an inability partially alleviated by heuristic and ambiguous "united atom" arguments.

Alternatively, we may define an R transition as any member of a series which obeys the Rydberg equation

$$E_{j\alpha} = I - \frac{1}{\nu_{j\alpha}^2} \tag{1}$$

where $E_{j\alpha}$ is the energy of that spectral feature thought to be the jth member of the αth R series converging on the ionization limit I and where $\nu_{j\alpha}$ is the effective quantum number. This characterization is empirically limited by the need for spectra which exhibit high resolution over large spectral regions; furthermore, it precludes interactions between R series.

The third alternative is operational: in this case, we say quite simply that an R state is any state defined with respect to an asymptotically hydrogenic hamiltonian. Several conclusions follow.

(i) Energy spacings of R states decrease as $1/\nu_{j\alpha}^2$ where $\nu_{j\alpha} = n_j - \mu_\alpha$ (n_j is an integer and μ_α is the quantum defect).

(ii) The average radius $\langle r \rangle$ of an R orbital is proportional to $\nu_{j\alpha}^2$. Hence, highly excited R states are spatially enormous, a characteristic embodied in the term "giant" molecule or atom.

(iii) For a fixed core the spin–orbit coupling parameter ζ remains approximately constant whereas the exchange integral K decreases at least as fast as $1/\nu_{j\alpha}^2$. Thus, the coupling regime index K/ζ is proportional to $\nu_{j\alpha}^{-k}$ where $k > 2$, a result indicating that highly excited R states are in a pure (Ω, ω) regime.

We shall adopt the above "asymptotic definition" and then investigate the scope and limitations of the concomitant operational definitions (i) - (iii). In this context we define the following one-electron hamiltonian:

$$H = \frac{\hbar^2}{2m}\left\{-\frac{d^2}{dr^2} + \frac{l(l+1)}{r^2}\right\} - \frac{Ze^2}{r} + V_{ra}(r) + V_{rm}(r) + V_{so}(r,\sigma) + V_v(r,\sigma,Q) + \mathcal{F} \tag{2}$$

The first term in eqn. (2) contains the (radial) kinetic energy operator and the centrifugal barrier, while the second term is the Coulomb potential. V_{ra} is the residual atomic potential and V_{rm} is the residual molecular potential; both of these potentials are short ranged, *i.e.*

$$\lim_{r\to\infty} rV_{ra} = \lim_{r\to\infty} rV_{rm} = 0$$

$V_{so}(r,\sigma)$ represents orbital–orbital and spin–orbital interactions- $V_v(r,\sigma,Q)$ includes vibronic and spin–vibronic interactions. Finally, $\mathcal{F}$ represents any imposed external field, whether electric, magnetic or molecular (*i.e.* condensed phase). This paper represents a justification of eqn. (2) for R states. In Section 2 we present an approximate treatment for V_{ra} and V_{rm} from the viewpoint of single-channel

quantum defect theory (SQDT). In Section 3 we refine this treatment and extend it to include part of V_{so} by the introduction of multichannel quantum defect theory (MQDT) interactions. In Section 4 strong perturbations (*i.e.* those perturbations arising from V_v and from anomalous exchange and spin–orbit coupling effects) are discussed. In addition, the importance and prevalence of Rydberg–valence mixing is investigated. Finally, electric and magnetic field effects are treated in Section 5, while condensed media effects are discussed in Section 6.

2. Single-channel quantum defect theory

2.1. One-electron Coulomb problem

We begin with the hydrogenic atom. The radial Schrödinger equation (in Rydberg units) is

$$\left\{\frac{d^2}{dr^2} - \frac{l(l+1)}{r^2} + \frac{2Z}{r} + 2\mathcal{E}_j\right\} f_j(r) = 0 \tag{3}$$

where

$$\mathcal{E} = -Z^2/k^2 \tag{4}$$

and

$$k = \begin{cases} \nu_j \text{ for } \mathcal{E} < 0 \\ i\gamma \text{ for } \mathcal{E} > 0 \end{cases} \tag{5}$$

The bound state ($\mathcal{E} < 0$) wavefunctions are given by the regular Coulomb function f which asymptotically is

$$f \sim u(\nu, r) \sin \pi\nu - v(\nu, r) \cos \pi\nu \tag{6}$$

where u is a rising exponential and v is a falling exponential in r. Since the bound state wavefunctions must vanish as $r \to \infty$, we find

$$\sin \pi\nu = 0 \tag{7}$$

Thus $\nu = n$ where n is an integer and

$$\mathcal{E} = -Z^2/n^2 \tag{8}$$

2.2. Introduction of the residual atomic potential

The Schrödinger equation for the residual atomic potential is

$$\left\{\frac{d^2}{dr^2} - \frac{l(l+1)}{r^2} + \frac{2Z}{r} - 2V_{ra}(r) + 2\mathcal{E}_{jl}\right\} F_{jl}(r) = 0 \tag{9}$$

Since $V_{ra}(r)$ is short ranged, this equation asymptotically reverts to eqn. (3) at distances greater than r_0, the cut-off distance for V_{ra}. In order to ensure smooth joining at $r = r_0$, we find

$$F_{jl} = f_j(r) \cos \pi\mu_l - g_j(r) \sin \pi\mu_l \tag{10}$$

Using the appropriate asymptotic forms for f and g, eqn. (10) becomes

$$F_{jl} \sim u_j(r)\sin\{\pi(\nu+\mu_l)\} - v_j(r)\cos\{\pi(\nu+\mu_l)\} \tag{11}$$

from which it follows that

$$\sin\{\pi(\nu+\mu_l)\} = 0 \tag{12}$$

or

$$\nu_j = n_j - \mu_l \tag{13}$$

From eqns. (4) and (5) then

$$\mathcal{E}_{jl} = -\frac{Z^2}{(n_j-\mu_l)^2} \tag{14}$$

Thus the Rydberg equation is established.

2.3. Introduction of the residual molecular potential

The procedure of Section 2.2 can be extended to molecules if V_{rm} is indeed short ranged. This in turn implies a significant similarity between an atomic R spectrum and a molecular R spectrum if, in both instances, the *total* residual potential were very nearly the same. That this assumption is reasonable in some cases is established [1] for Xe–CH_3I by a comparison of Figs. 1 and 2.

Further information concerning the residual potentials may be gained through introduction of the phase amplitude method [3]. This *ansatz* transforms the Schrödinger equation into two coupled first-order differential equations, thereby effecting the separation

$$F_{jl}(r) = a_{jl}(r)[f_{jl}(r)\cos\{\pi\mu_l(r)\} - g_{jl}(r)\sin\{\pi\mu_l(r)\}] \tag{15}$$

where $a_{jl}(r)$ is an amplitude function while $\mu_{jl}(r)$ is a quantum defect function. Within the phase amplitude method it is possible to show that

$$\pi\mu_{jl}(r) = 2W^{-1}\int_0^r \{V_{ra}(r') + V_{rm}(r')\}[f_{jl}(r')\cos\{\pi\mu_l(r')\} - g_{jl}(r')\sin\{\pi\mu_l(r')\}]^2\,dr' \tag{16}$$

where W is the wronskian of the f and g functions.

If the residual potentials are negative and monotonically increasing, it follows from eqn. (16) (and the detailed structure of the f and g functions) that [1]

$$\nu_{jl} - \nu_{(j-1)l} \geqq 1$$

However, if the residual potentials are positive and monotonically decreasing [1]

$$\nu_{jl} - \nu_{(j-1)l} \leqq 1$$

This is illustrated for the rare gases ($V_{rm} = 0$) in Fig. 3. Thus, we see that V_{ra} is attractive for each of the rare gases. Application of this procedure to CH_3I [1]

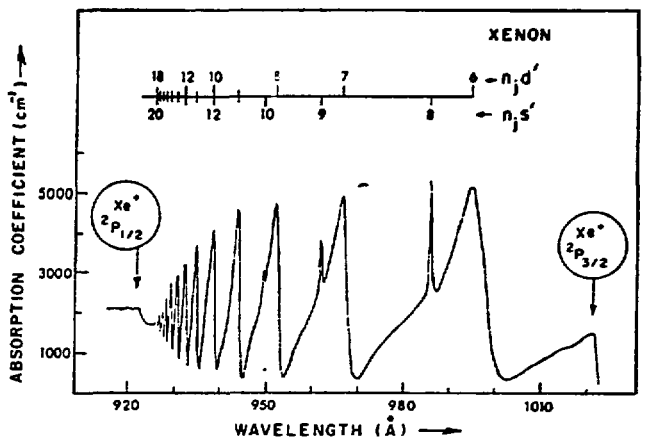

Fig. 1. The autoionization spectrum of xenon between the $^2P_{3/2}$ and $^2P_{1/2}$ ionization limits (adapted from ref. 2). The primed symbol nj' distinguishes series converging on $^2P_{1/2}$ from those converging on $^2P_{3/2}$.

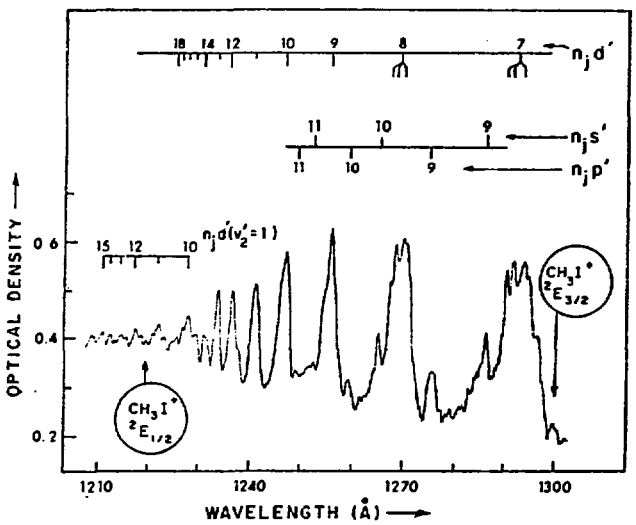

Fig. 2. The absorption spectrum of CH_3I between the $^2E_{3/2}$ and $^2E_{1/2}$ ionization limits. The primed symbol nj' distinguishes series converging on $^2E_{1/2}$ from those converging on $^2E_{3/2}$.

shows that V_{rm} is repulsive for $j < 2$ but becomes negligible at larger j because of the dominance of $V_{ra}(r)$ at larger r. The effect is even more pronounced for l waves with $l \geqq 2$ since, in this case, the centrifugal barrier acts to impose effective spherical symmetry even on the molecular system [1].

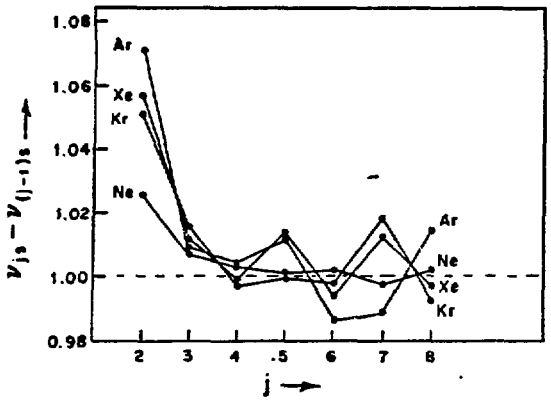

Fig. 3. A plot of $\nu_{js} - \nu_{(j-1)s}$ for the $n_0p^6\ {}^1S_0 \rightarrow n_0p^5n_j s_{3/2}{}^0, J = 1$ series ($^2P_{3/2}$ core) of the rare gases (data taken from ref. 4).

3. Multichannel quantum defect theory

If two or more ionization limits are adjacent, two R series (one converging on each limit) may interact, presuming, of course, that each series has the same total angular momentum [5]. Of even more importance, a discrete state of one series may interact with the continuum of the other series thereby preionizing (autoionizing). A "channel" is the union of the discrete members of an R series with the continuum of the same series, and interactions such as those described above are known as multichannel interactions. That such interactions occur in xenon [6] and CH_3I [1, 7] is shown in Figs. 1 and 2: we see the characteristic Beutler–Fano [8 - 10] autoionization profiles in both systems. Within the MQDT, however, the similarities between xenon and CH_3I can be further strengthened [11], as will now be shown.

In the spectral region of interest in xenon and CH_3I there are two ionization limits: $I_1 = I(^2P_{3/2}$ or $^2E_{3/2})$ and $I_2 = I(^2P_{1/2}$ or $^2E_{1/2})$. Thus each level must be referenced to both ionization limits:

$$E = I_1 - \frac{1}{\nu_1{}^2} = I_2 - \frac{1}{\nu_2{}^2} \tag{17}$$

Boundary conditions on the bound state wavefunc ions impose a consistency constraint which, when coupled with eqn. (17), allows us to fit experimental data to a ν_1(modulo 1) *versus* ν_2(modulo 2) plot and thus to determine quantum defects [6, 10, 12]. This procedure is illustrated in Fig. 4. The similarities between the two plots are striking and further indicate the close relationship of the non-coulombic potential terms for xenon and CH_3I.

Finally, we note that manifestations of autoionization in polyatomic systems are known [13] which are more esoteric (*e.g.* J dependence and q reversal) than that discussed above. In addition, rotational and vibrational preionization and molecular predissociation have been treated in an MQDT format [10, 14 - 16].

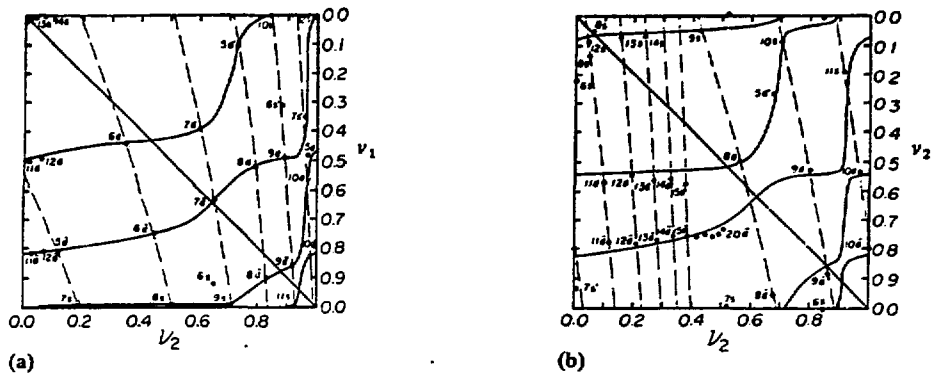

Fig. 4. Lu–Fano [6, 10, 12] plots for the discrete states of (a) xenon and (b) CH_3I. The xenon plot is adapted from ref. 6. ν_1 and ν_2 are effective quantum numbers (modulo 1) defined with respect to the first and second ionization potentials respectively (see text). The full diagonal lines are given by $\nu_1 = \nu_2$; the broken curves are plots of $\nu_2(\nu_1)$, the functionality being defined by eqn. (17) of the text. The full curves are the loci of the consistency constraint mentioned in the text and discussed more fully in refs. 6 and 11. The data point notation is as follows: $d = d_{5/2}(I_1)$; $\bar{d} = d_{3/2}(I_1)$; $s = s_{1/2}(I_1)$; $s' = s_{1/2}(I_2)$; $d' = d_{3/2}(I_2)$.

4. Strong perturbations

Most, if not all, of the strong perturbations considered here should be included within the channel framework of Section 3. Unfortunately, the theoretical basis for such an inclusion is not available for polyatomics and is even incomplete for diatomics [10, 14 - 16]. Indeed, even if the tactical approach were fully developed, considerations of the multichannel nature would require detailed high resolution data over large spectral ranges. Such data, unfortunately, are not often available.

The general type of high resolution data covers small spectroscopic ranges (*e.g.* the first s complex of CH_3I [17]) and perturbations may be evident which, because of the narrow observational range, require discussion in terms of interactions within that range. Even in the MQDT, sudden perturbations may occur which, because of artificial restrictions on the number of interacting channels, simply cannot be treated within the channel framework. The above two types of perturbations are referred to here as strong perturbations not because they are strong but because they are (or appear to be) sudden and therefore in some sense dominating.

As a result we now feel free to discuss a variety of strong perturbations of which at least one (*i.e.* spin–orbit coupling) has already been considered within the MQDT.

4.1. Spin–orbit coupling

We use the $5p \rightarrow 6s$ R excitation of HI as an example. It is found that the linear ≡C–I bond of alkyl, alkene and alkyne iodides dominates spin–orbit cou-

pling in these iodides and therefore that the HI considerations have a wider range of applicability than we might at first think. Indeed, because the spin–orbit coupling constants for chlorine, bromine or iodine are all much larger than that for carbon, these same considerations also apply to chlorides and bromides.

The states which arise from the 5p → 6s configurational excitation are shown in Fig. 5 in both the (Λ,S) limit and the (Ω,ω) limit. If the states shown in Fig. 5 are labelled 1, 2, 3 and 4 in order of increasing energy, then the intermediate coupling regime yields the following set [18] of energy differences and intensity ratios:

$$E(4)-E(2)=2(K^2+\zeta^2)^{1/2}$$

$$E(3)-E(1)=2\zeta$$

$$E(2)-E(1)=K-(K^2+\zeta^2)^{1/2}+\zeta$$

$$E(4)-E(3)=K+(K^2+\zeta^2)^{1/2}-\zeta$$

$$I(^2\Pi_{3/2})-I(^2\Pi_{1/2})=2\zeta$$

$$\frac{\mathcal{J}(4)}{\mathcal{J}(2)}=\left\{\frac{K}{\zeta}+\left(1+\frac{K^2}{\zeta^2}\right)^{1/2}\right\}^2$$

Here K is the exchange integral, ζ is the spin–orbit coupling constant ($K \equiv \langle 5p6s|\,1/r_{12}\,|6s5p\rangle$ and $\zeta \equiv \frac{1}{2}\langle 5p|\zeta|5p\rangle$) and $\mathcal{J}(\beta)$ is the absorptivity of the transition $\tilde{X} \rightarrow \beta$. The ability of this model in fitting details of intermediate coupling in the simple halides is extensive [19, 20], as may be seen in Fig. 6.

4.2. Vibronic and spin–vibronic coupling

If q, Q and σ represent sets of electron coordinates, atom coordinates and electron spin coordinates respectively, the spin–vibronic hamiltonian may be designated $H(q, \sigma, Q)$. If we assume that spin–orbit coupling is small, a Herzberg–Teller expansion in the normal coordinates Q_K about the equilibrium nuclear configuration Q° of a given electronic state yields

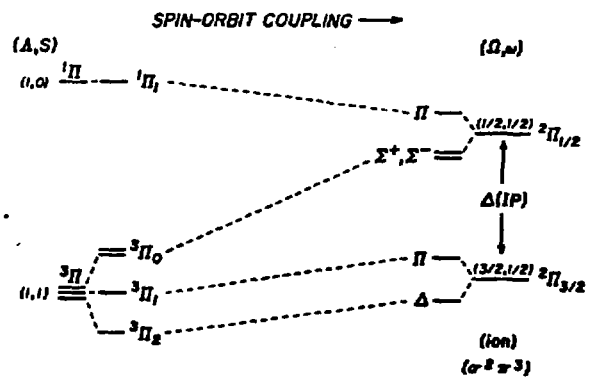

Fig. 5. Spin–orbit coupling in the $\ldots\sigma^2\pi^3 6s$ configuration of HI.

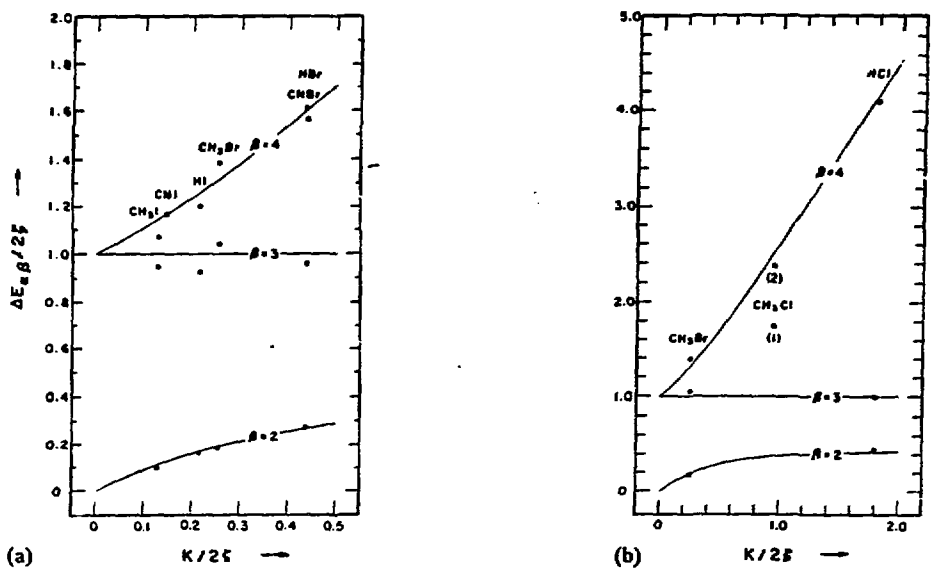

Fig. 6. A plot of $\Delta E_{\alpha\beta}$, $\alpha = 1$ and $\beta = 2, 3, 4$, *vs.* the exchange:spin–orbit ratio for various halides: ——, theoretical curves (see Section 4.1); O, ●, experimental data.

$$H(q, \sigma, Q) = H(q;Q^\circ) + H(q, \sigma; Q^\circ) + \sum_k \left[\left\{ \frac{\delta H(q.Q)}{\delta Q_K} \right\}_{Q^\circ} + \left\{ \frac{\delta H(q,\sigma,Q)}{\delta Q_K} \right\}_{Q^\circ} \right] Q_K + \ldots \tag{18}$$

which, on truncation, may be written

$$H(q,\sigma,Q) = H_e + H_{so} + H_v + H_{sv} \tag{19}$$

where H_e is the Born–Oppenheimer electronic hamiltonian at configuration Q°, H_{so} is the spin–orbit hamiltonian (also at Q°), H_v and H_{sv} (in obvious notations) are the vibronic and spin–vibronic hamiltonians and all coordinate dependences to the right of the semicolon are parametric. If the H_e–H_{so} separation is valid, then $H_{so} < H_e$ and hence H_v and H_{sv} respectively are first and second order in nature. If H_{so} is large, it is advisable to rewrite eqn. (18) as

$$H(q,\sigma,Q) = H(q,\sigma;Q^\circ) + \sum_k \{\delta H(q,\sigma,Q)\,\delta Q_K\}_{Q^\circ} Q_K \tag{20}$$

in which case H_{sv}, now the second term, is formally first order.

In the MQDT, as presented in Section 3, the zeroth-order electronic and spin–orbit interactions are included in the channel formalism and they need not be considered here. However, the vibronic and spin–vibronic interactions are

TABLE 1

State	$\{q_i\}$	$\{q_i,\sigma_j\}$	$\{q_i,\sigma_j,Q_{1,2,3}\}$	$\{q_i,\sigma_j,Q_{4,5,6}\}$
1	Π	Δ	Δ	Φ,Π
2	Π	Π	Π	Π,Σ^+,Σ^-
3	Π	Σ^+,Σ^-	Σ^+,Σ^-	Π
4	Π	Π	Π	Π,Σ^+,Σ^-

not a part of the MQDT, at least as we have formalized it. Hence these effects can give rise to spectroscopic perturbations which are not only *not* accounted for within the MQDT but which can also confuse the entire MQDT deperturbational tactic. Thus it is very important to recognize vibronic and spin–vibronic intrusions, particularly because these intrusions are both common and large.

We again adopt the linear HI molecule as an exemplar of vibronic and spin–vibronic coupling. This molecule possesses only one normal vibrational mode, which forms a basis for the Σ^+ representation of $C_{\infty v}$. The extension to the CH_3I molecule is accomplished here, for simplicity, by "permitting" HI to possess non-totally symmetric Π normal modes. Thus in the group $C_{\infty v}$ the CH_3I normal modes Q_1, Q_2 and $Q_3 \in \Sigma^+$ and Q_4, Q_5 and $Q_6 \in \Pi$. Consequently, we are now in a position to tabulate the representations of $C_{\infty v}$ for which the various vector collections form bases (Table 1).

Now, in the (Λ,S) regime (Table 1, second column) only the $\tilde{X}\rightarrow 4$ transition, namely $^1\Sigma^+ \rightarrow {}^1\Pi$, is electric dipole allowed. In the (Ω,ω) regime (Table 1, third column), spin–orbit mixing of states 2 and 4 confers allowedness the $\tilde{X}\rightarrow 2$ transition. The transitions $\tilde{X} \rightarrow 1$ and $\tilde{X} \rightarrow 3$, however, remain forbidden and retain this forbiddenness until vibronically coupled to either state 2 or state 4 by Π normal modes (Table 1, fifth column). We thus have the interesting result that states 2 and 4 may be coupled in a nominally first-order way by totally symmetric modes, whereas states 1 and 3 can couple with either of states 2 and 4 in ways which are nominally second order, and that such coupling is mediated only by non-totally symmetric modes. An example [21] of 3–4 state coupling in CD_3I mediated by the Q_6 mode is shown in Fig. 7. Examples [22] of 2–4 mixing abound. The matrix elements of the nominally first-order and second-order effects are as follows: C_2H_5Br [22] (2–4 mixing), 145 cm^{-1}; CNCl [23] (4–intravalence mixing), 180 cm^{-1}; CH_3I [21] (3–4 mixing), 15 cm^{-1}.

5. Field effects

5.1. Magnetic field effects

The application of a magnetic field $\boldsymbol{B}$ introduces the Zeeman term $H_B = \boldsymbol{\mu}\cdot\boldsymbol{B}$ (where $\boldsymbol{\mu}$ is the magnetic moment) into the hamiltonian. Given the normal bandwidths for polyatomic molecules, it is improbable that line splitting due to the Zeeman effect will be observed in such systems, at least for $B \leqq 20$ T. The observation of Zeeman effects then devolves on the measurement of band shape differences, *e.g.* the measurement of magnetic circular dichroism (MCD) [24],

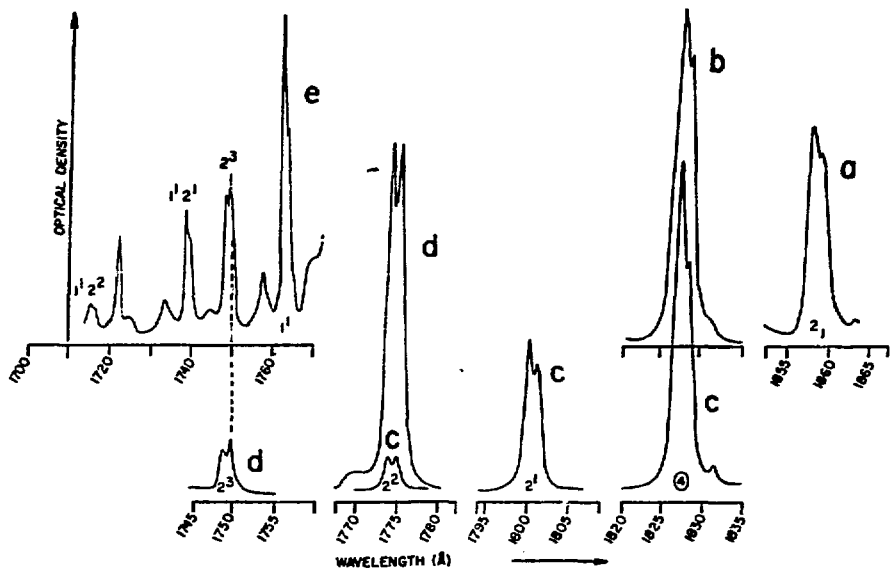

Fig. 7. Spin–vibronic doubling in CD_3I mediated by the non-totally symmetric (Π symmetry) mode Q_6. The interactions in this case occur between states $0 \rightarrow 3$ (ν_6) and states $0 \rightarrow 4$ and are carried throughout the ν_2 progression of Q_2 built on the transition $0 \rightarrow 4$. The alternation in intensity is associated with a slight difference in the frequency ν_2 in states 3 and 4. The doubling is absent in CH_3I because the increase in the ν_6 frequency in the fully protonated derivative destroys the near degeneracy.

which is the difference in molecular absorptivity of left and right circularly polarized light in the presence of a magnetic field. The primary aim of such studies is to make state assignments. Unfortunately, difficulties intrude. For example, μ is different in the various molecular spin–orbit limits of which, in contrast with the atom, there are more than two (*i.e.* (Λ,S) and (Ω,ω)). Indeed, the only well-defined quantum number is a resultant of molecular rotational and electronic motions. The situation, then, is very complicated in a diatomic molecule; in a polyatomic molecule, because of large coriolis effects it can become even worse.

It has been shown [20, 25], however, that MCD can lead to rather precise information. We exemplify again using the first s complex of CH_3I in a primitive $C_{\infty v}$ point group. In this instance we find the spectra shown in Figs. 8 and 9 [25]. The MCD signal is [25]

$$\Delta A^{H}(\bar{\nu}_0) = A^{H}_{-}(\bar{\nu}_0) - A^{H}_{+}(\bar{\nu}_0) = aB\left\{\frac{\delta A^{0}(\bar{\nu})}{\delta \bar{\nu}}\right\}_{\bar{\nu}_0} + bBA^{0}(\bar{\nu}_0) \qquad (21)$$

where A denotes absorptivity, the superscripts H and 0 denote the presence or absence of the field B and the subscripts + and – denote right circularly polarized light and left circularly polarized light respectively. Since the ground state $^1\Sigma^+$ possesses no angular momentum and therefore a is proportional to μ_B of the

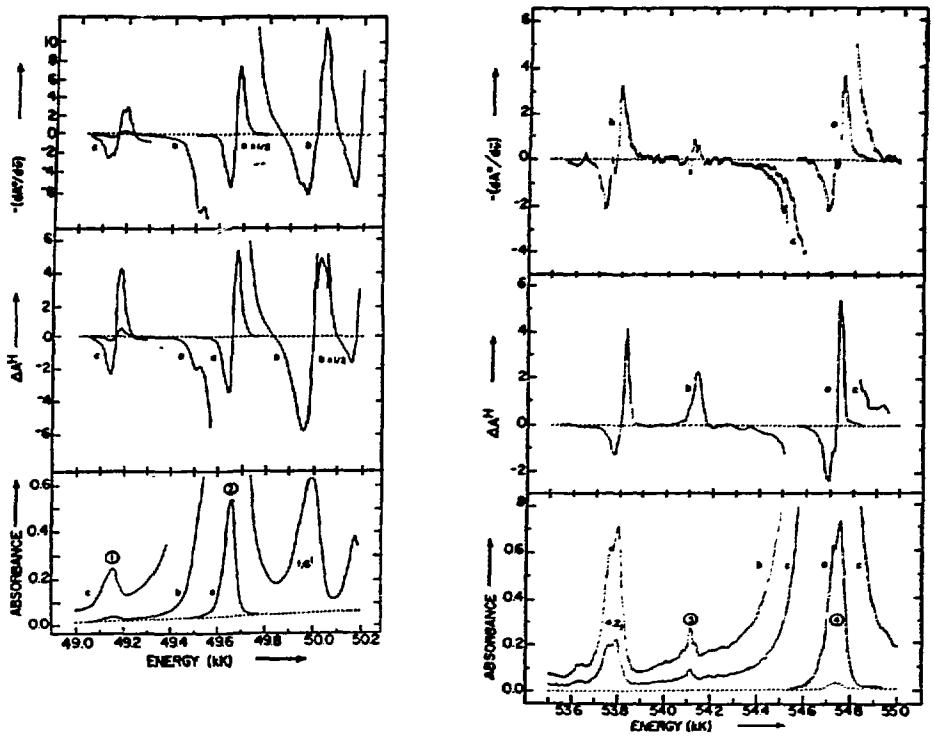

Fig. 8. Absorption spectra A^0, MCD spectra ΔA^H and derivative spectra $dA^0/d\bar{\nu}$ of CH_3I in the 6s Rydberg complex.

Fig. 9. Absorption spectra A^0, MCD spectra ΔA^H and derivative spectra $dA^0/d\bar{\nu}$ of CD_3I in the 6s Rydberg complex.

excited state β, the derivative component of eqn. (21) will be large when μ_β is large and absent when μ_β is zero. The second term in eqn. (21), attributable to field-induced mixing, is usually small and will only be important when a is zero. The relevant factors are that a derivative signal (+ or – phase) denotes an excited state magnetic moment whose size, $\mu_\beta = -(\Lambda_c + 2\Sigma_c + \lambda + 2\sigma)\hbar^{-1}\mu_{Bohr}$ in (Ω,ω) coupling, is proportional to signal height and that an absorptive-type signal (+ or – phase) denotes an excited state with zero magnetic moment.

The experimental magnetic moments of states 1, 2, 3 and 4, as evaluated [25] from the data of Figs. 8 and 9, are 1, 0.33, 0 and 0.27, whereas those obtained using the μ_β expression given above are 1, 0.33, 0 and 0.33, in excellent agreement with experiment. A great deal of other information is contained in the phasing and is discussed in refs. 25 and 26.

The quadratic field effect, attributable to diamagnetism, is usually very small. However, since the diamagnetic interactions are proportional to the Rydberg cross-sectional area, they increase as ν^4 whereas the electrostatic binding energies decrease as ν^{-2}. Thus the ratio of magnetic energy to electrostatic bind-

ing energy increases as ν^6 and at $n = 30$. for example, is about 10^9 times larger than for $n = 1$. In this case the quadratic field effect not only dominates the Zeeman effect but also overwhelms the electrostatic binding energy and converts the system into a "magnetic system". Quadratic field effects have been observed in atoms [27, 28] and although a thorough understanding is elusive it appears to be nascent. We [29] have searched CH_3I and C_6H_6 for quadratic field effects in the vicinities of both I_1 and I_2. Although distinct field perturbations were evident [29], no behavior reminiscent of a magnetic system was observed. The doublet intensification observed [29] at $n = 15$ in CH_3I is probably a $|\Delta J| = 2$ field-induced mixing of the s–d type.

5.2. Electric field effects

The investigation of molecules in strong external electric fields, while burgeoning [30], is still in its infancy. The goad for research is provided by the development of focused pulsed laser systems with power densities in the gigawatts per square centimeter range which are strong enough to produce massive distortions of molecular electronic charge distributions. The Rydberg regime provides a facile means of performing such "high field" investigations. Since the mean Coulomb field of a Rydberg molecule is $eZ/\langle r^2\rangle \propto \nu^{-4}$ it follows that even a very weak field can induce field ionization at large n values. Furthermore, since level densities increase as ν^5, it follows that weak-field-induced mixings and hence massive non-linearities can occur in high n Rydberg states. Unfortunately, few or no investigations of high n molecular states are known. Indeed, the little vacuum UV work known [24, 31, 32] is mostly concerned with state identifications.

The electron of a hydrogenic system in a static electric field finds itself in the potential

$$V(r) = -\frac{Z}{r} + E\cdot r \tag{22}$$

The effect of the term $H_E = E\cdot r$ is to couple the discrete states of the field-free atom, producing changes in the atom structure (*i.e.* Stark effects). However, it can also produce discrete state–continuum coupling, leading to field ionization and to a real alteration in the ionization limit. The situation in a molecule is very different from that in the atom: the molecule possesses dipole moments, different in both ground (unprimed) and excited (primed) states, which the atom does not. Thus, if we define $a = \mu - \mu'$, asserting that both dipole moments are either parallel or antiparallel to the principal molecular axis (which itself lies at an angle ϑ to E) and if we define $b = \alpha - \alpha'$ where α is a mean isotropic polarizability, we can write [31]

$$H_E(\vartheta) = \frac{a\cdot E}{hc} - \frac{bE^2}{2} \tag{23}$$

The total effects are considerably more complex than that implied above. Yet, as far as we are concerned, eqn. (23) contains the essence of our interests. Thus the Stark effect measurements (low n or low field) provide a way of measuring μ', and the effect of measurements at high n, quadratic because α' varies as ν^6, will yield a measure of α'.

Again, because of bandwidth problems, the measurement of molecular Stark effects usually devolves on the detection of band shape alterations. An applicable method has been discussed [24] and a few examples [31, 32] of its use are available. Briefly, the experimental format known as electric linear dichroism is preferable. If the electric vector ε of the incident light wave is plane polarized and at an angle β to the external electric field E (which in turn is perpendicular to the direction of light incidence), the field-on–field-off absorbance difference is [24]

$$\Delta A^{E}_{\beta}(\tilde{\nu}_0) \equiv A^{E}_{\beta}(\tilde{\nu}_0) - A^{0}(\tilde{\nu}_0)$$
$$= E^2\left(C_1^{\beta}A^{0}(\tilde{\nu}_0) + C_2^{\beta}\left[\left\{\frac{dA^{0}(\tilde{\nu})}{d\tilde{\nu}}\right\}_{\tilde{\nu}_0} - \frac{A^{0}(\tilde{\nu}_0)}{\tilde{\nu}_0} + \right.\right.$$
$$\left.\left. + C_3^{\beta}\left[\left\{\frac{d^2A^{0}(\tilde{\nu})}{d\tilde{\nu}^2}\right\}_{\tilde{\nu}_0} - \frac{2}{\tilde{\nu}_0}\left\{\frac{dA^{0}(\tilde{\nu})}{d\tilde{\nu}}\right\}_{\tilde{\nu}_0} + \frac{2A^{0}(\tilde{\nu}_0)}{\tilde{\nu}_0^2}\right]\right) \qquad (24)$$

This expression is obviously more complex than that in the magnetic field case primarily because of the presence of the second derivative. Expressions for the parameters C_1, C_2 and C_3 are available [24] in terms of dipole moments, polarizability tensor components and field-induced mixing coefficients, and experimental means of extracting them are known.

6. Rydberg series in the condensed phase

It is impossible to discuss molecular R series in solution without an understanding of them in the gas phase. Unfortunately, our understanding of gas phase behavior is not very good and for that reason we feel compelled to initiate our discussion of the condensed phase by a retreat to the gaseous phase.

6.1. Gas phase

In the vapor, molecules may exhibit the following characteristics: (i) a well-developed R series, almost hydrogen like in that the intensity decreases as $1/\nu^3$; (ii) a well-developed R series but with maximum intensity at intermediate values of n; (iii) a collapsed R series, often with only the lowest energy member observable (*e.g.* the lowest R (s) transitions in H_2O, amides, saturated hydrocarbons etc. which may be referred to, facetiously perhaps, as "virgin Rydbergs", characterized usually by being anomalously broad, intense and quantum defect deviant [33]); (iv) a series such as (i) or (ii) but with an anomalous quantum defect for the first few members [34] (see, for example, our discussion of SQDT).

Rydberg series may, of course, exhibit many perturbations, the recognition and identification of which has been the content of Sections 3 and 4. Now we concern ourselves primarily with the series characteristics (i) - (iv). It seems to us that the only model capable of rationalizing items (ii) - (iv) is a double-well model (Fig. 10).

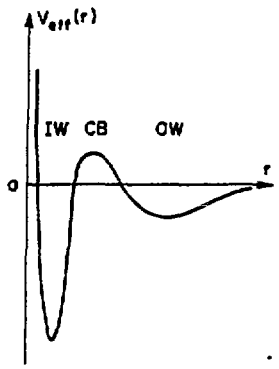

Fig. 10. A model double-well potential: IW, inner well; CB, centrifugal barrier; OW, outer well.

For atomic Rs, $V(r)$ is a monotonically increasing negative-definite function of r. However, the effective potential

$$V_{\text{eff}}(r) = V(r) + \frac{l(l+1)}{r^2}$$

is monotonic only for s waves. For l waves, $l \neq 0$, $V_{\text{eff}}(r)$ is generally double welled and exhibits a centrifugal barrier such that the bound states may be approximate eigenstates of either the inner well (IW) or the outer well (OW). The barrier controls the finite number of bound states, some perhaps resonant, which can be sustained in the IW. The OW potential is asymptotically hydrogenic and it sustains an infinite number of R states.

For molecular Rs, since $V_{\text{rm}}(r)$ is short ranged, the effective potential is essentially spherically symmetric at large r. At small r, however, the effects of $V_{\text{rm}}(r)$ are drastic. From an atomic point of view the imposition of $V_{\text{rm}}(r)$ on an atomic potential is a breaking of symmetry of the sphere group. Retaining $V_{\text{eff}}(r) = V_{\text{eff}}(r)$, the result is the induction of l wave mixing in a spherically symmetric potential. Thus, even for a parental s wave, the effective potential for a molecule will be of the double-well form but the barrier may be negative definite: $V_{\text{eff}}(r)$ may be a double-well potential for molecular R states regardless of the parental l value. As for atoms, the nature of the barrier determines the number of bound levels in the IW and, more importantly, the localization of wave amplitude in either the IW or the OW regions.

We now attempt to rationalize the gas phase characteristics. In order to do so, we note that the initiating orbital in the absorptive event is largely confined in the IW and, consequently, that only those terminal R orbitals with some IW amplitude will couple optically to the ground state. In this view, then, rationalization proceeds as follows: (i) the centrifugal barrier (CB) is either very weak or absent; (ii) the barrier is weak and narrow and, while the IW cannot sustain even one bound level, all levels are bimodal (*i.e.* possess IW and OW amplitude) and the bimodal IW component maximizes at intermediate n; (iii) one or more levels can be sustained in the IW, the barrier being such that all eigenfunctions

are either wholly IW or wholly OW and that little bimodality (*i.e.* mixing) occurs; (iv) there is always a bimodal component in the first s R member.

6.2. Condensed phase

Consider now a molecule-doped insulator, liquid or solid. The dopant molecules exhibit the following behavior forming the condensed phase: (v) virgin R states (see (iii) above) remain largely unaffected [33]; (vi) total quenching of R series (see (i) above) is common [34, 35]; (vii) a Wannier exciton behavior results and a few members of the exciton R series are observed in some instances [36]; (viii) anions which do not support any bound excited states in the gas phase may do so in the condensed phase (some of these states may be resonant and may lead to electron transfer (*i.e.* CTTS [37]) phenomena in aqueous solutions and single-crystal hosts [33]).

The alterations in $V_{\text{eff}}(r)$ caused by condensation of the guest into a condensed insulator host are as follows. To first order, $V_{\text{eff}}(r)$ remains unaffected by the crystal field of the host at small r; at large r the conduction band of the host will dominate $V_{\text{eff}}(r)$ so that

$$\lim_{r\to\infty} I(\text{dopant}) = E(\text{conduction band})$$

and at intermediate r further substructure (*i.e.* negative-definite barriers) may or may not appear in the OW region. If the dopant is a charged entity such as an anion, the resulting host–guest interactions become so drastic that even the IW region is grossly altered [38]. Indeed, in this case the deepening of the IW may support bound states and, if substructure appears in the intermediate r region, some of these states may become resonant (*i.e.* may autoionize to the host conduction band). The behavioral characteristics (v) - (viii), then, are rationalized as follows: (v) these states, already localized in the IW, remain largely unaffected by the environment; (vi) the host conduction band must lie near or below the first R series member and $V_{\text{eff}}(r)$ substructure in the OW region must be minimal; (vii) the host conduction band must lie above the first few R series members and/or a large substructure of $V_{\text{eff}}(r)$ must occur in the OW region; (viii) the events already discussed for a monopolar dopant must occur.

7. Conclusions

We have tried to assess the Rydberg area of molecular electronic structure and interactions in the frame of modern atomic physics, building on the appropriate molecular extensions where needed. In the course of this effort it became totally obvious that the chemical literature is not only *not* keeping pace with the rapidly advancing area of atomic physics but that it is also losing ground in molecular physics. We believe this to be most unfortunate because it puts the chemist at a distance from the cutting edge of his subject. As examples we note that progress in high energy chemistry is tied in a large measure to our understanding of R states; rare gas chemistry, a rather startling discovery in the first place, may well rely heavily on Feschbach resonances, and much preparative chemistry may well require CTTS intermediates.

Acknowledgment

This work was supported by the U.S. Department of Energy.

References

1 H.-T. Wang, W.S. Felps, G.L. Findley, A.R.P. Rau and S.P. McGlynn, *J. Chem. Phys., 67* (1977) 3940.
2 R.G. Huffman, Y. Tanaka and J.C. Larrabee, *J. Chem. Phys., 39* (1963) 902.
3 J.L. Dehmer and U. Fano, *Phys. Rev. A, 2* (1970) 304.
4 C.E. Moore, *Natl. Bur. Stand. Circ. 467*, 1958 (U.S. Government Printing Office, Washington, DC).
5 M.J. Seaton, *Proc. Phys. Soc., 88* (1966) 801, 815.
6 K.T. Lu, *Phys. Rev. A, 4* (1971) 579.
7 M.A. Baig, J.P. Connerade, J. Dagata and S.P. McGlynn, *J. Phys. B, 14* (1981) L25.
8 H. Beutler, *Z. Phys., 93* (1935) 177.
9 U. Fano, *Phys. Rev., 124* (1961) 1866.
10 U. Fano, *Phys. Rev. A, 2* (1970) 353.
11 J. Dagata, G.L. Findley, S.P. McGlynn, J.P. Connerade and M.A. Baig, submitted to *Phys. Rev. A.*
12 K.T. Lu and U. Fano, *Phys. Rev. A, 2* (1970) 81.
13 J.P. Connerade, M.A. Baig and S.P. McGlynn, *J. Phys. B, 14* (1981) L67.
14 O. Atabek and C. Jungen, in H. Kleinpoppen and M.R.C. McDowell (eds.), *Electron and Photon Interactions with Atoms*, Plenum, New York, 1976.
15 D. Dill and Ch. Jungen, *J. Phys. Chem., 84* (1980) 2116.
16 Ch. Jungen and D. Dill, *J. Chem. Phys., 73* (1980) 3338.
17 S. Felps, P. Hochmann, P. Brint and S.P. McGlynn, *J. Mol. Spectrosc., 59* (1976) 355.
18 R.S. Mulliken, *Phys. Rev., 57* (1940) 500.
19 W.S. Felps, G.L. Findley and S.P. McGlynn, *Chem. Phys. Lett.*, in the press.
20 S.P. McGlynn, J.D. Scott, W.S. Felps and G.L. Findley, *J. Chem. Phys., 72* (1980) 421.
21 S.P. McGlynn, W.S. Felps, J.D. Scott and G.L. Findley, *J. Chem. Phys., 73* (1980) 4925.
22 W.S. Felps, J.D. Scott, G.L. Findley and S.P. McGlynn, *J. Chem. Phys., 74* (1981) 4832.
23 W.S. Felps, S.P. McGlynn and G.L. Findley, *J. Mol. Spectrosc., 86* (1981) 71.
24 J.D. Scott, W.S. Felps and S.P. McGlynn, *Nucl. Instrum. Methods, 152* (1978) 231.
25 J.D. Scott, W.S. Felps, G.L. Findley and S.P. McGlynn, *J. Chem. Phys., 68* (1978) 4678.
26 J.D. Scott, W.S. Felps, G.L. Findley and S.P. McGlynn, in preparation.
J.D. Scott and S.P. McGlynn, MCD of non-linear molecules–viewed in a linear molecule basis, *36th Am. Chem. Soc. Northwest Regional Meet., Bozeman, MT, June 17 - 19, 1981.*
27 W.R.S. Garton and F.S. Tompkins, *Astrophys. J., 158* (1969) 839.
28 C.D. Harper and M.D. Levinson, *Opt. Commun., 20* (1977) 107.
29 J.P. Connerade, W.R.S. Garton, M.A. Baig, J. Hormes and S.P. McGlynn, Bonn Synchrotron Center, unpublished data, 1980.
30 J.E. Bayfield, *Phys. Rep., 51* (1979) 317.
31 J.D. Scott and B.R. Russell, *J. Chem. Phys., 63* (1975) 3243.
32 G.C. Causley, J.D. Scott and B.R. Russell, *Rev. Sci. Instrum., 48* (1977) 264.
33 S.P. McGlynn and G.L. Findley, *Proc. Workshop on Far VUV Spectroscopy and Photochemistry, Mülheim a.d. Ruhr, February 24 - 26, 1981*, pp. 99 - 102.
34 M.B. Robin, in M.B. Robin (ed.), *Higher Excited States of Polyatomic Molecules*, Academic Press, New York, 1975.
35 J.W. Lewis, R.V. Nauman, D.B. Bouler and S.P. McGlynn, *J. Am. Chem. Soc.*, in the press.
36 J. Jortner, in E.-E. Koch, R. Haensel and C. Kunz (eds.), *Vacuum Ultraviolet Radiation Physics*, Pergamon, Braunschweig, 1974, p. 263.
37 M. Fox, in A.W. Adamson and P.D. Fleischer (eds.), *Concepts of Inorganic Photochemistry*, Wiley-Interscience, New York, 1975, p. 333.
38 G.L. Findley, J.A. Dagata and S.P. McGlynn, submitted to *Chem. Rev.*

THEORETICAL ASPECTS OF NH_3^+

Angelo R. Rossi

Department of Chemistry
The University of Connecticut
Storrs, Connecticut 06268

ABSTRACT

The vibronic nature of the lowest energy photoelectron spectrum of the $^2A_1(NH_3^+) \leftarrow {}^1A_1(NH_3)$ will be discussed. Two dimensional Franck-Condon factor calculations are performed and theoretical spectra are constructed which include the effect of vibronic linewidth.

Results of *ab initio* calculations on the low-lying states of NH_3^+ will also be presented. These results include excitation energies, geometries and force field calculations. The calculations are performed by several different techniques and yield comparable results in agreement with known experimental quantities. The ^2E excited state of NH_3^+ which is Jahn-Teller active will be discussed in detail. The calculations show that ^2E state distorts to a Cs geometry yielding two components of $^2A'$ and $^2A''$ symmetry. The Jahn-Teller stabilization energy (JTSE) has been calculated and will be compared with the experimental value. It turns out that the JTSE varies with the level of calculation used. The $^2A'$ component of the undistorted ^2E must be obtained by MCSCF techniques and is slightly energetically higher than $^2A''$ component. The distorted geometries of the $^2A'$ and $^2A''$ components will also be presented.

Photolysis of cyclic ethers and acetals at 185 nm in the liquid phase

Clemens von Sonntag

Max-Planck-Institut für Strahlenchemie, Stiftstr. 34-36,
D-4330 Mülheim a.d. Ruhr, West-Germany

Abstract

Like open-chain ethers, cyclic ethers undergo C-O bond scission upon excitation at 185 nm. This reaction leads to oxylalkyl diradicals. The intermediacy of an oxylalkyl diradical can be monitored, for example, by the cis$\rightleftarrows$trans isomerisation of cis- and trans-2,5-dimethyltetrahydrofuran. Besides reclosure these diradicals undergo disproportionations and internal H abstractions. Depending on the structure of the cyclic ether fragmentation reactions may occur in some cases with high quantum yields. They are considered to be true molecular processes and not to involve the diradical intermediates.

In neat 1,4-dioxane a long-lived excimer reacts with N_2O by excitation transfer. In aqueous solutions either electrons are ejected (formation of solvated electrons) or the excited molecules transfer an electron to either N_2O or to a proton, a species that competes for the same intermediate.

Acetals behave very similar to ethers. Some features of their photolyses are discussed in detail.

NATO-ASI : PHOTOPHYSICS AND PHOTOCHEMISTRY IN THE VACUUM ULTRAVIOLET

Lake Geneva, Wisconsin : 15-29 August 1982

SUPEREXCITED AND IONIC STATE RELAXATION PROCESSES IN VACUUM ULTRAVIOLET EXCITED POLYATOMIC MOLECULES

Sydney Leach

Laboratoire de Photophysique Moléculaire du C.N.R.S.
Bâtiment 213 - Université Paris-Sud
91405 - Orsay Cédex, France

Vacuum ultraviolet excitation of molecules above the lowest ionization potential can produce ions by direct ionization or by the indirect process known as autoionization (preionization) of superexcited states. These lectures will be concerned with the study of the relaxation of superexcited and ionic states of polyatomic species.

SUPEREXCITED STATES AND THEIR DECAY

Just as for atoms, molecules have neutral states above the lowest ionization limit, which are thus known as superexcited states. Most superexcited states are of Rydberg type but some may be valence states or have mixed Rydberg-Valence parentage. For atoms the superexcited states can generally only relax by decay to one or more ionization continua. Atomic oxygen is an exception in having other competitive decay channels. The situation is markedly different for molecules, where there is a greater diversity of decay channels for superexcited states and a greater density of the latter which now include rovibronic levels of electronic states. As described on the independent particle approximation, these discrete (bound) states can

decay into ionization continua, or they may relax by nonionic processes such as fluorescence, neutral dissociation and predissociation and generally by intramolecular radiationless coupling to isoenergetic levels of lower electronic states. To a first approximation, each relaxation process can be considered as independent and competitive, and thus exhibit a distinct partial cross section. Interactions can also exist between these channels, leading to interference effects. The competing decay channels of superexcited states have been most extensively studies for H_2 and some other diatomic species, but relatively little is known for polyatomic species. One of the interesting relaxation processes of superexcited states involves dissociative autoionization and is manifest by the appearance of dissociative photoionization in Franck-Condon gap regions i.e. in energy regions where no ion levels can be generated by the direct ionization process.

A measure of the relative importance of nonionic relaxation channels is given by the photoionization efficiency or quantum yield. The photoionization efficiency γ_i is defined as the number of ions produced per photon initially absorbed. For atoms, γ_i is generally unity above the first threshold and in most atomic cases, photoionization cross sections can be considered as identical to those of photoabsorption. In general, it is found that the ionization efficiency for molecules does not reach unity until between $\sim$ 3 and $\sim$ 9 electron volts above the ionization threshold. This implies that nonionic channels must have decay rates that are comparable, to within a factor of 100, with autoionization rates over this energy region. There is little detailed work on the competitive processes for molecular species other than hydrogen.

When γ_i reaches unity, autoionization becomes the overwhelming decay process of the superexcited states. In this region, the photoionization cross-section curves show little or no structure as is consistent with the linewidths associated with ultrafast autoionization decay rates and the high densities of superexcited states at these energies.

Knowledge of the relaxation processes of superexcited states of polyatomic molecules can be obtained from several complementary

techniques, among which are the following.

1. High resolution absorption spectroscopy in the vacuum ultraviolet

From the absorption spectra one can measure the energies of the "superexcited" bands and determine the energies of their corresponding excited levels. Exact determination of zero-order band origins can be difficult because of interactions between the discrete superexcited level and autoionization or other continua. Nevertheless one uses the information so obtained to classify Rydberg series and establish quantum defects. The study of line and band profiles enables one, in principle, to explore interaction phenomena, including interferences between direct ionization and superexcited state decay.

2. Ion yield spectroscopy

Studies, as a function of incident photons, of the yield of parent and of fragment ions enable one to observe some autoionizing superexcited states and to follow the relative total cross sections for autoionization to stable, dissociative or predissociating ionic states. Monochromatized synchrotron and other continuum sources are used in such studies.

3. Threshold photoelectron spectroscopy and coincidence studies

In threshold photoelectron spectroscopy a variable photon energy source is used but only zero kinetic energy photoelectrons are detected. The states detected therefore have the same energy as that of the absorbed photon. Threshold photoelectron spectroscopy can thus provide information on both direct ionization and autoionization processes. Comparison with conventional photoelectron spectra enables one to separate the threshold photoelectron signal into its direct ionization and autoionization components. Studies can be made of coincidences between threshold photoelectrons and the products of superexcited state autoionization channels such as parent ions, fragment ions, fluorescence of excited ions, etc ...

Further useful information can be had from the photoelectron

energy distribution at specific excitation energies.

4. Fluorescence excitation spectra of neutral or ionic dissociation products

Fluorescence excitation spectroscopy can provide information on dissociative and predissociative channels of superexcited state relaxation when one or more of the dissociation products is in an excited state of non negligible quantum yield.

DECAY OF IONIC STATES

Ionic states formed can decay via three principal processes : 1) fluorescence ; 2) radiationless transition to bound states ; 3) radiationless transition to dissociation continua. In addition, collisions can modify these intramolecular processes and give rise to new, reactive, channels. We will be concerned only with intramolecular processes.

The theory of radiationless transitions, involving the coupling of two or more electronic states, and vibrational redistribution, has been extensively developed over the past few years, but the models and applications relate mainly to neutral species. Relatively little has been done to study these processes in molecular ions, although such transitions have often been invoked, in particular to account for ionic fragmentation. Advantages of molecular ions as objects for the study of radiationless transitions will be discussed.

A brief account will be given of the theoretical models used in 4 cases of radiationless transitions : 1) the resonance limit ; 2) the intermediate case ; 3) the statistical limit ; 4) predissociation. Chief among the experimental parameters to be determined are ion fluorescence quantum yields and lifetimes and ion fragmentation product yields. These are studied as a function of internal energy of the molecular ions. The experimental techniques used to study these processes include measurement of the following :

- Photoion-fluorescence photon coincidences ;
- Photoelectron-fluorescence photon coincidences ;

- Threshold photoelectron-fluorescence photon coindicences ;
- Photoelectron-photoion coincidences ;
- Threshold photoelectron-photoion coincidences ;
- Laser induced fluorescence excitation spectra ;
- Optical emission and lifetimes of electron beam excited species in supersonic jets ;
- Photoelectron energy distribution.

APPLICATIONS

Experimental results on superexcited and ionic state relaxation processes will be discussed for a number of polyatomic species, within the context of the above presentation. These species include carbon dioxide, sulfur dioxide, ammonia, monochloroacetylene, benzene, sym-trifluorobenzene and hexafluorobenzene. Some future directions in this general area will be considered.

General references

1) *R.S. Berry and S. Leach, Adv. Electron. Electron Phys. 57, 137 (1980)*

2) *J. Berkowitz, Photoabsorption, Photoionization and Photoelectron Spectroscopy, Academic Press, N.Y. (1979)*

3) *Molecular Ion Studies ; A special issue of the Journal de Chimie Physique (ed. S. Leach), J. Chim. Phys. 77, 587-777 (1980)*

4) *Vacuum Ultraviolet Radiation Physics Sixth Conference : Invited papers. Appl. Phys. 19, 3881-4122 (1980)*

5) *M.B. Robin, Higher Excited States of Polyatomic Molecules, Vol. I and II, Academic Press N.Y. (1975)*

THEORETICAL CORRELATIONS OF ORGANIC PHOTOCHEMICAL REACTIONS IN THE FAR UV

Angelo R. Rossi

Department of Chemistry
The University of Connecticut
Storrs, Connecticut 06268

ABSTRACT

A general overview of calculations on molecules excited in the Far UV will be presented. Two specific examples will be discussed in detail:

A. Calculations on 1,4-Cyclohexadiene (1)

In this case the emphasis will be on pointing out the contrasting photochemistry of this molecule in both the Near and Far UV regimes from a theoretical point of view. Interestingly, the molecule (1) undergoes new reactions in the Far UV but does not give specific porducts which might be expected from lower energy excitations. The implications of these results will be presented from a theoretical point of view.

B. Theoretical Calculations of the Excited States of Methylenecyclopropane (MCP) and an Implicated Trimethylene Methane (TMM) Intermediate

The thermochemical reactivity of MCP is a problem of longstanding chemical interest. What happens to this molecule when it is excited with high energy photons? The second part of this talk will deal with excited states of both MCP and TMM from a qualitative point of view. These ideas lead to implications of photochemically important excited states in TMM which have not been looked at until now. An attempt will be made to correlate the excited state reactivity of MCP with an involved TMM intermediate.

Photochemistry of saturated alcohols and open-chain ethers at 185 nm in the liquid phase

Clemens von Sonntag

Max-Planck-Institut für Strahlenchemie, Stiftstr. 34-36,
D-4330 Mülheim a.d. Ruhr, West-Germany

Abstract

The first absorption band of saturated alcohols and ethers has been attributed to an n-Rydberg transition. The 185 nm line of the Hg-low-pressure arc excites these compounds close to the maximum of this band. The two major processes of neat primary and secondary alcohols undergone on excitation are (i) homolytic scission of the O-H bond and (ii) elimination of H_2 whereby the corresponding carbonyl compound is formed. Neat tert-butanol does not homolytically cleave the O-H bond but C-C bond cleavage (homolytical and molecular) are the major modes of reaction. Only in alkane solutions homolytic O-H bond cleavage becomes the predominant process. There C-C bond scission is suppressed.

In ethers C-O bond cleavage (homolytical and molecular) clearly predominates whereby the smaller alkyl fragment is released in preference. The question why ethers readily cleave the C-O bond but alcohols do not is discussed in the light of theoretical calculations. The strong effects that solvents can exert in these systems will be demonstrated by some selected examples.

Circular Dichroism and Magnetic Circular Dichrosim Studied In the Vacuum Ultraviolet

A. GEDANKEN

Chemistry Department, Bar-Ilan University

Ramat-Gan, Israel 52100

Circular Dichroism (CD) and Magnetic Circular Dichroism (MCD) measurements were carried out in the VUV over the range of 2000-1350 Å. The experimental set-up which has been described elsewhere includes a biotite reflecting element as a linear polarizer. This enables us to extend the lower wavelength limit beyond the 1450 Å obtained with a MgF_2 Wollaston prism. The chromophores studied in our CD measurements were an olefin, ethylene oxide and ethylene sulfide. The optically active olefin studied was (R)-3-methylcyclopentene. This molecule was chosen because it is small enough so that ab-initio SCF calculations could be carried out on it. This is advantageous since all the previous quantum mechanical calculations of the rotational strength of chiral olefins were performed on a model twisted ethylene. The assignment of the measured spectra, based on the results of the calculations, shows that the first three observed bands can be identified with $\pi\rightarrow\pi^*$ and $\pi\rightarrow$ Rydberg type excitations of the olefin chromophore and $\sigma\rightarrow$R transitions of the skeletal frame. The first band is probably a combination of $\pi\rightarrow$R and $\sigma\rightarrow$R transitions.

.../2

The ethylene oxide chromophore was studied via CD measurements of (-) (S,S) - 2,3 - dimethyloxirane and (-) - S - 2 - methyloxirane. The first three observed bands in these molecules were assigned on the basis of ab-initio SCF calculations as n→Rydberg transitions. Similar results were obtained for (+) (R,R)-2,3 dimethyl thiirane which was the optically active compound containing the ethylene sulfide chromophore.

MCD measurements were carried out on DABCO (1,4 diazabicyclo 2,2,2 octane) in the gas phase. The characterization of the n→3p Rydberg transition is discussed in length in the literature and two different assignments were proposed. The observation of derivative line-shape A-term signal for all the vibrational bands belonging to this transition provides an unambiguous assignment of this state as a degenerate $^1E'$ state. We have also observed a regular line-shape band (B-term) at 430 cm^{-1} to the red side of the origin which does not have a corresponding transition in the absorption. We assign it as a A_2'' state (n→3pz transition) on the basis of group theory arguments.

PERTURBATION SPECTROSCOPY

John D. Scott
Department of Chemistry
University of Montana
Missoula, MT 59812

I. INTRODUCTION; DEFINITIONS AND MODELS

Perturbation Spectroscopy will be defined as the absorption spectroscopy of samples which are exposed to an externally applied perturbation. The experiments to be discussed are (1) Magnetic Circular Dichroism (MCD), (2) Electric Linear Dichroism (ELD) and Electrochromism and (3) Pressure-Effect Spectroscopy.

Two problems which arise when interpreting perturbation effects on spectra are:

- The deducing of observables from theories of micrscopic structure; i.e., determination of a model idealy structured to make certain molecular parameters (properties) addressable by experiment.
- The mode of spectral analysis to enable practical realization of these quantities.

The model may be more or less well structured; those for MCD and electric-field effects are very clear, that for pressure-effect studies is less clear, a result of the complex nature of the perturbation.

The following presentation is the generalization of a model for the analysis of perturbation-induced spectral effects. The philosophy underlying this approach is based on assumption of two effects produced by the perturbation;

- An energy shift of absorption; the absorption band retains its shape, but it is dispersed according to a distribution of the ground-state molecules in the perturbing field.

- A change in intensity caused by (a) a change in absorber-coordinate distribution and (b) a change in the transition probability caused by a perturbation of the absorber wavefunction.

Measurable quantities include the magnitude and, possibly, coordination distribution of the perturbation, $A^P(\tilde{\nu})$ and $A^0(\tilde{\nu})$, which are the absorption spectra with and without perturbation applied and/or $A_1(\tilde{\nu})$ and $A_2(\tilde{\nu})$, which are the absorption spectra with the same perturbation applied but with two different polarizations of the excitation radiation. Two coordinate systems must be considered. The energy shift, $D(\underline{Q})$, of the transition is a function of the absorber/perturber coordinate, $\underline{Q}$; $D(\underline{Q})$ must be realized in terms of $\Omega(\underline{Q})$, the molecular distribution in $\underline{Q}$. The excitation mechanism is a function of the laboratory frame-of-reference coordinate, $\underline{q}$; the absorber distribution in $\underline{q}$ is $\omega(\underline{q})$. For the magnetic and electric perturbations $\{\underline{Q}\}$ and $\{\underline{q}\}$ are identical sets because the perturbation is fixed in the laboratory frame, for pressure-effect studies $\underline{Q}$ and $\underline{q}$ are independent. One more important quantity is the absorption probability. This can be considered and expressed relative to the zero-perturbation probability and will be given as a product of two functions, $\Gamma(\underline{Q})$ and $\gamma(\underline{q})$. $\gamma(\underline{q})$ arises from an orientation effect different from that at zero perturbation and $\Gamma(\underline{Q})$ arises because of wavefunction perturbation.

Formulation of these effects involves expression of $A^P(\tilde{\nu})$ as a Taylor-series expansion in $A^0(\tilde{\nu})$;

$$A^P(\tilde{\nu}) = \tilde{\nu} \sum_{i=0} a_i \, d^i[A^0(\tilde{\nu})/\tilde{\nu}]/d\tilde{\nu}^i \qquad (1)$$

where the a_i's are parametrically dependent on the perturbation, temperature and radiation polarization and are expressed as

$$a_i = \frac{(-1)^i/i! \int_{\underline{q}} \int_{\underline{Q}} \Omega(\underline{Q})\, \omega(\underline{q})\, D^i(\underline{Q})\, \Gamma(\underline{Q})\, \gamma(\underline{q})\, dv_q\, dv_q}{\int_{\underline{q}} \int_{\underline{Q}} \Omega(\underline{Q})\, \omega(\underline{q})\, dv_q\, dv_Q} \qquad (2)$$

The terms in the integrands depend on the particular experiment and are determined from theory. The experimental $A^P(\tilde{\nu})$ is analyzed in terms of $A^0(\tilde{\nu})$ and a set of experimental expansion coefficients is found; these are equated with respective theoretical a_i's and determination of certain molecular properties is made. How well theory is contacted is determined by knowledge of the theoretic forms of the a_i's.

In actual practice the perturbed spectrum is often measured as a difference spectrum, $\Delta A(\tilde{\nu})$, which also can be expressed as an expansion.

$$\Delta A(\tilde{\nu}) = \tilde{\nu} \sum_{i=0} c_i\, d^i[A^0(\tilde{\nu})/\tilde{\nu}]/d\tilde{\nu}^i \ . \qquad (3)$$

For a chromic effect

$$\Delta A(\tilde{\nu}) \equiv A^P(\tilde{\nu}) - A^0(\tilde{\nu}) \qquad (4)$$

and for a dichroic effect

$$\Delta A(\tilde{\nu}) \equiv A_1^P(\tilde{\nu}) - A_2^P(\tilde{\nu}) \ . \qquad (5)$$

The derivations of the c_i's in Eq.(3) from the a_i's in Eq.(1) should be obvious for both definitions of $\Delta A(\tilde{\nu})$.

The following three sections are discussions of the specific perturbations.

A. Magnetic Circular Dichroism: MCD is circular dichroism induced by a magnetic field, $\underline{H}$, applied parallel to the radiation-propagation vector. In applying Eq.(5), polarization "1" is taken to be left-circular polarization and "2", right-circular polarization. Stephens[1] has written a comprehensive

review of MCD. Application of MCD to the study of Rydberg transitions[2] is relatively recent; the wealth of information available from such studies certainly warrants further investigations, both experimental and theoretical. The technical aspects of MCD measurement in the VUV are recorded in the literature.[3]

It is observed that for modest field strengths ($H<5T$, $H\equiv|\underline{H}|$) the intensity of $\Delta A(\tilde{\nu})$ is linear in H and the expansion need be carried through only the first derivative if the molecule is C_{3v}, D_{3h}, D_{2d} or higher symmetry; if lower, then only C_0 is non-zero. The molecules in this presentation have closed-shell ground states and, in addition, rotational magnetic moment contribution is neglected; thus, the coefficients are

$$c_0 = bH \tag{6}$$

where b results from field-induced intensity (the integrated effect of $\Gamma(\underline{Q})$) and

$$c_1 = \underline{\mu}_H \cdot \underline{m}_k \, H/|\underline{m}_k| \tag{7}$$

where $\underline{\mu}_H$ is the electronic magnetic moment of the excited state created by absorbance of right ($\underline{m}_k = \hbar\underline{e}_3$) or left ($\underline{m}_k = -\hbar\underline{e}_3$) circularly polarized radiation and $\underline{e}_3$ is a unit vector in the molecular figure axis. It should be noted that this simple form is applicable only over spectral regions corresponding to transitions for which there is no mixing of electronic states and for which the vibrational and rotational parts are Franck-Condon allowed or are made allowed by the same coupling mechanisms. The reason for presenting c_1 as above will become apparent.

B. Electric-Field-Effect Spectroscopy: This study can be made as either a "chromic" (electrochromism) or a "linear-dichroic" (ELD) investigation. The underlying principle is that of the electro-optical Kerr effect.[4] The theoretical form[5] of $A^P(\tilde{\nu})$ has been known for ca. twenty years and application to Rydberg states was first reported in the middle of the last decade.[6] Technical aspects of spectral measurements in the VUV are summarized in the literature.[3]

An electric field, $\underline{E}$, is applied perpendicular to the propagation vector of a beam of monochromatic radiation, plane polarized at angle β with respect to $\underline{E}$. For modest field strengths ($E \equiv |\underline{E}| < 100$ kV/cm) $\Delta A(\tilde{\nu})$ is simple quadratic in E and expansion through the second derivative is sufficient. For electrochromism the coefficients are

$$c_i = \ln(10)\,[c_i' - (1-3\cos^2\beta)c_i'']\,E^2 \qquad (8)$$

where c_i' and c_i'' are given in terms of molecular parameters in Table I. For ELD, the coefficients are

$$c_i = \ln(10)\,3(\cos^2\beta_1 - \cos^2\beta_2)\,c_i''\,E^2 \qquad (9)$$

The techniques employed in actual measurement are discussed in the literature. The values given in Table I are for molecules with principal symmetry axes (i.e., C_{2v} or higher symmetry) and the symbols (//) and ($\perp$) signify transition-moment orientation parallel and perpindicular to the figure axis respectively.

The current status of electric-field-effect spectroscopy is that permanent-electric-dipole-moment changes and excited-state electronic symmetries have been determined for Rydberg states. Soon, it is hoped that temperature-dependance studies will make accurate determinations of other properties possible.

TABLE I

ANALYTIC EXPRESSIONS FOR c_i' AND $c_i''^2$

i	c_i'	$c_i''(//)$	$c_i''(\perp)$
0	$\frac{1}{3}[\frac{R^{(1)}\mu_e}{kT} + S^{(1)}]$	$\frac{1}{30}[\frac{2\mu_e^2}{k^2T^2} + \frac{3(\alpha_{ii} - \bar{\alpha})}{kT} - 2(\frac{R^{(1)}\mu_e}{kT} - S^{(1)}) + 3(\frac{R^{(2)}\mu_e}{kT} - S^{(2)})]$	$c_1''(//) - \frac{\mu_e^2}{10k^2T^2}$
1	$\frac{1}{hc}[\frac{\mu_e\Delta\mu_e}{3kT} + \frac{\Delta\bar{\alpha}}{2} + \frac{R^{(1)}\Delta\mu_e}{3}]$	$\frac{1}{15hc}[\frac{2\mu_e\Delta\mu_e}{kT} + \frac{3}{2}(\Delta\alpha_{ii} - \Delta\bar{\alpha}) + \frac{1}{2}(2R^{(1)} - 3R^{(2)})\Delta\mu_e]$	$c_2''(//) - \frac{\mu_e\Delta\mu_e}{5kThc}$
2	$\frac{(\Delta\mu_e)^2}{6h^2c^2}$	$\frac{(\Delta\mu_e)^2}{15h^2c^2}$	$-\frac{(\Delta\mu_e)^2}{30h^2c^2}$

$\underset{\sim}{\mu}_e$ and $\underset{\sim}{\mu}_e'$ are ground- and excited-state permanent dipole moments, respectively; $\mu_e = |\underset{\sim}{\mu}_e|$; $\Delta\mu_e \equiv (\underset{\sim}{\mu}_e' - \underset{\sim}{\mu}_e)\cdot\underset{\sim}{\mu}_e / |\underset{\sim}{\mu}_e|$; $\bar{\alpha}$ and $\bar{\alpha}'$ are ground- and excited-state mean electric polatizabilities, respectively; $\Delta\bar{\alpha} = \bar{\alpha}' - \bar{\alpha}$; α_{ii} and α_{ii}' are elements of the ground- and excited-state polarizability tensors, respectively, i being the Cartesian, molecule-fixed axis in which the transition moment lies; $\Delta\alpha_{ii} = \alpha_{ii}' - \alpha_{ii}$; $\underset{\sim}{R}^{(1)}$ and $\underset{\sim}{R}^{(2)}$ are vectors which originate in a 1st order treatment of intensities*; $S^{(1)}$ and $S^{(2)}$ are scalars which arise from a 2nd order treatment of intensities*; $R^{(1)} \equiv \underset{\sim}{R}^{(1)}\cdot\underset{\sim}{\mu}_e / |\underset{\sim}{\mu}_e|$; $R^{(2)} \equiv \underset{\sim}{R}^{(2)}\cdot\underset{\sim}{\mu}_e / |\underset{\sim}{\mu}_e|$.

*See reference 5 for derivations and analytical forms of $S^{(1)}$, $S^{(2)}$, $\underset{\sim}{R}^{(1)}$ and $\underset{\sim}{R}^{(2)}$.

C. Pressure-Effect Spectroscopy: This chromic effect can be studied by measuring the absorption spectrum of a gas sample, the "absorber," in the presence of a non-absorbing "perturber" gas. Analysis of $A^P(\tilde{\nu})$ in the context of Eq.(1) will produce the various coefficients, a_i. A theoretic context must be available to analyze the coefficients for the purpose of obtaining particular molecular properties. However, the interaction mechanisms for this perturbation are not as simple as for the external fields discussed in the previous two sections and the choice of a theoretical model is not as clearly defined. The following discussion presents a model we are currently developing for utilization in this study.

First, the several approximations and assumptions are listed:

- The approximation is made that the chromic effect results from an energy shift only. No wavefunction perturbation is considered (i.e., $\Gamma(Q) = 1$).
- Only single absorber/perturber-pair interactions are considered.
- The only absorber/perturber coordinate considered is the intermolecular separation, r (i.e., $Q = r$).
- The interaction potentials for the ground (unprimed system) and excited (primed system) absorber states are of the van der Waals type;

$$U(r) = 2D_e(-r_e^6/r^6 + r_e^{12}/2r^{12})$$

and (10)

$$U'(r) = 2D'_e(-r_e'^6/r^6 + r_e'^{12}/2r^{12})$$

where D_e and D'_e are the respective potential-well depths and r_e and r'_e, the positions of potential minimum.

- Each perturber molecule is assigned the ideal-gas volume

$$v = kT/P \qquad (11)$$

(k=Boltzmann constant, T=absolute temperature and P=pressure). It is assumed that each volume is a sphere of radius

$$R = (3kT/4\pi P)^{1/3} \tag{12}$$

and R is the upper integration limit.

- A Boltzmann distribution of the ground-state absorber/perturber orientation is assumed. Also, a continuum energy distribution for both ground and excited states is assumed.

The energy shift, D(r), is

$$D(r) = U'(r) - U(r) \ . \tag{13}$$

By defining

$$D_p^n \equiv \int_0^R D^n(r)\ \exp[-U(r)/kT]\ r^2\ dr \ / \int_0^R \exp[-U(r)/kT]\ r^2\ dr \tag{14}$$

the coefficients, a_i, of Eq.(1) can be written

$$a_i = (-1)^i D_p^i/i! \tag{15}$$

The dependence of the a_j's on the perturbation (pressure), the interaction parameters (D_e, D_e', r_e and r_e') and temperature is apparent. The first three D_p^i's are

$$D_p^0 = 1 \ , \tag{16}$$

$$D_p^1 = \{2[D_e - D_e' r_e'^6/r_e^6]\ F_{-1}(b,r_e/R) - [D_e - D_e' r_e'^{12}/r_e^{12}]\ F_1(b,r_e/R)\}/F_{-3}(b,r_e/R) \tag{17}$$

and

$$D_p^2 = \{4[D_e - D_e' r_e'^6/r_e^6]^2\ F_1(b,r_e/R) - 4[D_e - D_e' r_e'^6/r_e^6][D_e - D_e' r_e'^{12}/r_e^{12}]\ F_3(b,r_e/R) + [D_e - D_e' r_e'^{12}/r_e^{12}]^2\ F_5(b,r_e/R)\}/F_{-3}(b,r_e/R) \tag{18}$$

where

$$b \equiv D_e/kT \tag{19}$$

and

$$F_n(b,r_e/R) \equiv \int_{(r_e/R)}^{\infty} 6 \exp[-b(x-1)^2]\, x^{n/2}\, dx \tag{20}$$

We propose to analyze the experimentally determined coefficients in terms of Eq.'s (15)-(18) to obtain the molecular properties, excited- and ground-state D_e and r_e.

The possibility of problems arising because of the various approximations and assumptions must be considered.

- If analysis gives a value of $a_0 \neq 1$ then the neglect of wavefunction perturbation will be known to be invalid. It is expected that this effect on a_0 would be the largest effect of this aspect of the perturbation; therefore, the inadequacy of this approximation can be measured through knowledge of a_0.
- The appearance of satellite bands would imply break-down of the continuum-distribution assumption and/or the fact that the set of zero-order absorber wavefunctions does not form a basis for representation of the absorber/perturber pair.
- Divergence from expected values of coefficients with increasing pressure would indicate inadequacy of the spherical model and/or the need to consider interactions of higher order than pair-wise.

These are areas that may have to be dealt with, especially for higher Rydberg states and at higher pressures.

The study of pressure effect on band shape is, of course, not new. A classic work in the area by Margenau and Watson[7] appeared in the literature

in 1936. This paper included a discussion of low-energy shifts of higher Rydbergs in the alkali metals. Robin and Kuebler[8] published a paper in 1970 dealing specifically with pressure effects on Rydberg transitions. Other models have appeared; viz., an harmonic potential[9] and a Morse potential.[10] Our approach is unique in that we are attempting to analyze experimental data along the lines common to other chromic measurements. It is felt that this form of analysis will be more sensitive than determining changes in intensity maxima, band widths and energies of band maximum since it involves all points within the band as opposed to only a few.

II. PERTURBATION THEORY AND MCD SPECTROSCOPY

Since the phenomena underlying MCD spectroscopy are most easily understood and explained in term of angular momentum that is a constant of motion we choose first-order perturbation approaches that utilize expansions in a linear-molecule basis. Consider the linear molecules A-C and A-B-C, which belong to the $C_{\infty v}$ point group ($D_{\infty h}$, if A = C), with nuclei fixed in the Z axis. For an n-electron molecule the electron positions can be given in cylindrical coordinates ρ_j, z_j and ϕ_j (j = 1,..., n). By defining $\phi_{j'} \equiv \phi_j - \phi_1$ the potential energy can be made independent of ϕ_1. The result is a (non-relativistic) wavefunction

$$\psi_{e+} = F(\rho_j, z_j, \phi'_j: j = 1,..., n)e^{i\Lambda\phi} \quad (21)$$

and

$$\psi_{e-} = \psi_{e+}^*$$

for states with $\Lambda \neq 0$. The conserved orbital angular momenta, $\underset{\sim}{\Lambda}$, for ψ_{e+} and ψ_{e-} respectively are

$$\underline{\Lambda}_+ = \Lambda\hbar\underline{e}_3$$

and (22)

$$\underline{\Lambda}_- = -\Lambda\hbar\underline{e}_3$$

where $\underline{e}_3$ is a unit vector in the Z axis.

For this discussion the importance lies in the ϕ_1-dependent element of the wavefunction;

$$\Phi_{\pm}(\phi_1) = e^{\pm i\Lambda\phi_1} \tag{23}$$

It is in this function that the angular-momentum information resides and it is this function that determines how a particular perturbation Hamiltonian operator manifests itself. Several perturbation operators are considered and the results expected for MCD spectroscopy are presented. The models are more heuristic than computational, as presented; however, they are very useful when interpreting MCD data.

A. Molecules of symmetry lower than $C_{\infty v}$ or $D_{\infty h}$:

The important effect of lowering the molecular symmetry is to introduce potential energy dependence on ϕ_1 and thus destroy the quantization of axial angular momentum. In our perturbation format this is accomplished by mixing states of different Λ.

As an example of this technique consider a C_{mv} or D_{mh} (m = finite interger) molecule as a perturbed linear molecule. The approximate perturbation Hamiltonian we use is

$$\hat{H}'_m = \sum_{j=0}^{\infty} \sum_{k=1}^{n} a_j(\rho_k, z_k)\cos jm\phi_k$$

$$= \tfrac{1}{2} \sum_{j=0}^{\infty} \sum_{k=1}^{n} a_j(\rho_k, z_k)[e^{ijm\phi_k'} e^{ijm\phi_1} + e^{-ijm\phi k'} e^{-ijm\phi_1}]$$

$$= \sum_{j=0}^{\infty} [v_j e^{ijm\phi_1} + v_j^* e^{-ijm\phi_1}] \qquad (24)$$

where $v_j = v_j(\rho_k, z_k, \phi'_k: k = 1,\ldots, n)$. While the v_j terms determine the magnitude of the perturbation effect, the primary symmetry constraints reside in the $\exp(\pm ijm\phi_1)$ terms. These effects will manifest themselves by

- changing the energy bary center of the states
- lifting the degeneracy of some states for which $\Lambda \neq 0$
- mixing the states having different Λ.

The bary-center change, V_0, is

$$V_0 = \int \psi^* v_0 \psi d\tau \qquad (25)$$

As there is no experimental quantity from which to derive an empirical V_0 we will not dwell on this term. The second and third effects can be addressed experimentally and are discussed in the following sections.

1. First-order energy correction: Application of first-order degenerate perturbation theory to the degenerate pairs of zero-order states is standard. Solution of the 2x2 secular determinant

$$\begin{vmatrix} H_{++}-E' & H_{+-} \\ H_{-+} & H_{--}-E' \end{vmatrix} = 0 \qquad (26)$$

for states where $\Lambda \neq 0$ gives E'. The matrix elements are

$$H_{++} = \int \psi_{e+}^{*}\hat{H}'\psi_{e+}d\tau = V_0$$

$$H_{--} = V_0$$

$$H_{+-} = \int \psi_{e-}^{*}\hat{H}'\psi_{e+}d\tau$$

$$= \sum_{j=0}^{\infty} \int F^2 v_j \, e^{2i\Lambda\phi_l} e^{-ijm\phi_l} d\tau \qquad (27)$$

$$= \sum_{j=0}^{\infty} V_j \int \exp[i(2\Lambda - jm)\phi_l] d\phi_l$$

and

$$H_{-+} = H_{+-}$$

It can be seen that when $2\Lambda/m$ is an integer there will be symmetry-forced degeneracy lifting, otherwise $H_{+-} = 0$. The energy correction, through first order, and the corresponding proper zero-order wavefunctions are

$$E_S' = V_0 + V_\ell, \; \psi_S = (2)^{-1/2}[\psi_{e+} + \psi_{e-}]$$

and (28)

$$E_a' = V_0 - V_\ell, \; \psi_a = (2)^{-1/2}[\psi_{e+} - \psi_{e-}]$$

when $\ell(=2\Lambda/m)$ is an integer. Otherwise the degeneracy is not lifted and the wavefunctions remain ψ_{e+} and ψ_{e-}. This is, of course, exactly the result recorded in tables giving resolution of linear-molecule species into those of lower-symmetry molecules.[11]

2. First-order wavefunction correction: While MCD will yield information regarding degeneracy lifting ($C_1 \neq 0$), it will also give information regarding states that remain degenerate. We investigate the symmetry properties of integrands containing two different state functions. Consider

a "parent" state $\underline{1}$ which mixes with a "contaminant" state $\underline{2}$ via the perturbation $\hat{H}'$. The wavefunction expanded in the linear-molecule bases set is

$$\psi = \psi_1^0 + c_2^1\psi_2^0 + \ldots \tag{29}$$

where

$$c_2^1 = \frac{\int \psi_2^{0*}\hat{H}'\psi_1^0 d\tau}{E_1^0 - E_2^0} \tag{30}$$

$$= \{\sum_{j=0} [\int F_2^{0*}\nu_j F_1^0 d\tau_A \int e^{\mp i\Lambda_2\phi_1} e^{ijm\phi_1} e^{i\Lambda_1\phi_1} d\phi_1$$

$$+ \int F_2^{0*}\nu_j^* F_1^0 d\tau_A \int e^{\mp i\Lambda_2\phi_1} e^{-ijm\phi_1} e^{i\Lambda_1\phi_1} d\phi_1]\}/(E_1^0 - E_2^0)$$

($d\tau_A$ is the differential volume element excluding $d\phi_1$)

The coefficient, C_2^1 is non-zero only when at least one of the following conditions is satisfied:

$$\begin{aligned} &\text{condition 1} \quad \Lambda_1 + \Lambda_2 = jm \\ &\text{condition 2} \quad \Lambda_1 - \Lambda_2 = \pm jm \end{aligned} \tag{31}$$

where j can be any integer. For condition 1, states 2 and 1 combine such that $\underset{\sim}{\Lambda}_2$ and $\underset{\sim}{\Lambda}_1$ are antiparallel. For condition 2, $\underset{\sim}{\Lambda}_2$ and $\underset{\sim}{\Lambda}_1$ are parallel. In interpreting MCD spectra this alignment feature will be shown to be important.

Tables II and III present summaries of the effects of $\hat{H}_3'$ and $\hat{H}_6'$ perturbations in "creating" C_{3v} (or D_{3h}) and C_{6v} (or D_{6h}) molecules.

B. Vibronic Coupling: The coupling of vibrational and electronic motions can be treated by first-order degenerate perturbation theory to yield results that are easily interpreted from MCD spectra. We present this for linear triatonics first (Renner-Teller effect) followed by non-linear polyatonics (addition of Jahn-Teller effects).

TABLE II

EFFECT OF THE PERTURBATION ASSOCIATED WITH m=3

PARENT Λ	CONTAMINANT STATE $\Lambda^{\dagger}$			SYMMETRY SPECIES IN C_{3v}
	k=0	k=1	k=2	
1	1	(-)2,4	(-)5,7	E
2	2	(-)1,5	(-)4,8	E
3††	3	0,6	(-)3,9	$A_1(\psi_s), A_2(\psi_a)$
4	4	1,7	(-)2,10	E
5	5	2,8	(-)1,11	E
6††	6	3.9	0,12	$A_1(\psi_s), A_2(\psi_a)$

†The sign indicates the relative directions of the vector $\underset{\sim}{\Lambda}$ in the mixing and parent states.

††Levels for which degeneracy is removed.

TABLE III

EFFECT OF THE PERTURBATION ASSOCIATED WITH m=6

PARENT Λ	CONTAMINANT STATE Λ†			SYMMETRY SPECIES IN C_{6v}
	k=0	k=1	k=2	
1	1	(-)5,7	(-)11,13	E_1
2	2	(-)4,8	(-)10,14	E_2
3††	3	(-)3,9	(-)9,15	$B_1(\psi_s), B_2(\psi_a)$
4	4	(-)2,10	(-)8,16	E_2
5	5	(-)1,11	(-)7,17	E_1
6††	6	0,12	(-)6,18	$A_1(\psi_s), A_1(\psi_a)$
7	7	1,13	(-)5,19	E_1

†,††See footnotes for Table II.

1. Linear Molecules: Of the four normal vibrational modes of a $C_{\infty v}$ triatomic molecule two are totally symmetric (Σ^+) and the remaining two transform as π. For a $D_{\infty h}$ triatomic the symmetry species are Σ_g^+, Σ_u^+ and π_u. A transition from a ground electronic state, having no π vibration excited, to an excited electronic state to which singly excited π vibration is coupled is nominally forbidden by the Franck-Condon principle. The occurrence of such a transition must involve vibronic interaction.

The potential energy introduced by the nuclear motions associated with a π vibration is considered here as a static perturbation. The nuclear positions are given in cylindrical coordinates; considering center-of-mass and rotational coordinates as separable and employing two equations of constraint, the potential energy may be expressed in terms of electronic coordinates and two nuclear coordinates, ρ_N and ϕ_N. The form of the perturbation Hamiltonian we use is

$$\hat{H}'_{C\infty v} = \sum_{j=0} \sum_{k=0} a_{jk}(\rho_\ell, z_\ell, \phi'_\ell: \ell = 1,\ldots, n)\, \rho_N^j\, e^{ik\phi_1} e^{-ik\phi_N}$$

$$+ a^*_{jk}(\rho_\ell, z_\ell, \phi'_\ell: \ell = 1,\ldots, n)\, \rho_N^j\, e^{-ik\phi_1} e^{ik\phi_N} \qquad (32)$$

The zero-order wavefunction is

$$\psi^0_{ev} = \psi^0_e \psi^0_v$$

where ψ_e is the electronic wavefunction [see Eq.(21)] and ψ_v is[12]

$$\psi_v = \psi_{v\pm} = f_{n',\ell}(\rho_N)\, e^{\pm i\ell\phi_N} \qquad (33)$$

where n' is the number of excited quanta and

$$\ell = n', n'-2,\ldots, 1 \text{ or } 0 \qquad (34)$$

The function $f_{n',\ell}(\rho_N)$, while numerically important, contains no symmetry restrictions in $C_{\infty v}$ vibronic perturbation and we do not consider it.

When the electronic and vibrational states are each doubly degenerate the wavefunction is

$$\psi_{ev} = \psi_{e\pm}\psi_{v\pm} \tag{35}$$

All four combinations are possible; they are denoted

$$\begin{aligned} \psi_1 &= \psi_{e+}\psi_{v+} \\ \psi_2 &= \psi_{e+}\psi_{v-} \\ \psi_3 &= \psi_{e-}\psi_{v+} \\ \psi_4 &= \psi_{e-}\psi_{v-} \end{aligned} \tag{36}$$

The perturbation energy is found by solving the 4x4 determinant

$$\left| H'_{tu} - \delta_{tu}E' \right| = 0 \tag{37}$$

where

$$H'_{tu} = \int \psi_u^* \hat{H}' \psi_t d\tau \tag{38}$$

The only non-zero off-diagonal elements are H'_{23} and H'_{32} where

$$H'_{23} = H'_{32} \tag{39}$$

These are non-zero only if $\ell = \Lambda$, otherwise second-order perturbation must be employed to account for the degeneracy splitting of states 2 and 3 away from 1 and 4.

Information regarding a property of interest to us, the presence of a non-zero electric-dipole transition moment for a nominally forbidden transition, lies in the perturbation wavefunctions. The perturbation Hamiltonian must mix a Franck-Condon-allowed "contaminant" into a forbidden "parent". *Allowed* from the standpoint of our basis functions means that

$$\begin{aligned} &\Delta\Lambda = 0, \pm 1 \qquad \Sigma^+ \longleftrightarrow \Sigma^- \\ &\Delta\ell = 0 . \end{aligned} \tag{40}$$

Consider a Σ^+, non-vibrationally-excited ground state as an example. The Franck-Condon, electric-dipole-allowed excited state must have

$$\Lambda = 0 \text{ or } 1 \quad (\Sigma^+ \text{ or } \Pi) \tag{41}$$
$$\ell = 0$$

If the parent state, ψ_I, is forbidden and a contaminant state, ψ_{II}, is allowed, that state function may be written

$$\psi = \psi_I + C_{II}\psi_{II} + \ldots \tag{42}$$

where

$$C_{II} = \frac{\int \psi_{II}^* \hat{H}' \psi_I d\tau}{E_I^\circ - E_{II}^\circ} \tag{43}$$

Considering the form of $\hat{H}'$ and zero-order wavefunctions, the possibilities of $C_{II} \neq 0$ (by symmetry), where ψ_{II} is allowed, are listed for a few forbidden transitions in Table IV. It should be noted that in some instances $\underset{\sim}{\Lambda}_I$ and Λ_{II} are parallel and in others, antiparallel.

2. Non-linear polyatomics: We assume that the zero-order functions used in previous sections provide an adequate representation of the electronic states of a C_{mv} (or D_{mh}) molecule. We also assume that the wavefunctions of the doubly degenerate vibrations can be given in form of Eq.(33), the coordinate ϕ_N being defined as

$$\phi_N = \cos^{-1} \frac{\xi_a}{\sqrt{\xi_a^2 + \xi_b^2}} \tag{44}$$

where ξ_a and ξ_b are the normal coordinates of a doubly degenerate vibration.

The vibronic perturbation Hamiltonian for a C_{mv} molecule differs somewhat from that of the linear case;

TABLE IV

VIBRONIC COUPLING IN $C_{\infty v}$

ELECTRONIC STATE		VIBRATIONAL STATE		ALLOWEDNESS[†]		SYMMETRY OF ALLOWED ELECTRONIC CONTAMINANT WHICH IS FRANCK-CONDON ALLOWED[††]
Λ	SYMMETRY SPECIES	ℓ	SYMMETRY SPECIES	ELECTRIC DIPOLE	FRANCK-CONDON	
0	Σ^+	1	π	a	f	Π
1	Π	1	π	a	f	Σ^+
		2	δ	a	f	$(-)\Pi$
2	Δ	1	π	f	f	Π
		2	δ	f	f	Σ^+

[†]The allowedness refers to that of the non-interacting electronic/vibrational state. Symbol a means allowed, f, forbidden.

[††](-) indicates antiparallel orientation of parent and contaminant-state $\underset{\sim}{\Lambda}$.

$$\hat{H}_{C_{mv}} = \sum_{j=1} \sum_{k=1} \sum_{n=0} a_{jkn}\rho^j \cos nm\phi_1 \cos k(\phi_1-\phi_N)$$

$$= \sum_{j=1} \sum_{k=1} a_{jko}\rho^j [e^{ik\phi_1} e^{-ik\phi_N} + e^{-ik\phi_1} e^{ik\phi_N}]$$

$$+ \sum_{j=1} \sum_{k=1} \sum_{n=1} a_{jkn}\rho^j [e^{i(k+nm)\phi_1} e^{-ik\phi_1} + e^{-i(k+nm)\phi_1} e^{ik\phi_N}]$$

$$+ [e^{i(k-nm)\phi_1} e^{-ik\phi_1} + e^{-i(k-nm)\phi_1} e^{ik\phi_N}]$$

The Renner-Teller terms from Eq.(32) are recognizable. The additions are the Jahn-Teller terms which increase the possibilities for inducing allowedness into vibronically forbidden transitions. Table V is a compilation of the intensity-conferring aspects of vibronic coupling in a C_{3v} molecule. Note again the parallel/antiparallel alignments of parent and contaminant $\underset{\sim}{\Lambda}$ vectors.

TABLE V

VIBRONIC COUPLING IN C_{3v}[†]

ELECTRONIC STATE			VIBRATIONAL STATE			ALLOWEDNESS		SYMMETRY OF ALLOWED ELECTRONIC CONTAMINANT WHICH IS FRANCK-CONDON ALLOWED
Λ	SYMMETRY SPECIES $C_{\infty v}$	C_{3v}	ℓ	SYMMETRY SPECIES $C_{\infty v}$	C_{3v}	ELECTRIC DIPOLE	FRANCK-CONDON	$C_{\infty v}$
0	Σ^+	A_1	1	π	e	a	f	Π
1	Π	E	1	π	e	a	f	$\Sigma^+,(-)\Pi$
			2	δ	e	a	f	$\Sigma^+,(-)\Pi$
2	Δ	E	1	π	e	f	f	Σ^+,Π
			2	δ	e	f	f	Σ^+,Π

[†]See footnotes of Table IV.

BIBLIOGRAPHY

[1]P.J. Stephens, Adv. Chem. Phys. 35, 197 (1976).

[2]J.D. Scott, W.S. Felps, G.L. Findley and S.P. McGlynn, J. Chem. Phys. 68, 4678 (1978).

[3]J.D. Scott, W.S. Felps and S.P. McGlynn, Nuc. Instrum. and Meth. 152, 231 (1978).

[4]H. Labhart, Tetrahedron 19, 223 (1963).

[5]W. Liptay, Z. Naturforsch. 20A, 272 (1965).

[6]J.D. Scott and B.R. Russell, J. Chem. Phys. 63, 3243 (1975).

[7]H. Margenau and W.W. Watson, Rev. Mod. Phys. 8, 22 (1936).

[8]M.B. Robin and N.A. Keubler, J. Mol. Spectrosc. 33, 274 (1970).

[9]H.G. Drickamer, C.W. Franck and C.P.S. Lichter, Proc. Nat. Acad. Sci. U.S.A. 69, 933 (1972).

[10]R.C. Tompkins, J. Chem. Phys. 72, 3449 (1980).

[11]G. Herzberg, Molecular Spectra and Molecular Structure (III) Electronic Spectra and Electronic Structure of Polyatomic Molecules (Van Nostrand, Princeton, 1966) p. 576.

[12]L. Pauling and E.B. Wilson, Introduction to Quantum Mechanics (McGraw-Hill, New York, 1935) pp. 105-111.

Valence-Shell and Rydberg Transitions of Larger Molecules

C. Sandorfy and L.S. Lussier

Département de Chimie

Université de Montréal

Montréal, Québec, Canada

H3C 3V1

Abbreviations used: VS valence-shell

UA united atom

Abstract

This review contains a discussion on the definition of Rydberg states, a very brief account of the vacuum UV spectra of organic molecules and a report on a search for the Rydberg states of a transition metal complex.

Introduction

The Rydberg bands of most polyatomic molecules are located in the far ultraviolet, beyond 200 nm. In most cases the lowest Rydberg bands are found between 200 and 120nm, or 50000 and 80000cm^{-1}, or 6 and 10eV. While the spectra of some molecules in this spectral region have been known for a long time, the systematic conquest of this part of the far UV spesctrum started only in the nineteen-forties by W.C. Price and his Coworkers.(1) A large number of far UV spectra have been measured in the last twenty years. Robin (2) summed up the state of the far UV art until 1975. Shorter reviews are also available. (3,4)

It is not intended here to review the field again. Instead an attempt is made to give a succint account of the remaining difficulties and uncertainties.

I. The Rydberg Concept

For atoms the definition of Rydberg states is simple: when in the transition leading to a given state the principal quantum number increases it is called Rydberg. The corresponding band is a member of a Rydberg series and the size of the orbital of the excited electron is large compared to the core.

The Hydrogen Molecule

For simple molecules the correlation diagrams might offer a basis for a definition. Let us take the well known diagram for homo-diatomic molecules as given by Herzberg (5) and consider the hydrogen molecule.

It would be hard to avoid using the LCAO-MO language. Then from the 1s atomic orbitals of the two hydrogen atoms we can build two molecular orbitals. Omitting normalization factors these are $1s_A + 1s_B$ ($\sigma_g 1s$) and $1s_A - 1s_B$ ($\sigma_u 1s$). Between the two levels a transition is possible:

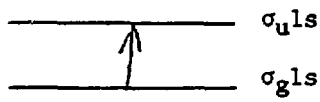

Since both the ground and excited states are built from atomically unexcited AOs this is a valence-shell (VS) transition and the molecular excited state is a VS state. However, the $\sigma_u 1s$ orbital correlates, in the united atom (UA) approximation to the $2p\sigma$ orbital and at the UA limit to 2p while the principal quantum number increased from 1 to 2. Thus if we wish to maintain the definition given for atoms we have to call definition given for atoms we have to call the $\sigma_u 1s$ state Rydberg, at least for short distances. This illustrates well the difficulty inherent in the Rydberg concept. Orbitals and states that are VS at normal molecular distances may become Rydberg at the UA limit or, approximately, at short distances. Mulliken (6) calls this Rydbergisation.

Now, if the above electronic transition was the only one possible for the H_2 molecule, its spectrum would consist of only two bands: a singlet and a triplet. There are many others, however. (see (5), p. 340). So the higher orbitals have to be built from AOs which are atomically excited. These will be truly Rydberg, at any distance. The one of lowest energy is the 2s + 2s ($\sigma_g 2s$) orbital. At short

distances it becomes 2sσ and at the UA limit, 2s. Its energy may be higher or lower than that of 2pσ, depending on the internuclear distance. This immediately raises the question: what comes first, (2s + 2s), a bonding combination but built from higher AO's or (1s - 1s), an antibonding combination but built from lower AO's? The answer is given by the correlation diagram: it depends on geometry for any given molecule. This implies that the lowest excited state might be truly Rydberg, intermediate or of VS type.

Methane

Now we turn our attention to a "simple" polyatomic molecules, methane. Disregarding the carbon 1s ($1a_1$) orbital, the MO of lowest energy is ($2a_1$) or 2s at the UA limit. It has the LCAO form:

$$(2s_C) + \lambda(1s_{H1} + 1s_{H2} + 1s_{H3} + 1s_{H4}) \qquad [1]$$

Next we find two orbitals, $3a_1$ and t_2, which are very close to each other at long C-H distances, but in the actual molecule t_2 is definitely more stable and it is fully occupied in the gorund state while 3a is empty. They become 2p and 3s respectively at the UA limit. Thus, the band of lowest frequency in the UV spectrum corresponds to transtion $3a_1 \leftarrow t_2$. Since both t_2 and a_1 are built from atomically unexcited AO's this can be considered a VS transition. However, since at the UA limit $3a_1$ becomes 3s, this is again a case of Rydbergisation and the orbital is best described as being of an intermediate, Rydberg - VS type. The LCAO function corresponding to

$3a_1$ is

$$(2s_C)-\lambda'(1s_{H_1}+1s_{H_2}+1s_{H_3}+1s_{H_4}) \qquad [2]$$

It has nodes between the carbon and each of the hydrogens, therefore at short distances it resembles the 3s orbital of the UA.

We may, however, construct a MO of the same symmetry by using the positive combination of the carbon $3s_C$ orbital with the $1s_H$:

$$(3s_C)+\lambda''(1s_{H_1}+1s_{H_2}+1s_{H_3}+1s_{H_4}) \qquad [3]$$

Since it is essentially $3s_C$ this MO is truly Rydberg. Having two radial modes, at the UA limit it would also become 3s. This raises a problem which has been the object of much controversy. (See the next section.)

A way out of this difficulty could follow from an argument by Schwarz (7). While the conservation of symmetry is mandatory when UA - separated atoms correlations are considered, the conservation of the number of radial nodes may not be an absolute criterion. Thus in the isoelectronic series HCl, H_2S, PH_3, SiH_4 the lowest empty orbital is VS for HCl but Rydberg for SiH_4 so that the 4s Rydberg orbital of HCl is correlated with the 5s orbital of SiH_4, the UA being Ar for both. Following a procedure inspired by Herzfeld (8) Schwarz shows that when we transform Ar into HCl "...by a repeated transfer of small amounts of positive charge from the heavy nucleus to the point where the proton is located in HCl, ... the molecular potential will change continoustly, as will the orbital functions", but "... the nodes of the orbitals may change in number and topology". So it appears to be possible that for methane [3] correlates not to the 3s of the UA but to 4s. This would

go some way in solving the problem. It implies, that 4s may have a lower energy than 3s. This is, of course strange; however, [3] is an "all-plus" combination, while [2] is antibonding in the C-H bonds. Crossing between the two curves must be avoided, so that mixing will occur.

Ethylene

As a last example we take ethylene but we consider only the π electron orbitals. The problem resembles that of H_2 except that instead two 1s AO's we have two $2p\pi$ AO's. Under D_{2h} symmetry the originating MO is B_{3u} and the empty LUMO is B_{2g}. (With the Z axis taken along the C-C bond and X perpendicular to the molecular plane.) These are, of course, the well known $(2p_{x_1}+2p_{x_2})$and $(2p_{x_1}-2p_{x_2})$ MO's respectively. The $b_{2g}\leftarrow b_{3u}$ transition leads to a VS state. However, b_{2g} "Rydbergizes to a $3d\pi$ UA_AO, so again it is of a mixed Rydberg-VS type. (We have the vertical transition in mind and disregard to fact that ethylene becomes perpendicular in the π^* state.) It is, of course, known as the V←N transition of ethylene.

The lowest Rydberg state of ethylene is, however, not b_{2g} but a_1; it is of the 3s type and the corresponding band is well known. (9 and references therein) While in ethylene itself it is in coincidence with the V←N band, in many derivatives it is clearly detached and is the singlet-singlet band of lowest energy. (10,11) According to Merer and Mulliken (9) this 3s ($4a_g$) orbital is "... the same MO as the first CH antibonding MO". However, the positive combination of the two $3s_C$ AO's also has the required properties; it is truly Rydberg and

might be of lower energy.

It follows from the above that there is a difference between Rydberg orbitals which become Rydberg only at short distances and are built from atomically unexcited AO's on the one hand, and Rydberg orbitals built from atomically excited AO's which are Rydberg at any distance, on the other. It would be probably better to call the former united atom Rydberg, or pre-Rydberg (12), or intermediate type orbitals and reserve the name Rydberg to the latter.

For further informaton on this problem the Reader might consult (6 and 13).

More important than all this is that Rydberg and valence-shell orbitals mix more often than not. This, it is believed, is still not fully realized and has far-going consequences.

It is almost certainly a major cause of the broadening of the spectrum at higher frequencies where the Rydberg bands are numerous. It can also be a reason of increased collision broadening. The sensitivity of Rydberg bands to intermolecular interactions has been stressed by Evans (14) and by Robin (15); this is used as a criterion to distinguish between Rydberg and VS bands. Now, if VS bands have partial Rydberg character this can be a cause of increased sensitivity of these bands to the field of approaching other molecules which in turn may result in increased band width.

Any comparison between observed spectra and the results of quantum chemical calculations may be misleading if no account is taken of the existance of Rydberg states and of Rydberg/VS mixing.

The photochemical consequences of these conditions have only recently begun to be explored. (See the next section)

The Problem of the Negative Combinations of Rydberg AO's

In 1970 Salahub and Sandorfy (16) proposed a quantum chemical treatment in which Rydberg atomic orbitals were included in the base. The results obtained then might appear naive after the spectacular developments due mainly to Buenker, Peyerimhoff (17-20 and many other publications) and their coworkers during the subsequent decade. That method was a semiempirical, Rydberg-CNDO scheme. It yielded many orbitals and many states. Conditions may be illustrated on an exmple which was touched upon by Salahub and Sandorfy. Neopentane, $C(CH_3)_4$ has five carbons. If we are looking for MO's that can be built from, say, 3s AO's we have to form linear combinations from them. Other σ type AO's should also be included but we shall disregard this for simplicity's sake. The five 3s AO's yield five MO's of the type: $c_1 3s_1 + c_2 3s_2 + c_3 3s_3 + c_4 3s_4 + c_5 3s_5$.

So the question is: are all five of these acceptable MO's? Can we build states of them and expect the related bands to appear in the spectrum? This problem has been the subject of some controversy. Let us summerize briefly the various opinions.

Sinanoglu put it the following way (12). In conventional LCAO-MO calculations in which only unexcited AO's are used, one obtains as many MO's as were AO's. This situation might change, however, if some of

the AO-AO overlap integrals approach unity, $S_{ab} \to 1$, or the overlap matrix equals zero. Even the example of H_2 can illustrate this. If the internuclear distance $R=0$, S_{ab} 1; then $(1s_a+1s_b)$ and $1s_a-1s_b)$ are two independent MO's. But if $R \to 0$, $S_{ab} \to 1$ and $(1s_A+1s_B) \to 1s_a=1s_b$, the MO becomes a one center AO, very similar to any of the separate AO's. Furthermore $(1s_a-1s_b) \to 0$. The negative combination disappears at zero internuclear distance!

A way out of the problem may seem to be to look at the normalized form:

$$1\sigma_u = \frac{1}{\sqrt{2(1-S_{ab})}} (1s_a-1s_b) \to \frac{0}{0} \text{ , as } R \to 0$$

and take $2p\sigma_u$ as the limit. As Sinanoglu points out, however, there are objections against this procedure. "Taking the limit is not an operation within the linear vector space on which the AO→MO, LCAO theory is based. $2p\sigma_u$ cannot be expressed by any coefficients at $R \sim 0$ in terms of the original AO's,

One of the two AO's has actually disappeared due to the linear dependence. Needing still two independent orbitals, one has simply invoked from outside of the 2-dimensional linear vector space, a new one, $(2p_u)$." There are other difficulties too. (12) It is not so easy to reach $R=0$ and the UA concept will perhaps be reassessed one day.

The situation is much worse with the large Rydberg orbitals where S_{ab} has values very close to unity, even at molecular distances. So Sinanoglu recommends the elimination of all but the "all-plus" MO for

Rydberg orbitals.

This idea is pleasant to spectroscopists. They normally presume that, if all degeneracy is lifted, there can be one ns, three np and five nd, ... type Rydberg series originating with any given ground state orbital. This is, of course, so for atoms and if the molecule can have no other states than those which can be extrapolated to the UA, the assumption is logical.

Mulliken's argument (6) is slightly different but it comes to the same conclusion. Since at R=0 the function $1\sigma_u$ goes over the $2p\sigma$, at intermediate distances it can be written as the linear combination

As $R\to 0$, $B\to 0$ and $A\to 1$. "If one looks at the limiting form of the normalized (1s-1s) function at R=0, this becomes $1p\sigma$, i.e. $\cos\theta e^{-\alpha r}$ that is unacceptable as an eigenfunction of the Schrödinger equation. In short, it then becomes redundant".

For methane the $3a_1$ orbital becomes 3s at the UA limit so, according to Mulliken, at intermediate C-H distances it is:

$$C_1 3s + C_2(\lambda 2s_C - 1s_a - 1s_b - 1s_c - 1s_d) \qquad [4]$$

In the UA, neon, $C_1=1$ and $C_2=0$. This does not mean that there are two orbitals, a 3s and a $(\lambda 2s_C - 1s_a - 1s_b - 1s_c - 1s_d)$; just as in the case of the $(1s_a - 1s_b)$ orbital of H_2 the second one becomes redundant at the UA limit and should be eliminated. This is the continuity argument.

However, the 3s in [4] is an orbital of the UA. There is no objection against forming an orbital of $3s_C$ and the $1s_H$ which would be the first truly Rydberg orbital:

$$3s_C+\lambda"(1s_{H_1}+1s_{H_2}+1s_{H_3}+1s_{H_4}) \qquad [3]$$

(Our eq. [3].) It is essentially a carbon $3s_C$ orbital, so it would become 3s at the UA limit too, for neon. Do we have to eliminate this too? Certainly not, it is an "all-plus" combination. (The formation of [3] corresponds to forming the (2s+2s) orbital of H_2, except that at the UA limit the latter becomes $2s\sigma$, not $2p\sigma$.) Yet, both [2] and [3] possess two radial nodes and seem to correlate to the UA 3s. In our opinion this shows the weakness of the procedure which is the bases of the construction of correlation diagrams. Both Mullikeu and Sinanoglu appear to be right in suggesting that for Rydberg AO's the negative combinations should be eliminated but when the negative combination is valence-shell and the "all-plus" combination is Rydberg both of them should exist. This should be the case of methane and similar molecules yielding what Robin called "VS/Rydberg Conjugates". Just which one is of lower energy if a matter of calculations. According to Pauzat, Ridard, and Levy (21), in the case of methane the Rydberg orbital has a much lower energy. The frustrating point is that it might never be possible to find both related bands in the spectrum. One of them may be at high frequencies, possibly beyond the ionizaton potential; it could be broad and lost in the background.

For methane [2] and [3] are of the same symmetry and can mix. This is generally so for Rydberg and VS orbitals of close enough

energies. If they are of different symmetry they can still mix vibronically. Thus after eliminating the negative combinations of Rydberg AO's the theoretical treatment of electronic spectra, in the LCAO-MO language, becomes largely a matter of mixing between Rydberg and VS orbitals. In this respect the Reader is referred to a review by Peyerimhoff (13) and numerous papers from the Buenker and Peyerimhoff group.

What introduces ambiguities into the treatment of Rydberg levels is not the molecular orbital approach but the use of LCAO functions and the required reference to the united atom. An interesting attempt to avoid this has been made by Roberge and Salahub (22) who applied the Xα method to the ground and a number of excited states of H_2S. In this method the space around the molecule is divided into a) spherical regions surrounding the atoms, b) an intersphere region, and c) the rest of space which lies outside of sphere surrounding the entire molecule. This suggests a natural definition for Rydberg character of a given orbital as being "the fractional charge for that orbital contained in the outersphere region". (22) This does not depend on the choice of the basis set. The solutions of the Xα equations are obtained by the use of Johnson's scattered wave method (23) in which the radial functions are found independently for each level and are not constructed from a fixed set of basis functions. Roberge and Salahub (22) were able to match the best available configuration intereaction calculations (24) as close as 0.24eV for the 26 lowest excited states of H_2S. Most of the excited states had about 90% Rydberg character;

the lowest two $6a_1 \leftarrow 2b_1$ and $3b_2 \leftarrow 2b_1$, however had Rydberg characters of 83% and 47% respectively meaning that the latter should be considered as VS. No Rydberg/VS conjugates were found.

This method avoids the uncertainties involved with the use of diffuse Rydberg AO's with an LCAO function. Significant advances could be expected if it could be applied to more complex molecules.

II. From Spectra to Photochemistry

After a period of intensive research on π-electron systems and a more recent era of investigations on σ-electron systems and Rydberg transitions, we now have a basic understanding of the spectra of typical organic molecules down to about 125 nm or 80,000 cm^{-1}. Photoelectron spectroscopy (25) and highly computerized quantum chemistry (17-20) have been of indispensable help in achieving this. The field was reviewed several times. Here we are attempting to do this in a nutshell. (For references see (2) (3) or (4)).

Paraffin hydrocarbons are the only organic molecules having only bonding σ electrons. They have relatively high ionization potentials; it decreases from about 13eV to about 10eV from methane to n-decane; a behavior not so different from that of conjugated chains. All the known excited states of n-paraffins are of intermediate type but closer to the Rydberg type. Except for methane they have three close-lying originating orbitals, one of them degenerate in ethane. This is probably a major cause of the broadness of the bands in these spectra;

most of them are almost certainly composite. Ethane is the only member of the series exhibiting vibrational fine structure in its spectrum. The transition leading to the lowest excited state leaves the hole mainly in the C-H bonds. This is likely to be connected with the fact that the photolysis of n-paraffins yields mainly H_2 molecules at low energies. The many intersecting potential surfaces, at least a part of them repulsive makes the diffuse appearance of these spectra understandable.

Cyclopropane and cyclobutane have spectra about midway between σ and π type spectra. Transitions to Rydberg and valence-shell type excited states intermingle among their bands of lowest frequency. The 3s band of cyclopropane has not yet been identified; it may be photochemically important.

Highly branched paraffins have spectra of a different appearence. Contrary to n-paraffins the first band is intense and it is usually followed by a pronounced minimum. These spectra resemble the one of methane while the normal chain paraffins have spectra similar to ethane. The difference is connnected with the simple fact that under tetrahedral symmetry the first transition is allowed while for ethane (D_{3d}) the center of symmetry makes it forbidden. The two types tend to persist in the more complicated molecules; their spectra resemble to that of either methane or ethane. They also exist in the analogous silane derivatives. (26) The lower bands in n-paraffins undergo a regular bathochromic shift with increasing number of carbons; it comes to a halt for C_5 or C_6 at about 160 nm. Highly branched

paraffins absorb about 10 nm to longer waves. Bands due to singlet-triplet transitions have not so far been identified. According to Buenker and Peyerimhoff (27) they must be very close to the corresponding singlets.

The spectra of perfluorocarbons are of the C-C σ type since orbitals associated with either C-F bonds or F lone pairs have high energies (beyond about 15.5eV) due to the high electronic attracting power of fluorine. There is some ambiguity with respect to the Rydberg or valence-shell character of the bands in their spectra. Contrary to hydrocarbons, the bathochromic shift does not come to a halt at C_5 or C_6. These observations are still waiting for an explanation.

Saturated, heteroatomic molecules like halides, alcohols, amines have lone pairs of electrons; actually the orbitals occupied by the lone pairs are the originating orbitals for the photoelectron band of lowest energy and for all the known UV absorption bands. For halides (X=Cl, Br, I) the first excited state is valence-shell, an C-X antibonding state. For alcohols, ethers and amines it of the intermediate, Rydberg-V.S. type. The first 3s and 3p bands are usually well distinguished for these compounds. Alcohols present an interesting case of a largely split 3p manifold due to the non-linearity of the C-O-H unit. Saturated molecules containing two or more hetero atoms have not been as extensively studied as they have been in the π electronic case.

In mono-olefins the (π,π^*) band coincides with or is preceded by the 3s Rydberg band. In ethylene itself the Rydberg band is

superposed on the low frequency wing of the (π,π^*) band while in highly methylated or fluorinated olefins the 3s band becomes the first band and it is well separated from the (π,π^*) band. Like ethane, ethylene has been a test-case for both theory and experiment. Ethylene is coplanar in its ground state, perpendicular in the singlet and triplet (π,π^*) states, and has an angle of 25° between the two CH_2 planes in the 3s Rydberg state. The protracted long wavelength tail of the singlet (π,π^*) band has been the topic of much discussion. McDiarmid (28) has shown that the longest wavelength part of it was due to traces of molecular oxygen but even so the tail is quite long demonstrating the great structural difference between the ground and the excited state. The vibrational intervals correspond to C–C stretching and doubles of torsional frequencies. Molecules alter their geometry after excitation if thereby they can stabilize the energy of the adiabatic excited state and if the potential barrier opposed tc this is not too high.

Butadiene and the series of conjugated polyenes are at present the target of intensive research. One reason for this is the relevance of these studies to the functioning of visual pigments and carotenoids. Butadiene could exist in either cis and trans configuration with C_{2v} and C_{2h} symmetries respectively. Now, as is well known, the selection rules are more liberal for the C_{2v} group which does not contain a center of symmetry, than for C_{2h} which does. For this reason two of the four (π,π^*) bands of trans-butadiene, which is the isomer encoutered in practice, are forbidden by the

Laporte rule. Such bands can be found, however, by two photon spectroscopy in which the selection rules make these g↔g bands allowed. Furthermore the two states can interact by configuration interaction (in a mathematical sense) and this could push one of them, the A_g band to lower frequencies. That an A_g^- could lie at energies lower than the allowed B_u band is an exciting possibility, first put forward by Koutecky in 1967. (29) For the last ten years everal attempts have been made to locate these bands in a number of conjugated polyenes. (30-32) The problem is rendered difficult by the existence of the weak 3s Rydberg bands which are also g↔g. Recently McDiarmid (33) investigated the problem of the A_g bands of butadiene by electron impact spectroscopy and found no such bands at frequencies lower than the B_u bands. As to the higher polyenes Birge et al. (34) found an A_g band for all-trans retinol by two photon spectroscopy. Its maximum is approximately 1600 cm^{-1} from the one-photon absorption maximum, at its long wavelength side.

The chromophore of visual pigments (rhodopsin) is the Schiff base of 11-cis retinal which is covalently linked to the protein opsin on he nitrogen and is placed in the field of polar groups of the aminoacid residues of the protein. The knowledge of the excited state in which the photochemical primary step of vision occurs is, of course, of atmost importance. There is general agreement at present that it is the singlet (π,π^*) state of lowest energy. (35-37) If there was an A_g^- state at frequencies lower than the (π,π^*) state, this would change all our ideas on the mechanism of vision.

This does not appear to be the case, however. Quantum chemical calculations show that the presence of a nitrogen atom in the polyene makes move the A_g band to higher, not lower, frequency and that this is even more so for a protonated Schiff base. (38)

Theoreticians has been greatly concerned with butadiene for the last few years. Among the main problems are the geometrical changes upon excitation and the extent of Rydberg-VS mixing in excited states. (39)

The π electron spectra of benzene and other aromatic compounds are among the most studied ones in molecular spectroscopy. There are, in general, three of four (π,π^*) bands before the Rydberg bands are encountered. For benzene itself the ns bands which are g↔g have not been observed except, perhaps, the 3s band. The np series is known ad a few (nd or nf) series with a very low quantum defect are also known. They all converge to the first π ionization potential at 9,247eV. Beyond that a wealth of superexcited states are found.

Most organic molecules have bonding σ, bonding π and lones pairs (n) of eletrons. There are often two originating orbitals, an n and a π, whose order depends on cases.

Simple aldehydes and ketones have only the well known (n,π^*) band in the near UV. This is followed, in the VUV by three Rydberg bands: 3s, 3p and 3d. The (π,π^*) band is thus at very high frequencies; in the case of formaldehyde it is superexcited. This, it is believed, is photochemically important and has been disregarded in the past. Non-aromatic Schiff bases have spectra intermediate between those of

olefins and carbonyl compounds. Because of the two relatively close originating orbitals and the many possibilities for crossing among potential surfaces, their spectra usually consist of broad bands. Their Rydberg bands are difficult to locate. Olefins have π spectra, aldehydes and ketones have lone pair spectra, Schiff bases have π and lone pair spectra. (4)

IN the spectra of amides the bands are, in order of increasing energy: (n,π^*), Rydberg, (π,π^*), Rydberg, (π,π^*). This is typical of amides, acide halides, carboxylic acids, esters, etc. In these molecules there are three π levels instead of two in ketones and aldehydes; this puts the n level close to the second π level, pushes the (n,π^*) band to higher frequencies and gives rise to close-lying n and π Rydberg bands.

So if a molecule contains n and/or π-electons, their transitions dominate even in the vacuum UV of 200 to 130 nm. The bands due to σ-electron transitions can only be seen when no other electrons are present; otherwise they readily move to higher energies. They are strongly bound and do not come out easily to the limelight. Their excitations often cause dissociation. (Not always, however, remember the vibrational fine structure of ethane or cyclopropane.)

At this point it is convenient to refer to books and review papers for further study.

It is a pleasant task, however, to say a word about the photochemical consequences of the Rydberg - valence-shell distinction. The idea that the photochemical primary steps should be expected to be

different for photolytical reactions occurring in Rydberg states from those occurring in valence-shell excited states has been put forward by the writer in 1975 and was subsequently advocated in several papers. (40-44) Previously, in 1973 Kropp pointed out that to interpret the photochemical reactions of olefins both VS and Rydberg excited states have to be invoked. (44,45)

Since most known photochemical reactions occur in the lowest excited states, for organic molecules the 3s state is expected to be photochemically the most important Rydberg state. Let us first suppose that it is a true Rydberg state remaining so at any internuclear distance. Unlike the higher ns orbitals 3s is not extremely large. It has two radial nodes, one of which will lie, in molecules like methane or ethane, between the carbon and the hydrogens. This is perhaps an important point. When referring to the bonding or antibonding character of orbital wave funcitons, it is usually the angular part that is meant. If, however, higher AO's, 2s, 3s, 3p,... are involved, the radial nodes enter into play. they might cause antibonding character, as well as the angular nodes.

On the other hand, since ns orbitals are totally symmetrical, the 3s orbital will provide some bonding between atoms which are not chemically bound together. In other words it will act as a weak one-electron bond.

Then, reasoning in terms of Koopmans' theorem, one can say that if we excite to a 3s orbital, or ionize an electron from an orbital which is bonding in a given bond that bond is likely to break in the

excited state, the main reason being the loss of bonding character, and a lesser reason being that the 3s orbital contributes some antibonding character because of its radial nodes. Rydberg orbitals are typically non-bonding rather than antibonding but the most important 3s orbitals are, to some extent, an exception to this. Furthermore, the 3s orbital will bring together symmetrically related atoms which are not chemically connected. Therefore one would expect that the preferred primary process for photolysis from a 3s state be molecular elimination rather than a simple bond cleavage. An example for this is ethane, or any other normal paraffin, for which the most important primary process is elimination of H_2 molecules. (Not 2H) (46,47)

If, on the other hand, the orbital of the excited electron is a valence-shell type orbital which is typically antibonding, the expected primary process is simple bond cleavage. Typical examples are alkylchlorides, or bromides, or iodides. The first excited state of these molecules is due to a (C-Cl)*←n, etc. transition where the (C-Cl)* orbital is antibonding; they all produce halogen atoms in the primary step.

There is no point in giving more examples. These ideas are evidently too simple to be applied to individual problems. It is believed, however, that they contain significant elements of truth. The importance or radial nodes in producing antibonding character and the ability of Rydberg orbitals of establishing one electron bonds should not be dismissed lightly.

Such simple reasoning can at most apply to the vertical excited

state. It is reminiscent of the static indices used in the early times of quantum chemistry. Naturally, in order to interpret the course of a photochemical reaction we have to examine the potential surfaces and their evolution with time. Every reaction must be considered in its own right and particular conditions. In this respect we refer to the recent works of Evleth and his coworkers (48-50) and of Malrieu. (51) As to experimental photochemistry, results obtained by Kropp (44,45) von Sonntag and Schuchmann (52) (53), Collin (54,55), Tschouikow-Roux (56), Wijnen (57) and others have shown that while these problems are complicated, the Rydberg - valence-shell distinction is indeed important for the understanding of photochemical reactions.

III. Rydberg States of Transiton Metal Complexes

There is an immense literature and accumulated knowledge on transition metal complexes. (See, for example (58-61)) All we need to do here is to state the present position and then see what we could expect to find in the vacuum UV, the spectral region which is at present the target of our deliberations. We shall choose Cr(III) hexafluoroacetylacetonate (hfaa) as a typical example. (hfaa) complexes are sufficiently volatile to be studied in the gas phase; their photoelectron spectra have been determined by Orchard et al (62) and by Furlani and Cauletti (63). The gas phase VUV spectra of the (hfaa) complexes of Al(III), Sc(III), V(III), Cr(III), Fe(III), Mn(III) and Cu(II) have now been measured. From the point of view of the present discussion they all yielded similar results. The VUV

absorption spectrum of Cr(III) $(hfaa)_3$ is shown in Fig.1. (Lussier and Sandorfy, to be published).

Under octahedral symmetry (O_h) the degeneracy of the five 3d atomic orbitals is partly lifted, and two orbitals are obtained. The one of lower energy is triply degenerate, t_{2g}, the one of higher energy is doubly degenerate, e_g. (They are also called dε and dγ, respectively.) According to literature data (Cf 62), the actual symmetry of trishexafluoroacetylacetonates is actually only D_3 in the crystal phase and this is likely to be so in the gas phase too. Under D_3 symmetry t_{2g} becomes a_1+e_a while e_g remains degenerate and is called e_b.

Free Ion	O_h	D_3
5(3d)	e_g	e_b
	t_{2g}	a_1+e_a

It is instructive, however, to consider both symmetries.

Cr(III) has three 3d electrons which occupy half of the places in the t_{2g} orbital. Form this configuration (d^3) of three equivalent d electrons several states are issued:

$$^2P, ^2D(2), ^2F, ^2G, ^2H, ^4P \text{ and } ^4F$$

(The quantum number of the orbital angular momentum L may take any integer value from 6 to 0.) Among these many states, according Hund's rules, the ^4F term has the lowest energy. Under O_h symetry ^4F splits into three omponents: $^4A_{2g}$, $^4T_{2g}$ and $^4T_{1g}$ of which $^4A_{2g}$ is lowest. So we have three states issued from the d^3 configuration for the 4F term:

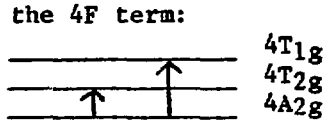

This yields two transitions which correspond to the two well known characteristic visible bands of the Cr(III) complexes. These bands are very weak, being g →g. Under D_3 symmetry A_{2g} will be A_2, T_{1g} becomes A_2+E, and T_{2g} becomes A_1+E. Then from the A_2 ground state transitions to A_1 and E will be allowed, but transition to another A_2 state will be forbidden. (D_3 does not possess a center of symmetry.) The bands will be still weak, however, since departure of O_h symmetry is not very great.

The next higher state would correspond to the ^4p_g configuration of the free ion which becomes T_{1g} under O_h and A_2+E under D_3 symmetry. The band is often covered by the much more intense charge transfer bands but for $[Cr(III)(H_2O)_6]$ it is found at about 3800 cm^{-1}, 14,300 cm^{-1} higher than the second ^4F_g band. Naturally, all states issued from the d^3 configuration are gerade. The bands to the doublet configurations are, of course, even weaker being not only symmetry but also spin forbidden. (Although for the heavy Cr(III) ion the rule is only approximately valid.) So the contribution of these bands to the overall appearance of the spectrum is expected to be negligible.

The (hfaa) ligand has a π orbital as its HOMO, π_3. Towards higher energies the n_- and n_+ orbitals follow which are combinations of the two oxygen lone pair AO's. There are two empty π^* levels, π_4 and π_5. Under C_{2v} symmetry the π_3 and n_- orbitals are respectively b_2 and b_1. With three ligands under O_h symmetry both π_3 and n_- are t_{1g} and, under D_3 symmetry, a_2+e and are only slightly

split. Mixing between the metal and ligand orbitals has been examined by previous authors and we shall not be involved with this here.

Orchard et al. obtained 10.74 and 11.25eV respectively for the Koopmans ionization potentials of the free ligand related to π_3 and n_- respectively. For Cr(III) $(hfaa)_3$ the first photoelectron band comes from 3d ionization, 9.57eV, ($^4A_2$, top orbitals a_1e_2) preceding π_3 ionization at 10.18 and n_- ionization at 11.10 and 11.61eV. Thus metal ionization preceds ligand ionization (approximate language) but the difference is only 0.61eV.

The UV spectrum of (hfaa) has been published by Nakanishi, Morita and Nagahura. (64) They assigned the two intense bands at 37400 and 63700cm^{-1}, with oscillator strengths of 0.20 and 0.30 respectively, to (π,π^*) transitions but the second band is double containing an (n,σ^*) band. A shoulder at about 57300 cm^{-1} was attributed to a (π,σ^*) transition. The band at 70400 (f=0.15) was assigned to another (n,σ^*) transition.

FIG. 1

Now we are ready to have a look at the UV spectrum of Cr(III) $(hfaa)_3$. The two visible d-d bands, typical of Cr(III) complexes are not shown. Towards higher frequencies, at 29200 cm^{-1} we find an intense band which is known to be a metal to ligand charge transfer band; 3d to π_4. (See references 65 to 68) Under D_3 symmetry the band may split which could explain the shoulder on the band.

At 35000-36750 cm^{-1} there are two intense mutually overlapped bands. This is quite certainly the first ligand (π,π^*) band; π_3 to π_4. It is not dramatically displaced from its position in the free

ligand. The second (π,π^*) band (or rather mixed π,π^* and n,σ^*) is also readily identified at 60500 cm^{-1}. Both bands are evidently composite.

In the 44000-46000 cm^{-1} region there is a broad shoulder which could be assigned to a charge transfer transiton n to 3dγ that is, ligand to metal (65,68,59) The band at about 50000 cm^{-1} might contain still other charge transfer bands. Several other CT bands can be deduced from the orbital scheme of the complex (59). These are often invoked in a general way as well as transitions to σ^* orbitals. One is wondering, however, if purely valence-shell considerations are an adequate language to interpret the bands found at higher frequencies in the spectum.

The bands shown in Fig.1 are quite intense. Although we could not determine the molar absorption coefficients with precision we can estimate their values from vapor-solution comparisons in the part of the spectrum in which both vapor and solution spectra can be obtained. Thus ε is of the order of 20000 for the 44000-46000 cm^{-1} region; for the band at 50000 cm^{-1} ε is about 40000 and for the broad band at 60500cm^{-1} it is about 74 000. Under these cirucmstances the many forbidden d-d bands which were mentioned above cannot make any significant contribution.

Beyond the valence-shell bands discussed so far Rydberg bands must exist. The question is if we may expect any intense, allowed bands among them?

First we look at the Rydberg states which the three d electrons can generate.

a) The d^2s configuration. (first level: $3d^24s$)

The terms are:

$^2S, ^2D, ^2G, ^4P, ^2P, ^4F, ^2F$

with ^4F the lowest, all gerade.

Under O_h symmetry ^4F splits in to $^4A_{2g}+^4T_{2g}+^4T_{1g}$

All transitions from the $^4A_{2g}$ ground state are forbidden by the Laporte rule. Even if the actual symmetry is only D_3, we expect them to be very weak. Transitions to the next state, ^4P is $^4T_{1g}$ under O_h symmetry, also forbidden. Transitions to the doublet terms are even more strongly forbidden.

b) The d^2p configuration (first member $3d^24p$) gives a different picture. The terms are:

$^2P, ^2F, ^2D, ^2P, ^2H, ^2G, ^2F,$

$^4D, ^4P, ^4S, ^2D, ^2P, ^2S,$

$^4G, ^4F, ^4D, ^2G, ^2F, ^2D$

All these terms are ungerade.

The lowest term is ^4G. Under O_h symmetry it splits up into $A_{1u}+E_u+T_{1u}+\underline{T_{2u}}$. Transition from the $^4A_{2g}$ ground state to $^4T_{2u}$ is allowed, the other are symmetry forbidden.

The ^4F and ^4D terms also yield allowed components but not ^4P and ^4S:

^4F becomes $^4A_{2u}+^4\underline{T_{2u}}+^4T_{1u}$

^4D " $^4E_u+^4\underline{T_{2u}}$

^4P " $^4T_{1u}$

^4S " $^4A_{1u}$

So among the $3d^2 4p$ terms there are four allowed transitions even under O_h symmetry. (There are two ^4D terms.) These are both symmetry and spin allowed and are expected to be intense. They are also atomically allowed. ($L=\pm 1$)

c) All terms issuing from the $d^2 d$ configuration will be $g \leftrightarrow g$ and forbiden.

d) The $d^2 f$ configuration yields the following terms, all "u":

$^2F, ^2H, ^2G, ^2F, ^2D, ^2P, ^2J, ^2I, ^2H, ^2G, ^2F, ^2D, ^2P$

$^4G, ^4F, ^4D, ^2G, ^2F, ^2D$

$^4I, ^4H, ^4G, ^4F, ^4D, ^4P, ^4S$

$^2I, ^2H, ^2G, ^2F, ^2D, ^2P, ^2S$

All the quadruplet terms except the P and S warrant allowed transitions, altogether eight series.

But how can we locate these states? The Rydberg term values for Cr(III) are not known. A look at the ionization potentials is of interest (Data from Moore's tables (69)).

Cr(III)	49.6eV	400,000 cm^{-1}
Cr(II)	30.95	249,700
Cr(I)	16.48	133,060
Cr	6.76	54,565

The ionization potential of the complex is 9,57eV or 77190 cm^{-1}. Now the electron configurations of these different ions of Cr and the very high number of states that are issued from them preclude to any

meaningful comparison. Yet, it is tempting to guess from these data that the net positive charge around the central ion in the complex is much less than +1, perhaps +0.3 or so. Furthermore the IP, 9.57eV is very much of the order of magnitude of those of organic molecules. The first s and p terms for most organic molecules are between 27000 and 22000cm^{-1} and 20000 and 16000 cm^{-1}, respectively. With this and the partial positive charge one would expect strongly penetrating Rydberg orbitals, wih terms of the order of perhaps 35000 for the s and 30000cm^{-1} for the p. this would lead us, for the first p type Rydberg bands to about 47000 cm^{-1}. Then four allowed p type Rydberg term might well be in the 42000-52000 cm^{-1} region where we actually see absorption which is neither ligand-ligand nor valence-shell d-d absorption. Instead of, or in addition to invoking possible but higher charge-transfer transitions it is pleasant to propose that allowed Rydberg transitions contribute a significant part of the absorption intensity in this part of the spectrum.

There must be also ligand to Rydberg transitions. Taking π_3 for the originating orbital, under O_h symmetry transitions to s type Rydberg orbitals would be t_{1g} to a_{1g} or $^4A_{1g}$ to T_{1g} and forbidden. Transitions to p type Rydberg orbitals would be t_{1g} to t_{1u} or $^4A_{2g}$ to $^4A_{2u}+^4E_u+^4T_{1u}+^4T_{2u}$, $^4T_{2u}$ being allowed.
In this case one might safely use the term values know from organic spectroscopy. This, with the second IP (10,18eV or 82100 cm^{-1}) would give p bands near 62000-640000 cm^{-1}. They might contribute to the very broad (π,π^*) band which is found there. d type Rydberg bands would be

again forbidden. Both s and d might have some more strength under D_3 symmetry.

To what extent the Rydberg orbitals, both metal to Rydberg and ligand to Rydberg, cover the metal and the ligands seems to be a problem for the future. Many of them might have some harge transfer character.

It is not intended to go any further. Let us conclude only that transition metal complexes must have allowed Rydberg bands and that these constitute a worthwhile target for future research.

Legend to the Figure

Fig.1. The ultravolet absorption spectrum of Cr(III) $(hfaa)_3$

References

(1) W.C. Price, Advan. Spectrosc. 1, 56 (1959).

(2) M. B. Robin, Higher Excited States of Polyatomic Molecules. Vols. 1 and II. Academic Press, New York 1974-1975.

(3) C. Sandorfy, J. Mol. Structure 19, 183 (1973).

(4) C. Sandorfy, in Topics in Current Chemistry. Vol. 86. Springer Verlag, Berlin, 1979. pp. 91-138.

(5) G. Herzberg, Molecular Spectra and Molecular Structure. Vol. I. Spectra of Diatomic Molecules. Van Nostrand, Princeton, 1950.

(6) R.S. Mulliken, Acc. Chem. Res., 9, 7 (1976).

(7) W.H.E. Schwarz, Chem. Phys. 9, 157; 11, 217 (1975).

(8) K.F. Herzfeld, Z. Naturforschung 3a, 457 (1948).

(9) A.J. Merer and R.S. Mulliken, Chem. Rev. 69, 639 (1969).

(10) M. B. Robin, R.R. Hart and N.A. Kuebler, J. Chem. Phys. 44, 1803 (1966).

(11) G. Bélanger and C. Sandorfy, J. Chem. Phys. 55, 2055 (1971).

(12) O. Sinanoglu, in Chemical Spectroscopy and Photochemistry in the Vacuum Ultraviolet. C. Sandorfy, P.J. Ausloos and M.B. Robin, editors. Reidel, Dordrecht, Holland, 1974, p.337.

(13) S.D. Peyerimhoff, Gazz. Chim. Ital., 108, 411 (1978).

(14) D.F. Evans, Proc. Chem. Soc. London 378 (1963).

(15) M.B. Robin and N.A. Kuebler, J. Mol. Spectrosc. 33, 247 (1970).

(16) D.R. Salahub and C. Sandorfy, Theoret. Chim. Acta 20, 227 (1971).

(17) S.D. Peyerimhoff and R.J. Buenker, Advances in Quantum Chemistry 9, 69 (1975).

(18) R.J. Buenker and S.D. Peyerimhoff, Theoret. Chim. Acta 39, 217 (1975).

(19) R.J. Buenker and S.D. Peyerimhoff, Chem. Rev. 74, 127 (1974).

(20) R.J. Buenker and S.D. Peyerimhoff in Excited States in Quantum Chemistry. C.A. Nicolaides and D.R. Beck, editors, Reidel, Dordrecht, Holland, 1979. pp.45, 79, 403.

(21) F. Pauzat, J. Ridard, and B. Levy, Mol. Phys., 23, 1163 (1972).

(22) R. Roberge and D.R. Salahub, J. Chem. Phys. 70, 1177 (1979).

(23) K.H. Johnson, Adv. Quantum Chem., 7, 143 (1973).

(24) S. Shih, S.D. Peyerimhoff and R.J. Buenker, Chem. Phys., 17, 391 (1976).

(25) D.W. Turner, C. Baker, A.D. Baker and C.R. Brundle, Molecular Photoelectron Spectroscopy. Wiley-Interscience, New York, 1970.

(26) R. Roberge, C. Sandorfy, J.I. Matthews, and O.P. Strausz, J. Chem. Phys., 69, 5105 (1978).

(27) R.J. Buenker and S.D. Peyerimhoff in Chemical Spectroscopy and Photochemistry in the Vacuum Ultraviolet. C. Sandorfy, P.J. Ausloos and M.B. Robin editors. Reidel, Dordrecht, Holland, 1974, p.257.

(28) R. McDiarmid, J. Chem. Phys., 55, 4669 (1971).

(29) J. Koutecky, J. Chem. Phys., 47, 1501 (1967).

(30) B.S. Hudson and B.E. Kohler, Chem. Phys. Lett., 14, 299 (1972).

(31) K. Schulten and M. Karplus, Chem. Phys. Lett. 14, 305 (1972).

(32) B. Hudson and B.E. Kohler, Ann. Rev. Phys. Chem., 25, 437 (1974).

(33) R. McDiarmid and J. P. Doering, Chem. Phys. Lett., in press.

(34) R.R. Birge, J.A. Bennett, B.M. Pierce, and T.M. Thomas, J. Amer. Chem. Soc., 100, 1533 (1978).

(35) B. Honig, Ann. Rev. Phys. Chem., 29, 31 (1978).

(36) B.E. Kohler, Biophys. Struct. Mechanism, 3, 101 (1977).

(37) C. Sandorfy, J. Photochem., 17, 297 (1981).

(38) J.-M. Leclercq, to be published.

(39) R.J. Buenker, S. Shih and S.D. Peyerimhoff, Chem. Phys. Lett., 44, 385 (1976).

(40) C. Sandorfy, Rev. React. Species. Chem. React., 1, 159 (1975).

(41) C. Sandorfy, Z. Phys. Chem., 101, 307 (1976).

(42) C. Sandorfy in Applications of MO Theory in Organic Chemistry. I.G. Csizmadia, editor. Elsevier, Amsterdam, 1977. p. 384.

(43) C. Sandorfy, Int. J. Quantum Chem., 19, 1147 (1981).

(44) P.J. Kropp, E.J. Reardon, Z.L.F. Gaibel, K.F. Williard, and J.H. Hattaway, J. Am. Chem. Soc., 95, 7058 (1973).

(45) T.R. Fields and P.J. Kropp, J. Am. Chem. Soc., 96, 7559 (1974).

(46) H. Okabe and J.R. McNesby, J. Chem. Phys., 34, 668 (1961) and subsequent papers.

(47) S.G. Lias, G.J. Collin, R.E. Rebbert, and P.J. Ausloos, J. Chem. Phys., 52, 1841 (1970).

(48) E. Kassab, J.T. Gleghorn, and E.M. Evleth, Chem. Phys. Lett., 70, 151 (1980).

(49) E. Kassab, E.M. Evleth, J.J. Dannenberg, and J.C. Rayez, Chem. Phys., 52, 151 (1980).

(50) E.M. Evleth and E. Kassab, J. Am. Chem. Soc., 100, 7859 (1978).

(51) J. P. Malrieu, Theoret. Chim. Acta, 59, 251 (1981).

(52) C. von Sonntag and H.P. Schuchmann, The Chemistry of Functional Groups. Supplement E, Vol. 2, Chapter 21, 1980.

(53) C. von Sonntag and H.P. Schuchmann, in Advances in Photochemistry, Vol. 10, Wiley-Interscience, New York, 1977.

(54) G.J. Collin, H. Deslauriers, and A. Wieckowski, J. Phys. Chem. 85, 944 (1981).

(55) G.J. Collin, Rev. Chem. Int., 2, 377 (1979), Verlag-Chemie, Weinhem, 1979.

(56) T. Yano and E. Tschouikow-Roux, J. Chem. Phys., 72, 3401 (1980).

(57) R. Ausubel and M.H.J. Wijnen, J. Photochem., 4, 241 (1975).

(58) H.L. Schläfer and G. Gliemann, Basic Principles of Ligand Field Theory. Wiley-Interscience, New York, 1969.

(59) F.A. Cotton and G. Wilkinson, Advanced Inorganic Chemistry. Third Edition. Interscience, New York, 1972.

(60) C.J. Ballhausen, Introduction to Ligand Field Theory. McGraw-Hill, New York, 1962.

(61) C.K. Jorgensen, Absorptin Spectra and Chemical Bonding in Complexes. Pergammon Press, Oxford, 1962.

(62) S. Evans, A. Hamnett, A. F. Orchard, and D.R. Lloyd, Disc. Faraday Soc., 54, 227 (1972).

(63) C. Furlani and C. Cauletti, in Structure and Bonding. Vol. 35. Springer-Verlag, 1978, p.119.

(64) H. Nakanishi, H. Morita, and S. Nagakura, Bull. Chem. Soc. Japan, 51, 1723 (1978).

(65) R.H. Holm and F.A. Cotton, J. Am. Chem. Soc., 80, 5658 (1958).

(66) D.W. Barnum, J. Inorg. Nucl. Chem., 21, 221 (1961).

(67) D.W. Barnum, J. Inorg. Nucl. Chem., 22, 183 (1961).

(68) I. Hanazaki, F. Hanazaki, and S. Nagakura, J. Chem. Phys., 49, 276 (1968).

(69) C.E. Moore, Atomic Energy Levels. Vols. 1 and 2, Natl. Bur. Stand. (U.S.), NSRDS-NBS 35, 1971.

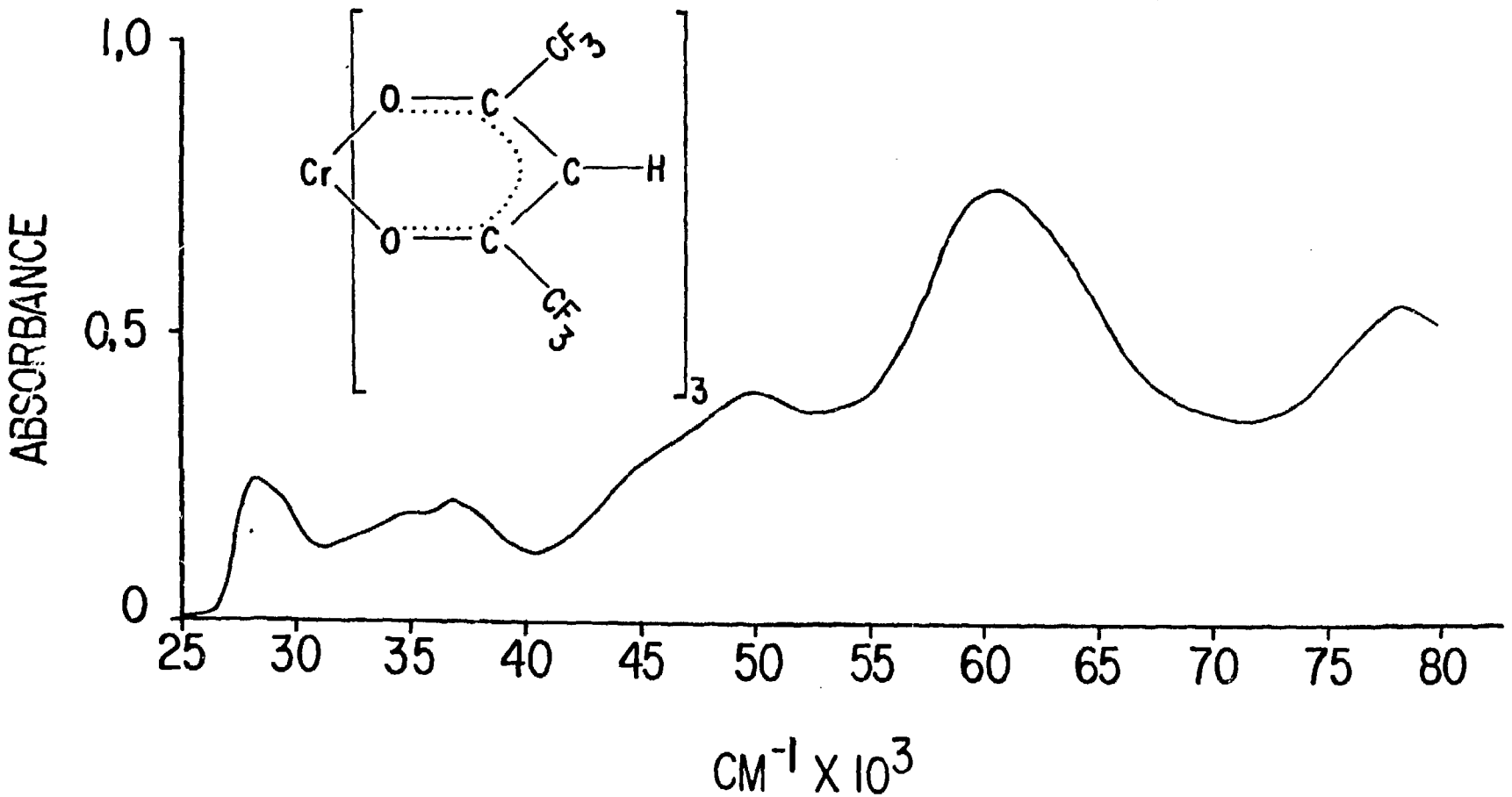
1,0
0,5
0
ABSORBANCE
25
30
35
40
45
50
55
60
65
70
75
80
CM⁻¹ X 10³
Cr
O
C
CF3
H
3

DYNAMICS OF HIGHLY EXCITED STATES OF LARGE ISOLATED MOLECULES

J. Jortner

Department of Chemistry
Tel Aviv University
Tel Aviv, Israel

This review will be concerned with the spectroscopy and excited-state relaxation of large molecules, van der Waals complexes and clusters in seeded supersonic expansions. Experimental studies in this novel area applied the techniques of laser-induced fluorescence, energy-resolved emission spectroscopy and absorption spectroscopy, utilizing CW and pulsed axisymmetric jets, expanded through a pinhole, and planar supersonic jets, expanded through a nozzle slit. This approach allows for a remarkable increase of spectral resolution in electronic-vibrational spectroscopy of large, "isolated", ultracold molecules, complexes and clusters. Nonreactive and reactive intramolecular relaxation processes from well-characterized photoselected

vibrational states of large molecular systems were interrogated. We shall consider the perspectives of supersonic beam spectroscopy for the exploration of excited-state energetics and dynamics of "isolated" large molecular systems excited in the vacuum ultraviolet region of 6-25 eV.

References

[1] Levy, D.H., 1980, Ann. Rev. Phys. Chem. 31, p. 197.

[2] Amirav, A., Even, U. and Jortner, J., 1981, J. Chem. Phys. 75, p. 2489.

[3] Leutwyler, S., Even, U. and Jortner, J., 1982, Chem. Phys. Letters 86, p. 439.

[4] Amirav, A., Even, U. and Jortner, J., 1981, Chem. Phys. Letters 83, p. 1.

EXCITONS AND ENERGY TRANSFER IN CONDENSED PHASES

J. Jortner

Department of Chemistry
Tel Aviv University
Tel Aviv, Israel

These talks will be concerned with the electronic structure and excited-state relaxation phenomena in pure and doped insulators in the vacuum ultraviolet region (energy range 6-50 eV). Both ordered and disordered systems will be considered with an emphasis on pure rare-gas solids, solid rare-gas alloys, solid two component mixtures, liquid rare gases and doped liquids. We shall focus attention on the following general problems:

(1) The interrelationship between the electronic level structure and the geometric structure of condensed phases, establishing the effects of structural and compositional disorder on electronic excitations.

(2) The relation between the state of aggregation and excited-state relaxation phenomena. In this context we shall focus attention

on the effects of the state of aggregation on localization of excited states in condensed phases. Important implications pertaining to electronic energy transfer in condensed phases will be considered subsequently.

(3) The elucidation of the diverse nonradiative decay channels of electronic excitations in insulators pertains to the basic aspects of energy storage, conversion and disposal in condensed phases.

The following information concerning energy levels will be considered: (a) Wannier exciton states in pure materials and excitonic atomic and molecular impurity states, (b) band gaps in pure substances and impurity ionization potentials in doped solids, (c) characteristics of conduction bands, e.g., electron effective mass and energetics, and (d) extended and localized states, exciton screening effects and metal-nonmetal transitions in metal rare-gas mixtures.

The information concerning the electronic structure provides basic input data for the elucidation of dynamic relaxation phenomena in insulators. The fate of electronically excited states in ordered

and disordered condensed rare gases involves a variety of non-radiative relaxation processes, exciton trapping, energy transfer between impurity states and autoionization phenomena. The experimental relaxation data establish general relations and correlations which can be used as a testing ground for theoretical ideas.

References

[1] Jortner, J.: 1974, in "Vacuum Ultraviolet Radiation Physics", Koch, E.E., Haensel, R. and Kunz, C., Edrs, Pergamon, New York, p. 263.

[2] Sonntag, B.: 1977, in "Rare Gas Solids, Klein, N.K. and Venables, J.A., Edrs, Academic Press, London, Vol. II, p. 1021.

[3] Schwentner, N.: 1978, in " Luminescence of Inorganic Solids", Di Bartolo, B., Edr, Academic Press, New York, p. 645.

[4] Fugol, I.Y.: 1978, in " Excitons in Rare Gas Crystals", 1978, Advances in Physics 27, p. 1.

LECTURES ON ATOMIC DIAMAGNETISM

J.C. GAY

Laboratoire de Spectroscopie Hertzienne de l'ENS - Tour 12 E01 - 4 place Jussieu

75230 PARIS.

NATO ADVANCED STUDY INSTITUTE

PHOTOPHYSICS AND PHOTOCHEMISTRY IN THE VACUUM ULTRAVIOLET

LAKE-GENEVA - WISCONSIN

ABSTRACT OF THE LECTURES ON ATOMIC DIAMAGNETISM (J.C. GAY)

The fundamental aspects of the problem of atoms in magnetic fields are connected with diamagnetism and basically with what happens to the motion of the electron when submitted to the joint actions of the Coulomb and Lorentz forces. This is still an unsolved question, but recent experimental and theoretical advances in atomic physics are renewing the current understanding of the phenomena.

The interest of the problem comes firstly from its fundamental simplicity making it really the prototype of a wide class of questions. It is a non separable problem in R^3 with two forces of different symmetries and of comparable strengths acting on the electron. Major questions are then those of the stability of the classical trajectories, of convenient semi-classical quantization and of the existence of adiabatic invariants. The conceptual importance of the problem follows from the fact that two limiting cases are the only two exactly separable situations known in classical or quantum physics - that is the Coulomb and Landau (oscillator like) problems - associated with the early Bohr-Sommerfeld and Landau quantizations.

Secondly, all the questions connected with atomic diamagnetism have wide applications in various domains of physics, for example in solid state physics of excitonic systems where studies were developped long ago, although without any success so far as a general solution of the problem is concerned. Astrophysical implications are also of importance but the range of field strengths relevant to pulsars and white dwarfs is quite different from the previous one and far outside practical possibilities under laboratory conditions. Plasma physics applications may also turn out to be of extreme importance although they are not developped. Firstly for Tokamaks as the magnetic field action completely modifies basic processes as electronic recombination, ionization and finally the energy balance. Secondly it is now well established that self generation of ultra intense magnetic fields occurs due to various kinds of magnetohydrodynamical processes in the plasma with as a consequence a complete alteration of the local atomic properties in the surroundings.

Historically, the understanding of the interaction between atoms or atomic vapours and a magnetic field was a source of constant interest since 1850. This was long ago before the advent of quantum mechanics which happened rather in consequence of this early interest in the field actions. Studies from Faraday to Lorentz and Zeeman have allowed to settle up the theory. But these early investigations were only concerned with one aspect of the magnetic interaction in atoms that is paramagnetism which is indeed the dominant feature for low lying atomic states. The second aspect, associated with diamagnetism and with Faraday's law, was not obviously revealed in the atomic spectra as it is usually a small perturbation for low lying atomic states.

The importance of the diamagnetic interaction for weakly bound electronic systems was first established by Landau, who gave the quantum mechanical spectrum of "free" particles in a magnetic field. This spectrum is basically oscillator like. The first experimental attempt directed towards the effects of diamagnetism in the atomic spectra was performed by Jenkins and Segre, in 1939, on Rydberg series of Sodium atoms. They studied the region where the diamagnetic interaction is still small compared to the Coulomb binding energy. On the other hand, the existence of a Landau regime in the exciton spectrum, which is nearly coulombic in zero-field, was demonstrated in the fifties. But the story of diamagnetism really began in 1969. Garton and Tomkins first demonstrated on Barium the existence near threshold of a new signature of the atomic spectrum, later called "strong field mixing regime" by A.R.P. Rau, which was neither the coulombic nor the Landau one. Basically, this regime was characterized by the existence of broad modulations, with a spacing of about 1.5 $\hbar\omega_c$ which extend far beyond the ionization limit into the continuum.

What appears to be extremely important in this result is the evidence that the atomic spectrum still presents some organization in a region where the Coulomb and magnetic forces acting on the electron are of the same magnitude. As their symmetry properties differ deeply, intuitous arguments would be in favour of a featureless but certainly complicated spectrum.

The fact that, really, the key features of the problem of diamagnetism lies in the region where the Lorentz and Coulomb forces are of the same order of magnitude becomes clear from the following elementary classical analysis. The

expression of the Coulomb force is just :

$$F_C = \frac{\alpha}{n^4 a_o^2} \qquad (1)$$

where $\alpha = q^2/4\pi\varepsilon_o$, a_o the Bohr radius and n the degree of excitation of the electron's motion associated with the Coulomb regime. On the other hand, the expression of the Lorentz force is just :

$$F_L = \frac{\alpha}{n a_c^2} \qquad (2)$$

where a_c is the cyclotron radius, $a_c = [\hbar/qB]^{1/2}$, that is the unit of length in the magnetic Landau problem. The coupling constant in the problem is of the order of the ratio of these two forces :

$$\xi = \frac{F_L}{F_C} = n^3 . (\frac{a_o}{a_c})^2 \qquad (3)$$

This allows to introduce a parameter γ which is independant of the degree of excitation of the motion and which can be expressed in terms of either the units of lengths or in terms of the units of energies (or magnetic field) in the two problems. That is, one gets

$$\gamma = (\frac{a_o}{a_c})^2 = \frac{\hbar\omega_c}{2R} = \frac{B}{B_c} \qquad (4)$$

where $\omega_c = qB/m$ is the cyclotron frequency (unit of energy in the Landau problem) while R is the Rydberg constant. B_c is the unit of magnetic field in the Coulomb problem for which the cyclotron frequency equals the Rydberg. The value of B_c is

$$B_c = 2.35.10^9 \text{ Gauss}$$

meaning that in practical laboratory conditions the value of γ is certainly smaller than 10^{-4}.

The important point is that the coupling constant in the problem is of the order of $n^3\gamma$ which is nearly 1 for $n \underline{\sim} 30$ atomic states. One can expect a dramatic alteration of the atomic spectrum when $\xi \underline{\sim} 1$ that is when

$$n^3 . B \sim B_c \qquad (5)$$

with correlatively a complete modification of the atomic properties. Of course, when $\xi \ll 1$, that is for low lying atomic states or for low excitation of the electron's motion, the atomic spectrum will still be of Coulomb type with some small magnetic alterations. To the contrast, for high ξ values, the magnetic force will completely overwhelm the Coulomb one. This means that for high degree of excitation of the electron's motion, the behaviour will mainly be of Landau type, that is, that of a free particle in a magnetic field. This is especially valid for continuum states, with positive energies. The usual continua of energy of the atomic spectrum will no longer exist and will be replaced with some discrete structures. From fromula (5), it is quite clear that such a deep alteration of the atomic structure will occur once a field is applied on the atom, whatever the field strength provided it is non-zero !

Indeed, the previous model is a very coarse one and suffers from some difficulties. Obviously, it is not at all clear whether the previous effects are associated with the paramagnetic or diamagnetic terms. It is well-known that changing to Larmor frame (rotating with the angular velocity $\omega_c/2$) allows the cancellation of the Lorentz force with the Coriolis one. The motion of the electron in this new frame is the field-free motion but for the presence of the diamagnetic interaction. It is responsible for the axial diamagnetic force

$$F_D = - \frac{q^2 B^2}{4m} \vec{\rho} \qquad (6)$$

where $\vec{\rho}$ is the vector radius in cylindrical coordinates. It is then straightforward to get the expression of the coupling constant :

$$\xi = \frac{F_D}{F_C} \sim \frac{1}{4} \gamma^2 \, n^6 \qquad (7)$$

which is just the square of the expression (3) previously derived. These simple arguments allow to conclude about the true origin of the alterations in the atomic spectrum. The fact that the paramagnetic force disappears in Larmor frame only means that the paramagnetic term (of the order of $\hbar\omega_c/2$) is essentially constant throughout the atomic spectrum and does not depend on the degree of excitation of the electron's motion. It is then straightforward to be get rid off it and it cannot be the origin of a fundamental alteration of the atomic spectrum. To the contrast, the diamagnetic term, proportional to $B^2 \rho^2$, strongly depends on the degree of excitation of the motion. It is really negligible for low n values

(low lying atomic states) while it is completely dominant over the Coulomb terms in highly excited states or continua. The fundamental problems associated with the behaviour of the atom in a magnetic field are then those connected with diamagnetism.

Finally, one can remark that the value of ξ does not depend on the way of evaluation. One can as well evaluate the ratio F_D/F_C using the Landau type quantization instead of the Coulomb one. The only difference lies in the fact that r is then proportional to $n^{1/2}$ (oscillator type spectrum) instead of n^2 in the Coulomb regime. One then gets :

$$\xi_L = \frac{F_D}{F_C} \sim (\gamma . n^3)^{1/2} \qquad (8)$$

The functional dependance is not the same but the quantization law (5) obeyed in the strong mixing regime for $\xi \gtrsim 1$, is still fulfilled.

Qualitative arguments allow to get some more ideas on this strong mixing regime. First of all, it is quite obvious that condition (5) is equivalent to :

$$\frac{2R}{n^3} \sim \hbar\omega_c \qquad (9)$$

taht is the classical frequencies associated with the Coulomb and Landau problems are equal. Moreover, as the coulombic contribution to the energy is of the order of $(-R/n^2)$ while the magnetic contribution is $(n + \frac{1}{2})\hbar\omega_c$ (oscillator like), the total energy of the electron, when condition (5) is fulfilled, is nearly 0. This means that the strong mixing regime takes place near the zero field ionization threshold. Then $Bn^3 \sim B_c$ looks like a new quantization condition obeyed at constant energy ($E \gtrsim 0$) and an intermediate one between the Coulomb and Landau limiting cases. At the end, condition (5) is strictly equivalent to :

$$n^2 a_o \sim \sqrt{n}\, a_c \qquad (10)$$

meaning that in the regime near threshold the atomic orbits have a finite extension and begin to re-organize following the Landau rule for free charged particles in a magnetic field. This means that there is some condensation of the atomic dimensions due to the magnetic field action.

Finally, if one tries to think about this problem in term of harmonic oscillators, that is assuming that the Coulomb force can be approximated by an almost harmonic one, the frequency of the resulting motion is

$$\Omega = \left[\left(\frac{2R}{n^3}\right)^2 + \omega_c^2\right]^{1/2}$$

that is $\sqrt{2}\omega_c$ when (5) is fulfilled. Making use of the correspondence principle, one deduces that the spacing in the quantum mechanical problem is $1.4\ \hbar\omega_c$. Within 10 %, this is basically the experimental result got in the experiments by Garton and Tomkins, near the zero-field threshold.

Of course, all the previous qualitative derivations suffer from various shortcomings ; for example, no attention has been paid to the very different symmetry properties of the two forces. The very simple and basically classical in nature characters of the arguments show that the phenomena are general ones and do have some conceptual importance in physics. This has been earlier stressed upon by A.R.P. Rau.

NATO ADVANCED STUDY INSTITUTE

PHOTOPHYSICS AND PHOTOCHEMISTRY IN THE VACUUM ULTRAVIOLET

LAKE GENEVA WISCONSIN

SUMMARY OF THE LECTURES ON ATOMIC DIAMAGNETISM

(J. C. GAY)

6) QUANTUM MECHANICAL APPROACH

6.1. HAMILTONIAN FOR THE TWO PARTICLES PROBLEM
6.2. NON-SEPARABILITY AND EQUIVALENCE TO THE CROSSED (E,B) FIELDS PROBLEM
6.3. THE ONE PARTICLE PROBLEM
6.4. CONSTANTS OF THE MOTION
6.5. QUALITATIVE ANALYSIS OF THE VARIOUS REGIMES
6.6. COULOMB INTER 1 AND INTER n MIXING REGIMES
6.7. PROPERTIES OF THE WAVE FUNCTIONS IN THE INTER 1 MIXING REGIME
6.8. USE OF THE ADIABATIC INVARIANT
6.9. WAVE FUNCTIONS IN THE INTER n MIXING REGIME
6.10. GROUP THEORETICAL INTERPRETATION
6.11. OTHER METHODS AND ANALYSIS
6.12. THE STURMIAN APPROACH OF THE STRONG MIXING REGIME
6.13. LACK OF APPROACH OF THE LANDAU REGIME
6.14. THE ULTRA HIGH FIELD SITUATION

7) SEMI-CLASSICAL METHODS

7.1. THE USEFULNESS OF THE SEMI-CLASSICAL METHODS
7.2. THE FAILURE OF BOHR-SOMMERFELD QUANTIZATION FOR NON SEPARABLE PROBLEMS..E.B.K. QUANTIZATION
7.3. QUANTIZATION OF THE TRANSVERSE MOTION
7.4. AN OLD SEMI-CLASSICAL THREE DIMENSIONAL MODEL
7.6. RIGOUROUS SEMI-CLASSICAL QUANTIZATION IN THE COULOMB LIMIT USING THE ADIABATIC INVARIANT
7.7. A BAND MODEL OF THE SPECTRUM NEAR THRESHOLD

8) EXPERIMENTAL STUDIES IN ATOMIC PHYSICS

8.1. THE IDEAL EXPERIMENTAL SITUATION
8.2. SUMMARY OF EXPERIMENTAL APPROACHES
8.3. ATOMIC BEAM EXPERIMENTS
8.4. VAPOUR CELL EXPERIMENTS
8.5. FUTURE EXPERIMENTS AND PROSPECTS

9) MISCELLEANEOUS QUESTIONS AND PROSPECTS

9.1. THE CROSSED (E,B) FIELDS PROBLEM. THE VARIOUS PREDICTIONS.
9.2. THE HIGH FIELD SITUATION FOR THE LOOSELY BOUND PARTICLES
9.3. THE HIGH FIELD LIMIT AND QUANTUM ELECTRODYNAMICS

1 - INTRODUCTION

The fundamental aspects of the problem of atoms in magnetic fields are connected with diamagnetism and basically with what happens to the electron when submitted to the joint actions of the Coulomb and diamagnetic forces. This is still an unsolved question, but recent experimental and theoretical advances in atomic physics are renewing the current understanding of the phenomena.

The interest of the problem comes firstly from its fundamental simplicity making it really the prototype of a wide class of questions. It is a non separable problem in R(3) with two forces of different symmetries and of comparable strengths acting on the electron. Major questions are then those of the stability of the classical trajectories, of convenient semi-classical quantization and of the existence of adiabatic invariants. The conceptual importance of the problem follows from the fact that two limiting cases are the only two exactly separable situations known in classical or quantum physics - that is the Coulomb and Landau (oscillator like) problems - associated with the early Bohr-Sommerfeld and Landau quantizations.

Secondly, all the questions connected with atomic diamagnetism have wide applications in various domains of physics, for example in solid state physics of excitonic systems [1][2] where studies were developped long ago, although without any success so far as a general solution of the problem is concerned. Astrophysical implications[3] are also of importance but the range of field strengths relevant to pulsars and white dwarfs is quite different from the previous one and far outside practical possibilities under laboratory conditions. Plasma physics applications may also turn out to be of extreme importance although they are not yet developped. Firstly for tokamaks as the magnetic field action completely

modifies basic processes as electronic recombination, ionization and finally the energy balance. Secondly, it is now well established that self generation of ultra intense magnetic fields occurs due to various kinds of magnetohydrodynamical processes in the plasma with as a consequence a complete alteration of the local atomic properties in the surroundings.

Historically, the understanding of the interaction between atoms or atomic vapours and a magnetic field was a source of constant interest since 1850. This was long ago before the advent of quantum mechanics which happened rather in consequence of this early interest in the field actions. Studies from Faraday to Lorentz and Zeeman have allowed to settle up the theory. But these early investigations were only concerned with one aspect of the magnetic interaction in atoms that is paramagnetism which is indeed the dominant feature for low lying atomic states. The second aspect, associated with diamagnetism and with Faraday's law, was not obviously revealed in the atomic spectra as it is usually a small perturbation for low lying atomic states.

The importance of the diamagnetic interaction for weakly bound electronic systems was first established by Landau [4], who gave the quantum mechanical spectrum of "free" particles in a magnetic field. This spectrum is basically oscillator like. The first experimental attempt directed towards the effects of diamagnetism in the atomic spectra was performed by Jenkins and Segre, in 1939, on Rydberg series of Sodium atoms [5]. They studied the region where the diamagnetic interaction is still small compared to the Coulomb binding energy. On the other hand, the existence of a Landau regime in the exciton spectrum, which is nearly coulombic in zero-field, was demonstrated in the fifties. But the story of diamagnetism really began in 1969. Garton and Tomkins first demonstrated on Barium [6] the existence near threshold of a new signature of the atomic spectrum, later called "strong field mixing regime" by A.R.P. Rau, which was neither the coulombic

nor the Landau one [7]. Basically, this regime was characterized by the existence of broad modulations, with a spacing of about 1.5 $\hbar\omega_c$ which extend far beyond the ionization limit into the continuum.

What appears to be extremely important in this result is the evidence that the atomic spectrum still presents some organization in a region where the Coulomb and magnetic forces acting on the electron are of the same magnitude. As their symmetry properties differ deeply, intuitous arguments would be in favour of a featureless but certainly complicated spectrum. But for all atoms this turns out to be far from being true. Since 1969, experiments have supplied with the striking evidence that for all atoms, the general behaviour was the same meaning that the intermediate regime at threshold was as basic as the Coulomb or Landau ones.

In sections 2 and 3, we will recall the classical and quantum properties of the COulomb and Landau problems which will be used in the following sections. General considerations on the atom in a magnetic field follow in section 3. Then, one comes back to a classical analysis of the phenomena which is presently a source of numerous discoveries and advances. Especially the nature of classical trajectories is discussed and the consequences of the discovery of an adiabatic invariant in the COulomb limit are drawn. Section 6 is devoted to the quantum approach at the spectrum from the Coulomb limit. Then in the lack of any other approach, semi-classical methods are discussed for dealing with the strong mixing and Landau regimes. In section 8, some important aspects of experiments are stressed upon, which have allowed recent progresses in the understanding of the problem. This seems the rule as all the basic features have been experimentally discovered before being theoretically understood. We will conclude with a few prospects, some of them are already under experimental realization.

2 - THE COULOMB SPECTRUM

In this section, we recall some well-known results on the pure Coulomb spectrum of atomic hydrogen. These results have obviously wide generality whatever the atomic specy.But, in addition, purely coulombic potentials lead to fundamental degeneracies in the atomic spectrum which are associated with the underlying group structure [8][9].

2.1 - CLASSICAL MECHANICS

The expression of the Coulomb potential being :

$$V_c = -\frac{q^2}{4\pi\varepsilon_o}\,\frac{1}{r} = -\frac{e^2}{r} \qquad (1)$$

the equation of the motion of the electron in the Coulomb field is :

$$m\,\ddot{\vec{r}} = m\,\vec{\gamma} = \vec{F}_c = -e^2\,\frac{\vec{r}}{r^3} \qquad (2)$$

while the hamiltonian for the problem is readily written as :

$$H = \frac{p^2}{2m} + V_c(r) \qquad (3)$$

The angular momentum $\vec{L}$ is defined as :

$$\vec{L} = \vec{r} \wedge \vec{p} \qquad (4)$$

It is straightforward to verify that H and $\vec{L}$ are constants of the motion that is :

$$\frac{d\vec{L}}{dt} = \vec{0} \qquad (5)$$

which expresses nothing but the conservation of $\vec{L}$ for any motion in a central potential, due to the rotational invariance of the system around any axis in space.

But in addition to this very well known result, there is another constant of the motion which is <u>specific</u> of the Coulomb potential and called the LAPLACE-RUNGE-LENZ VECTOR $\vec{A}$ (10) :

$$\vec{A} = \vec{p} \wedge \vec{L} - m e^2 \frac{\vec{r}}{r} \qquad (6)$$

Using equation (2), it is straightforward to show that

$$\frac{d\vec{A}}{dt} = \vec{0} \qquad (7)$$

Obviously, $\vec{L}$ and $\vec{A}$ fulfill :

$$\vec{L}.\vec{A} = 0 \qquad (8)$$

while the energy can be expressed as a function of L^2 and A^2 :

$$A^2 = -2m H L^2 + m^2 e^4 = -2mE.L^2 + m^2 e^4 \qquad (9)$$

The trajectories are easily deduced by taking the scalar product $(\vec{r}.\vec{A})$. One gets :

$$(\vec{r}.\vec{A}) = -(\vec{r} \wedge \vec{p})^2 + me^2 r$$

Hence :

$$\frac{1}{r} = \frac{me^2}{L^2}\left(1 - \frac{A}{me^2}\cos\varphi\right) \qquad (10)$$

and the trajectories are the well-known KEPLER ellipses shown on Figure (1). The Lenz vector is directed along the major axis of the ellipse. The focus is at the nucleus while the excentricity of the ellipse is given by :

$$\xi = \frac{A}{me^2} \qquad (11)$$

From equation (9), it is clear that the classical motion is highly degenerated, as the trajectory and its energy are completely defined once $\vec{L}$ and $\vec{A}$ are given. The existence of the extra constant of motion $\vec{A}$ is responsible for this feature and for the closed character of the trajectories.

2.2 - THE COULOMB QUANTUM SPECTRUM

The hamiltonian is given by equation (3). One will take advantage of the existence of the two constants of the motion in the classical problem for deriving the Coulomb quantum spectrum. One will firstly introduce the following quantum expression of the Runge-Lenz vector :

$$\vec{A} = \frac{1}{2}(\vec{p} \wedge \vec{L} - \vec{L} \wedge \vec{p}) - me^2 \frac{\vec{r}}{r} \qquad (12)$$

The commutation relations of H, $\vec{L}$ and $\vec{A}$ are the following ones [8][11] :

$$\begin{aligned}
&[H, L_i] = [H, A_i] = 0 \\
&[L_j, L_k] = i\hbar\,\epsilon_{jke}\,L_e \\
&[L_j, A_k] = i\hbar\,\epsilon_{jke}\,A_e \\
&[A_j, A_k] = \frac{\hbar}{i}\,\epsilon_{jke}\,L_e \quad (2mH)
\end{aligned} \qquad (13)$$

and $\vec{L}.\vec{A} = \vec{A}.\vec{L} = 0$ $\qquad A^2 = -2mH(L^2 + \hbar^2) + m^2e^4$ (14)

As $\vec{L}$ and $\vec{A}$ commute with the hamiltonian H, equation (13) suggests to consider a subspace belonging to the eigenvalue E (E < 0). In this subspace, one introduces the operator a :

$$\vec{a} = (-2mH)^{-1/2}\,\vec{A} \tag{15}$$

From the new sets of commutation relations, it becomes clear that $\vec{j}_1 = (\vec{L} + \vec{a})/2$ and $\vec{j}_2 = (\vec{L} - \vec{a})/2$ build up two commuting sets of operators, each one satisfying the commutation relations of ordinary angular momentum. Hence, their eigenvalues are readily derived :

$$\begin{aligned} j_1^2 &= \hbar^2\, j_1(j_1 + 1) \\ j_2^2 &= \hbar^2\, j_2(j_2 + 1) \end{aligned} \tag{16}$$

According to equation (14), $\vec{L}.\vec{A} = \vec{A}.\vec{L} = 0$ so that $j_1 = j_2 = j$. Then, from equation (14), it is straightforward to show that :

$$a^2 + L^2 + \hbar^2 = (2j_1 + 1)^2\,\hbar^2 = -\frac{me^4}{2E} \tag{17}$$

writing $n = 2j + 1$, one recovers the usual Coulomb spectrum, as j is allowed to take every half integer value :

$$E = -\frac{me^4}{2\hbar^2}\frac{1}{(2j+1)^2} = -\frac{me^4}{2\hbar^2}\frac{1}{n^2} \tag{18}$$

The possible values of L for each n follow from the definitions of $\vec{j}_1$ and $\vec{j}_2$. These are L = 0, 1, 2 ... 2j. The degeneracy of each n level is then :

$$\sum_{\ell=0}^{2j} (2\ell + 1) = (2j + 1)^2 = n^2 \qquad (19)$$

2.3 - BASIS SET IN SPHERICAL COORDINATES

Due to the fundamental degeneracy of the problem, or equivalently to the existence of several independant sets of operators commuting with the hamiltonian, there are several possible choices of a basis of eigenvectors.

The first well-known one is associated with the eigenvectors of $\{H, L^2, L_z\}$. The angular part of the wavefunction is then the usual spherical harmonics $Y_\ell^M(\theta,\varphi)$ while the solution of the radial equation is a Laguerre polynomial. One gets (using atomic units) (11)(12)(13) :

$$\langle r\theta\varphi | n\ell m\rangle = R_{n\ell}(r).Y_{\ell m}(\theta,\varphi)$$

with

$$R_{n\ell}(r) = \frac{2}{n^{\ell+2}(2\ell + 1)!} \left(\frac{(n + \ell)!}{(n - \ell - 1)!}\right)^{1/2} (2r)^\ell \; e^{-r/n} \; F(-n+\ell+1, 2\ell+2, \frac{2r}{n}) \qquad (20)$$

with F the confluent hypergeometric function and

$$n = n_r + \ell + 1 \qquad (21)$$

where n_r is the radial Coulomb quantum number.

2.4 - BASIS SET IN PARABOLIC COORDINATES

The set of wave functions which are eigenstates of $\{H, A_z, L_z\}$ is also of importance. It is associated to the separability of Schrödinger's equation in parabolic coordinates :

$$\xi = r + z$$
$$\eta = r - z \qquad (22)$$

It turns out to be extremely useful for studying the Stark effect of hydrogenic species [13]. The expression of the wavefunctions is then (in atomic units) :

$$\langle \xi, \eta, \varphi | n_1, n_2, M \rangle = \frac{1}{\sqrt{\pi}} \frac{1}{n^2} e^{iM\varphi} F_{n_1 M}(\frac{\xi}{\eta}) . F_{n_2 M}(\frac{\eta}{n})$$

with

$$F_{pM}(x) = \frac{1}{|M|!} \left(\frac{(p + |M|)!}{p!}\right)^{1/2} F(-p, |M| + 1, x) e^{-x/2} x^{|m|/2} \qquad (23)$$

with $n = n_1 + n_2 + |M| + 1$ (24)

In this basis, the z component of the Lenz vector is diagonal :

$$A_z = 2 \frac{n_2 - n_1}{n} \qquad (25)$$

while L^2 and parity are no longer defined, as they do not commute with A_z.

2.5 - GROUP THEORETICAL MEANING

L^2 and L_z are constants of the motion. This allows to infer that the Coulomb problem has the O(3) symmetry in coordinate space. A^2 and A_z are also constants of the motion meaning that the problem has another O(3) symmetry which is independant of the previous one. The group O(3) x O(3) is O(4). This O(4) symmetry allows to explain the specific degeneracy of the Coulomb problem.

The O(4) symmetry is much more evident using the Fock method [9] in momentum space $\{\vec{p}\}$. It is especially clear using this approach that the passing from the spherical harmonics basis to the parabolic ones is straightforwardly performed through a rotation. The coefficients of the expansions are Clebsch-Gordan coefficients. Within a given n manifold, it is of course possible to define other basis sets which may be more appropriate for the study of more specialized questions. Some more details can be found in reference [9].

3 - THE LANDAU SPECTRUM

We recall here some well-known classical and quantum mechanical results on the motion of a free charged particle in a uniform magnetic field. This problem is as basic as the Coulomb problem [12]. It is the second and last example of a physical system for which exact quantum and classical solutions can be got as it is a separable problem in R(3). Indeed this is because the Landau problem is almost equivalent to that of the two dimensional harmonic oscillator.

3.1 - CLASSICAL MECHANICS

The equation of motion of the particle in a magnetic field is :

$$m\vec{\gamma} = m\ddot{\vec{r}} = \vec{F}_{\ell} = q\,\vec{v} \wedge \vec{B} \qquad (26)$$

This leads after one integration to :

$$\vec{\Pi} = m\vec{v} = q\,\vec{r} \wedge \vec{B} + \vec{\Pi}_o \qquad (27)$$

where $\vec{\Pi}_o$ is a constant vector and $\vec{\Pi}$ the momentum of the velocity. After projection of equation (27) on the field axis and on the plane perpendicular to the field,

one gets with obvions notations ($\vec{\rho}$ the vector radius in cylindrical coordinates) :

$$\Pi_{//} = m v_{//} = \Pi_{o//}$$
$$\vec{\Pi}_{\perp} = m \vec{v}_{\perp} = q \vec{\rho} \Lambda \vec{B} + \vec{\Pi}_{o\perp} \qquad (28)$$

As $\Pi_{//}$ is a constant, the motion along B field is a uniform motion. Writing $\vec{\Pi}_{o\perp} = - q \vec{r}_o \Lambda \vec{B}$, one gets straightforwardly :

$$\vec{\Pi}_{\perp} = q(\vec{\rho} - \vec{r}_o) \Lambda \vec{B} \qquad (29)$$

The motion in the plane perpendicular to the field is a uniform circular motion with the following characteristics : the angular velocity is the cyclotron frequency ω_c

$$\omega_c = - \frac{qB}{m} \qquad (30)$$

and the position of the center of the circle is :

$$\vec{r}_o = \vec{\rho} + \frac{\vec{\Pi}_{\perp} \Lambda \vec{B}}{qB^2} \qquad (31)$$

which is a constant of the motion. These conclusions are summarized in Figure 2

An additional constant of the motion can be derived from equations (28), using the momentum $\vec{\ell}$ of $\vec{\Pi} = m\vec{v}$ taken at the origin. One gets :

$$\frac{d}{dt}\vec{\ell} = \frac{d}{dt}(\vec{r} \Lambda m\vec{v}) = \vec{r} \Lambda (q\vec{v} \Lambda \vec{B}) \qquad (32)$$

while projecting on the z axis parallel to the field direction, one obtains :

$$\frac{d\ell_z}{dt} = -q(\vec{\rho} \cdot \vec{v}_\perp)B = -q(\vec{\rho}\cdot\vec{\rho})B$$

that is the quantity

$$M_z = \ell_z + \frac{qB}{2}\rho^2 \tag{33}$$

is a constant of the classical motion. Obviously, $\vec{\ell}$ the angular momentum of $m\vec{v}$ is no longer a constant of motion in the presence of an external $\vec{B}$ field, in the laboratory frame. Performing a rotation to Larmor frame rotating at the constant angular frequency $\omega_c/2$ allows to show that M_z coïncides with the momentum of the impulsion in this new frame and then has obvious physical meaning. Moreover in the Larmor frame, the equations of motion are just :

$$m\vec{\gamma}_L = -\frac{q^2B^2}{4m}\vec{\rho} \tag{34}$$

making clear the equivalence with the problem of the two dimensional symmetric harmonic oscillator. Trajectories in this frame are then ellipses with the center at the origin.

Writing the expression of the energy of the system in the laboratory frame is straightforward. One gets :

$$H = \frac{1}{2}m\vec{v}^2 = \frac{\vec{\Pi}^2}{2m} = \frac{\Pi_\perp^2}{2m} + \frac{\Pi_{//}^2}{2m} = E_\perp + E_{//} \tag{35}$$

where $E_\perp$ and $E_{//}$ are respectively the energies associated with the transverse and longitudinal motions which from (28) are conserved independently. From (29) and (35), one deduces immediately the relation between the radius Γ of the circle and the transverse part of the energy. This is :

$$\Gamma^2 = \frac{2.E_\perp}{m\omega_c^2} \qquad (36)$$

To sum up, as shown in Figure 2 , the classical trajectories are circular helices described at the cyclotron frequency ω_c. The constants of the classical motion are the coordinates $\vec{r}_o(x_o, y_o)$ of the center of the circle, the radius Γ of the circle which is proportional to the transverse part of the energy, and M_z defined through equation (33). One can derive another expression for M_z which is :

$$M_z = \frac{qB}{2}(r_o^2 - \Gamma^2) \qquad (37)$$

Equation (36) has an obvious physical consequence. It proves that the classical two dimensional problem, in the plane perpendicular to the field, is highly degenerated as the set of trajectories with fixed Γ but with different values of $\vec{r}_o$ will have the same energies. Indeed, in Larmor frame, the problem has been shown previously to be equivalent to that of the symmetric two-dimensional harmonic oscillator the high degeneracies of which are well known [12]. This allows to explain why trajectories are closed ones.

3.2 - THE LANDAU QUANTUM SPECTRUM

The main differences with the previous classical derivation are associated with the use of the hamiltonian formalism. This implies one has to perform a choice of gauge. Whatever this choice of a gauge, the physical results will not depend on it. But the mathematical expressions of the physical constants of the motion in terms of the canonical variables will do.[11][12]

The hamiltonian of a free charged particle in a magnetic field is

$$H = \frac{\Pi^2}{2m} \tag{38}$$

$$\text{with } \vec{\Pi} = m\vec{v} = \vec{p} - q\vec{A} \tag{39}$$

where $\vec{A}$ is the vector potential ($\vec{\nabla} \Lambda \vec{A} = \vec{B}$). We assume the $\vec{B}$ field parallel to the z axis. The $\vec{p}$ and $\vec{r}$ canonical operators fulfill the standard commutation relations :

$$\begin{aligned} [p_i, p_k] &= 0 \\ [x_i, p_k] &= i\hbar\, \delta_{ik} \end{aligned} \tag{40}$$

while the $\vec{\Pi}$ (velocity) operators do not obey the canonical relations as :

$$\begin{aligned} [\Pi_x, \Pi_z] &= [\Pi_y, \Pi_z] = 0 \\ [\Pi_x, \Pi_y] &= i\, q\, \hbar\, B \end{aligned} \tag{41}$$

and

$$[x_i, \Pi_j] = i\,\hbar\,\delta_{ij} \tag{42}$$

Although the $\vec{p}$ canonical operator fulfills the usual canonical relations, the velocity operator is the one having physical meaning.

The angular momentum $\vec{L}$ is defined from $\vec{p}$ as :

$$\vec{L} = \vec{r} \Lambda \vec{p} \tag{43}$$

while the momentum of the velocity operator $\vec{\ell}$ is :

$$\vec{\ell} = \vec{r} \Lambda \vec{\Pi} \tag{44}$$

The $\vec{L}$ operator obviously fulfills the usual canonical commutation relations of an angular momentum :

$$\begin{aligned} [L_i, x_k] &= i \hbar \varepsilon_{ik\ell} x_\ell \\ [L_i, p_k] &= i \hbar \varepsilon_{ik\ell} p_\ell \\ [L_i, L_k] &= i\hbar \varepsilon_{ik\ell} L_\ell \end{aligned} \tag{45}$$

while $\vec{\ell}$ does not fulfill these relations and is not an angular momentum :

$$[\ell_i, \ell_k] = i \hbar \varepsilon_{ik\ell}(\ell_\ell + q\, x_\ell\, \vec{r}.\vec{B}) \tag{46}$$

although it does possess physical meaning.

The constants of the motion can be straightforwardly deduced from their classical analogs. The hamiltonian in equation (38) can be shared into two parts, $H_{//}$ and $H_{\perp}$. One gets

$$H = H_{\perp} + H_{//}$$

$$\text{with } H_{\perp} = \frac{1}{2m} \Pi_{\perp}^2 = \frac{1}{2m}(\Pi_x^2 + \Pi_y^2) \tag{47}$$

where $H_{//}$ and $H_{\perp}$ have a null commutator. The motion parallel to the $\vec{B}$ field is a free motion. Then

$$H_{//} = \frac{\Pi_z^2}{2m} = \frac{1}{2} m v_z^2 \qquad (48)$$

associated with a continuous spectrum. So far as the transverse motion is concerned the operators associated with the constants of the motion in the classical problem are respectively :

$$x_o = x + \frac{\Pi_y}{qB}$$

$$y_o = y - \frac{\Pi_x}{qB} \qquad (49)$$

$$r_o^2 = x_o^2 + y_o^2$$

(x_o, y_o) being associated with the position of the center of the classical trajectory and

$$M_z = \ell_z + \frac{qB}{2} \rho^2 = \frac{qB}{2} (r_o^2 - \Gamma^2) \qquad (50)$$

$$\text{with } \Gamma^2 = (x - x_o)^2 + (y - y_o)^2 = \frac{2H|}{m\omega_c^2} \qquad (51)$$

where Γ is associated with the radius of the classical circle. One can verify that these operators commute with the hamiltonian H :

$$[H, x_o] = [H, y_o] = [H, r_o^2] = [H, M_z] = [H, \Gamma^2] = 0$$

But to the contrast of what is clearly evident in classical mechanics, the operators x_o and y_o do not commute :

$$[x_o, y_o] = i \frac{\hbar}{qB} = i a_c^2 \qquad (52)$$

where a_c is the unit of length in the problem and is called the cyclotron radius. One can also remark that

$$[M_z, x_o] \neq 0$$

$$[M_z, y_o] \neq 0 \qquad (53)$$

$$[r_o^2, x_o] \neq 0$$

One must stress upon the fact that

$$[H, \ell_z] \neq 0$$

and usually $[H, L_z] \neq 0$ that is the z projection of the angular momentum is usually not a constant of the motion. Indeed, L_z has no physical meaning and its expression depends on the choice of gauge. Then, it is likely that it will not be a constant of motion for an arbitrary choice of the gauge.

Without any choice of gauge, one can derive the quantum spectrum of the transverse hamiltonian. From the expression of $H_\perp$ and from the commutation relations obeyed by Π_x and Π_y, that is :

$$[H, \Pi_x] = - i \hbar \omega_c \Pi_y$$

$$[H, \Pi_y] = i \hbar \omega_c \Pi_x \qquad (54)$$

One can interpret $H_\perp$ as the hamiltonian of a one-dimensional harmonic oscillator in which Π_x and Π_y respectively play the role of the impulsion and coordinate.

Writing :

$$u = \Pi_y/(-\hbar qB)^{1/2}$$

$$v = \Pi_x/(-\hbar qB)^{1/2} \qquad (55)$$

one gets :

$$[u, v] = i$$

$$\text{and } H_\perp = \frac{\hbar\omega_c}{2}(u^2 + v^2) \qquad (56)$$

which is really the hamiltonian of a one-dimensional harmonic oscillator. Rewriting (56) in terms of the usual ladder operators b and b^+ :

$$b = \frac{1}{\sqrt{2}}(u + iv) \qquad (57)$$

one gets : $$H_\perp = \hbar\omega_c(bb^+ + \frac{1}{2}) \qquad (58)$$

Then the Landau spectrum is given by :

$$E = \hbar\omega_c(N + \frac{1}{2}) + \frac{\Pi_z^2}{2m} \qquad (59)$$

As concerns its discrete part, the Landau spectrum is equivalent to a one-dimensional harmonic oscillator spectrum. Continua are associated to the free motion along $\vec{B}$ field. Such a spectrum is shown on Figure 3 . Nevertheless, this does not mean that such an equivalence is complete. The expression of b in equation (57) allows to understand that the degeneracy of each discrete state is in-

finite as expected from the classical behaviour. To the contrast of what happens for a true one-dimensional oscillator, equation (57) depends on the two coordinates (x, y) meaning that the ground state of the equivalent harmonic-oscillator does have infinite degeneracy. And so for the excited states which are proportionnal to $(b^+)^N|0>$.

3.3 - CHOICES OF GAUGES

Getting the expression of the wavefunctions needs to choose a particular gauge. One must remark that the physical results will not depend on this choice of a gauge. But the mathematical expressions for the various operators will do.

The two gauges which are more widely used in this problem are the Landau[13] gauge and the so-called symmetric gauge. The $\vec{A}$ vector potential in the Landau gauge is expressed with :

$$A_x = - B \cdot y$$
$$A_y = A_z = 0 \qquad (60)$$

The use of this gauge is of interest in problems exhibiting some translational invariance, e.g. in solid state physics applications. The second possible choice of a gauge which is more convenient for atomic physics applications is the so-called symmetric gauge in which :

$$\vec{A} = - \frac{1}{2} \vec{r} \wedge \vec{B} \qquad (61)$$

as it allows to exhibit the rotational invariance along the $\vec{B}$ field direction.

Aside from a trivial phase factor, the eigenfunctions of the problem in the two gauges will be the same, although the mathematical expressions of the constants of the motion (x_o, y_o, r_o^2, M_z, $H_\perp$) as a function of the canonical operators ($\vec{p}$, $\vec{L}$) will not.

Some striking examples of such features are the following. Using the Landau gauge, it is straightforward to show that the expression of y_o is just :

$$y_o = - p_x/qB \tag{62}$$

meaning that p_x is here a constant of motion. The problem is readily reduced to a one dimensional harmonic oscillator along the y axis, with its equilibrium position shifted at y_o [13]. The associated wavefunctions are those of the one dimensional shifted harmonic oscillator along Oy and proportional to Hermite polynomials. The translational invariance along the x axis is clear from the fact that y_o being defined, x_o cannot from (52). The fundamental degeneracy of the problem is described here through the continuous index y_o. These wavefunctions are associated with the set of observables $\{H_\perp, H_{//}, y_o\}$. Neither L_z nor M_z are defined in this representation.

Using the symmetric gauge, one finds immediately that the situation is of interest for atomic physics applications. From relations (37), (43) and (50), one gets :

$$L_z = \ell_z + \frac{qB}{2} \rho^2 = M_z \tag{63}$$

that is, the z component of the angular momentum in this gauge does coïncide with the constant of the motion M_z. The rotational invariance around the z axis is explicit here. The wavefunctions associated with this $\{H_\perp, H_{//}, L_z\}$ representation are labelled with the integer index $M = L_z/\hbar$ associated with the quantized projection of the angular momentum. This provides with a discrete description of the fundamental degeneracy. From (50), it is clear that r_o^2 is defined in this representation and that $(r_o^2 - \Gamma^{-2})$, then r_o^2, that is the distance to the center of the classical circle, is quantized.[11]

A schematic representation of these two main types of wavefunctions is given on Figure 4 .

3.4 - FOCK REPRESENTATION OF THE LANDAU SPECTRUM

We will hereafter adopt the symmetric gauge formulation in order to exhibit the rotational invariance of the problem [12]. The expression of the transverse part of the hamiltonian is :

$$H_\perp = (p_x + \frac{qB}{2} y)^2/2m + (p_y - \frac{qB}{2} x)^2/2m \qquad (64)$$

and the expression of the four basic constant of the motion is then :

$$\begin{aligned} \Pi_z &= mv_z = p_z \\ x_o &= \frac{x}{2} + p_y/qB \\ y_o &= \frac{y}{2} - p_x/qB \\ M_z &= L_z = \frac{qB}{2}(r_o^2 - \Gamma) \end{aligned} \qquad (65)$$

From equation (64), one gets :

$$H_{\perp} = \frac{1}{2m}(p_x^2 + p_y^2) + \frac{\omega_c}{2} L_z + \frac{m\omega_c^2}{8}(x^2 + y^2) \qquad (66)$$

But for the paramagnetic term $(\frac{\omega_c}{2} L_z)$ this is the hamiltonian of a two dimensional symmetric harmonic oscillator. Introducing the usual ladder operators (a_x, a^+_x, a_y, a^+_y) associated with annihilation and creation of excitation along respectively the x and y axis is a source of difficulties as these obviously do not commute with L_z. It is far better to use the (a, a^+) operators associated with annihilation and creation of left and right handed circular excitation in the system. That is :

$$a_d = \frac{1}{\sqrt{2}}(a_x - ia_y)$$
$$a_g = \frac{1}{\sqrt{2}}(a_x + ia_y) \qquad (67)$$

They fulfill the usual commutation rules :

$$[a_i, a^+_k] = \delta_{ik} \qquad (68)$$

The expressions of the various constants of the motion are then :

$$= (a^+_d a_d + \frac{1}{2})\hbar\omega_c$$
$$= (a^+_d a_d - a^+_g a_g)\hbar \qquad (69)$$

$$(\hbar/2m\omega_c)^{1/2}(a^+_g + a_g)$$
$$(\hbar/2m\omega_c)^{1/2} i(a^+_g - a_g) \qquad (70)$$

$$r_o^2 = x_o^2 + y_o^2 = a_c^2 \, (a^+_g \, a_g + a_g \, a^+_g)$$

$$\Gamma^2 = (x - x_o)^2 + (y - y_o)^2 = a_c^2 \, (a^+_d \, a_d + a_d \, a^+_d) \tag{71}$$

One then gets the transverse part of the energy, with n_d, n_g the number of right and left handed circular excitations in the system:[12]

$$E_\perp = (n_d + \tfrac{1}{2}) \, \hbar\omega_c \tag{72}$$

Then, for the electron, the energy of the system does not depend on n_g (number of left handed circular excitations in the system) making clear the infinite degeneracy of each n_d Landau manifold. The angular momentum is given by :

$$L_z = (n_d - n_g)\hbar = M \hbar \tag{73}$$

that is, in a given n_d manifold, the degeneracy can be labelled with the discrete integer index n_g varying from 0 to + ∞. Or, equivalently, M varies between n_d and - ∞. A straightforward choice for the wavefunctions is :

$$|n_d, n_g\rangle = (n_g! \, n_d!)^{-1/2} \, (a^+_d)^{n_d} \, (a^+_g)^{n_g} \, |0,0\rangle \tag{74}$$

In cylindrical coordinates $\langle \rho\varphi\theta | n_d, n_g \rangle$ can be expressed as a generalized Laguerre polynomial.[11]

Such a choice of the wavefunction is associated with the $\{H, H_\perp, H_{//}, L_z\}$ representation. The values of r_o^2 and Γ^2 are then defined as :

$$\Gamma^2 = (2n_d + 1) \, a_c^2$$
$$r_o^2 = (2n_g + 1) \, a_c^2 \tag{75}$$

That is, coming back to the classical picture, the radius Γ of the circle is $(2n_d + 1)^{1/2} a_c$ which is constant in a given Landau band. The degeneracy of the Landau band is associated with the distance $r_o = (2n_g + 1)^{1/2} a_c$ between the origin and the center of the circle. From (74) it is clear that any choice of a basis is possible within a given n_d manifold provided one has :

$$|\psi> = (a^+_d)^{n_d} |0> . |f>$$

with $|f>$ a linear combination of $|n_g>$ states only. For example, one can build in a given manifold quasi-classical states in the sense of Glauber [12] on left handed circular excitations for which the fluctuations $\Delta x_o . \Delta y_o$ take the minimum value $a_c/\sqrt{2}$ while the energy is still defined. These states will have the general form :

$$|n_d, \alpha_g> = \frac{(a^+_d)^{nd}}{(nd!)^{1/2}} \; e^{\alpha_g . a^+_g - \alpha^*_g a_g} |0,0> \qquad (76)$$

Of course, L_z will not be diagonal in such a basis.

As well, the other usual set of wavefunctions associated with the $\{H, y_o\}$ representation can be obtained while choosing another basis for the left handed circular excitations. An obvious one is associated with the wavefunction of the one-dimensional left handed harmonic oscillator in impulsion space

$$|p_x = - q B y_o> = \sum_{n_g} \varphi^*_{n_g}(p_x) |n_g>$$

where the $\varphi^*_{n_g}$ are the usual wavefunctions of the one-dimensional harmonic oscillator . The complete wavefunction is then

$$|n_d, p_x = - q B y_o> = \sum_{n_g} \varphi^*_{n_g}(p_x) |n_d, n_g> \qquad (77)$$

Of course it is nothing but the wavefunction which has been got at the beginning of section 3.3. L_z, r_o^2 are no longer defined in this representation in which

the wavefunctions exhibit a clear translational invariance.

Finally the last remark about the pure Landau problem is connected with the building of semi-classical wave packets. Writing D(α) the Glauber operator

$$D(\alpha) = e^{\alpha a^{+} - \alpha^{*} a} \qquad (78)$$

one gets :

$$|\alpha_d, \alpha_g\rangle = D(\alpha_d).D(\alpha_g)|00\rangle \qquad (79)$$

It is possible to show that, with :

$$\alpha_d = \Gamma/(\sqrt{2}\, a_c).\ e^{i\varphi_d}$$

$$\alpha_g = \Gamma_o/(\sqrt{2}\, a_c)e^{i\varphi_g}$$

the state $|\alpha_d, \alpha_g\rangle$ represents the motion of a particle on the circle (r_o, radius Γ) which is followed with the minimum possible fluctuations [12].

4 - THE ATOM IN A MAGNETIC FIELD

We will consider here the simplest atomic situation that is the two-particles problem, in a magnetic field. To the contrast of what happens in the purely coulombic situation, the two (interacting) particles problem in a magnetic field does not separate in the centre of mass frame.[14][15][16]

4.1 - CLASSICAL MECHANICS OF THE TWO-PARTICLES PROBLEM

Writing (q_i, m_i) the charges and masses of the two particles, the classical equations of motion are :

$$\begin{aligned} m_1 \ddot{\vec{r}}_1 &= q_1 \dot{\vec{r}}_1 \Lambda \vec{B} + \frac{q_1 q_2}{4\pi\varepsilon_o} \frac{(\vec{r}_1 - \vec{r}_2)}{|\vec{r}_1 - \vec{r}_2|^3} \\ m_2 \ddot{\vec{r}}_2 &= q_2 \dot{\vec{r}}_2 \Lambda \vec{B} + \frac{q_1 q_2}{4\pi\varepsilon_o} \frac{(\vec{r}_2 - \vec{r}_1)}{|\vec{r}_1 - \vec{r}_2|^3} \end{aligned} \qquad (80)$$

we will write these equations in terms of the center of mass variables. That is :

$$\begin{aligned} \vec{R} &= \Sigma\, m_i \vec{r}_i \,/\, (m_1 + m_2) \\ \vec{r} &= \vec{r}_1 - \vec{r}_2 \end{aligned} \qquad (81)$$

Combining these equations, one gets :

$$(m_1 + m_2)\, \ddot{\vec{R}} = (q_1 \dot{\vec{r}}_1 + q_2 \dot{\vec{r}}_2) \Lambda \vec{B}$$

One further integration allows to get with $q_1 = - q_2 = q$:

$$(m_1 + m_2)\, \dot{\vec{R}} - q\, \vec{r} \Lambda \vec{B} = \vec{C} = \text{Cste} \qquad (82)$$

Equation (82) implies that the motion of the reduced particle and of the center of mass are always coupled in the presence of the magnetic field, for the two particles interacting through the Coulomb field [14].

4.2 - QUANTUM APPROACH OF THE TWO-PARTICLES PROBLEM

The hamiltonian of the system is, in the presence of the $\vec{B}$ field :

$$H = \frac{\Pi_1^2}{2m_1} + \frac{\Pi_2^2}{2m_2} - \frac{q^2}{4\pi\varepsilon_o|\vec{r}_1 - \vec{r}_2|} \tag{83}$$

with

$$\vec{\Pi}_i = \vec{p}_i - q_i \vec{A}(\vec{r}_i) \tag{84}$$

It is straightforward to show that the operator

$$\vec{C} = \vec{\Pi} - q \vec{r} \Lambda \vec{B} \tag{85}$$

associated with relation (82) in classical mechanics commutes with the hamiltonian and

$$[C_i, C_j] = 0 \tag{86}$$

Then, although the problem is not separable in the sense that the reduced particle motion and the motion of the center of mass are not decoupled, the existence of the operator $\vec{C}$ allows a quasi-separability in the equations [14][17]. Choosing the symmetric gauge, one gets :

$$\vec{C} = \vec{P} - \frac{q}{2} \vec{r} \Lambda \vec{B} \tag{87}$$

where $\vec{P}$ is the momentum of the center of mass in this gauge (that is $\vec{P} = -i\hbar\nabla_{\vec{R}}$).

The reduction of the two-particles problem follows. Performing a translation on the wavefunction :[15]

$$\Psi_{\vec{C}}(\vec{R}, \vec{r}) = \exp\left(\frac{i}{\hbar}(\vec{C} + \frac{q}{2}\vec{r} \Lambda \vec{B}).\vec{R}\right) \cdot \varphi_{\vec{C}}(\vec{r}) \tag{88}$$

Upon substitution in (83), one gets the expression of the reduced hamiltonian H_C :

$$H_C = \frac{C^2}{2M} - \frac{q}{M}(\vec{C} \wedge \vec{B})\vec{R} + \frac{p^2}{2\mu} - \frac{q}{2}(\frac{1}{m_1} - \frac{1}{m_2})\vec{B}.\vec{L} + \frac{q^2}{8\mu}(\vec{r} \wedge \vec{B})^2 - \frac{q^2}{4\pi\epsilon_o}\frac{1}{r} \qquad (89)$$

where $\vec{p}$ and $\vec{L}$ are the canonical operators associated with the reduced particle of mass $\mu = m_1 m_2/(m_1/m_2)$, and $\vec{C}$ is the eigenvalue of the operator of equation (87).

4.3 - PHYSICAL MEANING OF THE REDUCED TWO-PARTICLES HAMILTONIAN

The fact that the problem is not separable in the center of mass frame follows from the $\vec{C}$ dependance of H_C. Clearly, $\vec{C}$ is not the eigenvalue of the momentum of the center of mass and is responsible for a coupling between the center of mass motion and the reduced particle one. The interpretation of the various terms in H_C is the following. The first term $\frac{C^2}{2M}$ in H_C represents the translational energy of the system. The second term couples the relative motion and the translational one. The quantity $(\frac{\vec{C}}{M} \wedge \vec{B})$ is the motional electric field seen in the rest frame of the reduced particle and is crossed to $\vec{B}$. The other field depending terms are respectively the paramagnetic interaction (in which the gyromagnetic ratio is altered) and the diamagnetic term proportional to B^2.

To conclude, it is clear that the motion of the center of mass and the motion of the reduced particle are no longer independant in a magnetic field. Especially the energies are no longer conserved independantly, which means that the problem is non separable, though soluble [16][17]. Complete solution of the one electron atom problem in a magnetic field really needs to get the solution of an infinite set of one particle problems in crossed electric and magnetic fields. Doing that is presently outside practical possibilities. Nevertheless,

making the approximation oe an infinite mass for the proton is justified for the most situations of atomic physics. But of course, no longer correct, if one deals with positronium !

4.4 - ONE-PARTICLE HAMILTONIAN IN A $\vec{B}$ FIELD

Assuming $\frac{\vec{C}}{M} \simeq \vec{0}$ and $m_1 << m_2$ in equation (89), one gets :

$$H = \frac{p^2}{2m} + \frac{\hbar\omega_c}{2} L_z + \frac{q^2 B^2}{8m} (x^2 + y^2) - \frac{e^2}{r} \qquad (90)$$

which is the expression of the hamiltonian in the symmetric gauge.

By putting B = 0 in the equations, one recovers the Coulomb hamiltonian while putting e = 0 one recovers the Landau problem. There are two field dependant terms in the hamiltonian. The first one which is linear in B field is the well-known paramagnetic term associated with Zeeman effect. It is essentially constant throughout the spectrum and does not depend on the degree of excitation of the electron's motion.

The second term is the diamagnetic interaction depending on the square of the B field strength. It also strongly depends on the degree of excitation of the electron's motion and in some situations, it can completely overwhelm the Coulomb interaction. This is especially true for high lying Rydberg states for which the Coulomb interaction becomes fainter and for continua states.

4.5 - CONSTANTS OF THE MOTION

From the analysis of sections 2 and 3, it is clear that the only constants of the motion in this problem are L_z and parity. More generally, whatever the choice of a gauge, the operator M_z as defined in relation (50) is a constant of the motion.

As the diamagnetic interaction breaks the spherical symmetry of the atomic problem, L^2 is no longer a constant of the motion. The same conclusions are valid for the Lenz vector $\vec{A}$ which no longer commutes with the hamiltonian, especially with the diamagnetic interaction. Then, the diamagnetic interaction is responsible for a break-down of the super symmetry of the Coulomb problem.

The same conclusions are valid for the constants of the motion which have been deduced in the Landau problem. None among them, but for L_z and parity, are constants of the motion in the present situation, as they do not commute with the Coulomb interaction.

Really, one can verify that the hamiltonian in equation (90) is not separable in any of the 13 sets of coordinates of R(3). This means that there will not exist any additional constant of the motion aside of L_z and parity. Then a major question is laid out : what are the various aspects of the atomic spectrum in a magnetic field ? How does the Coulomb energy levels branch to the Landau ones when the field or energy are varied ?

4.6 - PHENOMENOLOGY OF THE VARIOUS MAGNETIC REGIMES

Associated with the various terms in equation (90), there are special characteristics and alterations of the atomic spectra and approximate sets of constants of the motion [18].

For low-lying excited states, the diamagnetic term is negligible. The dominant term is the Zeeman one proportional to B and small compared to the Coulomb interaction. These regimes do not have any mystery and basically are associated with a removal of the L_z degeneracy of the spectrum.

The more fundamental aspects of the problem are those connected with diamagnetism. The diamagnetic interaction tremendously depends on the degree of excitation of the electron's motion and is of the order of :

$$H_D \sim \frac{q^2B^2}{8m} n^4.a_o^2 \qquad (91)$$

It will then totally dominate the Zeeman contribution in high Rydberg states and in some conditions; the electrostatic contribution to the binding energy, especially for continuum states.

Four characteristic regimes associated with diamagnetism have been recognized in the atomic spectrum though they are really the expression of the same feature [19]. The inter ℓ mixing regime occurs for $\frac{2R}{n^3} >> H_D \sim \frac{e^2B^2}{8m} n^4.a_o^2$. L^2 is no longer a constant of motion while the Coulomb radial quantum number is still defined. Energies behave as B^2 with some deviations associated with quantum defects in non hydrogenic situations. In the inter n mixing regime for which $\frac{2R}{n^3} \sim H_D$, the atomic spectrum is completely altered through merging of the various adjacent hydrogenic manifolds. The third regime is the most important one and has been called "strong field mixing regime" [ ]. It takes place when the electrostatic and magnetic contribution to the energy of the electron are comparable and $\frac{2R}{n^3} \sim \hbar\omega_c$.

Finally, when the magnetic force completely overwhelms the Coulomb one, far into the continuum, the Landau regime of the atomic spectra is reached. The way of passing from the Coulomb regime to the Landau one in the atomic spectra is discussed in the following sections.

5 - CLASSICAL MECHANICS OF DIAMAGNETISM

The difficulties for finding the quantum spectrum of a non separable problem are basically of the same nature that those encountered in studying the behaviour of the classical trajectories. In addition, classical studies are of importance for settling up proper semi-classical quantization of a problem (see section 7). In the present situation of atomic diamagnetism, they have allowed recent theoretical progress with the discovery of an adiabatic invariant in the Coulomb limit. Moreover, they allow to prove that the so-called strong field mixing regime is somewhat analogous to the classical resonance region or Hill's region which exists in the problem of the coupled harmonic oscillators.

5.1 - CLASSICAL EQUATIONS OF MOTION

Assuming the proton to be infinitely massive, the motion of the electron is described with :

$$m\ddot{\vec{r}} = q\vec{v} \wedge \vec{B} + \vec{F}_c \qquad (92)$$

The Lorentz force which linearly depends on B field recovers the two classes of magnetic interactions, that is paramagnetism and diamagnetism. Changing to Larmor frame rotating at constant $\omega_c/2$ angular velocity around the $\vec{B}$ axis allows to be get rid off any effects of the paramagnetic interaction. One gets in Larmor frame :

$$m\ddot{\vec{r}}_L = \vec{F}_c - \frac{q^2B^2}{4m}\vec{\rho} \qquad (93)$$

meaning that the Lorentz force just cancels with the Coriolis term in the transformation ($\vec{\rho}$ the vector radius in cylindrical coordinates). The second term in equation (93) is the diamagnetic force as appearing in equation (34). If one

neglects this term, one recovers the usual equation of motion for the Coulomb problem in Larmor frame. As expected this shows that the trajectories in Larmor frame are the field-free ones, i.e. ellipses with the focus at the origin, a well-known result of Larmor theorem.. At the opposite, if one neglects F_c in equation (93), the trajectories are the Landau ones in Larmor frame, i.e. ellipses with the center at the origin. Between these two limits where closed trajectories exist, no general solution of the problem is known.

The diamagnetic force is a two dimensional attractive harmonic force with cylindrical symmetry. It derives from the harmonic potential $H_D = \frac{q^2B^2}{8m}\rho^2$ which is got in the hamiltonian formulation, in the symmetric gauge (see for example (90)).

5.2 - SYMMETRIES AND COUPLING CONSTANT

From a classical point of view, the problem of the one-electron atom in a magnetic field is equivalent, in Larmor frame, to that of a particle experiencing the joint actions of a central Coulombic force and of an axial harmonic force associated with the diamagnetic interaction. The axial character of the diamagnetic force is responsible for a break-down of the super-symmetry of the field-free problem, whatever the strength of the magnetic field. The conclusions are the same from the Landau approach in equation (93). Indeed, none of the 13 sets of coordinates of R(3) [17] allows to separate equation (93). No clear evidence of an inner symmetry of the motion is existing in the intermediate regime where the two forces are both acting on the electron.

Another key point in equation (93) follows from the evaluation of the relative strengths of the diamagnetic(F_D) and Coulomb (F_C) forces. Using atomic units (a_o the Bohr radius) the coupling parameter ξ can be written as :

$$\xi = \frac{F_D}{F_C} = \frac{1}{4} \left(\frac{a_o}{a_c}\right)^4 (\rho . r^2) \qquad (94)$$

where a_c is the cyclotron radius defined through (52). (ρ, r) are dimensionless parameters of the order of the atomic dimensions, that is they depend on the degree of excitation of the electron's motion. One then introduces the coupling constant γ :

$$\gamma = \left(\frac{a_o}{a_c}\right)^2 = \frac{\hbar\omega_c}{2R} = \frac{B}{B_c} \qquad (95)$$

which measures the relative strength of the magnetic and electrostatic interactions. B_c is the critical value of magnetic field for which the Larmor frequency equals the Rydberg constant :

$$B_c = 2.35.10^9 \text{ Gauss} \qquad (96)$$

Under laboratory conditions, B is at maximum of the order of 25 T in D.C. operation that is γ is at maximum of the order of 10^{-4} , and then fairly small, as expected. One can conclude that the diamagnetic interaction is always negligible compared to the Coulomb one provided the degree of excitation of the electron's motion is weak, that is the sizes of the orbits are a few atomic units. But, fortunately, these conclusions are no longer correct if one deals with high lying atomic states as the coupling parameter ξ not only depends on γ but also on the degree of excitation of the electron's motion through $(\rho . r^2)$:

$$\xi = \frac{1}{4} \gamma (\rho . r^2) \qquad (97)$$

To the contrast, the paramagnetic interaction, associated with the rotation to Larmor frame, is always of the order of $\hbar\omega_c/2$ and constant whatever the degree

of excitation of the motion. In addition, it never breaks the symmetry of the problem.

An order of magnitude of the coupling constant in (97) can be obtained assuming that the degree of excitation of the electron's motion is described with an index n such that r or ρ are of the order of $n^2 a_o$. Then, ξ takes the form [19] :

$$\xi = \frac{F_D}{F_C} = \frac{1}{4} (\gamma . n^3)^2 \qquad (98)$$

This means that the coupling parameter in the problem is γn^3 instead of γ. Although γ is fairly small under normal atomic physics conditions, the ratio of the two forces can take every values meaning that the diamagnetic force may completely overwhelm the coulombic one.

5.3 - PHENOMENOLOGY OF THE VARIOUS REGIMES

Three types of motion follow from (98).[7]

• If $\gamma n^3 \ll 1$, the diamagnetic force is negligible compared to the Coulomb one. The motion of the electron is quasi-coulombic. Such a regime does not exist if $B > B_C$ ($\gamma > 1$).

• If $\gamma n^3 \gg 1$, the diamagnetic force is dominant over the Coulomb one. The motion of the electron is mainly of Landau type in the plane perpendicular to the field while the Coulomb force still has some binding action along $\vec{B}$ field.

• If $\gamma n^3 \sim 1$, the diamagnetic and Coulomb forces are of comparable strength but have far different symmetry properties. This is what has been called strong

field mixing regime or quasi-Landau regime [7][19][20]. No perturbative approach of such a regime from the Coulomb and Landau limits can be valid. The very different symmetries of the forces and the lack of separability suggest that the motion of the electron in such a regime might be completely featureless and inorganized. But surprisingly experiments have shown that for all atoms, this was far to be true [3][6]. Then, in between the two regimes of Coulomb and Landau where trajectories are closed and periodic ones a third one exists in which the trajectories may have some regularity, although intuitious arguments suggest exactly the opposite.

A further remark is that the classical problem obviously depends on two parameters which are the energy of the electron and the magnetic field strength. The analysis of the motion can be performed either at constant field varying the energy or at constant energy varying the field. The somewhat equivalent role of E and B can be rendered much more explicit using a R(4) formulation of the problem (see section 5.6). Several ways of investigating the behaviour of the classical trajectories are then possible, playing with initial conditions in equation (92). The increase of the energy at fixed field will result in a more important role of the diamagnetic force while the increase of the field at fixed energy will result in a decrease of the diamagnetic contribution. The region where $\gamma n^3 \underset{\sim}{} 1$ is associated with a transition curve in the (E, B) plot.

5.4 - PHASE SPACE TRAJECTORIES

Phase space studies of the motion of the particle are extremely useful for the exhibition of the inner symmetries and pecularities of the problem. Presently, as the two limiting situations are quite interesting because of their highly degenerated character, it is natural to try to have some insights on what happens in between.

The study of trajectories can be performed in cylindrical coordinates.[21] As L_z is a constant of motion, the φ angle is a cyclic coordinate and the relevant dimension of phase space is 4 associated with $(\rho, \dot{\rho}, z, \dot{z})$. Some aspects of these trajectories are shown on Figure (5) which represents two-dimensional projections of the 4 dimensional motion (at constant energy). Figure (5-a) is a plot in (ρ, z) for low field values such that the diamagnetic term is almost negligible. The projection is a well-defined curve which is stable over more than 100 times the period. It is nothing but the projection of a Kepler ellipse. Other aspects in $(\dot{\rho}, \dot{z})$ are shown in Figure (5-b). The plot in Figure (5-c) has been got for the same set of initial conditions but for a far greater value of the magnetic field. The perturbation of the coulombic trajectory is no longer negligible and distorsions of the Kepler ellipse appear in the (ρ, z) projection. Here, a complete interpretation of the evolution can be achieved using the analysis of section 5.7. For the sake of illustrating some other aspects of the classical behaviour, we have plotted in Figure 6 some of the two-dimensional projections obtained at several values of the energy, at fixed magnetic field. The initial conditions have been chosen such that the excitation of the motion along $\vec{B}$ field is weak, the initial value of ρ at $t = 0$ being increased successively. Trajectories are expected to lie close to the $z = 0$ plane. In Figure (6 (-a to -d)) $(\rho, \dot{\rho})$ plots are shown for increasing values of the diamagnetic contribution to the energy. In Figure (6-a) the curves are still well defined and quasi-periodic. On Figure (6-b) a complete destabilisation of the trajectory occurs due to the onset of the strong mixing regime as the diamagnetic contribution to the energy is now extremely important. On Figure (6-c) one sees an example of ionization occuring in the z direction. If the diamagnetic part in the energy is still increased, one recovers a very simple situation where the trace is a closed curve followed over more than 100 times the period of the motion (Figure 6-d). For these very positive values of the energy, the motion is once again quasi

periodic as one enters the Landau regime [21]. On Figure (6 -e) one can see that in the strong field mixing regime there are still some regularities in (z, ż) plots although they are completely different in nature from those seen in the highly degenerated Landau and Coulomb regimes [22]. The purpose of Figure (5) and (6) is illustrative, allowing to understand that the passing from the Coulomb to the Landau regime fondamentally modifies the behaviour of the system which becomes more or less chaotic although some regular features are still remnant The initial conditions which have been adopted in the strong field mixing regime are the worse ones in the sense that they are very close to an hyperbolic point as found in the linear analysis of the stability of the system [21].

5.5 - POINCARE SURFACES OF SECTIONS

The more general trajectory in phase space takes place on a 3 dimensional surface. To the contrast the Coulomb and Landau situations are associated with one-dimensional surfaces, that is closed curves. Finding an extra constant of motion in a problem will allow to reduce by one the dimension of the surface. For probing such a possibility one is lead to show that for a set of trajectories having the same energy, 2-dimensional sections of phase space do not exhibit a random distribution of points. At the opposite, the distribution must be organized in curves which are sections of torus. Poincaré surface of sections are the intersections of the 4-dimensional phase space trajectory $(\rho(t), \dot{\rho}(t), z(t), \dot{z}(t))$ with the plane $z = 0$ as projected onto the $(\dot{\rho}, \rho)$plane when $\dot{z} > 0$. If the section is a closed curve, it means that an extra constant of motion will exist (in addition to the energy) which confines the 4 dimensional motion to the surface of a Torus.

Several attempts at this problem have been done recently [23][24][25][26] which give evidence of the existence of approximate constants of the motion.

Under some conditions, the aspects of the surface of sections follow the coarse classification of section 5.3. For energies and field values such that $E < E_c \sim -0.5(\gamma)^{2/3}$ (24) where E_{crit} is a critical energy the electronic motion is regular, that is, as shown on Figure (7) the Poincaré section give evidence of the existence of an approximate constant of the motion. The trajectories take place on Torus of phase space, the sections of which are seen on the plot of Figure (7) . These trajectories are quasi-periodic ones and obviously are associated with two very different classes of symmetries. This aspect which will be interpreted in section (5.7) is connected with the existence of an adiabatic invariant in the Coulomb limit. One must remark that the critical energy fulfills :

$$(\gamma/E_c^{3/2})^{2/3} \sim (n_c^3 B)^{2/3} \sim (n_c^3 \gamma)^{2/3} \sim \xi^{1/3} \sim 1 \qquad (99)$$

and is associated with the onset of the strong mixing regime as expected.

If one crosses the critical line of formula (99), irregular features appear in the motion of the electron as shown in Figure (8) . That is part of the trajectories at a given energy are no longer quasi-periodic. This is the onset of classical chaos in the system. A Poincaré section for such trajectories is shown on Figure (9) . Clearly the generic point almost fills the whole volume of phase space bounded by the caustics. Nevertheless this does not preclude the existence of remnant structures of Torii and of quasi-periodic orbits coexisting with regions where classical chaos takes place. This is clear in Figure (8) where the two types of behaviours can be seen.[26]

For higher values of the energy and field, when

$$E > \gamma L_z/2 = E_I \qquad (100)$$

where E_I is the ionization energy, it is likely one will recover more regular behaviours associated with the onset of the Landau regime. As in the Coulomb limit, adiabatic invariants will exist although they have not been found so far. They will allow to explain the transition to the pure Landau situation.

To conclude, these Poincaré sections allow to understand the evolution of the trajectories in between the Coulomb and Landau limits where highly degenerated motion will take place. The first kind of mechanisms are those associated with the high degeneracies of the two limiting situations. This allows the electron to choose among the set of classical ellipses at constant energy (either in the Coulomb or in the Landau limit) a trajectory which is still an ellipse but with the parameters slowly evolving with the perturbation (the diamagnetic one or the Coulomb one). In between, in the strong mixing regime, the existence of Torus is not forbidden but a large part of the motion is irregular. In some sense, this region is quite similar to the so-called classical resonance region or Hill's region in the problem of coupled harmonic oscillators.[27][28]

5.6 - THE STRONG MIXING REGIME AS A CLASSICAL RESONANCE REGION

Well-known examples of classical systems exhibiting instabilities and classical chaos are those dealing with coupled harmonic oscillators. As usually the equation of motion reduces to the Whittaker - Hill's form the instability regions are called Hill's or classical resonance regions [28]. This is also true for a lot of phenomena associated with paramagnetic resonance. One will show here that the strong mixing regime of diamagnetism shares some common character with these interesting questions of Modern Physics [29][30][31].

How can the present problem be put into the form of two harmonic oscillators interacting through anharmonic corrections ? This can be obtained using a

convenient set of coordinates in R(4) [9][17]. The hamiltonian for the Coulomb problem is then transformed into the one for a 4 dimensional isotropic harmonic oscillator :

$$\hat{H} = \vec{p}^2 - E_o \vec{r}^2 \qquad (101)$$

($\vec{p}$ and $\vec{r}$ are the 4 dimensional impulsion and coordinate), E_o is the Coulombic energy which plays the role of $(-\omega^2)$ where ω is the frequency of the oscillator. The Coulomb problem is equivalent to solving the harmonic oscillator problem in R(4) but for a constant value of its energy [9]. A particular choice of the coordinates in R(4) is of interest for dealing with the diamagnetic interaction [17]. It is :

$$\mu = (r + z)^{1/2} = \xi^{1/2}$$
$$\nu = (r - z)^{1/2} = \eta^{1/2} \qquad (102)$$

where ξ and η are the usual parabolic coordinates. This allows to reduce the 4 dimensional oscillator problem to two 2-dimensional uncoupled harmonic oscillators problems in perpendicular planes [17]. The expression of the diamagnetic interaction is then :

$$H_D = \frac{\gamma^2}{4} \mu^2 \nu^2 \qquad (103)$$

A further straightforward reduction of the problem can be achieved writing the equations in terms of a new parameter τ such that $\frac{dt}{d\tau} \alpha (\rho^2 + z^2)^{1/2}$. Neglecting the rotational term in the equations of motion, one gets the new form of the hamiltonian in (μ, ν) coordinates :

$$\tilde{H} = p_\mu^2 + p_\nu^2 - E(\mu^2 + \nu^2) + \frac{\gamma^2}{4}\mu^2\nu^2(\mu^2 + \nu^2) \qquad (104)$$

showing the equivalence with the problem of two harmonic oscillators having the same frequency, coupled through anharmonic corrections. The solutions of (105) which are relevant to the physical problem for the energy E, are those for which $\tilde{H} = 4$. These results have been obtained in a slightly different form using the Levi-Civita regularization procedure [32] by several authors [23][26].

An interesting feature comes from the aspect of the potential which is shown on Figure (10) where rotational energy is included. The $\mu = \nu$ line corresponds to motion in the plane $z = 0$ in R(3) and is associated with a ridge where the potential energy is maximum and varying as $\gamma^2\mu^6$. Two valleys are on each side of the ridge. Fano [33][34] earlier pointed out the importance of motion near this ridge for the dynamics and understanding of the quantum mechanical problem. Writing $E = 0$ in (104) allows to solve exactly the equations of motion. One then gets the exact condition :

$$n\,\gamma^{1/3} = 1.16 \qquad (105)$$

associated with the strong mixing regime [17][21]

The study of the stability of the motion along the ridge can be done after changing to a new sets of coordinates :

$$u = \frac{1}{\sqrt{2}}(\mu + \nu)$$

$$v = \frac{1}{\sqrt{2}}(\mu - \nu)$$

The motion along the ridge is then associated with $v \underset{\sim}{\sim} \epsilon \underset{\sim}{\sim} 0$. The u(t) solution of theequations of motion is then periodic :

$$u(t) \sim u_o \cos(\alpha t)$$

while replacing in the second equation, v(t) obeys :

$$\frac{d^2v}{ds^2} + (A + B \cos s + C \cos 2s) = 0 \qquad (106)$$

Equation (106) is of Whittaker - Hill's type and the regions of unstability are well known [28] and bounded with some curves depending on (A, B, C), then on the energy E. One can show that for energy values greater than $E_c \sim - 0.40$ the system enters an unstable region thus allowing to explain the coexistence of chaotic and regular motion in the plot of Figure (8) for E = - 0.35. The motion along the ridge is then not necessarily stable. Such an analysis (which has obvious limitations) shows that the strong field mixing phenomena is partly governed with the same kind of equations as in the coupled oscillators problem.

The fact that classical chaos appears in the strong mixing regime does not necessarily exclude the existence of an approximate dynamical symmetry. The true physical problem is that of the sizes of the regions of classical chaos compared to $\hbar^4$. From preliminary results by W.P. Reinhardt [26], it seems that there is still a possibility of building up an invariant which would be valid in this intermediate regime.

5.7 - ADIABATIC INVARIANT IN THE COULOMB LIMIT

The explanation of the regular behaviours observed below the transition energy and described in sections 5.3 and 5.5 has become possible with the

recent discovery of an adiabatic invariant valid in the Coulomb limit [35]. The search for it was up to that time not really unsuccessful[21][24] but no mathematical self consistent formulation was found. This was really existing as a by-product in an earlier paper of 1976 [36] dealing with group theory. The basic idea is that the problem is separable in impulsion space on the R(4) Fock hypersphere (in elliptico-cylindrical coordinates) [35]. This does not mean at all any separability in coordinate space, which really does not exist. Nevertheless this result is of importance for the classification of the quantum spectrum. But firstly it allows to derive the expression of the adiabatic invariant in the Coulomb limit, which is :

$$\Lambda = 4\,A^2 - 5\,A_z^2 \qquad (107)$$

where $\vec{A}$ is the Lenz vector as defined in equation (6). Λ is an adiabatic invariant and not a constant of the motion. Λ allows to describe how the zero-field Kepler ellipses are perturbed once the magnetic field is applied on the system and breaks the supersymmetry of the Coulomb problem. Classical trajectories are still ellipses at any time but their parameters are slowly evolving under the field action. How does this occur can be investigated using classical perturbation theory in averaging the equation of the classical motion on the unperturbed coulombic ellipse. Then it is possible to show that :

$$\frac{d}{dt}\langle\Lambda\rangle = 0\,(B^4) \qquad (108)$$

to fourth order in B field. The average value $\langle\rho^2\rangle$ of ρ^2 (proportional to the diamagnetic interaction) on the unperturbed ellipses is :

$$\langle\rho^2\rangle = -\frac{1}{2E^o}\left(4A^2 - 5A_z^2 + L_z^2 - \frac{1}{E^o}\right) \qquad (109)$$

where E^o is the unperturbed energy which fulfills equation (9) ot in atomic units

$$A^2 - 1 = E^o.L^2 \qquad \text{with} \tag{110}$$

$$\vec{A}.\vec{L} = 0$$

The perturbed energy E is then :

$$E = E^{(o)} - \frac{\gamma^2}{8E^{(o)}} \left(- \frac{1}{E^{(o)}} + L_z^2 - \frac{\Lambda}{E^{(o)}}\right) \tag{111}$$

or writing $E^o = - 1/n^2$

$$E = E_o + \langle H_D \rangle = - \frac{1}{n^2} + \frac{\gamma^2}{8} n^2(n^2 + M^2 + n^2\Lambda) \tag{112}$$

Practically, this means that the adiabatic turning on of the diamagnetic perturbation on an hydrogenic orbit specified with $(\vec{A}, \vec{L})$ will induce a slow evolution of the parameters of the trajectory (excentricity, directions of the axis) such that Λ is conserved to fourth order. Of course, such an analysis is valid provided the period of the evolution of the parameters of the ellipse is much larger than the period of the motion of the electron on the ellipse that is :

$$\gamma.n^3 << 1 \tag{113}$$

Direct numerical simulations allow to show that Λ is no longer constant if $\gamma n^3 \sim 1$ (21).

The existence of the adiabatic invariant allows to get some qualitative ideas on the evolution of the classical ellipse and very important results about

the symmetries of the trajectories in the Coulomb limit. From formula (107) to (112) one gets easily (in atomic units - n and m not necessarily integers here !) :

$$0 \leqslant A^2 < n^2 - m^2$$

$$-n^2 \leqslant \Lambda \leqslant 4(n^2 - m^2) \qquad (114)$$

$$0 \leqslant \langle \rho^2 \rangle \leqslant \frac{5}{2} n^4$$

and the highest value of Λ does correspond to the highest value of $\langle \rho^2 \rangle$ and of the energy. The evolution and symmetries of the orbits will be completely different following the sign of Λ. During the slow deformation of the ellipse, the extremity of the Lenz vector $\vec{A}$ moves on the surface :

$$4A_x^2 + 4A_y^2 - A_z^2 = \Lambda = \text{Cste} \qquad (115)$$

It is a one sheet hyperboloïd if $\Lambda > 0$ and a two-sheet one if $\Lambda < 0$. The orbits will then belong to two different classes. This is shown on Figure (11-a and -b).

When $\Lambda < 0$ the $\vec{A}$ vector (which is parallel to the major axis of the ellipse and fulfills (11) that is the excentricity is $\xi = A/n$) is on the average directed along the $\vec{B}$ field axis, one side of the plane $z = 0$ perpendicular to the field. The ellipse which is highly excentric if $\Lambda \lesssim -n^2$ will have a stretching and vibrational motion in the $\vec{B}$ direction. The same kind of motion will take place on the other side of the $z = 0$ plane. No coupling between these two kinds of trajectories can take place in classical mechanics.

On the other hand, if $\Lambda > 0$ the motion is completely different as can be seen on Figure (11-b). The $\vec{A}$ vector is allowed to move on the one-sheet hyperboloïd each side of the $z = 0$ plane. Thus, this set of trajectories will have some rotational symmetry around the $\vec{B}$ field direction. If Λ is close to its maximum value the $\vec{A}$ vector will be confined in the $z = 0$ plane. The very excentric motion of the electron will take place in the plane perpendicular to the field.

The evidence of the existence of two extreme types of symmetries of the classical trajectories in the Coulomb limit, roughly associated with libration and rotation, is an important result. The orbits having mainly a rotational symmetry are associated with motions in the plane $z \sim 0$ or motion along the ridge $\mu = \nu$. This appears to be an important indication for tackling the strong field mixing regime. On the other hand, it is clear that Λ is no longer an invariant in this regime.

5.8 - ADIABATIC INVARIANT IN THE LANDAU LIMIT

The search for an adiabatic invariant in the Coulomb limit and its discovery is probably a major step in the understanding of the present problem. Of course, another major step would be to have an explicit analytical form of the adiabatic invariant which is likely to exist in the other limit, the Landau one. This turns out to be complicated using classical perturbation theory [21]. Nevertheless, one can get a coarse idea about the structure of such an invariant using the various constants of the motion (r_o^2, x_o, y_o) in the Landau limit (see section 3).

5.9 - OTHER MEANINGS OF THE STRONG MIXING REGIME

We will end these considerations on classical mechanics by giving some equivalent formulations of the strong field mixing regime [19] [20]

From the equality of the diamagnetic and Coulomb forces, one has deduced that it takes place when :

$$\gamma . n^3 \simeq 1 \qquad (116)$$

As the Coulomb contribution to the energy is of the order of $(-1/n^2)$ while the diamagnetic one is of the order of $n\gamma$ (in atomic units), this means that when (116) is fulfilled, then :

$$E \simeq E_c + E_D \simeq 0 \qquad (117)$$

that is the regime takes place near the zero-field ionization threshold.

Now, considering the atomic sizes, the Coulomb radius is of the order of $n^2 a_o$ while of the order of $\sqrt{n}\, a_c$ in the Landau approach. When (116) is fulfilled, $n^2 a_o \sim \sqrt{n}\, a_c$ meaning that the dimension of the orbit (n) is the same while evaluated in the two approaches. (116) also means that the classical frequencies associated with the Coulomb and Landau problems are just equal.

Finally, one can say that the strong field mixing regime takes place when the two forces are of the same order of magnitude, or the classical frequencies of the equivalent oscillators are equal. This occurs near zero energy of the electron close to the zero field ionization limit. The sizes of the atomic orbits are then condensed compared to the zero field situation due to the extra binding action of the diamagnetic force. A more rigorous formulation can be derived from generalized Bohr's models [3][37].

6 - QUANTUM MECHANICAL APPROACH

The quantum understanding of the diamagnetic spectrum is far from being complete. This is of course associated with the very few number of constants of the motion (L_z and parity) which commute with the hamiltonian of equation (90). In spite of the fact that the two limiting Landau and Coulomb situations are well understood and have conceptual importance, it is likely that no further attempts at this problem after those of Jenkins and Segree [5] and Schiff and Snyder [18] in 1939 would have been performed if experiments have not shown that, for all atoms, the atomic spectra still presents very simple characters in the intermediate regime near and above threshold. Such a simplicity in the quasi-Landau spectrum of Garton and Tomkins [6], in a situation where all intuitous arguments suggest on the contrary strong complexity reveals the basic conceptual importance of the situation [7].

So far as the quantum aspects are concerned, only few progresses have occurred since 1939 [37]. The problem is really a tremendous one, due to the necessity of dealing with continuum states. To compare, the Stark problem which shares some common characters can be solved easily as the hamiltonian is separable in parabolic coordinates due to the existence of an exact dynamical symmetry associated with the Lenz vector. The existence of such a symmetry being still an elusive question in the present problem, the quantum approaches are rather undeveloped. Near and above threshold no attempts have ever been done except in the framework of WKB theories (see section 7). Finally quantum attempts have been essentially developped for dealing with the unter ℓ and inter n mixing regimes. Really, they provide us now with deeper understanding of those regimes first studied by Schiff and Snyder [18]. But this in consequence of the recent discovery of an adiabatic invariant in the Coulomb limit, as discussed in section 5.

Hereafter, we will use atomic units. The one-particle hamiltonian (90) takes the form :

$$H = p^2 + \gamma L_z + \frac{\gamma^2}{4}\rho^2 - \frac{2}{r} \qquad (118)$$

where γ is defined through (95). The diamagnetic hamiltonian H_D is :

$$H_D = \frac{\gamma^2}{4}\rho^2 \qquad (119)$$

6.1 - COULOMB INTER ℓ MIXING REGIME

In this region the diamagnetic term is small compared to the zero-field hamiltonian. Nevertheless its role cannot be neglected as it breaks the supersymmetry of the Coulomb problem once the magnetic field is non-zero. Obviously, this is associated with the non-zero commutation rule of the diamagnetic hamiltonian H_D with both A_z and L^2. Neither ℓ, not $(n_2 - n_1)$ are good quantum number but the principal quantum number n is still defined. As a first step, the diamagnetic interaction can be considered as a perturbation acting on the degenerate hydrogenic manifold. The diamagnetic term being of the order of $\gamma^2 n^4$, this is valid provided the perturbation is small compared to the spacing $2/n^3$ of adjacent manifolds, that is :

$$\gamma . n^{7/2} \ll 1 \qquad (120)$$

As L_z and parity are constant of the motion, the diagonalization of H_D can be performed seperately on each subspace with fixed M and parity. From (119) diagonalizing H_D is equivalent to finding the eigenstates and eigenvalues of ρ^2 in the hydrogenic manifold. This can be done in one of the numerous basis of the Coulomb problem defined in section 2.

These eigenstates will be written $|n\ K\ M\ \Pi\rangle$ where K is a label replacing the ℓ or $(n_2 - n_1)$ value of the usual basis. They are field independant and solutions of the field free Coulomb problem although not of the usual type. Writing

$$H = H_o + H_D \tag{121}$$

one has :

$$H_o|n\ K\ M\ \Pi\rangle = (-\frac{1}{n^2} + \gamma M)\ |n\ K\ M\ \Pi\rangle$$

and

$$H_D|n\ K\ M\ \Pi\rangle = E^{NK}(M,\Pi)\ |n\ K\ M\ \Pi\rangle$$

Obviously at this order of perturbation theory, E^{NK} the diamagnetic correction to the energy varies as B^2 with B field and can be written under the general form :

$$E^{NK}(M,\Pi) = \frac{\gamma^2 n^2}{4}\ (n^2 + m^2 + m + n^2\ \Lambda_K) \tag{122}$$

where Λ_K is the eigenvalue of the quantum operator associated with the adiabatic invariant defined in (107)

The eigenstates $|n\ K\ M\ \Pi\rangle$ are the eigenstates of ρ^2 in the manifold. The label K varies from 1 to the maximum possible value of the order of n/2 as they have definite parities. They can be expressed as :

$$|n\ K\ M\ \Pi\rangle = \sum_{L} C_{L}^{NK}\ |n\ L\ M\rangle = \sum_{n_1 n_2} d_{n_1 n_2}^{nK}\ |n_1\ n_2\ M\rangle \qquad (123)$$

in the spherical $\{nL^2L_z\}$ or parabolic $\{nA_zL_z\}$ representations. Typical variations of the energies E^{NK} and the structures of the diamagnetic manifold are displayed in Figure (12). With the present convention, the K = 1 state is the one for which the energy increases the faster, that is from (122), Λ_K is maximum. States associated with maximum values of K on the contrary have the smaller increase in the energy.

6.2 - PROPERTIES OF THE EIGENFUNCTIONS IN THE INTER & MIXING REGIME

The $\{n\ K\ M\ \Pi\}$ are common eigenvectors of H_o and of the projection of ρ^2 on a given hydrogenic manifold. Calling $\{\tilde{n}K\ M\ \Pi\}$ the basis of eigenvectors of (118), it fulfills :

$$|\tilde{n}K\ M\ \Pi\rangle \rightarrow |n\ K\ M\ \Pi\rangle \qquad \text{where } \gamma^2\ n^7 \ll 1 \qquad (124)$$

showing that the $\{n\ K\ M\ \Pi\}$ are the limiting form of the eigenvectors in the Coulomb limit. They are the only set which respects the symmetry in the manifold which is broken once the field is non zero.[38][39]

The $\{n\ K\ M\ \Pi\}$ can be characterized by the means of their spatial electronic density and nodal surfaces distributions, which obviously have cylindrical symmetry around $\vec{B}$. Such a (ρ, z) plot of nodal surfaces is shown in Figure (13) for n = 17, M = $\pm$ 3 and odd parity states. The lines represent the ensemble of points where the $\langle\rho\varphi|nKM\rangle$ wavefunction is nul. Obviously these nodal surfaces are far different from those of the usual spherical basis (equation (20)) which are an ensemble of spheres and cones which cross each other (a result associated with the separability of the angular and radial equations and with the spherical

symmetry of the zero field problem). The eigenstates of the restriction of ρ^2 in the manifold cannot have these properties but for a rotational invariance around $\vec{B}$. From Figure (13) one can see how the nodal surfaces are built from the merging of cones and spheres of the usual spherical basis with as a result a completely new aspect of the patterns and of the symmetries. As shown on the enlargement of Figure (14) , the nodal lines here, never cross, meaning that no separability in coordinate space is allowed. But the spatial anticrossings are extremely small of the order of a_o while the extension of the wavefunction is of the order of $n^2 a_o$.(39)

The second important feature connected with nodal surfaces is that the drawings near the core are much more complicated that the one far from the core. Inside, the details suggest an analogy with what happens in bifurcation processes as for example for the two harmonic oscillator systems (27). Outside, the patterns are much more regular and can be associated with vibrational patterns along $\vec{B}$ field for the maximum K values.

The major feature in Figure (13) is the evidence of the very different symmetries of the wavefunctions following K. From K = 1 to K = 7, the symmetry evolves from rotation to vibration along B field. The diamagnetic structure of the hydrogenic manifold looks like the rovibrational bands of molecules. On Figure (14) , we have plotted the isoelectronic lines for which $|\Psi|$ is greater than 3.10^{-5} . Obviously, the K = 1 density distribution looks like that of a prolate spherical top with a maximum concentration in a disk around the z = 0 plane perpendicular to the field. The extension along the field direction is small compared to the one along the ρ axis. Indeed such a state can be shown to present an overall O(3) rotational symmetry (40), although not of the usual type. The electronic density distribution for the K = 7 state at the bottom of the diama-

gnetic band completely differs from the previous one. The extension along B field is several times greater than the transverse one. It looks like a vibrational state in the B field direction. Of course, it is not surprising that K = 1 and K = 7 states have very different transverse extensions. Indeed they are proportional to $\langle\rho^2\rangle_K$ which is maximum for K = 1 states in the manifold.

Such a rovibrational structure of the diamagnetic manifold can be justified using more powerful arguments of group theory (see section 6.5). In Figure (15) is a plot of the electronic densities of the (n K M,$\Pi = \pm 1$) states for the two values of the parity. The label k used here is slightly different from our previous definition, as it is used for each state in the (n M) manifold,[38] whatever the parity. These plots show that the previous conclusions are roughly valid but certainly not in detail.

Another interesting feature is that following the parity Π_z along z axis, the states will have or not a node in the z = 0 plane. In the plot of nodal surfaces of Figure (13) , the parity was odd with M = 3. That is the parity along z axis was even as :

$$\Pi_z = \Pi(-)^M \qquad (125)$$

with a non zero value of the electronic density in the z = 0 plane. Of course, for the other set of states belonging to the same manifold , with opposite value of the parity, there is a node in the z = 0 plane. This can be seen on the right part of the plot of Figure (15) . This feature is extremely important. The electronic density distribution in Figure (15) , for states with small K values and opposite parities, are completely different. Consequently their diamagnetic energies proportional to $\langle\rho^2\rangle$ will differ. Such states with rotational symmetry at

the top of the diamagnetic band are not likely to have the same properties and energies. On the other hand, as can be seen on Figure (15) , states with maximum values of K are strongly peaked along the z axis whatever the parity and present the same general vibrational symmetry. The fact that there is a node or not in the $z = 0$ plane is here not of importance as the wavefunction is almost zero in this region. This means that the states at the bottom of the diamagnetic band will have almost the same diamagnetic energy and will more or less be degenerated following the parity. This result has been previously derived by C.W. Clark [41].

Coming back to the classical analysis of section 5.7, all these results become evident. States with the minimum values of K, at the top of the diamagnetic band, are associated with maximum values of $\langle\rho^2\rangle$ and of the adiabatic invariant Λ which fulfills equations (114) They are associated with classical trajectories in which A^2 is maximum and $\vec{A}$ belongs to the one-sheet hyperboloïd of Figure (11) . Then it is not surprising that these states are concentrated near the $z = 0$ plane and exhibit an approximate O(3) symmetry. States at the bottom of the band are associated with minimum values and Λ and ρ^2 and with trajectories in which the Lenz vector $\vec{A}$ lies on the two sheet hyperboloïd of Figure (11) . Their symmetries will be roughly of vibrational type. Quantum mechanically speaking, $\vec{A}$ might jump from one sheet to the other one through tunnelling. This allows to understand why states with different parities at the bottom of the band will be almost degenerated.

Finally, one can remark that the states with minimum values of K are associated with motion near the plane $z = 0$ or motion along the ridge $\mu = \nu$ inFigure (10) . Following the values of K and Π_z, these states will be concentrated near the ridge or will have nodes on the ridge [33] and in the crossed direction [42]. But the states which are confined in the potential valleys of Figure (10)

, far from the ridge, will have an approximate O(2) x O(2) symmetry associated with vibration and only small couplings through the barrier. This is another way of explaining the degeneracy at the bottom of the diamagnetic bands. The very special patterns of the nodal surfaces for these states may possibly be a remnant of the chaotic behaviours of the classical trajectories observed in strong field mixing conditions. The patterns of nodal surfaces of K = 1 states associated with motion along the ridge are obviously much more regular.

The last important question is that of the properties of these eigenstates under optical excitation. The intensity of the various lines are proportional to $|\langle i|\vec{\epsilon}.\vec{r}|nKM\Pi\rangle|^2$ where $|i\rangle$ is the lower state of the transition usually unperturb by the diamagnetic interaction and proportional to a spherical harmonics. $\vec{\epsilon}$ is the polarization of radiation. From (123), all the $|n\ K\ M\ \Pi\rangle$ states with appropriate values of parity and M will be excited. But, following the parity Π_z, the $|nKM\Pi\rangle$ may have a node in the z = 0 plane. Then the efficiency of optical excitation will differ following the polarization $\vec{\epsilon}$. This is quite clearly shown on Figure (16) where a plot of the intensities of the lines is given for even and odd parity along the z axis. For even parity along z axis, the efficiency of optical excitation of K = 1 states is very important and decreases with the value of K. This means that the overlap of the $|n\ K\ M\ \Pi\rangle$ state with the spherical harmonics of lowest ℓ_o value in the manifold is maximum. The overlap between $|n\ \ell_o\ M\rangle$ and the other K states being smaller and smaller with K. Then in (129) the $C^{NK=1}_{L=\ell_o}$ coefficient is maximum for Π_z even. On the other hand, if the z parity is odd, the $|n\ K=1\rangle$ states have a node in the z = 0 plane meaning that the overlap with the lowest order spherical harmonics $|n\ \ell_o\rangle$ will be weaker. The optical absorption strength will be more sensitive to the spatial extension of the wavefunction and compared to the previous situation must be smaller as the ground state is peaked around the origin where $\langle\rho\varphi|n\ K=1\rangle$ does have a minimum at z = 0. Really,

as shown on Figure (16), the K = 1 state no longer has the greatest probability of optical excitation and the distribution of oscillator strengths is spread over the various values of K. These features turn out to be of extreme importance for the interpretation of the experimental data and for the understanding of the quasi-Landau phenomena. Some of these results could be derived using the classical analysis of section 5.7.

6.3 - INTER N MIXING REGIME

As shown on Figure (12), if the field or energy are increased, one enters the inter n mixing regime in which the diamagnetic manifolds merge. This occurs when :

$$\gamma^2 n^7 > 1. \qquad \gamma n^3 \ll 1 \tag{126}$$

The Coulomb principal quantum number n is no longer a good quantum number, but the diamagnetic interaction is not yet dominant over the Coulomb interaction. The eigenstates $|\tilde{n} K M \Pi\rangle$ are not known. They can be obtained with limited accuracy through the diagonalization of the hamiltonian in a $\{n K M \Pi\}$ basis involving as much manifolds as possible. That is :

$$|\tilde{n} K M \Pi\rangle = \sum_{n_o K_o} \alpha^{n_o K_o}_{nK} \; |n_o K_o M \Pi\rangle \tag{127}$$

where the α coefficients now depend on the magnetic field strength. No close form of (127) have ever been obtained as a consequence of the R(3) non-separability of the hamiltonian. The only way of getting the eigenvectors in the inter n mixing regime is through numerical calculations. But as H_D couples any state with, in particular, continuum states, there are practical limitations !

One can nevertheless develop some intuitous arguments helping to understand this regime. First of all, the diamagnetic contribution to the energy will no longer behave as B^2. This is the main result of the interaction of the n manifold with the other ones. As the repelling action of states above n is stronger, the increase of the energy will become smaller than B^2. This is to be expected as in the Landau limit, it must increase linearly with B field.

Secondly, important informations can be drawn from the fact that the states in the inter ℓ mixing regime have very different limiting symmetries. Numerical diagonalizations allowed to show, two years ago [38][39], that the $|n, K=1\rangle$ states and the $|n+1, K_{max}\rangle$ states are only weakly interacting through H_D. As shown in Figure (17) , the sizes of the anticrossings between these states are exponentially small varying as e^{-2n}. At the opposite, one can show that the states $|n, K=1\rangle$ and $|n+1, K=1\rangle$ are strongly interacting with as a consequence a smaller rate of increase of the energy with B field. Such features were considered as a clue of the existence of an hidden approximate dynamical symmetry in the problem [38]. But of course, this is now quite well understood from the symmetry arguments developped in sections 5.7 and 6.2 showing the existence of an adiabatic invariant in the Coulomb limit. The approximate O(3) and O(2) x O(2) symmetries of the $|n, K=1\rangle$ and $|n, K_{max}\rangle$ states are quite different ensuring the weakness of their anticrossings. The exponential size of the anticrossing comes from the fact that the spatial overlap of the wavefunctions occurs in classically forbidden regions where they behave as e^{-n}. This is also to be expected from the picture of motion along the ridge [33][34] as the two types of motion will take place respectively on the ridge or in the double valleys. The overlap will then be small.

One can conclude that the $|n\ K\ M\ \Pi\rangle$ states will essentially interact with the other ones belonging to the same class of symmetry. This supplies with

a coarse model in which the spectrum is composed of a set of several weakly interacting series [43]. Each serie is identified through {K M Π} where the Label K is associated with the Λ_K eigenvalue of

$$\Lambda = 4\,A^2 - 5\,A_z^2 \qquad -$$

in the low field limit. Such a view is in agreement with the analysis of section 6.4, as well as with experimental results.

In the lack of any real separability in coordinate space, and taking advantage of the previous remarks, it is likely that some clever choice of basis sets will simplify numerical calculations. Of course, suitable basis are not expected to be the same for K_{min} and K_{max} states because of their different symmetries.

For the states associated with small values of K, with approximate O(3) symmetry the use of a modified parabolic basis can be shown to be convenient [40][44], as the off diagonal elements of H_D become small in the transformation. This is innerly connected with the possibility of using various sets of generators of the Lie group in the R(4) approach of the Coulomb problem [9]. For example, using Wigner-Eckardt theorem, one gets

$$\vec{r} = \frac{3}{2}\, n\, \vec{A} \qquad (128)$$

in the manifold so that the diamagnetic interaction takes the form [44]:

$$H_D = \frac{\gamma^2}{4}\rho^2 = \frac{9\gamma^2}{16}(A_x^2 + A_y^2) \qquad (129)$$

The operator $\vec{\lambda}$ (A_x, A_y, L_z) possesses all the properties of an angular momentum as can be seen from the results of section 2.2. Then from (129), the restriction of H_D to the manifold is proportional to $(\lambda^2 - \lambda_z^2)$. From equations (14), (15), (16) which define $\vec{j}_1$ and $\vec{j}_2$, it is clear that a possible choice of representation for the Coulomb spectrum is $\{j_1^2\ j_2^2\ j_{1z}\ j_{2z}\}$ where the two angular momentum are not coupled. In a given manifold, the choice of the coupled representation $\{j_1^2\ j_2^2\ \lambda^2\ \lambda_z\}$ allows to diagonalize the diamagnetic hamiltonian. The wavefunctions are then linear combinations of the usual parabolic wavefunctions with convenient phase factors and the coefficients of the expansion are the Clebsch Gordan coefficients. These wavefunctions are certainly extremely useful for tackling the inter n mixing regime. In addition, as H_D is proportional to $(\lambda(\lambda + 1) - M^2)$ in this representation, the analogy with states of the oblate spherical top becomes clear. Due to the definition of $\vec{\lambda}$, one can also conclude that the O(3) symmetry of the states is not of the usual type.[40]

For states associated with large K values, at the bottom of the band, the symmetries are approximately O(2) x O(2) and an approximate set of constants of the motion is $\{A_z^2, L_z\}$. This means as first pointed out by C.W. Clark [41] that the use of the parabolic basis is appropriate, for dealing with such states in the inter n mixing regime.

6.4 - THE STURMIAN APPROACH OF THE INTER N AND STRONG MIXING REGIMES

The only accurate quantum study of these regimes has been done using a Sturmian representation of the Coulomb spectrum [42]. The Sturmian are complete sets of discrete non orthogonal functions allowing to represent the hydrogenic spectrum, while taking into account continuum states [45] through a discrete representation. The convergence of the expansions needs to use a large basis of Sturmian functions and the use of Cray computers. Some of these numeri-

cal simulations [42][43] are shown on Figure (18) for atomic hydrogen. They are limited to negative values of the energy due to accuracy and convergence requirements. The results partly confirm intuitous arguments given in 6.2 and 6.3. They are also in agreement with experimental results (see section 8).

First of all, one can see in Figure (18) that the atomic spectrum is far different following the parity of states along z axis. This was explained in 6.2 in inter ℓ mixing conditions and is still valid in inter n mixing conditions and also near the zero field threshold. The main result is that when the z parity is even (that is $(-)^{\ell-M} = +1$), the K = 1 lines are still dominant in the inter n mixing regime. To the contrast regular features are hardly distinguishable for odd z parity once the various manifolds are merging.

Secondly, in the plot for even z parity, the secondary lines associated with K = 2 ... states do not strongly interact with the other ones. This confirms the previous view of non interacting or weakly interacting series of lines associated with the various K states, precursors of the quasi-Landau spectrum in the low-field inter ℓ mixing regime. In addition, and this will be discussed in section 7, the positions of the various lines agree fairly well with the predictions of semi-classical theories in which one assumes a very weakly excited motion along B field. These various series for several K values are shown on Figure (19) .

6.5 - GROUP THEORETICAL MEANING

The fact that the wavefunctions have very nice symmetry properties in the inter ℓ mixing regime can also be deduced from group theoretical analysis in $\{\vec{p}\}$ representation on the Fock hypersphere [40]. This allows to deduce the form of the adiabatic invariant (107) and to get the wavefunctions in the inter ℓ regime. Such an analysis allows to point out the O(3) symmetry of the states at the top of

the band (with strong analogy with those of an oblate spherical top) while the states at the bottom of the band lie in a double potential well and have an approximate O(2) x O(2) vibrational symmetry. They are faintly coupled through tunnelling which explains their quasi-degeneracy in parity operation. The diamagnetic band looks like the rovibrational structure of a molecule. This approach allows also to confirm the relationship between the present problem and that of classification of doubly excited states in atoms. This was earlier pointed out by Fano [46] on the basis of the ridge behaviour shared by the two problems [40].

Of course, the fact that the problem separates in $\vec{p}$ space in R(4), in ellipso-cylindrical coordinates [9][35][40] does not mean it separates in real space, as this separability occurs on a given energy shell of R(4). In other words, this means that

$$\Lambda = 4\,A^2 - 5\,A_z^2$$

only approximately commutes with the hamiltonian.

6.6 - STRONG MIXING AND LANDAU REGIMES

The previous considerations, some of them are from very recent work, sum up the state of the art as concerns the quantum approaches at diamagnetism. Due to the lack of separability and to the involvement of continuum states, no quantum approach have been developped near and above threshold. Continua states obviously play an important role. Once the field is applied, whatever its strength, a complete discretization of continua occurs with the appearances of resonances rather than bound states recalling the possibilities of ionization along the B field direction. Actually no quantum description of these states exists and their properties are unknown. Then the problem of the correlation diagram between the Coulomb and Landau limits is still an open one.

6.7 - NON-HYDROGENIC ATOMS

The first role of non-coulombic corrections to the potential will be to break the supersymmetry of the Coulomb problem. This means that $|n, \ell\rangle$ states will no longer be degenerated in zero-field. For low field values, the diamagnetic interaction will be negligible compared to the quantum defects associated with neighbouring levels. A first regime will exist in which the only role of the diamagnetic interaction will be to increase the energy of the level by the amount

$$\Delta E_D = \langle n\ell m|H_D|n\ell m\rangle = \frac{q^2B^2}{8m} a_o^2 \frac{n^2[5n^2+1-3\ell(\ell+1)][\ell^2+\ell-1+m^2\ell]}{(2\ell-1)(2\ell+3)} \qquad (130)$$

which is derived from conventional first order perturbation theory. In addition, due to the mixing of the wavefunctions, several weaker lines will appear.

In a second regime, the diamagnetic term will become dominant over the non-coulombic contributions and the patterns will more or less look like the one got in the purely hydrogenic case, as concerns the energies. But with the main difference that the oscillator strengths associated with the various K components will be still extremely sensible to close range corrections to the potential. This means that the intensity patterns are extremely different from the one shown in Figure (16) and in Figure (18) . It is likely that in the absence of the dominant features associated with the K = 1 lines in purely hydrogenic situations, the interpretation of the experimental data will be difficult.

6.8 - ULTRA-HIGH FIELD LIMITS

If $B > B_c$ or $\gamma > 1$, the quantum problem is almost completely solved. This is the domain of ultra high fields [37], or of solid state physics of excitons [1]. The wavefunctions are then of Landau type as concerns the transverse

part while the longitudinal part is the solution of a one-dimensional Coulomb problem [47][48]. Such an approach is valid as $\gamma >> 1$ authorizes to perform the adiabatic approximation for the z motion. Several interesting questions are still unsolved but we will not discuss these high field aspects here.

7 - SEMI-CLASSICAL METHODS

Lacking any quantum theoretical approach of the strong mixing regimes, the only way of getting predictions is through semi-classical theories. It seems quite convenient as we deal with highly excited states. Indeed such attempts have been done earlier and allowed important advances in the understanding of the various mechanisms [49][50][51]. Unfortunately, there is still here a major difficulty which is, as expected, associated with the non-separability of the hamiltonian.

7.1 - SEMI-CLASSICAL QUANTIZATIONS OF NON-SEPARABLE PROBLEMS

The usual Bohr-Sommerfeld quantization conditions apply to one dimensional problem under the form (γ_i the Maslov index [52]) :

$$\oint p_i \, dq_i = (n_i + \gamma_i)h \tag{131}$$

and then cannot be used for non-separable ones. (131) is of no use except in the two limiting situations of Landau and Coulomb motions. This does not apply in between. The right way of performing a semi-classical quantization of the present problem is to use E.B.K; (Einstein - Brillouin - Keller) quantization which was first suggested by Einstein [53][26]

$$\oint c_i \vec{p} \cdot d\vec{q} = (n_i + \gamma_i)h \tag{132}$$

The paths C_i are not classical trajectories but topologically distinct fundamental paths on the surface of the torus in phase space, while the n_i are the quantum numbers associated with these independent paths. Such quantizations on Torii need the study of the classical motion. This is one of the reasons for which classical studies as those described in section 5 are of importance in the present situation Actually there is no real proof of the survival of Torus in the intermediate regime where $n^3\gamma \sim 1$. Then (132) may not apply. But more general methods based on the Feynmann path integral techniques do not require such an existence and can be used [31][54]. Nevertheless, although these methods are the only rigorc ones, they have not been applied so far to this problem, due to their evident complexity. Then the conclusions are clear : there is presently no correct semi-classical predictions available. But this does not mean that the various approximate semi-classical theories which have been developped are not of interest.

7.2 - APPROXIMATE SEMI-CLASSICAL QUANTIZATION OF THE TRANSVERSE MOTION

As shown in section 6, the dominant lines in the spectrum are associated with wavefunctions concentrated near the $z = 0$ plane and at least having low degree of excitation along B field. In addition the main reason for the non-separability of the hamiltonian in cylindrical coordinates is the coupling between the z and ρ motion. Making the approximation $z = 0$ in the hamiltonian allows to deal with a one dimensional problem in ρ. The Bohr-Sommerfeld quantization of such a problem is then possible. One gets (in atomic units) :

$$\int_{\rho_1}^{\rho_2} \left(E_\perp - \gamma^2\rho^2/4 + \frac{2}{\rho} - \left(|M| + \frac{1}{2}\right)^2/\rho^2\right)^{1/2} d\rho = (N_r + \alpha)\,\pi \qquad (133)$$

where (ρ_1, ρ_2) are the classical turning points, while the expression for the rotational term has been choosen in order to respect the low field diamagnetic behaviour for the $K = 1$ line. In this limit, n_r and the Coulomb quantum number n

are connected with

$$n = n_r + |M| + 1$$

assuming $\alpha = \frac{1}{2}$ in (133)

Obviously, such an approach suffers from various shortcomings and difficulties. It does not account for the effect of the motion along $\vec{B}$ field which will be responsible for the presence of the secondary lines or important effects as autoionization ! Furthermore, it does not reproduce correctly either the Coulomb limit (obtained with $\alpha = \frac{1}{2}$ in (133)) or the Landau one (got for $\alpha = \frac{1}{4}$ in (133). This means at least that α in (133) smoothly depends on the field and energy. Then (133) cannot afford exact predictions for the energy levels due to its 2 dimensional approximation of the real 3 dimensional problem.

Nevertheless formula (133) is of interest provided one does not need absolute predictions. Especially predictions through (133) are in good overall agreement with both the experimental results and the numerical simulations of Clark and Taylor for the K = 1 lines.[43] If one cannot trust (133) for absolute determinations of the positions, the predictions of the spacings of the lines are correct and in good agreement with the quantum calculations in the Coulomb inter n and inter ℓ mixing regimes. Then (133) fairly well describes the general behaviour of K = 1 lines, associated with wavefunctions concentrated near the z = 0 plane.

From (133), one easily derives the major features of the strong mixing regime ; that is near the zero energy threshold, one has :

$$n_r + \frac{1}{2} = 1,16\ (B_c/B)^{1/3} \qquad (134)$$

which is the exact form of the quantization law $n^3\gamma \sim 1$. The expression of the spacing of the resonances at threshold is [50][51] :

$$\frac{dE}{dn_r} = \frac{3}{2}\hbar\omega_c \qquad (135)$$

which is the spacing experimentally found by Garton and Tomkins [6][55]. This explains why (133) or modified forms are still widely used up to now.

7.3 - EXACT SEMI-CLASSICAL QUANTIZATION OF THE 3-DIMENSIONAL MOTION IN THE COULOMB LIMIT

The recent discovery of the adiabatic invariant Λ allows now to perform an exact semi-classical treatment of the three dimensional problem in the Coulomb limit. The problem being approximately separable, one can use the Bohr Sommerfeld conditions or quantization on invariant torii through (132) ; one gets[35] :

$$\int_{\theta_1}^{\theta_2} L_\perp(\theta).d\theta = \pi(K + \frac{1}{2}) \qquad (136)$$

where θ is the angle between the Lenz vector $\vec{A}$ and $\vec{B}$ and $L_\perp$ is the component of the angular momentum perpendicular to the $(\vec{A}, \vec{B})$ planes. The explicit expression of $L_\perp^2$ is :

$$L_\perp^2(\theta) = n^2(1 + \frac{\Lambda}{1 - 5\sin^2\theta}) - \frac{m^2}{\sin^2\theta} \qquad (137)$$

where n and m are associated with the quantization of the energy and L_z. From (136) one gets the quantized eigenvalues Λ_K of Λ and finally formula (112) for the energy. Such a procedure is rigorous in the Coulomb limit as the 3 integrals of

the motion (H_o, Λ , L_z) which are in involution, do define a Torus in phase space. This is then equivalent to the topological semi-classical E.B.K. quantization [26]. As a result the predictions are here in excellent agreement <u>for all the K states</u> in the manifold with the quantum calculations. Of course the method does not suffer from the various shortcomings described in section 7.2.

7.4 - 3-DIMENSIONAL SEMI-CLASSICAL APPROACH IN THE LANDAU LIMIT

Finally one must stress upon the fact that a very early attempt at this problem has been done in 1966 by Monozon and Zhilich [56][57]. Although the model has been developped in conditions where $\gamma >> 1$, it seems to have fairly wider validity. The basic idea is to use the adiabatic approximation in the Landau limit and a formula similar to (133) in which the classical turning points ρ_1 and ρ_2 depend on the z variable. This allows to deduce proper adiabatic potentials for the z motion. Further semi-classical quantization of the 3 dimensional motion allows to get two limiting formula for the energy spectrum :

- for excited motion along z with quantum numbers n

$$E = \gamma (2N_r + |M| + M + 1) - \frac{1}{(n + \delta_n)^2} \qquad (138)$$

- for low degree of excitation along B field :

$$E = (2N_r + 1)\gamma \left(1 - \frac{2}{\sqrt{2\gamma}} \frac{1}{(2N_r + 1)^{3/2}} + \left(\frac{1}{2\gamma}\right)^{1/4} \frac{(n + 1/2)}{(2N_r + 1)^{7/4}}\right. \qquad (139)$$

(138) is the well known [37] expression, valid if $\gamma >> 1$, in which the motion along B field is described through a one dimensional Coulomb type potential. While (139) is much more interesting for our present purposes, as it is a 3 dimensional approach of the spectrum when the degree of excitation of the longitudinal

motion is weak. Surprisingly, one gets from (139) :

$$\text{for } E \underset{\sim}{\sim} 0 \qquad \frac{dE}{dN_r} = \frac{3}{2}\hbar\omega c \qquad \text{and } N_r^3.B \sim B_c \tag{140}$$

while the secondary structures associated with the longitudinal motion fulfills :

$$E \underset{\sim}{\sim} 0 \qquad \frac{dE}{dn} = \frac{\hbar\omega_c}{2\sqrt{2}} \tag{141}$$

This means that in between two successive principal lines (N_r, n = 0) and (N_r + 1, n = 0), three secondary lines associated with (N_r, n = 1, 2, 3) will appear. As the frequencies are not commensurable and will slightly evolve with E and B, the spectrum will take a chaotic aspect as local reinforcements of lines will occur. This is not far from the pictures got by Clark and Taylor (see Figure (19)). From (139) quasi degeneracies of lines associated with (N_r, n), (N_r - 1, n + 4), ... will occur

With this model, K = 1 lines would be associated with (N_r, n = 0) states (with weak excitation along B field) while the other K lines would be with n = 1, 2 ... degrees of excitation along B field. Finally, (139) would suggest that the quasi Landau spectrum at threshold is band-structured [56], the bottom of the bands being associated with K = 1 states.

At the end, (139) suggests that a rigorous semi-classical quantization is possible from the Landau limit and only needs to discover the analytic form of an adiabatic invariant in this regime. This would be another major piece of the puzzle.

8 - EXPERIMENTAL STUDIES IN ATOMIC PHYSICS

So far as the advances in the understanding of this problem are concerned, the role of experiments has been a major one. This begins in 1969 with the experimental discovery of the quasi Landau resonances with $\frac{3}{2}\hbar\omega_c$ spacings near threshold. At that time, they were rather considered as smooth modulations of the continua oscillator strengths. Further experimental attempts have shown the general character of the phenomena for all atoms. These early experiments were performed using optical absorption, with classical sources and high resolution spectrometers. Since 1977, with the advent of pulsed and c.w. dye lasers, numerous kinds of new experiments have been developped [58][59][60][61]. Some of them using very high resolution techniques, have allowed major advances, experimentally probing that the quasi Landau phenomena affects well-defined series of discrete lines from the Coulomb to the Landau regions. The results of these experiments were a strong motivation for new theoretical works as discussed in section 7. We will review here the more striking features of these experiences. But before, we will stress upon the characteristics of the ideal experiment which certainly will be developped in the near future.

8.1 - THE IDEAL EXPERIMENTAL SITUATION - C.W. DYE LASER EXCITATION OF HYDROGEN IN ATOMIC BEAMS

So far as the ideal experiment is concerned with the experimental search of new ideas for solving the problem or stimulating the theory, it is clear that the simplest experimental situation should be retained. Atomic hydrogen is then the only possibility which does not mean that the effects of diamagnetism on non-hydrogenic species are not of interest ! But in the absence of any close range correction to the Coulomb potential in hydrogen, one will be sure that no extra effects of configuration interaction hinder the observation of the dia-

magnetic perturbation of the atomic spectra.

Furthermore, performing the experiments on atomic beams is highly suitable. This will allow a total control of motional Stark field effects. As shown in equation (89) of section 4.3, the center of mass motion is not separable. This should cause some alterations of the reduced particle's motion especially through the interaction with the motional Stark field. Indeed crossed ($\vec{E}$, $\vec{B}$) fields effects can produce a complete alteration of the quasi-Landau spectrum (see section 9). It seems highly desirable to reduce the possibility of motional Stark effects on the spectrum by choosing an arrangement in which the velocity of the atom in the beam and the magnetic field are parallel. This ensures from (89) that the Stark term is negligible provided the beam is sufficiently well collimated ( ). Another requirement is that the beam should be as monokinetic as possible due to the $\frac{c^2}{2M}$ term in equation (89). From (87) and (89), it is clear that any change in the overall motion of the two particles system will affect the relative motion. As the problem, equivalent to the one-particle problem in crossed ($\vec{E}$, $\vec{B}$) fields is not solved, it is impossible to draw final conclusions about the effects of a non-monokinetic beam on the spectrum. But they are likely to be small compared to the residual Stark broadening associated with imperfect collimation. Finally, low velocity beams or traps (for the neutral particle...) seem a good choice for observing the spectrum in good conditions.

Beam experiments allow accurate determinations of the parameters of Rydberg states. But the production of n values greater than 80 is hardly possible or needs huge optical powers which does not favour the other requirement about optical purity of the excitation.

Spectral purity and tunability of the optical source are obviously important factors for resolving all the details of the quasi Landau spectrum, the accidental

coincidence of lines or weak anticrossings, or for dealing with high Rydberg states with n greater than 100. For n = 140, for example, the quasi Landau regimes occur for field values of 150 Gauss when $n^3 B \sim B_c$! It is highly desirable for various purposes to study the spectrum under such conditions. It turns our to be possible [55] but under vapour phase conditions using single-mode c.w. dye laser excitation. Of course under such conditions, motional Stark field effects will exist thus requiring the choice of heavy atoms with low temperature and low field conditions.

Beam experiments on high Rydberg states of hydrogen, using pure c.w. dye laser excitation, have not yet been achieved but some progress are likely to occur in the near future. Untill now, beam experiments [62] have been done on alkali atoms using pulsed dye laser excitation. Usually, this does not allow a total control of the width and lineshape of the source and then of the intensity aspects of the experimental data. On the other hand, vapour phase experiments (also on alkali atoms) combined with the use of single mode c.w. dye laser of well controlled linewidth [63] are likely to suffer from the lack of control of the motional Stark field effects.

8.2 - ACTUAL EXPERIMENTS

A lot of experimental attempts have been done for a few years using either conventional light sources or dye laser excitation, cells or beam apparatuses, various kinds of atomic species and excitation schemes [59][60][61][62][63][64]. In some of these experiments, the choice of elements having strong departures from the hydrogenic behaviour was hindering any possible detailed interpretation of the spectrum especially of the intensities.

We will discuss here two recent experiments which allowed to prove that the quasi-Landau spectrum was of discrete nature and that the dominant lines in

this spectrum were associated with the K = 1 lines in the Coulomb limit as discussed in sections 6 and 7. These studies were performed in rather complementary ways either scanning the energy or scanning the magnetic field.

The first experiment uses beam techniques and excitation of sodium nD Rydberg states with pulsed dye lasers (with GHz widths). The experimental attempts have been limited to the bound spectrum below threshold.

The second experiment uses highly selective single mode c.w. dye laser excitation of cesium nF Rydberg series which are highly hydrogenic ($\delta \sim 0.033$). The pumping scheme is the so-called hybrid two photon process [17] which is a quite efficient one. Production of states with n up to 162 has been achieved[55]. These experiments were essentially performed at constant laser frequency, scanning the B field, which allows, in particular, to check the n^3B quantization law obeyed at threshold and the n.B law obeyed in the Landau regime.

8.3 - THE DISCRETE NATURE OF THE QUASI LANDAU SPECTRUM

These experiments first showed that the strong field mixing phenomena affects series of well defined sharp lines from the Coulomb to the Landau limit. The dominant serie is associated with K = 1 states (see sections 6 and 7) in the low field Coulomb inter ℓ mixing regime, and its components obey the approximate predictions of formula (133). The spacing of the components at threshold is $\frac{3}{2}\hbar\omega_c$ while the quantization law at constant energy is $nB^{1/3} = 1.16.B_c^{1/3}$. In addition other series of discrete lines are approximatively obeying the same quantization law and are associated with K = 2, 3... states of the Coulomb limit.

8.3.1 - The quasi-Landau spectrum in energy

The results of the beam experiment on Na atoms are shown on Figure (20) . Approximate quantum calculations are shown in comparison providing with a rough assignment of the lines. The intensity of the lines are not relevant

The results have been obtained below threshold.

In Figure (21) is shown a record on Sr atoms near and above threshold got in cell experiments [61] showing that the phenomena below and above threshold are in continuity, but for the lineshapes.

8.3.2 - Landau spectrum in magnetic field

A typical spectrum in the diamagnetic region is shown on Figure (22) against the laser frequency for the n = 40 M = + 3 state of caesium. The various components of the diamagnetic manifold are displayed and in good agreement with theoretical calculations [39]. The fact that the K = 1 line has not the maximum intensity is associated with the small perturbation $\delta = 0.033$ due to the quantum defect. At higher field values this spurious effect will disappear. A complementary aspect of the diamagnetic pattern is shown in Figure (23) where the magnetic field is scanned at constant laser frequency. Another aspect of the spectrum below threshold is shown in Figure (24) where successively the inter ℓ, inter n mixing regimes and the onset of the strong mixing regime are displayed at constant laser frequency.

Figure (25) is a scan in magnetic field for energies E = + 10 cm^{-1} above threshold. These states are quasi Landau states. The studies of the spectrum have been performed for constant energies ranging from 120 cm^{-1} below the ionization threshold (n = 30 Coulomb state) to 120 cm^{-1} above threshold for magnetic field strengths between 0 and 8 Tesla. The results for the dominant (K = 1) serie are plotted on Figure (26) against the approximate predictions from (133). Especially at threshold (E = 0) the quantization law $n_r^3.B = Cste$ is exactly obeyed. The average spacing in energy at threshold is $1.52\hbar\omega_c$. We have plotted in Figure (27) the radial quantum number against 1/B. Clearly for the upper values of the energy, the experimental points are alined indicating that the Landau limit of the

spectrum is almost reached. The spacing of the resonances for E $\sim$ 120 cm^{-1}, B $\sim$ 25 kG and $n_r \sim 90$ is experimentally $1.1\hbar\omega_c$. For this serie of dominant lines, which are discrete and associated with well defined states in the Coulomb limit, one passes, varying the field and energy from a Coulomb signature of the spectrum to a Landau one. The n^3B = Cste quantization law, obeyed at threshold, is the basic feature between these two limits. Indeed, the experimental results in the bound state region as well as in the resonance region above threshold converge at high field towards this new law. Of course, other series associated with the r other K states are likely to produce the same kind of pattern. But this is not still really proved theoretically or experimentally.

9 - PROSPECTS AND CONCLUSIONS

Among the various problems which are connected with atomic diamagnetism, there is one which attracts considerable attention. It is the crossed electric and magnetic field problem [65][66][67]. The hamiltonian is that of equation (89) with the additional $\vec{qr}.\vec{E}$ electric dipolar interaction. There is no longer any constants of the motion in this problem. Experiments have yet indicated that the atomic spectrum could be still organized, exhibiting set of resonances with a spacing $\frac{1}{2}\hbar\omega_c$ [59] near threshold.

Several regimes of the spectrum can be distinguished. In the first one, neglecting the diamagnetic interaction, one can consider that only the linear Stark effect and the paramagnetic term are present [68]. Under such conditions it may happen that the atomic spectrum for highly hydrogenic species still presents some regular features which are neither the Zeeman ones nor the Stark ones. This is connected with the existence of an adiabatic invariant [69] in this intermediate regime. Writing $\vec{\omega}_S$ the frequency associated with linear Stark effect :

$$\vec{\omega}_S = -\frac{3q}{2}\,\frac{\vec{E}}{\sqrt{-2mE}} \qquad (142)$$

and using perturbation theory in classical mechanics, the equation of evolution of the classical ellipses are :

$$\begin{aligned}\frac{d}{dr}\langle\vec{j}_1\rangle &= (\frac{\vec{\omega}_c}{2} - \vec{\omega}_S) \wedge \vec{j}_1 = \vec{\omega}_1 \wedge \vec{j}_1 \\ \frac{d}{dr}\langle\vec{j}_2\rangle &= (\frac{\vec{\omega}_c}{2} + \vec{\omega}_S) \wedge \vec{j}_2 = \vec{\omega}_2 \wedge \vec{j}_2\end{aligned} \qquad (143)$$

where $\vec{j}_1$ and $\vec{j}_2$ are defined through (14) and (15). (143) means that $\vec{j}_1$ and $\vec{j}_2$ are still precessing independantly but along the two axis $\vec{\omega}_1$ and $\vec{\omega}_2$.

Independant quantization can be performed along these two axis. The energy is then :

$$E = -\frac{1}{n^2} + \frac{\vec{\omega}_c}{2} \cdot \vec{L} + q\,\vec{r} \cdot \vec{E}$$

or (144)

$$E = -\frac{1}{n^2} + \vec{j}_1 \cdot \vec{\omega}_1 + \vec{j}_2 \cdot \vec{\omega}_2$$

that is : $E = -\frac{1}{n^2} + (m_1\omega_1 + m_2\omega_2)$ (145)

Then, in the general situation, the mixed Stark-Zeeman patterns of the manifold will be quite complicated. But if $\vec{E}$ and $\vec{B}$ are crossed, this implies :

$$\omega_1^2 = \omega_2^2 = \omega^2 = (\frac{\omega_c^2}{4} + \omega_S^2)$$

(146)

$$E = -\frac{1}{n^2} + (m_1 + m_2)\omega$$

This proves the existence of a new regular pattern which is neither the paramagnetic nor the Stark one. This is associated with the existence of an adiabatic invariant when the diamagnetic term is weak.

The second class of regimes is associated with the mixed effect of the diamagnetic, Coulomb and dipolar electric interactions. In some conditions as shown in Figure (28) a non coulombic valley might exist at large distances between the electron and the proton. In such a one dimensional valley resonances will exist with a spacing of $\frac{1}{2}\hbar\omega_c$ [51][65][67][68]. This regime can be considered as an intermediate one between the quasi-Landau and Stark resonances [51] situations.

Other kind of studies and developments are those connected with the physical properties of quasi-Landau resonances. Their collisional and radiative properties are likely to be quite interesting. The tunable character of the Landau ladder is certainly of interest for studies of superradiance or detection of radiation in the 100 GHz range. The partial discretization of atomic sontinua and local increase of oscillator strengths will completely modify the mechanisms of electronic capture or electronic collisions. Such features are already seen in cyclotron resonance experiments on cold plasma Finally, it could turn out that diamagnetism will be as fine a tool as Zeeman effect but for MQDT analysis of high Rydberg series and autoionizing resonances. What will really happen in this last situation is not elucidated. What is clear is the effects of the diamagnetic interaction on the core will be weak while the continuum channels will be discretized into Landau resonances. It is not unlikely that some important modifications of the properties of antoionizing resonances will be achieved, this way

Of course, a major achievement will be primarily to completely understand the basic problem of diamagnetism for the hydrogen atom. A major step this way would be an approach at the spectrum in the resonance region above threshold providing with approximate wavefunctions. Some major pieces of the puzzle have been put recently in the right place using one of the various possible methods. Some major ones are still missing.

REFERENCES

(1) H. HASEGAWA - Physics of solids in intense magnetic fields, E.D. Haidemenakis ed. (Plenum 1969)

(2) J.G. MAVROIDES - Optical properties of solids, F. Abeles ed. (North Holland 1972)

(3) R.H. GARSTANG - Rep. Progr. Phys. 40, 105 (1977)

(4) L.D. LANDAU - Z. Phys. 64, 629 (1930)

(5) F.A. JENKINS and E. SEGRE - Phys. Rev. 55, 52 (1939)

(6) W.R.S. GARTON and F.S. TOMKINS - Ap. J. 158, 839 (1969)

(7) A.R.P. RAU - Phys. Rev. A 16, 613 (1977)

(8) for example M. BANDER and C. ITZYKSON - Rev. Mod. Phys. 38, 330 (1966)

(9) B.R. JUDD - Angular momentum theory for diatomic molecules (Academic Press 1975)

(10) L.D. LANDAU and E.M. LIFSCHITZ - Mecanique ed. MIR (Moscou 1966)

(11) A. DURAND - Mécanique Quantique (Dunod, Paris 1970)

(12) C. COHEN-TANNOUDJI, B. DIU and F. LALOE - Mécanique Quantique (Hermann, Paris 1973)

(13) L.D. LANDAU and E.M. LIFSCHITZ - Mécanique Quantique ed. MIR (Moscou 1966)

(14) W.E. LAMB - Phys. Rev. 85, 259 (1952)

(15) L.P. GORKOV and I.E. DZYALOSHINSKII - J.E.T.P. 53, 717 (1967)

(16) B.P. CARTER - J. Math. Phys. 10, 788 (1968)

(17) D. DELANDE - Thèse 3e Cycle Paris (1981) unpublished

(18) L.I. SCHIFF and H. SNYDER - Phys. Rev. 55, 59 (1939)

(19) J.C. GAY - Comments At. Mol. Phys. 9, 97 (1980)

(20) A.R.P. RAU - Comments At. Mol. Phys. 10, 19 (1980)

(21) D. DELANDE and J.C. GAY - unpublished

(22) A.R. EDMONDS - J. Phys. Paris Colloque C4 31, 71 (1970)

(23) A.R. EDMONDS - unpublished - Reprints.Imperial College

(24) M. ROBNIK - J. Phys. A 14, 3195 (1981)

(25) M. ROBNIK - in Coll. Int. CNRS 334 (ed. de Physique, Paris) to be published

(26) W.P. REINHARDT and D. FARRELY in Coll. Int. CNRS 334 (ed. de Physique Paris) to be published

(27) E.J. HELLER, E.B. STECHEL and M.J. DAVIS - J. Chem. Phys. 73, 4720 (1980)

(28) W. MAGNUS and S. WINKLER - Hill's equation (Wiley, N.Y. 1966)

(29) I.C. PERCIVAL - Ad. Chem. Phys. 36, 1 (1977)

(30) M.P. STRAND and W.P. REINHARDT - J. Chem. Phys. 70, 3812 (1979)

(31) R. BALIAN and C. BLOCH - Ann. Phys. (NY) 85, 514 (1974)

(32) V. SZEBEHELY - Theory of orbits (Ac. Press NY 1967)

(33) U. FANO - J. Phys. B13, L519 (1980)

(34) U. FANO - Phys. Rev. A 22, 2660 (1980)

(35) E.A. SOLOVEV - J.E.T.P. Letters 34, 265 (1981)

(36) E.G. KALNINS, W. MILLER and P. WINTERNITZ - Siam. J. Appl. Math. 30, 630 (1976)

(37) for example J.C. GAY - Progress Atomic Spectroscopy, Part C. Hanle and Kleinpoppen ed. (Plenum) to be published

(38) M.L. ZIMMERMANN, M.M. KASH and D. KLEPPNER - Phys. Rev. Lett. 45, 1092 (1980)

(39) D. DELANDE and J.C. GAY - Phys. Lett. 82A 393 (1981)

(40) D.R. HERRICK - Phys. Rev. A 26, 323 (1982)

(41) C.W. CLARK - Phys. Rev. A 24, 605 (1981)

(42) C.W. CLARK and K.T. TAYLOR - J. Phys. B 15, 1175 (1982)

(43) C.W. CLARK and K.T. TAYLOR - J. Phys. B 13, L737 (1980)

(44) J.J. LABARTHE - J. Phys. B 14, L467 (1981)

(45) A.R. EDMONDS - J. Phys. B 6, 1603 (1973)

(46) U. FANO - Coll. Int. CNRS 283 (Paris ed. du CNRS 1977)

(47) G. WUNNER, H. HEROLD and G. RUDER - Phys. Lett. 88A, 344 (1982)

(48) J. VIRTAMO - J. Phys. B 9, 751 (1976)

(49) R.F. O'CONNELL - Phys. Letters 60 A, 481 (1971)

(50) A.F. STARACE - J. Phys. B 6, 585 (1973)

(51) A.R.P. RAU - J. Phys. B 12, L183 (1979)

(52) V.P. MASLOV - Théorie des Perturbations et Méthodes asymptotiques (Paris Dunod 1972)

(53) A. EINSTEIN - Verh. Deutsch. Phys. Ges. Berlin 19, 82 (1917)

(54) M.C. GUTZWILLER - Phys. Rev. Lett. 45, 150 (1980)

(55) J.C. GAY, D. DELANDE and F. BIRABEN - J. Phys. B 13, L720 (1980)

(56) A.G. ZHILICH and B.S. MONOZON - Sov. Phys. Sem. 1, 563 (1967)

(57) A.G. ZHILICH and B.S. MONOZON - Sov. Phys. Solid State 8, 2846 (1967)

(58) M.L. ZIMMERMAN, J.C. CASTRO and D. KLEPPNER - Phys. Rev. Lett. 40, 1083 (1978)

(59) K.T. LU, F.S. TOMKINS, H.M. CROSSWHITE and H. CROSSWHITE - Phys. Rev. Lett. 41, 1034 (1978)

(60) N.P. ECONOMOU, R.R. FREEMAN and P.F. LIAO - Phys. Rev. A 18, 2506 (1979)

(61) K.T. LU, F.S. TOMKINS and W.R.S. GARTON - Proc. R. Soc. A 364, 421 (1978)

(62) J.C. CASTRO, M.L. ZIMMERMAN, R.G. HULET and D. KLEPPNER - Phys. Rev. Lett. 15, 1780 (1980)

(63) D. DELANDE and J.C. GAY - Phys. Lett. 82A, 399 (1981)

(64) D. DELANDE, C. CHARDONNET and J.C. GAY - Optics Comm. 42, 25 (1982)

(65) H.M. CROSSWHITE, K.T. LU, U. FANO and A.R.P. RAU - Phys. Rev. Lett. 42, 963 (1979)

(66) G.P. DRUKAREV and B.S. MONOZON - J.E.T.P. 34, 509 (1972)

(67) J.C. GAY. L.R. PENDRILL and B. CAGNAC - Phys. Lett. 72 A. 315 (1979)

(68) A.R.P. RAU and K.T. LU - Phys. Rev. A 21. 1957 (1980)

(69) T.P. GROZDANOV and E.A. SOLOVEV - J. Phys. B 15. 1195 (1982)

FIGURE CAPTIONS

Figure 1 - Zero field Coulomb ellipse ($\vec{L}$ the angular momentum. $\vec{A}$ the Lenz vector).

Figure 2 - Classical Landau trajectory in the plane perpendicular to the field ($\vec{r}_o$, Γ constants of the motion).

Figure 3 - Landau spectrum of a charged particle.

Figure 4 - Schematic "semi-classical" representation of the wavefunctions with rotational and translational symmetries in the Landau problem.

Figure 5 - Two dimensional projections of the phase space motion for initial conditions $(\rho, z, \dot{\rho}, \dot{z}) = (0.816, 0577, 0,0)$ (atomic units) and $M = 1$. The trajectory is followed on a duration approximately 100 times the period. (a) and (b) are respectively (ρ, z) and $(\dot{\rho}, \dot{z})$ plots for $B = 100$ kG, $E = -0.5$ (a. u.) - (c) is a (ρ, z) plot for $B = 10^5$ kG $E = -0.4572$.

Figure 6 - Two dimensional projections of the phase space motion for $B = 1.175.10^5$ ($\gamma = 0.5$), $M = 1$ and initial conditions of the general form $(\rho, z, \dot{\rho}, \dot{z})$ $(\rho, 0, 0, 10^{-2})$ (a.u.). The initial value of ρ is successively increased so as to increase the relative diamagnetic contribution to the total energy. (a) to (d) are $(\rho, \dot{\rho})$ plots for $(\rho = 2, E = 10^{-4})$, $(\rho = 2.8, E = +0.40)$, $(\rho = 4, E = +1.06)$, $(\rho = 10, E = +6.56)$. (e) is a $(z, \dot{z})$ plot for $E = 10^{-4}$, $(2, 0, 0, 10^{-2})$.

Figure 7 - Poincaré surface of section for the energy E = - 1.0 (a.u.). The (p_v, v) coordinates are analogous to the ones defined in (102). Several trajectories are associated to this plot [26].

Figure 8 - Poincaré surface of section [26] for the energy E = - 0.35 showing partial destruction of the regular features in Figure 7.

Figure 9 - Poincaré surface of section at E = - 0.275, for a chaotic classical trajectory [26].

Figure 10 - Effective potential (including rotational energy) associated with equation (104). Motions in the z = 0 plane in real space are associated with motions along the ridge $\mu = \nu$ in this plot.

Figure 11 - Trajectories of the Lenz vector $\vec{A}$ associated with negative (a) and positive (b) values of the adiabatic invariant, in the Coulomb limit. The dotted curve corresponds to the requirements on the energy.

Figure 12 - Diamagnetic structure of the hydrogenic manifold in the inter ℓ mixing regime.

Figure 13 - Plot of the nodal surfaces of the {nKMΠ} wavefunctions (n = 17, M = 3 odd parity states) in the inter ℓ mixing regime.

Figure 14 - Details of the nodal surfaces in Figure 13. The shaded area in the curves corresponds to values of the wavefunctions (K = 1 and K = 7) greater than 3.10^{-5}. The sizes of the spatial anticrossing is of the order of $3a_o$.

Figure 15 - Plot of the electronic densities of the wavefunctions for N = 8 M = 0 and the two values of the parity. On the left part of the Figure, the Π_z parity is even while odd on the right. Only one among these two classes of states can be optically excited with polarized radiation.

Figure 16 - Efficiency of optical excitation of the various K components in the manifold following their parity Π_z along B field.

Figure 17 - Sizes of the anticrossings (in GHz) between (n, K = 1) and (n+1, K_{max}) for the lowest energy levels, in logarithmic coordinates, as a function of (n - M). The sizes are almost varying as e^{-2n} with n. Each broken curve corresponds to a fixed M value which is, from the upper to the lower one, M = 0 to M = 4. For M = 4, even parity along Z, the first anticrossing between (n, K = 1) and (n+1, K_{max} = 2) occurs for n = 8 at a magnetic field strength of 588 T while for (M = 4, even, n = 12) it is 144 T.

Figure 18 -Numerical Sturmian simulations of the spectrum for atomic hydrogen for B = 47 kG, for even and odd values of the parity along B field.

Figure 19 - Components associated with K = 1, 2, ... lines in the even parity spectrum of Figure 18.

Figure 20 - Results of the Beam experiment on Na atoms showing the evolution of the components of the K = 1 serie as a function of B^2.

Figure 21 - Complete patterns of the diamagnetic regimes as shown on Sr atoms, scanning the laser frequency.

Figure 22 - Structure of the n = 40 M = 3 diamagnetic manifold of Caesium (B $\sim$ 6 kG) scanning the c.w. dye laser frequency (against the molecular iodine spectrum).

Figure 23 - Diamagnetic patterns of the n = 50, 49, ... states scanning the B field at fixed laser frequency.

Figure 24 - Scan in magnetic field at constant laser frequency (fixed around the n = 50 Coulomb state) showing the various diamagnetic regimes in field.

Figure 25 - Spectrum in magnetic field at fixed laser frequency (electronic energy E = + 10 cm^{-1} above threshold).

Figure 26 - Experimental and theoretical plots of the radial quantum number against $(B/B_c)^{-1/3}$ at various energies for the dominant discrete series of the spectrum. Theoretical points (crossed or broken curves) are from semi-classical calculations. Experimental points are for energies 121.5 (top line), 99.5, 65.7, 37.3, 17.2, 11.5, 0, -10.9, - 20, - 29.3, - 43.6, - 66.6 cm^{-1} (lower line) respectively from the ionization limit. At the threshold the curve is a straight line. For positive and negative energies of the electron, the results curve in opposite directions towards the Landau and Coulomb regions.

Figure 27 - Plot of n_r as a function of 1/B for the resonances above threshold showing that the Landau limit is almost reached for E $\sim$ 100 cm^{-1}

Figure 28 - Plot of the approximate effective potential in the crossed ($\vec{E}$, $\vec{B}$) fields situation showing the non-coulombic valley at large distances between the electron and the proton.

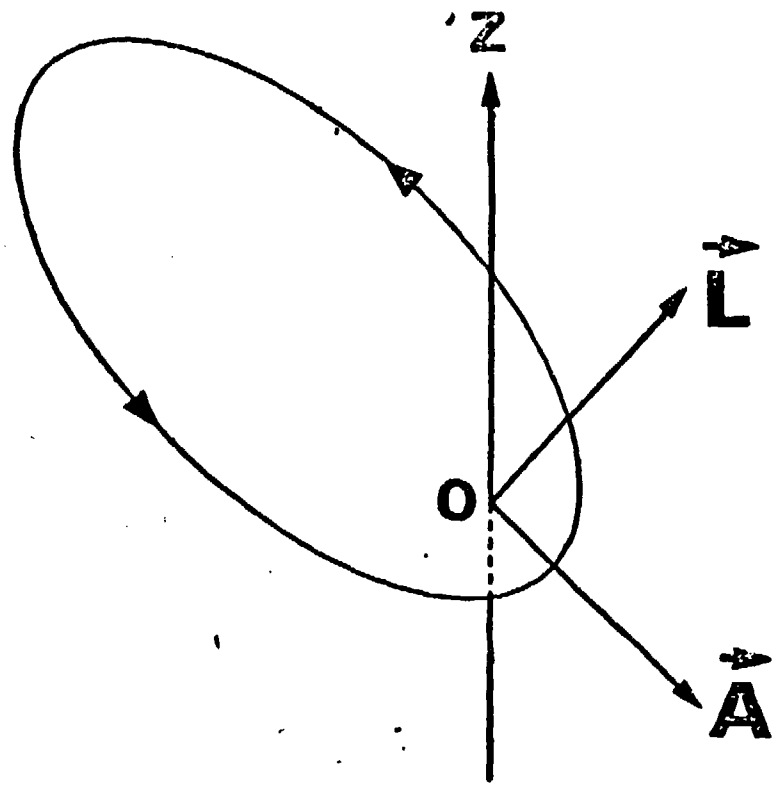

FIG 1

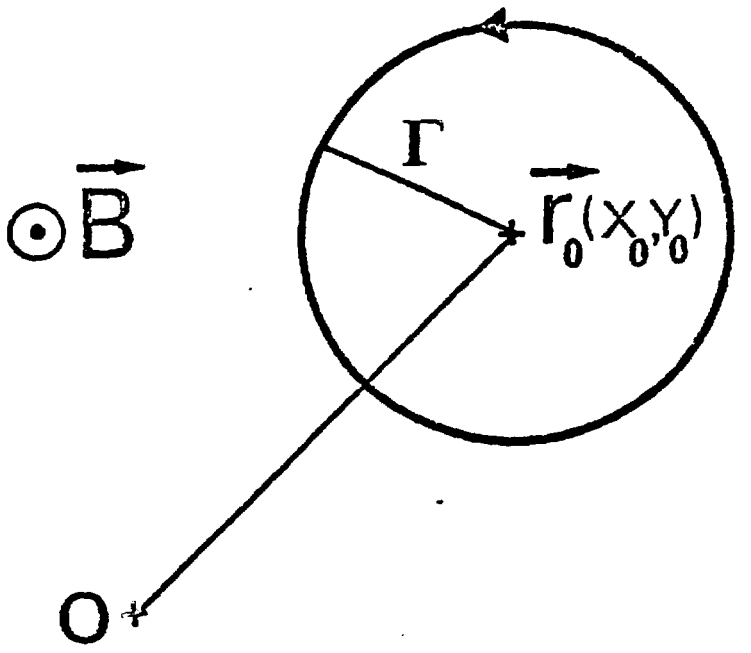

Fig 2

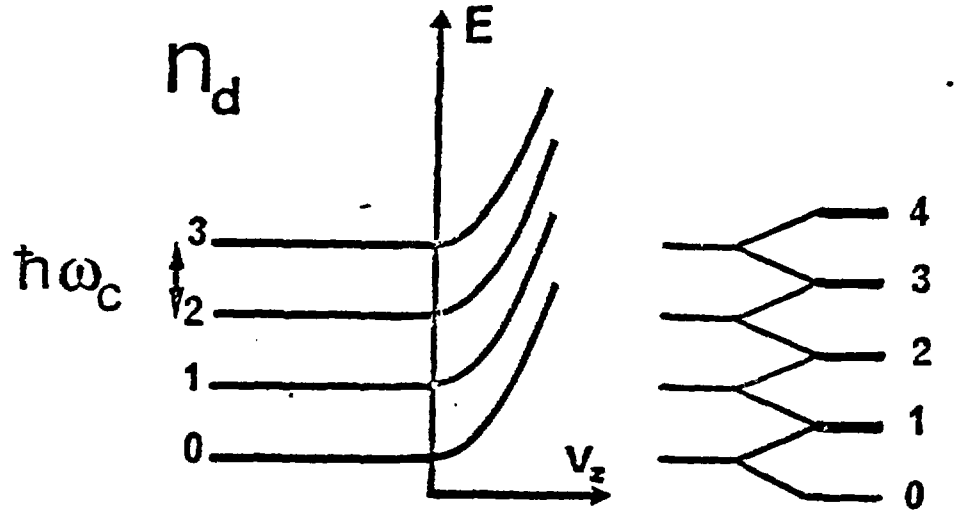
E
n_d
$\hbar\omega_c$
3
2
1
0
V_z
4
3
2
1
0

Fig 3

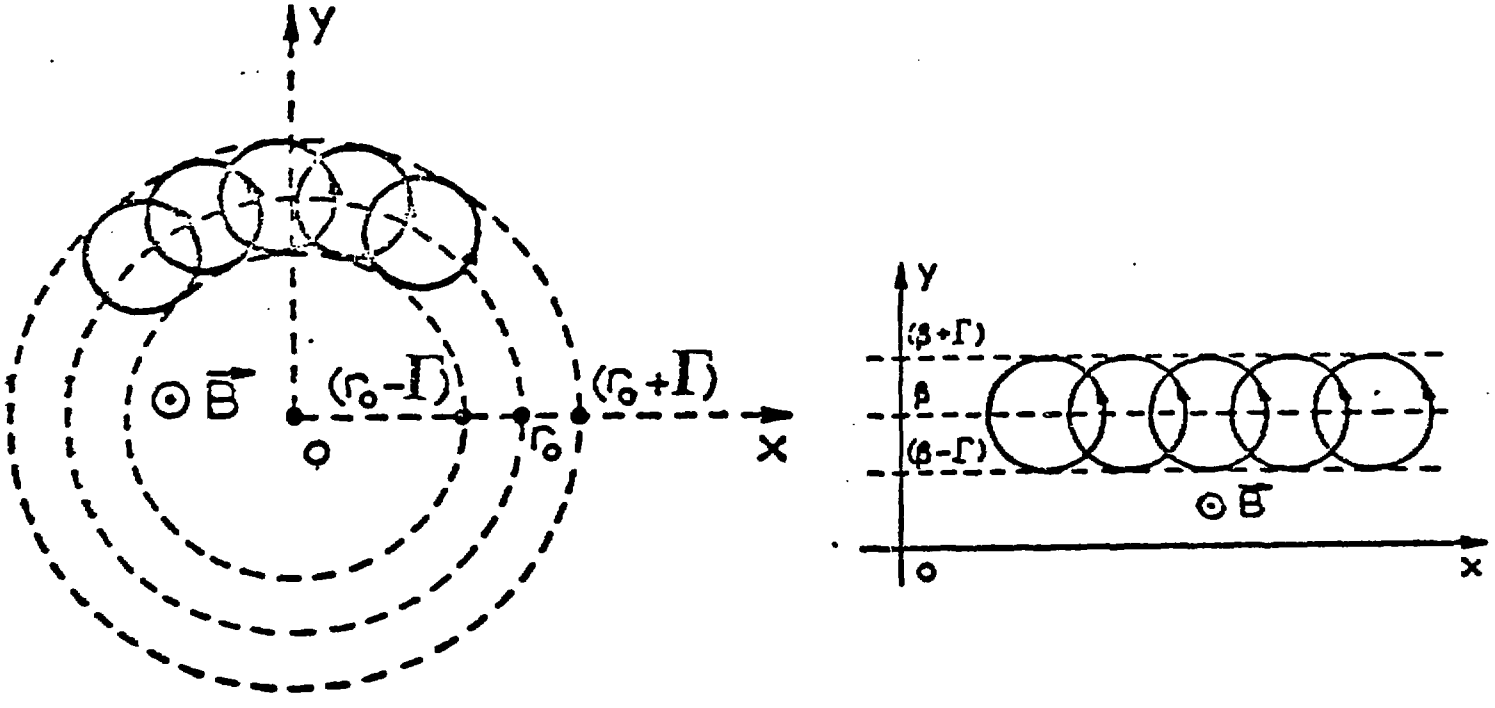
y
$\odot \vec{B}$
$(r_0-\Gamma)$
r_0
$(r_0+\Gamma)$
o
x
y
$(\beta+\Gamma)$
β
$(\beta-\Gamma)$
$\odot \vec{B}$
o
x

Fig 4

FIG 5

Fig 6

(e)

(d)

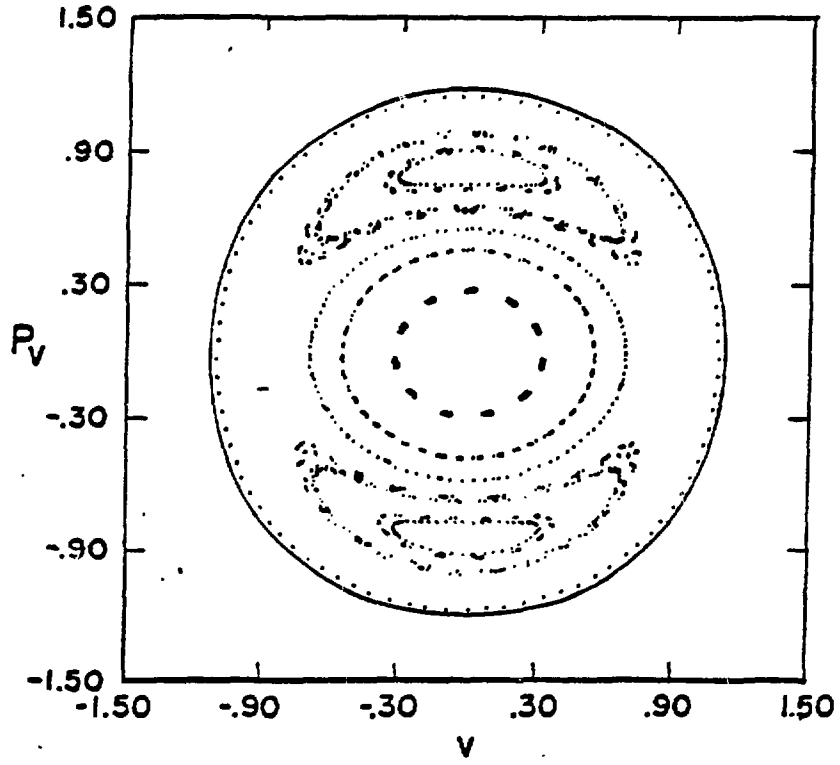
1.50
.90
.30
P_V
-.30
-.90
-1.50
-1.50
-.90
-.30
.30
.90
1.50
V

Fig 7

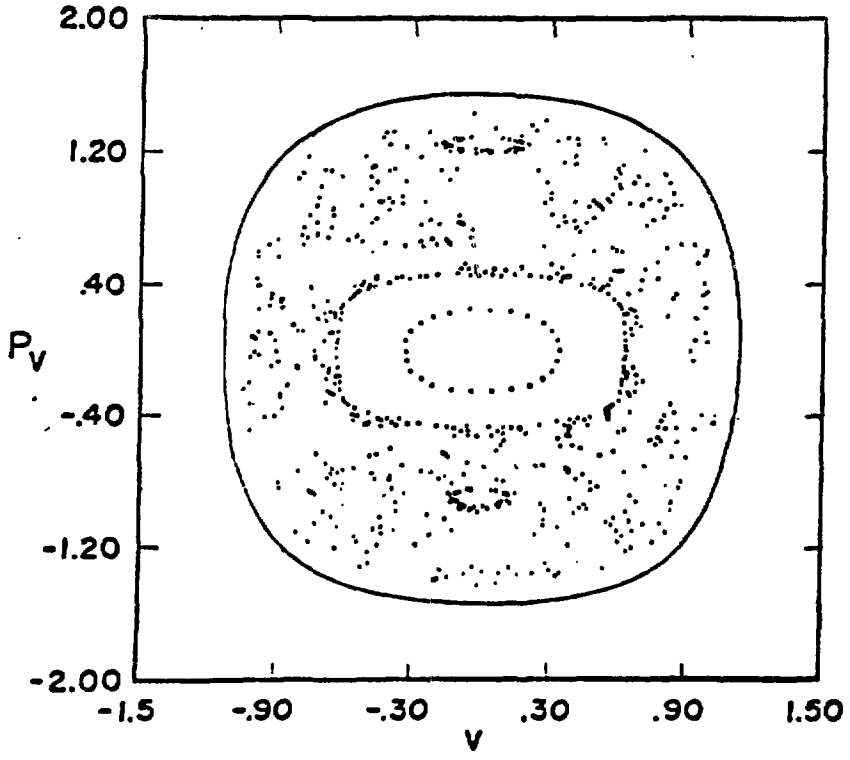
2.00
1.20
.40
P_V
-.40
-1.20
-2.00
-1.5
-.90
-.30
.30
.90
1.50
V

Fig 8

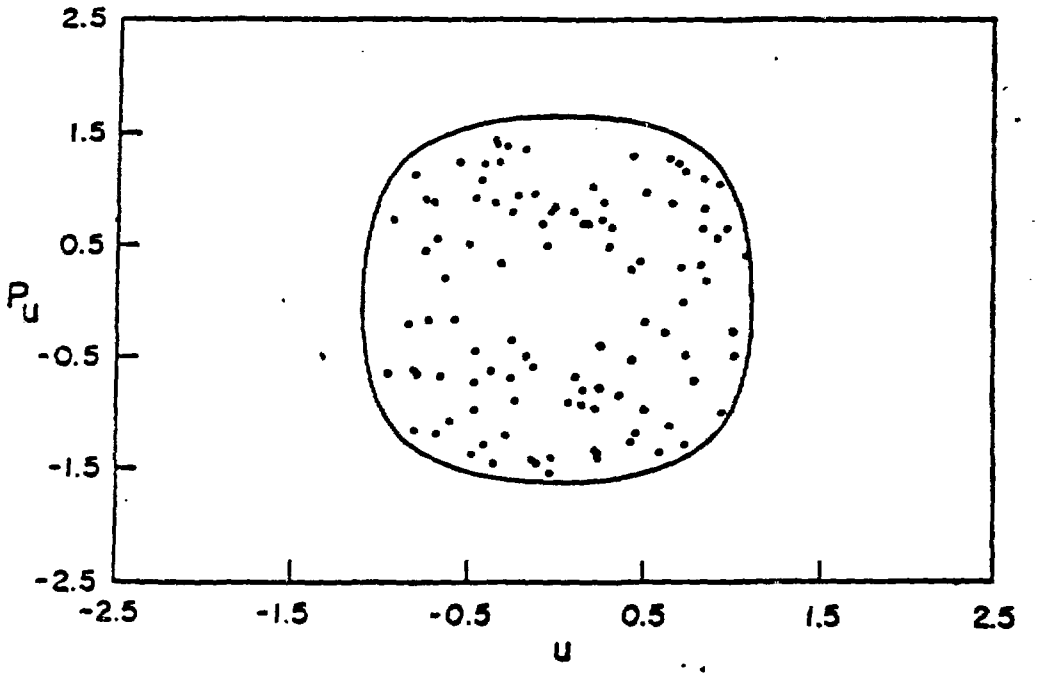

Fig 9

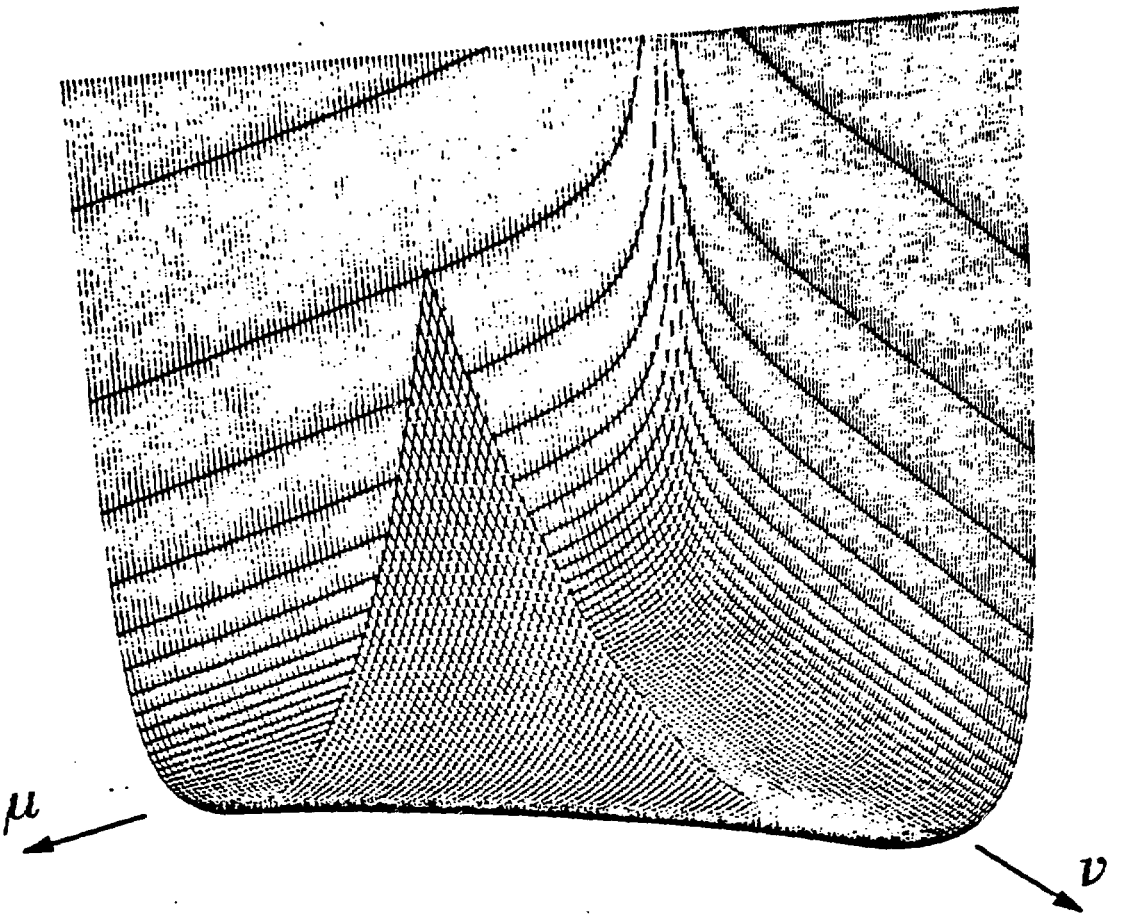

Fig 10

FIG 11 a)

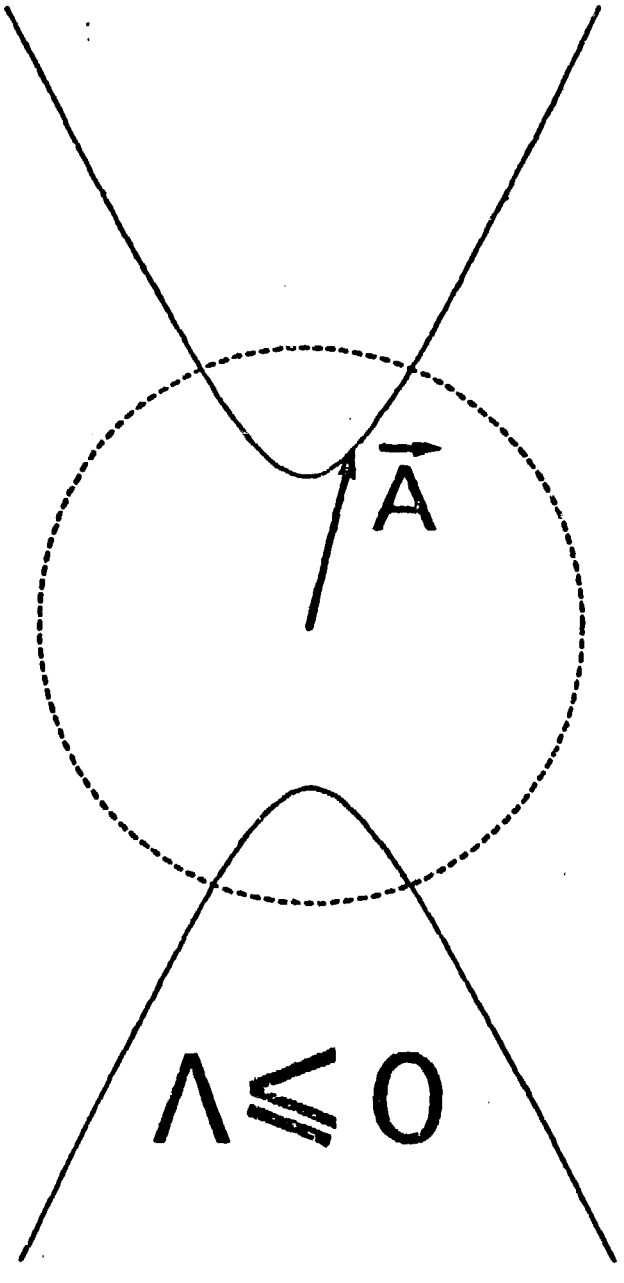

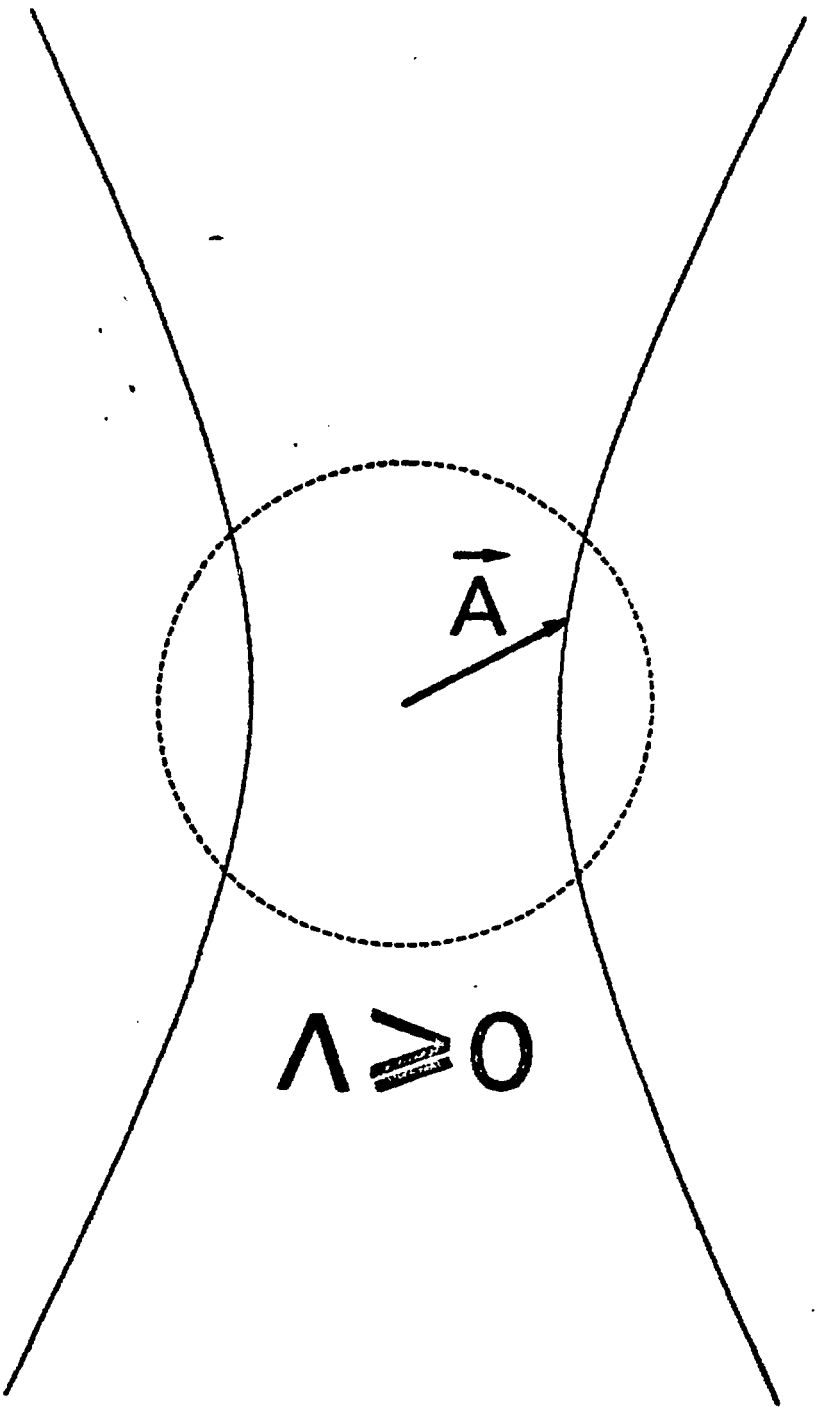

Fig 11 b)

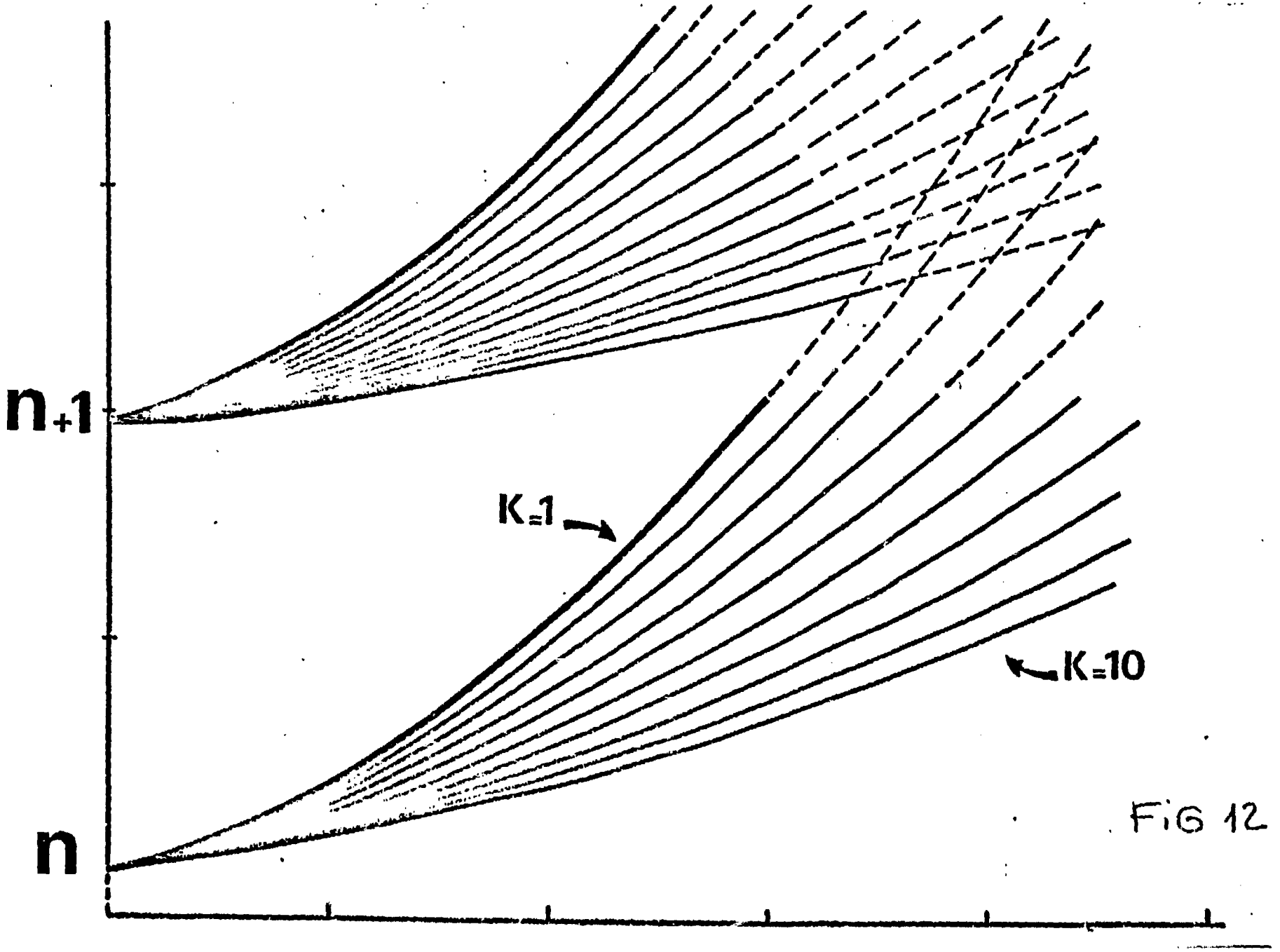

FIG 12

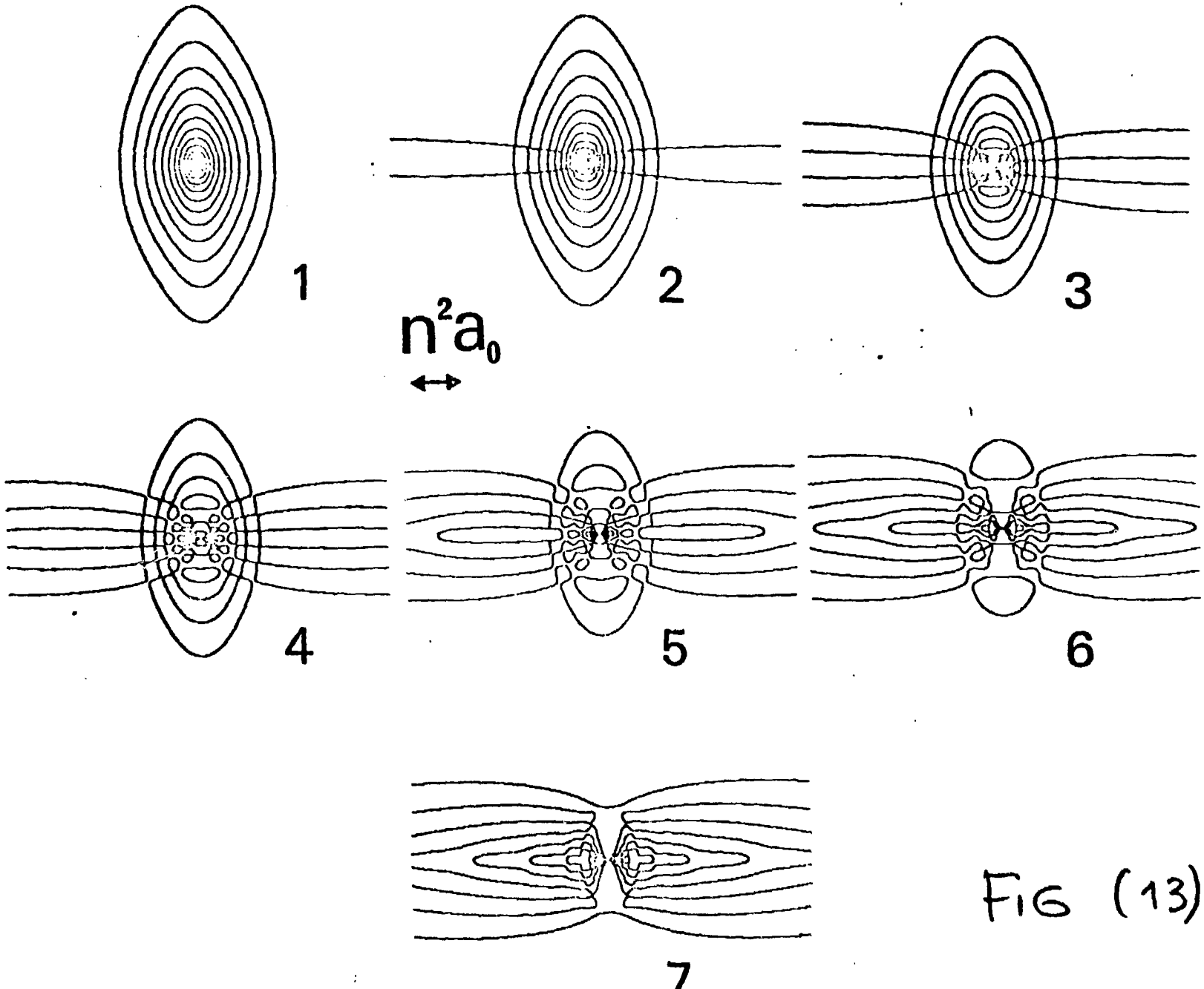

FIG (13)

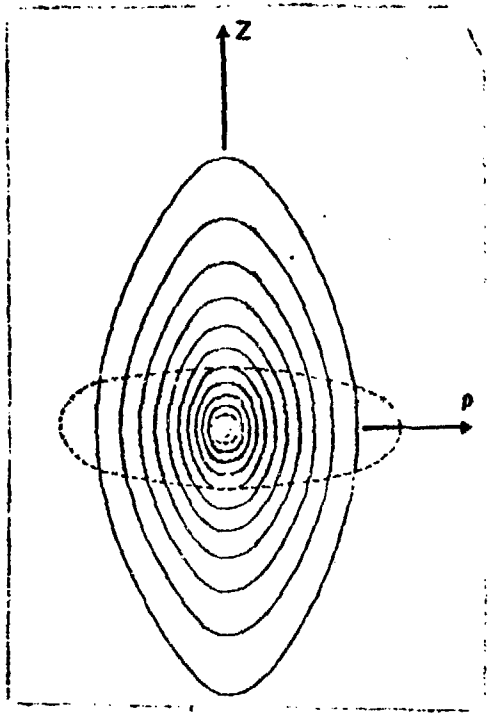

n^2a_0

1

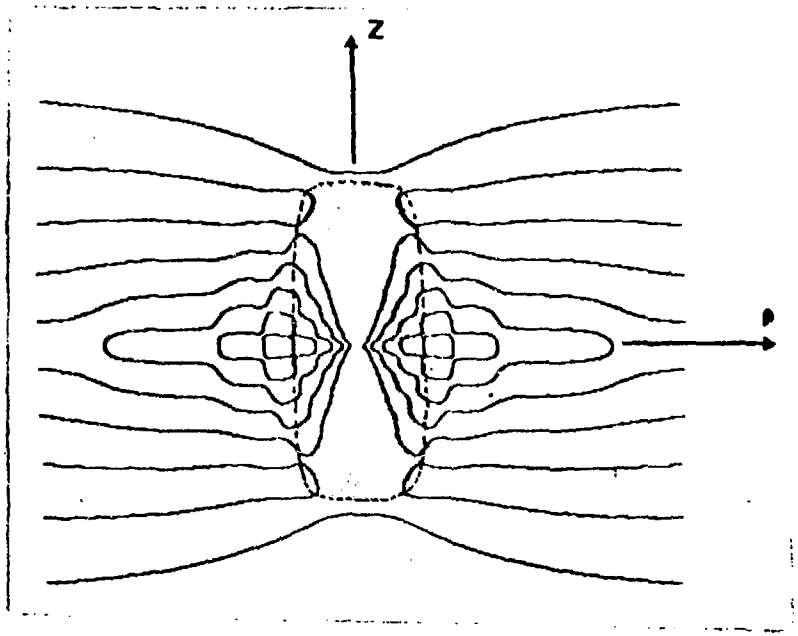

$n^2a_0/2$

7

FIG 14

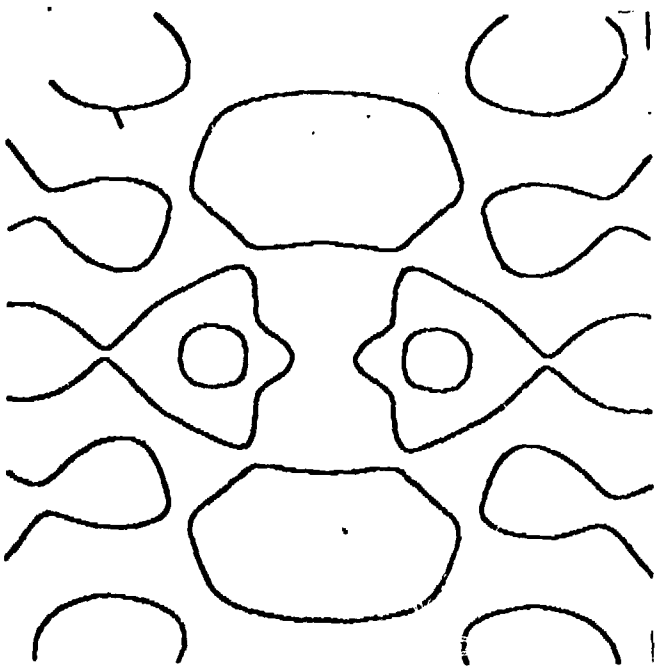

4

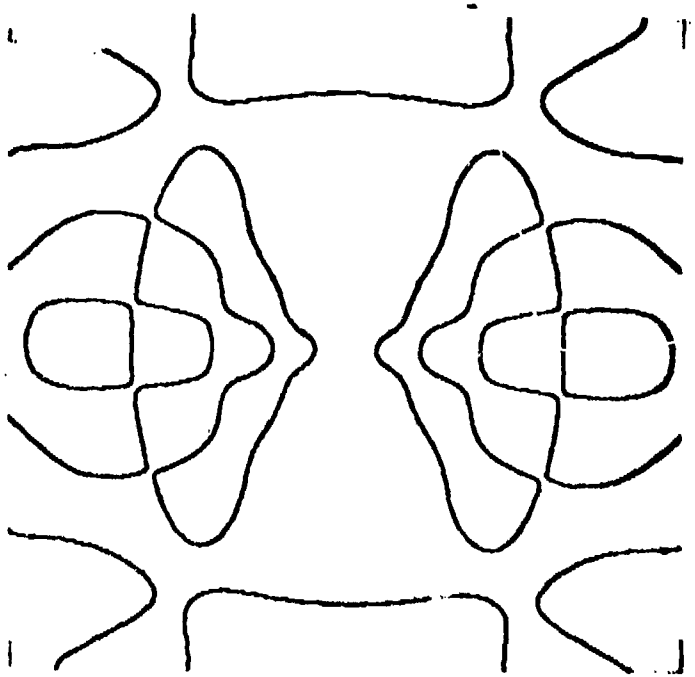

6

$n^2a_0/9$

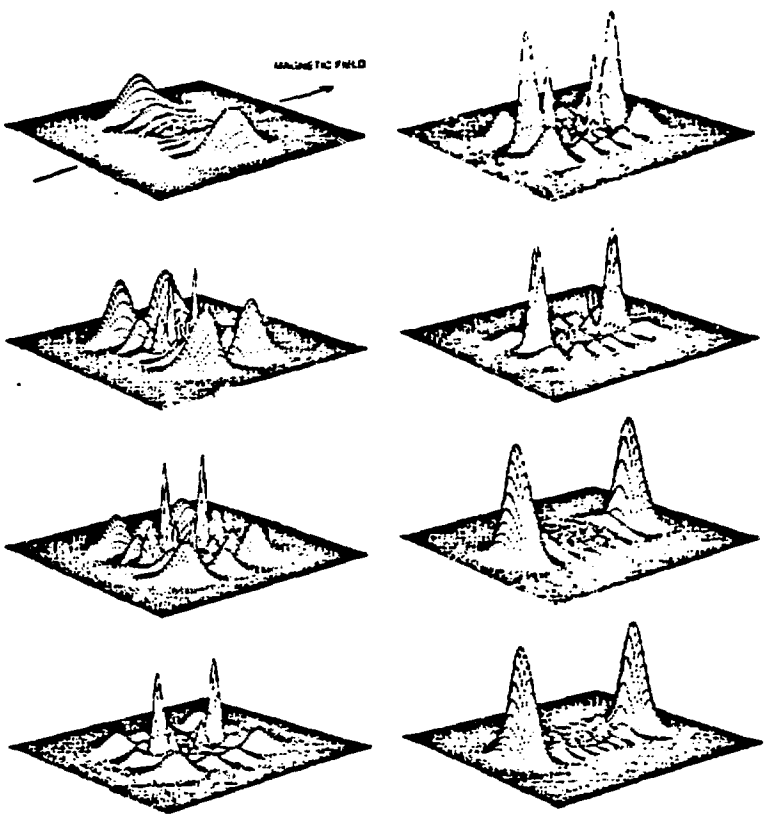

Fig 15

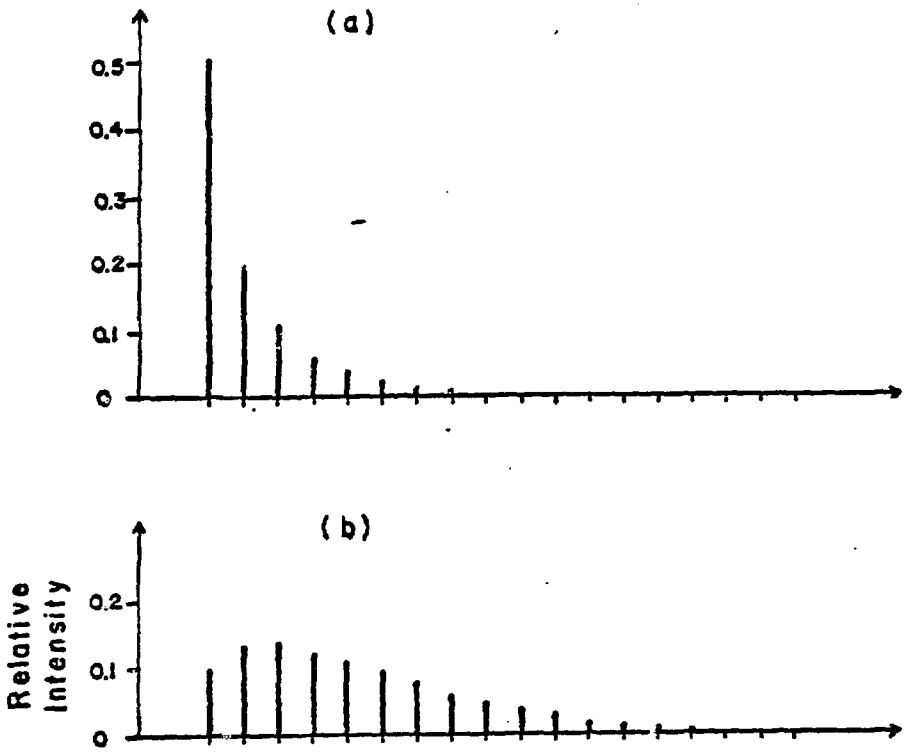

Fig 16

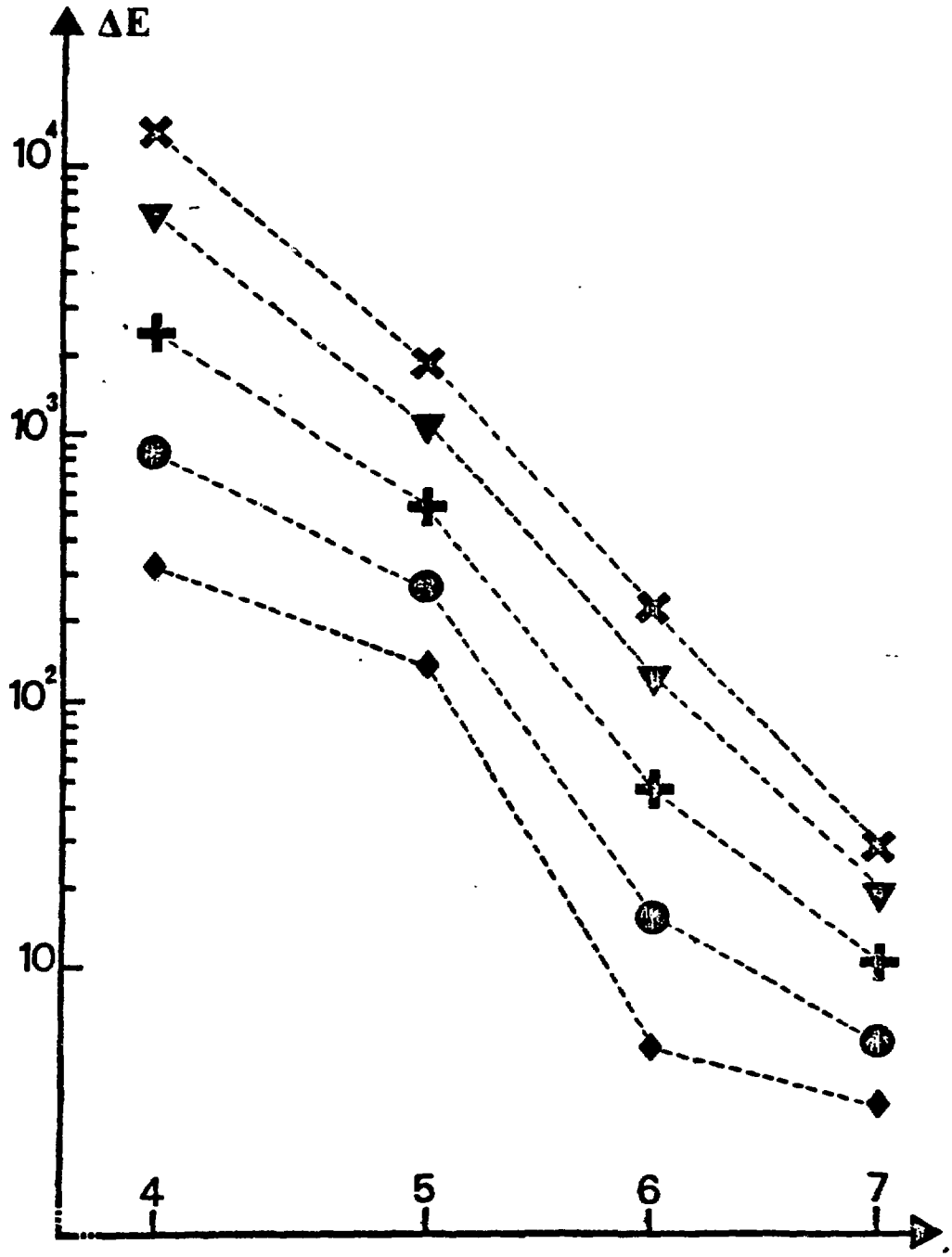

FIG 17

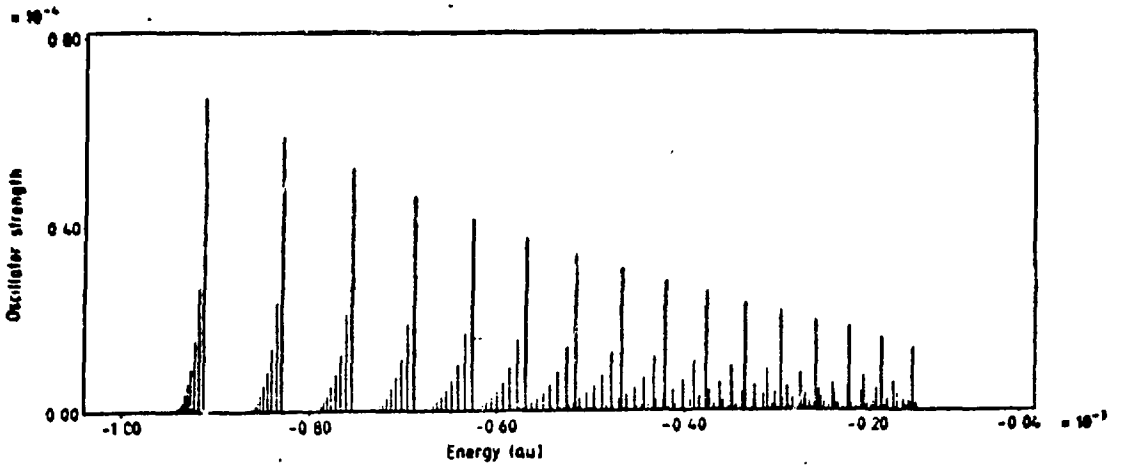
0 80
0 40
0 00
Oscillator strength
-1 00
-0 80
-0 60
-0 40
-0 20
-0 04
Energy (au)

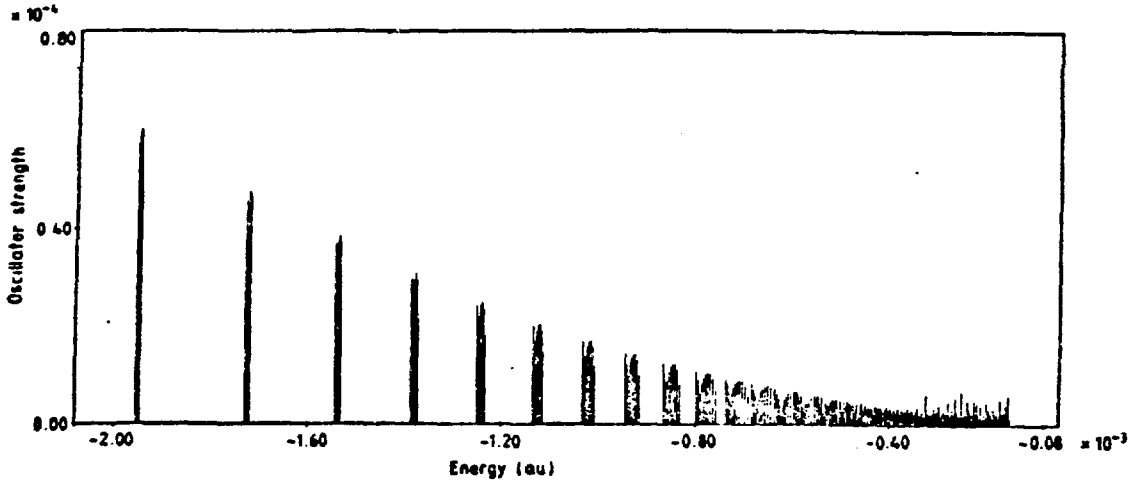
0.80
0 40
0.00
Oscillator strength
-2.00
-1.60
-1.20
-0.80
-0.40
-0.08
Energy (au)

Fig 18

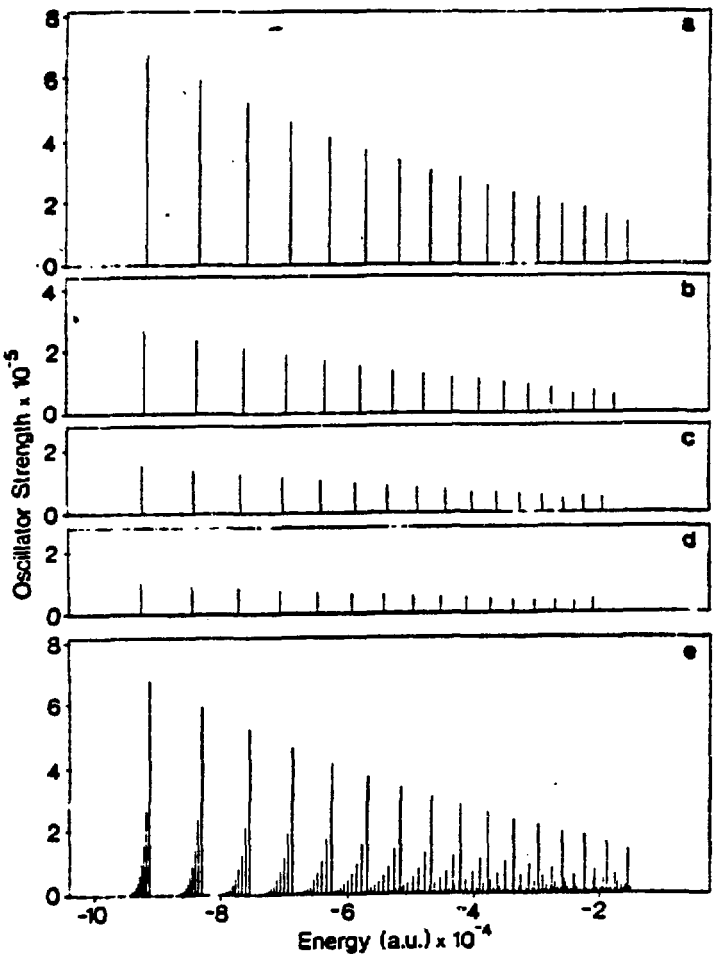

Fig 19

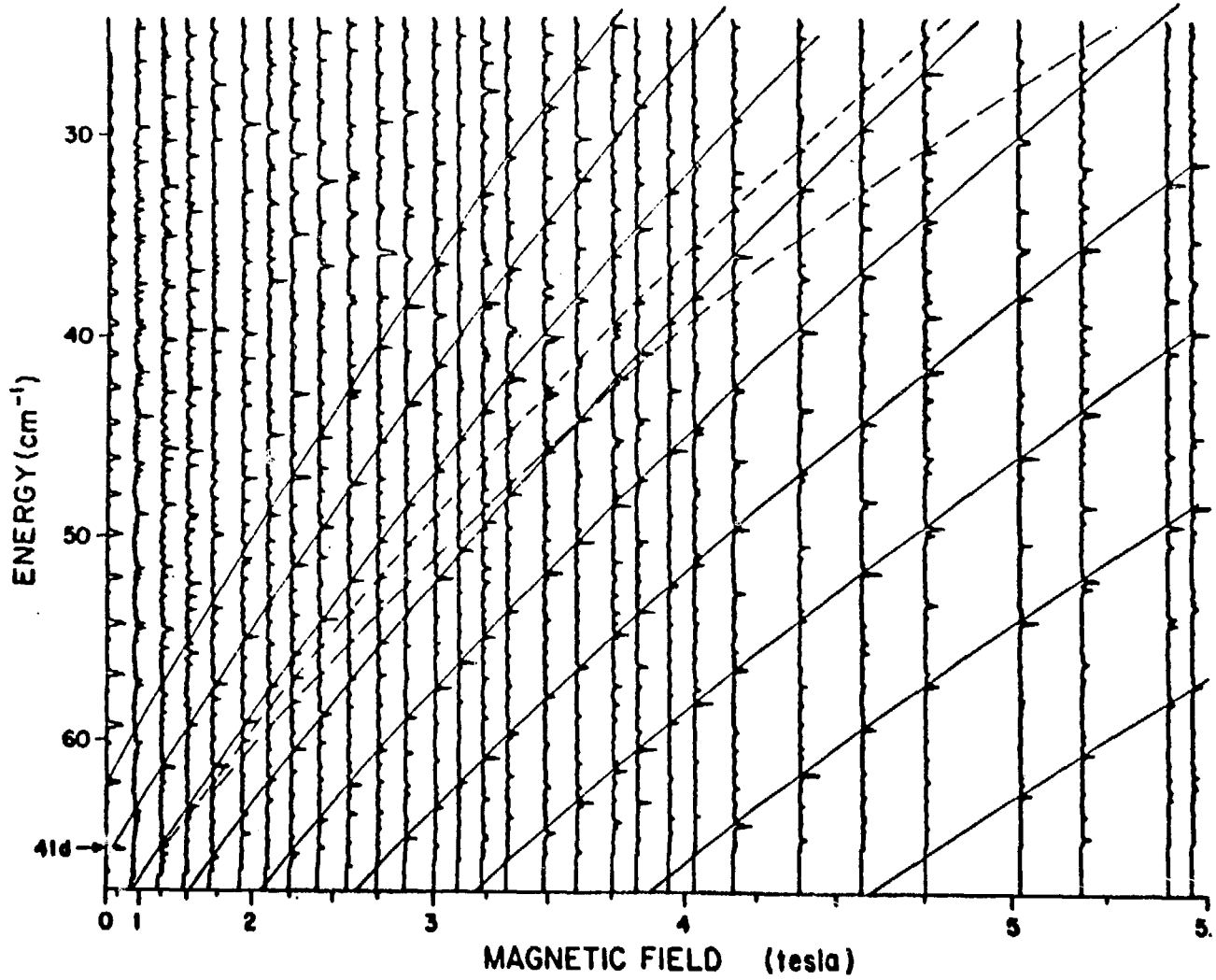

Fig 2

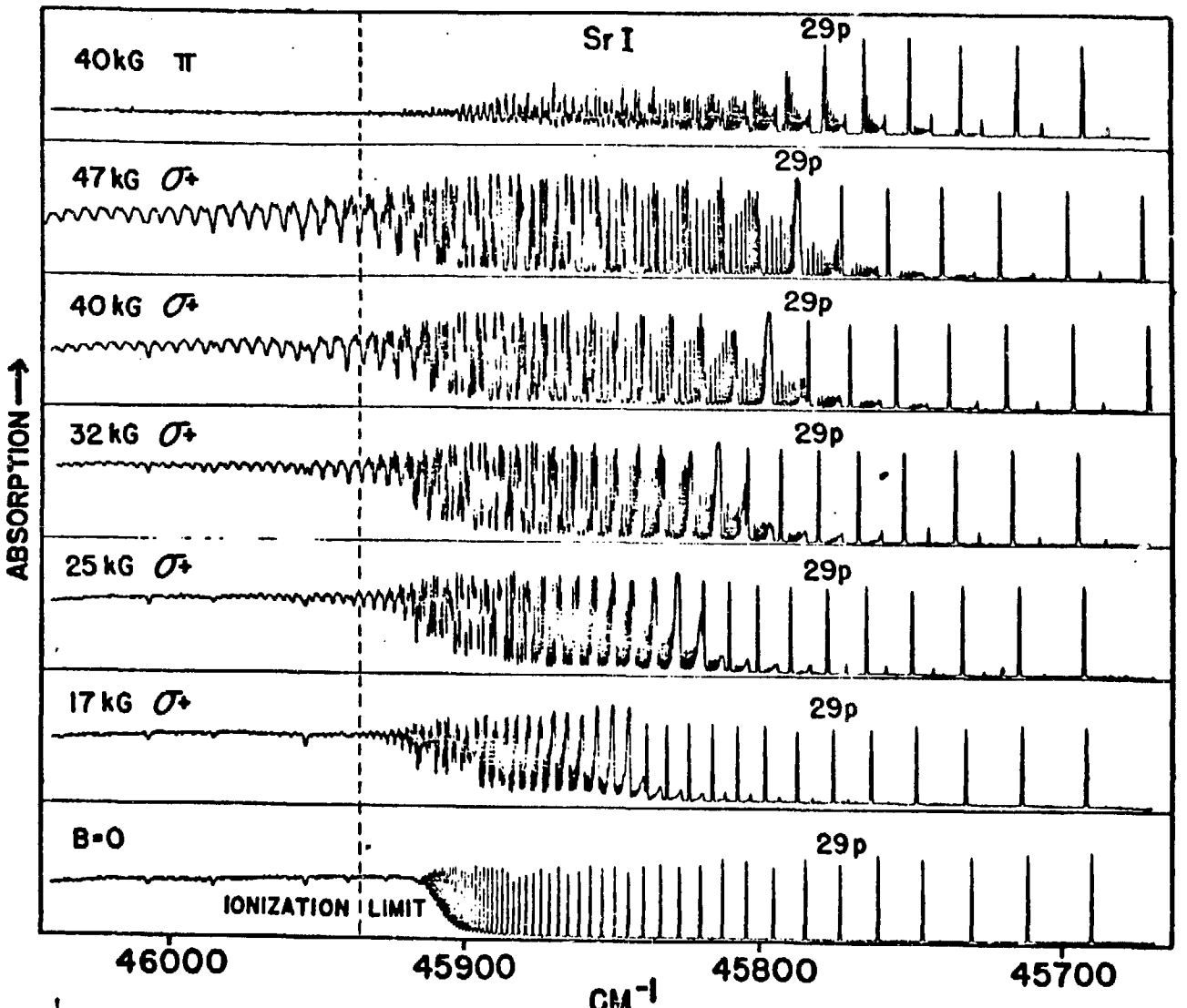
Sr I
40kG π
47kG σ+
40kG σ+
32kG σ+
25kG σ+
17kG σ+
B=0
29p
IONIZATION LIMIT
ABSORPTION
46000
45900
45800
45700
CM⁻¹

Fig. 2.1

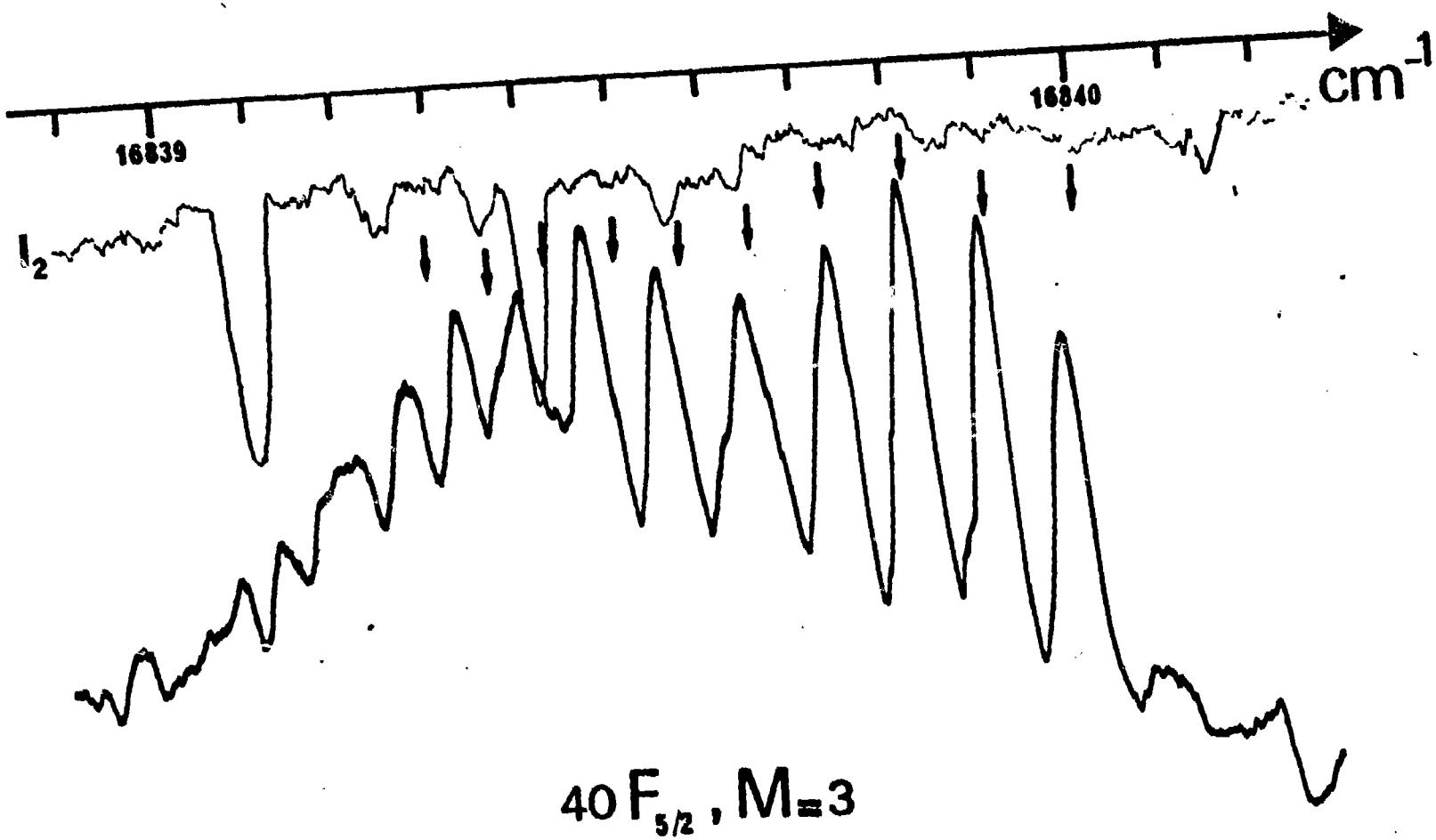

Fig 22

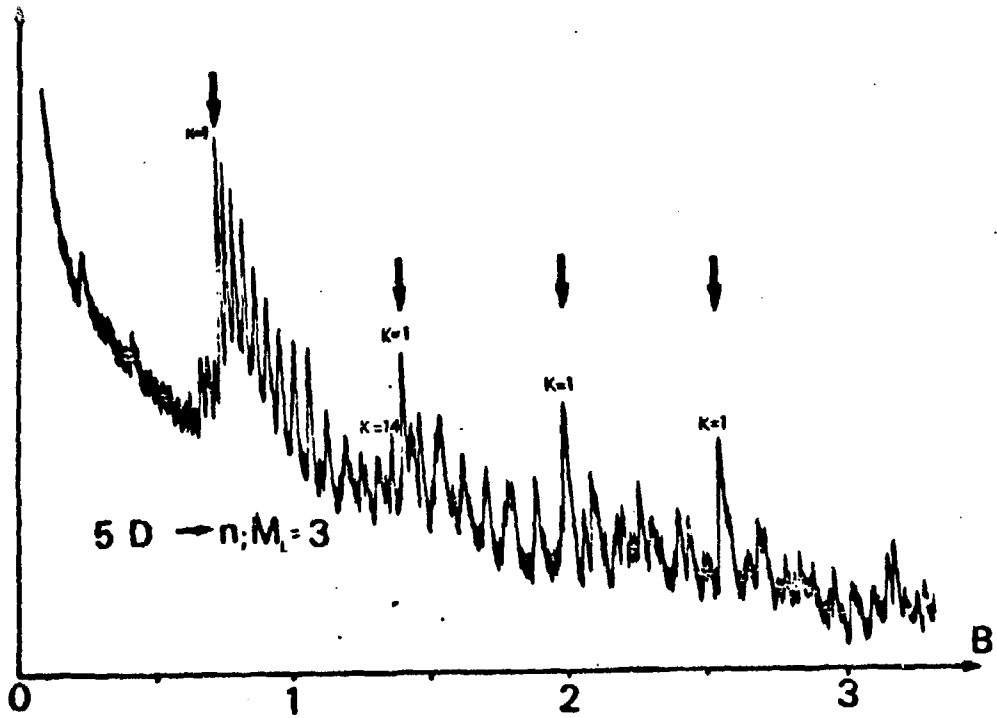

FIG 23

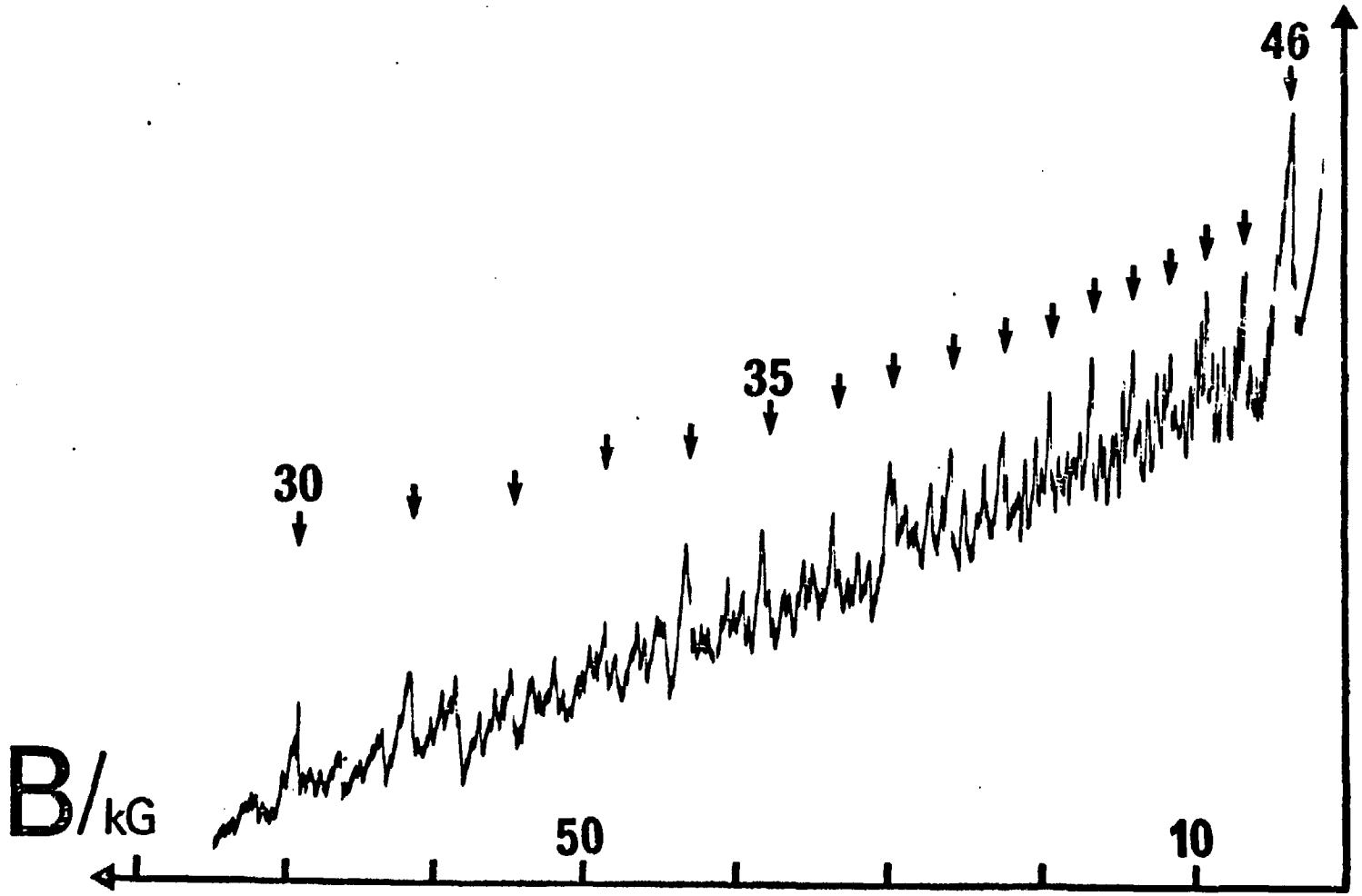

Fig 24

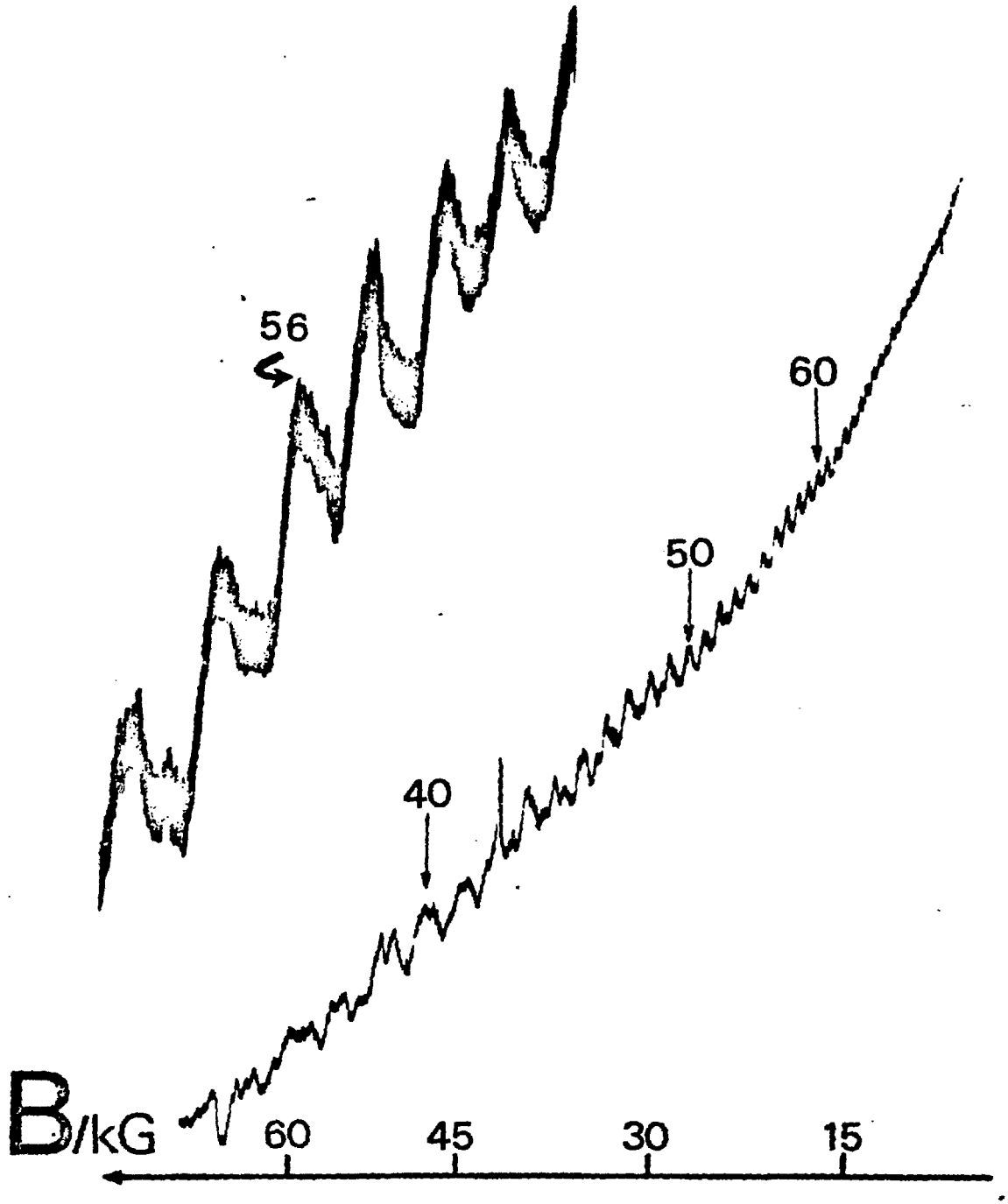

FIG 25

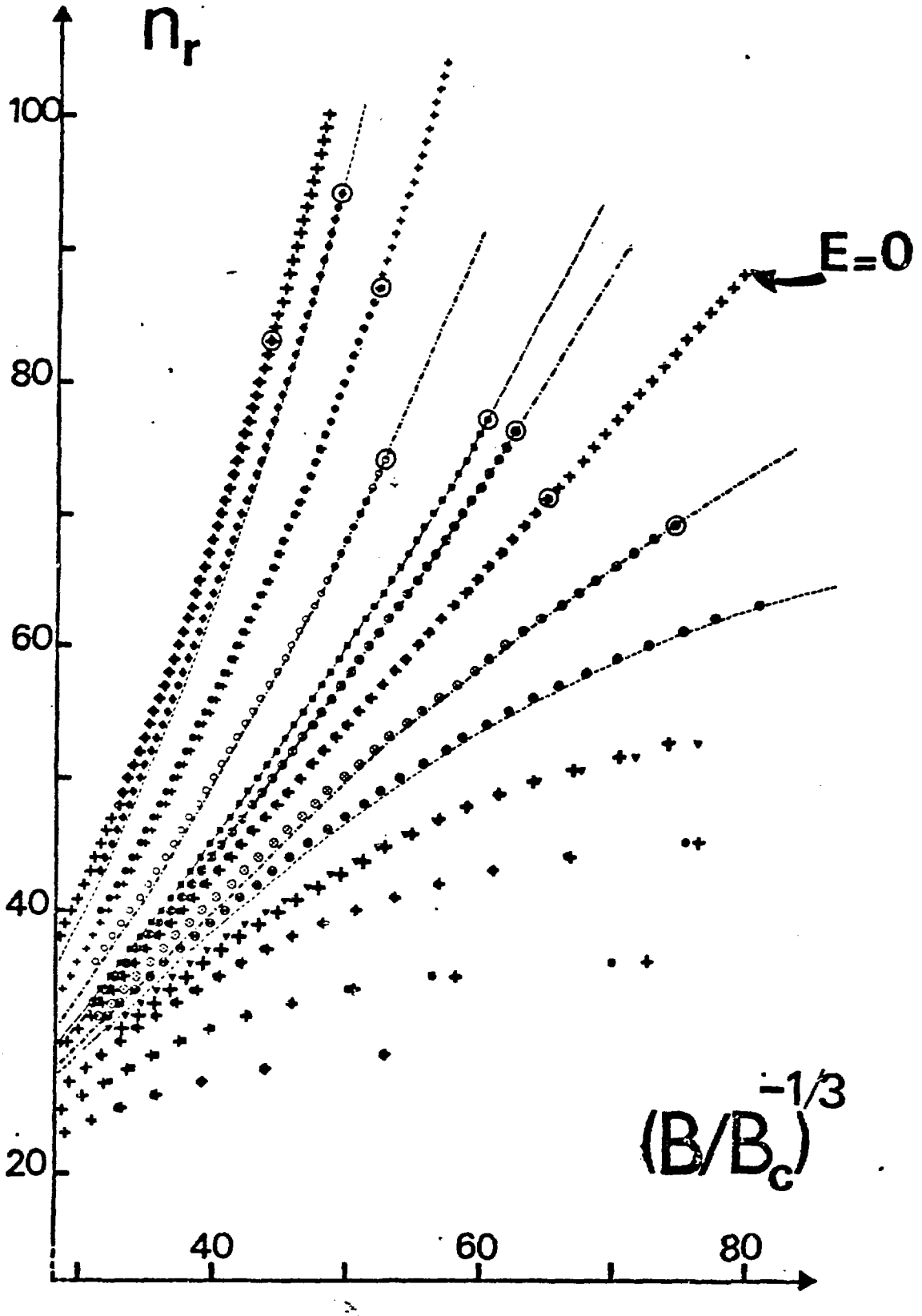

FIG 26

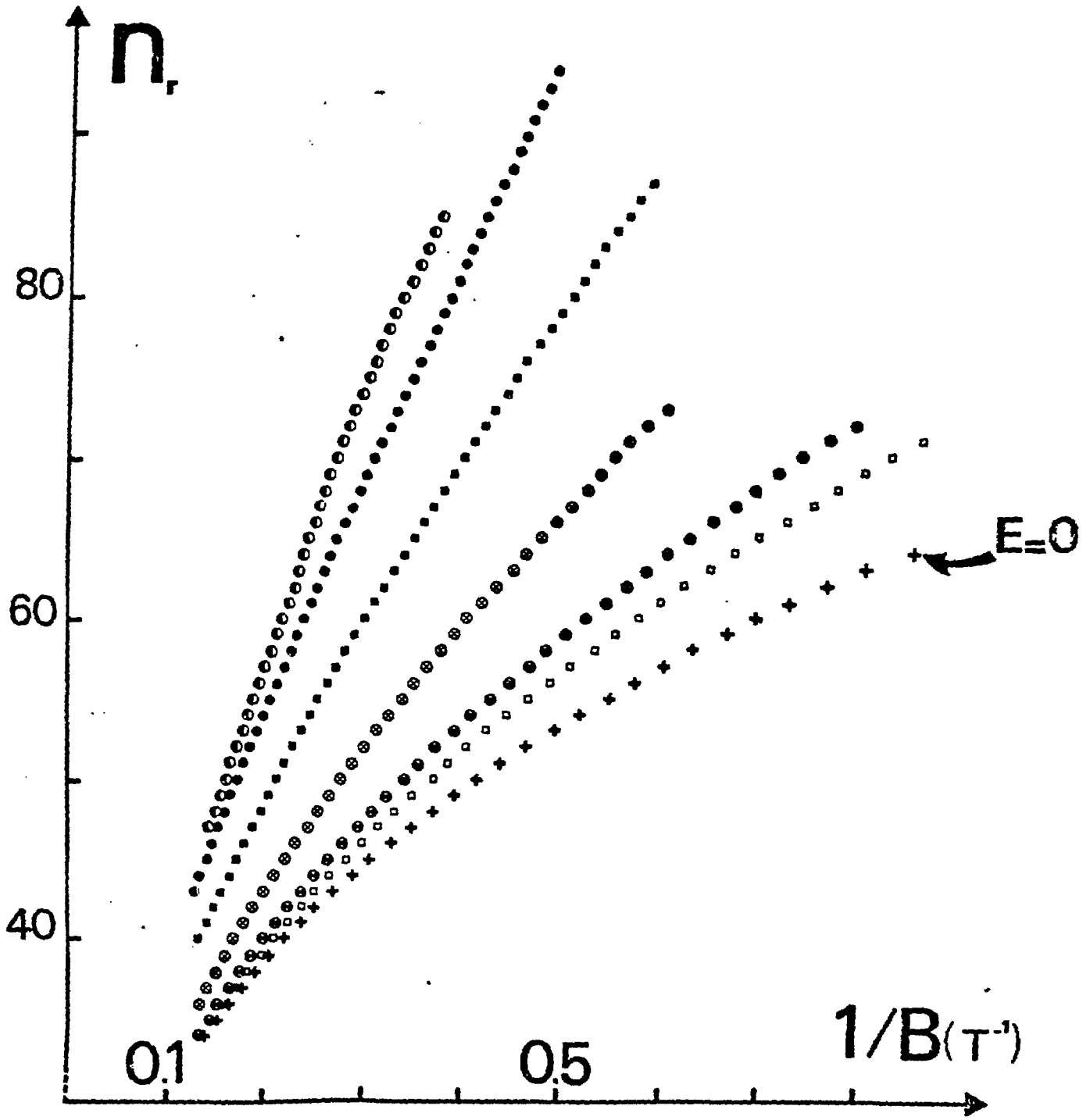

FIG 27

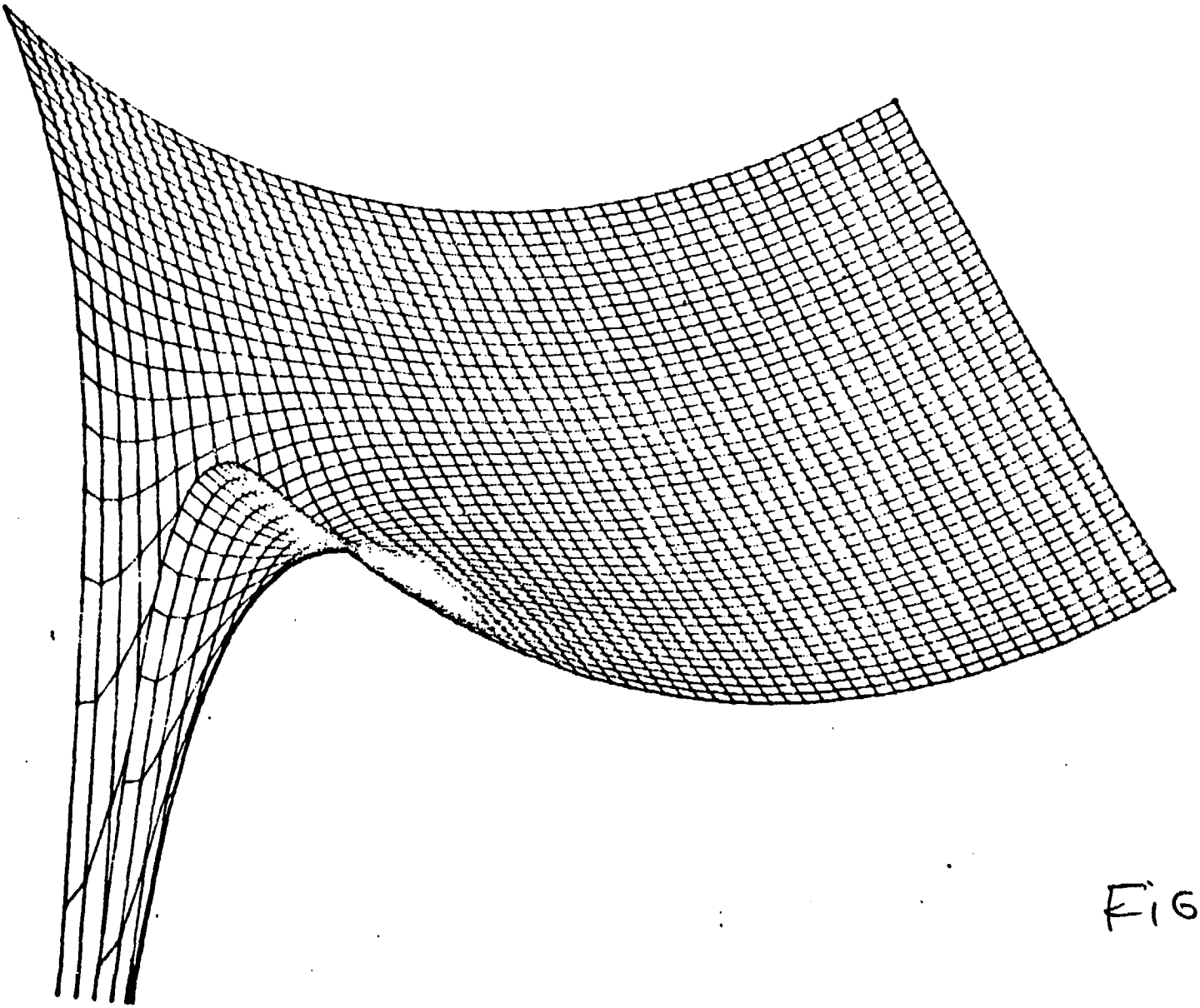

Fig 28

Photodissociation Dynamics of Small Gas Phase Molecules

M.N.R. Ashfold,

School of Chemistry, Bristol University,

Bristol, BS8 1TS, England

2 Tables

23 Figures

Introduction

Any detailed discussion of the vacuum ultraviolet (VUV) photophysics of simple polyatomic molecules must involve consideration of the strong interrelation between photochemistry and spectroscopy. This article will concentrate largely on just one photophysical aspect - photodissociation (i.e. molecular fragmentation as a result of photon absorption), since it represents one of the more probable, more interesting and, indeed, more studied consequences of the interaction of VUV photons with small gas phase molecules. Thus, in the specific examples considered later, neither fluorescence nor photoionisation significantly compete with photodissociation as the dominant decay process from the parent molecule excited states prepared by photon absorption.

Traditionally, photodissociation has been represented most simply in terms of the process:

$$AB + h\nu \longrightarrow A + B$$

Whilst there was a time not so long ago when the limit of a photochemist's aspiration involved mere identification of the product fragments A and B, the combined efforts of present day experiment and theory now render possible a fairly complete picture of the detailed dynamical aspects of the dissociation. In general, the absorbed VUV photon will carry energy, $h\nu$, greater than that required to break the A - B bond, $D_o^o(A-B)$; often in fact the excess energy will be sufficient to allow formation of one (or even both) of the fragments in electronically excited states - these may spontaneously fluoresce. In pre-laser times, the observation of this photofragment fluorescence represented the only possible route to a study of photodissociation dynamics under anything even approaching collision-free conditions. Hence, in part at least, the traditional emphasis on studies of small molecule photodissociations as a result of VUV (rather than less energetic near UV or even visible) photo-

excitation. Important photochemical and spectroscopic information may be derived from measurements of the branching ratios for the various energetically allowed decomposition pathways following photon absorption; studies of this kind will provide a useful point of entry into this survey of the VUV photophysics of a few selected gas phase small molecules.

Having characterised some, or preferably all, of the fragmentation channels further insight into the dynamics of any particular dissociation process will require completion of the detailed energy balance between reactants (parent molecule plus the photon) and the resulting photofragments. Overall energy conservation requires that the excess energy be partitioned into relative translational motion of the recoiling fragments and/or into their respective internal quantum states, i.e.

$$E_{int}^{AB} + h\nu = E_{int}^{A} + E_{int}^{B} + \frac{\underset{\sim}{P}^2}{2\mu_{AB}} + D_o^o(A\text{-}B)$$

where the product's relative translational energy is expressed in terms of their relative linear momentum $\underset{\sim}{P}$. Angular momentum conservation can influence the pattern of energy disposal through the requirement that:

$$\underset{\sim}{J}_{AB}^* = \underset{\sim}{J}_A + \underset{\sim}{J}_B + \underset{\sim}{L}$$

where $\underset{\sim}{J}_{AB}^*$, $\underset{\sim}{J}_A$ and $\underset{\sim}{J}_B$ are the rotational angular momenta of the photoexcited molecule and the resulting photofragments respectively, and $\underset{\sim}{L}$ is the relative orbital angular momentum of the recoiling fragments. As we proceed, the importance of angular momentum conservation in constraining the partitioning of the excess energy amongst the various product degrees of freedom will become increasingly apparent.

Product state detection methods are now sufficiently advanced to have enabled precise determination of the primary energy disposal in a number of photodissociations. For example, the translational energy disposal may be derived through measurement of the fragment velocity distributions using

molecular beams and time-of-flight methods. Internal vibrational, and even rotational, state distributions have been obtained by monitoring and analysing the wavelength resolved spontaneous fluorescence from electronically excited product species, or the laser induced fluorescence (LIF) from ground state photofragments under collision-free conditions. Nozzle expansion techniques are beginning to find a role in narrowing the thermal spread of energies E_{int}^{AB} and rotational states J_{AB^*} from which a given dissociation proceeds. Nevertheless, any attempt to provide a detailed interpretation of the observed energy partitioning is likely to remain somewhat speculative in the absence of reliable information concerning the properties of the excited state of the parent molecule from which dissociation occurs.

Thus necessarily we must concern ourselves also with some of the various types of study that attempt to probe the nature of the excited state or states populated through VUV photon absorption. One natural starting point involves analysis of the VUV absorption spectrum of the parent molecule. This, as we shall see, tends to be no easy matter since, even in simple molecules, many of the electronic transitions at these energies give rise to broad continua that can only be assigned through recourse to accurate theoretical calculations. Even in those instances where population of the excited state gives rise to a structured spectrum it is unusual for the predissociation rate out of the initially prepared state to be sufficiently slow for rotational structure to be adequately resolved and thereby allow assignment of the orbital symmetry and excited state geometry. The fact that both intravalence and Rydberg excitations can be expected in this wavelength region further complicates spectral analysis. Preparation of excited states possessing substantial Rydberg character will involve electronic promotions to large, diffuse molecular orbitals which to all intents may be envisaged as centred on an "atom-like" molecular core; details of the molecular geometry will therefore be expected to have relatively little effect on the orbital character.

Adopting the opposite viewpoint, the more spatially extensive the Rydberg orbital, the less influence will it have on the molecular bonding - the photo-excited molecule will therefore tend towards the equilibrium geometry associated with the molecular ion. If the ion itself is stable with respect to dissociation, then it is not unreasonable to suppose that the higher lying Rydberg states of the neutral molecule will also be comparatively stable. Thus it is that Rydberg transitions frequently manifest themselves as sharp, well defined features in VUV absorption spectra (see fig.1), especially in situations where the Rydberg state geometry differs appreciably from that associated with the neighbouring, near iso-energetic (dissociative) intravalence states since, in these circumstances, Franck-Condon considerations may restrict the predissociation rate from the initially prepared Rydberg state.

Complementary data for the excited states of the parent molecule can frequently be obtained through monitoring the wavelength dependence of the yields of the various primary photofragments. Judicious application of state to state correlation diagrams linking the parent molecule and the various product channels can aid assignment of excited state symmetries. We shall see that analysis of the collision-free photofragment angular distributions following dissociation brought about by an anisotropic photo-excitation (through use of a linearly polarised laser pulse, for example) can provide information about the excited state symmetry, geometric configuration and lifetime with respect to fragmentation. In cases where an electronically excited species is produced, much the same information can be derived through analysis of the polarisation of the resulting photofragment fluorescence.

Further elucidation of the VUV absorption spectra of small molecules can be anticipated as a result of the ever increasing experimental and theoretical interest being shown in multiphoton ionisation (MPI) processes.

A much enhanced ion yield is obtained whenever the overall MPI occurs via a longevous resonant intermediate excited state of the neutral parent molecule. Thus MPI spectra tend to reveal the structure due to Rydberg states without interference from those (predominantly dissociative) intravalence states that lie in the same wavelength region and normally complicate the more conventionally obtained VUV absorption spectrum [3-5].

In the remainder of this article we shall concentrate on studies of the photofragmentation of a few specific molecules which, hopefully, will serve to demonstrate the applicability of many of these currently available techniques to investigations of this kind. In no way is it the author's intention that this work should attempt to compete with any of the now numerous and comprehensive recent reviews of the VUV photochemistry and spectroscopy of small molecules [6-8] or their photofragmentation dynamics [9-13]. Rather it is hoped to provide (i) a feel for the kind of experimental information that is now obtainable, both in practice and in principle, (ii) the significance of these results in interpreting some of the finer details regarding the dynamics of photodissociation processes and (iii) some indication of the likely, and the desirable, directions that this kind of research should take.

The first of the three illustrative case studies will involve photofragmentation brought about using near UV excitation wavelengths; this largely reflects the continuing shortage of readily available and sufficiently intense, tunable sources of monochromatic VUV radiation.

ICN Photodissociation in the Near Ultraviolet

This temporary excursion into the near UV can be justified by the fact that this system, probably more than any other, has served to illustrate many of the various experimental and theoretical types of investigation currently available. That some of the studies have led to conflicting

conclusions merely serves to demonstrate that in photodissociation processes - as in so many other fields - that which might at first appear straightforward can, when probed in greater depth, reveal many hidden subtleties.

The first absorption feature in the electronic spectrum of ICN comprises an apparently structureless, weak continuum (the so-called $\tilde{A}$-continuum) spanning the wavelength region 220-300 nm, see Fig. 2. The current concensus associates this absorption with a purely intravalence $\pi \rightarrow \pi^*$ transition from the linear ground state of ICN, whose electronic configuration may be represented

$$....(1\pi)^4(6\sigma)^2(2\pi)^4$$

If we assume that a Russell-Saunders (Λ,S) description is the appropriate scheme for coupling the electron spin and orbital angular momenta in ICN, this electronic promotion will result in the possible population of singlet and triplet Δ, Σ^+ and Σ^- states. For a sixteen electron molecule such as ICN, Walsh's rules[15] predict that the excited states may be bent, in which case further complications will likely be introduced by Renner-Teller splitting of the degenerate Δ states. Table 1 provides a correlation between the excited $\pi^3\pi$ electronic state representations for both linear and bent molecular configurations. However, it may be more appropriate to consider the excited states of a relatively heavy molecule such as ICN in terms of a core $(2\pi^3)$, within which there is strong spin-orbit coupling, and an outer electron (3π). The projection of the total electronic angular momentum of each system (core and outer electron) along the molecular axis is quantised and represented by Ω_c and ω respectively. The axial projection of the <u>total</u> angular momentum, Ω, is then derived from the coupling of Ω_c and ω. A schematic correlation between the excited states derived using (Λ,S) and (Ω_c,ω) coupling schemes for the $\pi^3\pi$ configuration of the linear ICN molecule is presented in fig.3. Note that the latter coupling rules yield a total of ten possible excited states. Little of this potential complexity

is apparent from just a simple glance at the ICN absorption spectrum however.

The I-CN bond dissociation energy is 304±5 kJ mol^{-1}. Thus the following product channels are energetically accessible in the near UV photofragmentation of ICN:

$$ICN \longrightarrow I(^2P_{3/2}) + CN(X^2\Sigma^+) \qquad \lambda < 398 \text{ nm}$$
$$\longrightarrow I^*(^2P_{1/2}) + CN(X^2\Sigma^+) \qquad \lambda < 306 \text{ nm}$$
$$\longrightarrow I(^2P_{3/2}) + CN^*(A^2\Pi_i) \qquad \lambda < 292 \text{ nm}$$
$$\longrightarrow I^*(^2P_{1/2}) + CN^*(A^2\Pi_i) \qquad \lambda < 239 \text{ nm.}$$

ICN was one of the first polyatomic molecules to be investigated by the technique of Photofragment Spectroscopy, as pioneered by Wilson and coworkers[6]. In these experiments the pulsed output of a linearly polarised, frequency quadrupled Nd-YAG laser was used to photodissociate a molecular beam of ICN molecules at 266 nm. The resultant CN and I fragment densities reaching the ionisation region of a mass spectrometer located a fixed distance along an axis orthogonal to the crossed laser-molecular beam interaction region were recorded separately and selectively as a function of (i) the time after the 10 ns photodissociating laser pulse (fig. 4) and (ii) the direction of fragment recoil relative to that of the electric vector of the linearly polarised laser beam (fig.5) (17). This latter variation was achieved with the fixed geometry configuration by using a quartz half-wave plate to rotate the $\underline{\varepsilon}$-vector of the linearly polarised laser beam.

Two peaks are observed in the flight time distributions of both products. The more translationally excited set of fragments giving rise to the early time peak must, through total energy conservation, carry less internal excitation. Note that the heavier atomic iodine products display

substantially longer flight times than the CN fragments as is to be expected from linear momentum conservation in the centre of mass frame. The peaks in the I atom time of flight spectrum are less well resolved because the parent molecules from which dissociation occurs themselves possess a distribution of velocities. The fragment recoil velocity distributions are necessarily therefore superimposed on this range of parent molecular velocities and, when the relevant fragment is heavy and therefore relatively slow moving, this parent molecular velocity distribution will to some extent smear out the detail in the laboratory recoil velocity distribution of the fragments. Since D_o^o(I-CN) is known and the average internal energy of the parent molecule E_{int}^{ICN} is readily estimable, it should be possible to calculate how the excess energy provided by the monochromatic photo-excitation is partitioned between the product internal and translational degrees of freedom. This requires that the fragment velocity distribution measured in the laboratory frame of reference be transformed into a translational energy distribution in the centre of mass frame of the molecule (see fig.6). Then the average internal energy associated with each peak in the centre of mass translational energy distribution can be estimated and possible product states deduced. In this particular instance, the photodissociation of ICN at 266 nm, the low internal energy peak ($\downarrow E_{int}$) can only be associated with formation of I atoms and CN fragments both in their ground electronic states, with vibrational and rotational excitation within the CN(X) fragments accounting for the spread of translational energies observed. This channel accounts for ~40% of the total fragmentation yield. Interpretation of the 'slow' peak in the fragment time-of-flight spectrum (labelled $\uparrow E_{int}$) is less clear cut. Figure 5 reveals that its associated internal energy could allow any of three possible fragmentation channels namely (i) I and CN in their ground electronic states

with considerable vibrational and rotational excitation in the molecular fragment, (ii) excited $I^*(^2P_{1/2})$ atoms with ground state, vibrationally unexcited CN or (iii) electronically excited $CN^*(A^2\Pi_i)_{v=0}$ together with ground state I atoms. Alternative experimental techniques have subsequently been applied in order to determine the relative importance of these various decomposition channels; these will be described later.

As mentioned previously, photofragment spectroscopy can also be used to provide information regarding the nature of the photo-excited state of the parent molecule. When, as in this case, linearly polarised light is used, those molecules whose electric dipole transition moments $\underset{\sim}{\mu}$ are aligned parallel to the electric vector $\underset{\sim}{\xi}$ of the polarised light will be excited preferentially. Thus, provided that (i) the subsequent photofragmentation occurs before significant molecular rotation has had the opportunity to wash out the anisotropically oriented ensemble of photo-excited molecules and (ii) the relative translational energy of the separating fragments is much greater than the rotational energy of the parent molecule, this anistropy should be reflected in the angular distribution of the resulting photofragments. In the centre of mass coordinate system this will take the general form characteristic of a dipole radiation pattern.

$$I(\theta) = \frac{1}{4\pi}\{1 + \beta\ P_2(\cos\theta)\}$$

where θ is the angle between the polarisation vector of the exciting beam and the direction of recoil of the separating fragments and $P_2(\cos\theta)$ is the second order Legendre polynomial

$$P_2(\cos\theta) = \frac{1}{2}\ (3\cos^2\theta - 1)$$

The asymmetry parameter β depends on χ, the angle between the electric dipole transition moment $\underset{\sim}{\mu}$ and the direction of fragment recoil through the relationship

$$\beta = c\ P_2(\cos\chi)$$

and can range in value from $\beta = +2$ ($I(\theta)$ shows a $\cos^2$ distribution) to $\beta = -1$ ($I(\theta)$ is a $\sin^2$ distribution). For a diatomic molecule (except, for example, in the case of 'near threshold' dissociations where the relative velocity of the separating fragments is sufficiently low that a significant tangential velocity contribution can arise from the rotational motion of the photo-excited molecule) fragment recoil must occur along the internuclear axis and χ is therefore restricted to the values $\chi = 0^o$ (a 'parallel' transition) or $\chi = 90^o$ (when the transition moment lies perpendicular to the molecular axis). For polyatomics however there is no such restriction upon the direction of fragment recoil and in general there will be a range of χ values reflecting the distribution of excited state geometries, vibrational and rotational motions.

Through its dependence on c, the asymmetry parameter β also depends on the lifetime of the excited state. The quantity $c = 2$ if the photoexcited molecules do not rotate at all prior to fragmentation; it decreases smoothly to a value of 0.5 if the photoexcited state survives for a number of rotations. Thus the previously quoted limits to the range of possible β values are reduced by a factor of four if the rotational period is short compared to the excited state lifetime |18| and the observed angular distribution will be more uniform.

Figure 5 shows the laboratory angular distribution of the CN fragments for both the $\downarrow E_{int}$ and $\uparrow E_{int}$ peaks arising in the 266 nm photodissociation of ICN. Since the CN fragment relative velocities are much greater than the average velocity of the ICN parents, transformation into the centre of mass coordinate system little affects the form of the angular distributions, both product channels show a maximum centred at $\theta \approx 0^o$. This result implies that the photo-excited state (or states) leading to both product channels is accessed via a parallel transition, with the transition dipole moment lying predominantly along the I-C bond in ICN from which it follows that

the excited state (or states) has $\Omega = 0$ if linear or, if it is bent, has A' symmetry. Values of the asymmetry parameters β for the two angular distributions ($\beta = 1.40$ for $\dot{+}E_{int}$ and $\beta = 1.12$ for $\dot{+}E_{int}$) were estimated |17| by fitting the experimental data points to the appropriate expression for $I(\theta)$ in the laboratory frame. The reduction from the theoretical value of $\beta = 2$ for a 'pure' parallel process could be attributable to any of four factors: (i) parent molecular rotation, (ii) a contribution from a perpendicular transition that gives rise to the same products, (iii) a bent geometry for the photo-excited ICN and / or (iv) lifetime of the ICN excited state. If one attributes <u>all</u> of the 'lost' asymmetry to (iv) an absolute upper limit for the excited state lifetime(s) can be estimated. This analysis yields maximum lifetimes of 0.2 psec and 0.1 psec. respectively for the excited state or states leading to the $\dot{+}E_{int}$ and $\dot{+}E_{int}$ product peaks. |17|.

In summary then, photofragment spectroscopy reveals that ICN photodissociation at 266 nm yields (at least) two product channels derived from one (or more) short lived photo-excited states which, if bent, have predominantly A' symmetry or, if linear, have $\Omega = 0$. One fragment channel, which comprises ~40% of the total dissociation yield, gives rise to I and CN fragments in their ground electronic states; the internal energy partitioning within the fragments arising from the other 60% of dissociations cannot be unambiguously ascertained. Clearly this information is required if we wish to gain a deeper insight into this particular photodissociation process.

Fortunately a number of recent studies have provided much complementary information. For example, West and Berry |19|, using synchroton radiation, measured the relative quantum yield for formation of electronically excited $CN(A^2\Pi_i)$ fragments in the photodissociation of ICN as a function of wavelength and found <u>no</u> CN(A→X) emission following excitation at wavelengths

longer than 210 nm, thus ruling out one possible attribution for the 'slow' peak in the photofragment time-of-flight spectrum. Quantum yield measurements have also been used to establish the relative importance of another of the possible dissociation channels:

$$ICN \longrightarrow I(^2P_{1/2}) + CN(X^2\Sigma^+)$$

following excitation of ICN at various wavelengths within its $\tilde{A}$ - continuum [20]. By measuring the intensity of the $L(^2P_{1/2} \rightarrow {}^2P_{3/2})$ emission at 1.315μm following ICN photolysis at any particular wavelength and comparing it with the $I(^2P_{1/2})$ emission intensity observed from photolysis of either $i\text{-}C_3F_7I$ or CF_3I (for both of which the $I(^2P_{1/2})$ quantum yields are known) under identical conditions, these measurements can be put on an absolute scale. The product of these experimentally determined quantum yields, Φ_{I^*}, multiplied by the molar extinction coefficient of ICN, ε_{ICN}, at each wavelength provides the absorption profile for the electronic state(s) correlating with $I(^2P_{1/2}) + CN(X)$. This is shown in fig.7, along with the 'difference' spectrum obtained by the subtraction $\varepsilon_{ICN} - \phi_{I^*}\varepsilon_{ICN}$: in view of West and Berry's observation, these latter absorptions must correlate with ground electronic state I and CN fragments. The results therefore strongly suggest that (at least) three excited states contribute to the broad $\tilde{A}$-continuum in the ICN absorption spectrum, all of which may well be accessed by photon absorption at 266 nm. The two peaks observed in the translational photofragment spectrum following 266 nm photodissociation of ICN can be assigned to electronic branching in the atomic iodine product, with the channel leading to I^* formation accounting for 61% of the total dissociation yield at this wavelength. Finally, the observation that the product branching ratios display such a sensitive dependence upon photolysis wavelength should sound a cautionary note when attempting to interpret results from broadband flash photodissociation experiments.

Laser Induced Fluorescence (LIF) has been used to estimate the partitioning of internal (vibrational and rotational) energy within the CN(X) fragments formed in the 266 nm photodissociation of ICN |21-23|. A tunable dye laser is used to selectively excite CN fragments in a specific quantum state (or states) to fluorescence; a plot of the resulting LIF intensity against the probing laser wavelength yields an LIF spectrum. Fig.8 shows such a spectrum obtained following laser excitation on the CN(B←X) violet transition. |22|. Nascent product state distributions can be determined by arranging for the pulsed dye laser to probe at a sufficiently short time delay after the photolysis pulse that collisional relaxation is unimportant. Relative quantum state populations can be extracted with confidence from well resolved spectra such as fig. 8 when the appropriate Franck-Condon factors and rotational line strengths are known. Analysis of this particular spectrum reveals that >95% of the CN(X) fragments formed in the collisionless 266 nm photodissociation of ICN are produced in their v"=0 level with a markedly non-statistical distribution of rotational state populations that peaks at very low rotational quantum number, N"≈1-2; however, the tail of the distribution extends to high rotational levels (population of the level v"=0, N"=56 can be discerned from fig.8) |22|.

Unfortunately, in view of the previous analysis, we recognise that this rotational state distribution in the CN(X) fragment must represent the superposition of the two separate rotational state distributions resulting from the two product channels yielding $I(^2P_{3/2})$ and $I(^2P_{1/2})$ respectively. This does not prevent a qualitative estimate of how the total available energy is partitioned: for both the dominant fragmentation channels product vibrational excitation is clearly negligible, roughly 10% of the excess energy goes into CN rotation, with the balance appearing as relative translational excitation of the separating fragments |22|. This preferential partitioning of the available energy into interfragment recoil apparently

occurs for ICN photodissociation throughout its Ã-continuum. LIF has been used to show that the CN(X) fragments produced in the broadband flash photolysis of ICN at λ>220 nm exhibit a very similar overall energy partitioning amongst their various degrees of freedom |24|. Collision-free quantum state distributions for the CN(X) fragments produced in the 299.4 nm photodissociation of ICN have recently been reported |23|. From the interpretative viewpoint, excitation at this wavelength (which may be obtained as the first Stokes shifted line in the stimulated Raman scattering of 266 nm radiation in H_2) provides two potentially significant advantages. Firstly, the previously described quantum yield measurements |20| have been interpreted |23| as showing that ICN absorption at this wavelength is principally due to just one (admittedly uncharacterised) electronically excited state; secondly, the dissociation channel leading to excited iodine atom product formation is barely accessible energetically. Thus it may be hoped that the observed product state distributions, which whilst again showing that translational fragment recoil accounts for the bulk of the available energy also reveal a slightly higher level of vibrational excitation and more simple, Boltzmann-like rotational state distributions in the CN(X) product, should prove more amenable to detailed theoretical analysis.

Results for the vibrational and rotational energy partitioning within the CN(X) fragments produced in the photodissociation of ICN in its Ã-continuum have proved popular with theoreticians for testing various models of the photodissociation process |25-29|. Despite the apparent wealth of experimental data for this system, the continuing inadequate characterisation of the nature and geometry of the photoexcited state or states involved makes this a far from ideal test case. Discussion of the principle features of some of the models for the photodissociation process will therefore be reserved for a later section.

The following points should be stressed in concluding this section. Despite the fact that considerable selectivity has been exercised in this presentation it should be clear that the photodissociation of ICN, at 266 nm in particular, has been the subject of intensive study. For this wavelength at least we feel confident in our identification of the primary product channels and their relative branching ratios, and we have a fair idea of the energy partitioning within these product channels. Yet our understanding of the dissociation process remains poor, and will remain so, in the absence of more precise information on the identity, geometry and indeed the number of photoexcited states from which these dissociation channels arise.

VUV photodissociation of HCN

In contrast to the extensively studied ICN photofragmentation summarised in the previous section, comparatively few investigations of this process have been reported. Nevertheless we shall see that those results which have appeared are able to provide a more complete picture of this particular photodissociation.

The first intense features in the VUV absorption spectrum of HCN lie in the wavelength region 130 nm $<\lambda<$ 150 nm. These take the form of a progression of strong bands separated by 750 - 850 cm^{-1} (see Fig.9), and have been attributed to excitation of the ν_2' bending vibrational mode in the $\tilde{C}$ electronic state |30-32|. Some of the more intense members of a second, weaker progression are apparent to shorter wavelengths; these correspond to the series (0, ν_2',1) in which one quantum of the HC-N stretching frequency ν_3', as well as the bending mode ν_2', have been excited. Franck-Condon considerations immediately suggest that these progressions in ν_2' indicate an electronic promotion from the linear $\tilde{X}^1\Sigma^+$ ground state to a <u>bent</u> excited state. However in this instance spectroscopy can tell us far more. Despite the facts that all of the bands in the vibrational progression show some diffuseness - indicative or predissociation in the excited state - and that this diffuseness increases rapidly with increasing ν_2' quantum number,

sufficient rotational structure has been discerned and analysed |30| for the first members of the $\tilde{C}$-$\tilde{X}$ transition to allow identification of the symmetry, A', and equilibrium geometry, $\angle HCN \sim 141^{\circ}$, of the photoexcited state. The ground state electronic configuration of HCN may be represented:

$$....(4\sigma)^2\ (5\sigma)^2\ (1\pi)^4 \qquad \tilde{X}^1\Sigma^+ \qquad (C_{\infty v})$$

or $$....(4a')^2\ (5a')^2\ (1a'')^2\ (6a')^2 \qquad \tilde{X}^1A' \qquad (C_s)$$

(for a correlation see fig.10). There is now reasonable concensus [8] that the $\tilde{C}$ state may be assigned to the A' component of the $^1\Pi$ state arising from the $5\sigma \rightarrow 2\pi$ (or $5a' \rightarrow 7a'$) electronic excitation; such a transition is electric dipole allowed for both linear and bent geometries which accounts for its strong showing in the HCN absorption spectrum.

Additional support for this analysis and assignment has been provided by studies of photofragment fluorescence excitation spectra, relative quantum yield and photofragment fluorescence polarisation measurements, and by study of the isotopic species DCN. Three photodissociation channels are energetically accessible to HCN and DCN in this wavelength region:

$$H[D]CN \longrightarrow H[D]\ (^2S_{\frac{1}{2}}) + CN(X^2\Sigma^+) \qquad \lambda<238\ nm$$

$$\longrightarrow H[D]\ (^2S_{\frac{1}{2}}) + CN(A^2\Pi_i) \qquad \lambda<190\ nm$$

$$\longrightarrow H[D]\ (^2S_{\frac{1}{2}}) + CN(B^2\Sigma^+) \qquad \lambda<149\ nm$$

The latter two fragmentation pathways yield electronically excited fragments which can be readily monitored through observation of their spontaneous fluorescence. The $CN(A^2\Pi_i)$ state fluoresces in the red and near infrared and has a relatively long radiative lifetime, τ_{rad}~4.2μs, whilst the higher energy $CN(B^2\Sigma^+)$ state radiatively decays to the ground state in the violet region of the spectrum with a lifetime of ~60 ns. Photofragment Fluorescence Excitation Spectra (PFES) for HCN have been obtained by measuring either the total CN(A→X) emission |31| or the total CN(B→X) emission |31,32| as a

function of the excitation wavelength using either a synchrotron or a microwave powered rare gas discharge as the continuously tunable source of VUV radiation. These spectra are displayed in fig.11. Although each spectrum only provides a record of the branching into one particular dissociation channel, comparison of the appropriate PFES with the parent molecular absorption spectrum can give a measure of the relative decomposition rate via that channel as compared with the total fragmentation rate from the excited state or states prepared by photoexcitation. Such quantum yield measurements have the potential to reveal specific excited state → product channel correlations. In the case of HCN the ($\tilde{C}\rightarrow\tilde{X}$) absorption spectrum and PFES (figs.9 and 11) show a qualitative similarity which on closer inspection reveals that the dissociation channels leading to formation of electronically excited CN products increase in importance at the shorter excitation wavelengths, though never represent much more than ~20% of the total fragment yield.

The absorption and photofragment CN(B→X) fluorescence excitation spectra associated with the equivalent $\tilde{C}\rightarrow\tilde{X}$ transition in DCN display a more complex appearance (see fig.12). In addition to the progressions $(0,\nu_2',0)$ and $(0,\nu_2',1)$ which were identified in the HCN($C\rightarrow\tilde{X}$) system, another strong series of bands can be recognised in which each member is displaced from a corresponding band in the $(0,\nu_2',0)$ sequence by a frequency appropriate to one quantum of the D-CN stretching frequency, ν_1'. Just as for HCN, the quantum yield for forming CN(B) in the predissociation of DCN gradually increases as the excitation wavelength decreases. A recent ab initio calculated potential energy surface for the $\tilde{C}^1A'$ state of HCN and DCN has provided a plausible interpretation for the much greater simplicity of the CN(B→X) PFES from HCN. |33| The topography of the surface is such that excitation of the ν_2' bending mode allows the ν_1' stretching motion to sample a variety of different tunnelling barriers. Near the $\tilde{C}$ state equilibrium

configuration ($\angle$HCN ~ 141°), the radial potential shows no barrier and thus motion along the H-CN stretching coordinate will, for this particular dissociation channel, be either bound or directly dissociative depending upon whether the stretching energy is less than or greater than that of the asymptotic dissociation limit for H + CN(B). As the bending mode is excited and the H atom moves away from its equilibrium angular position, the radial potential energy curves exhibit barriers which can give rise to predissociative behaviour. Thus, structure in figure 12 reveals predissociation from levels $(1,\nu_2',0)$ in DCN($\tilde{C}$) where ν_2' = 5-12. However, the increased energy associated with one quantum of ν_1' when D is replaced by H raises all of the corresponding excited levels in HCN ($\tilde{C}$) above their respective dissociation barriers from where direct dissociation simply generates a structureless contribution to the continuum underlying the CN(B→X) PFES of HCN in this region (figure 11).

Thus in the VUV photodissociation of HCN and DCN, and in marked contrast to the previously considered near UV photofragmentation of ICN, conventional spectroscopic techniques are able to provide a fairly detailed picture of the photoselected excited state. Confirmation of the excited state symmetry has been provided through use of the technique of polarised photofluorescence excitation spectroscopy [32,34,35]. The physical principles underlying this technique are essentially the same as those described previously which allow identification of excited state symmetries from product angular distributions in photofragment spectroscopy. In this case, however, the anisotropic distribution of photoexcited molecules is revealed in the polarisation of the fluorescence from electronically excited fragments produced in the dissociation process.

By way of a general illustration, consider the photodissociation of a bent triatomic molecule ABC by a beam of linearly polarised light in which an electronically excited fragment is produced. As before, preferential

photoselection of those molecules whose transition dipole moment $\underset{\sim}{\mu}$ lies in the direction of the electric vector $\underset{\sim}{\varepsilon}$ of the linearly polarised light beam will occur, leading to a spatially anisotropic distribution of photo-excited ABC^* molecules. Again, provided that the subsequent dissociation occurs on a timescale that is rapid in comparison to the rotational period of the photoexcited ABC^*, some of this anisotropy will be transferred to the fragments. Since intramolecular motions in a bent triatomic molecule will lie in a plane, the trajectory of the departing atomic fragment C will tend to be confined within the molecular plane of the photoexcited ABC^* whilst the electronically excited diatomic AB^* will tend to be formed with its angular momentum vector $\underset{\sim}{j}_{fragment}$ directed perpendicular to this plane. The dissociation dynamics will be important in determining the magnitude of $\underset{\sim}{j}_{fragment}$. Overall angular momentum conservation requires that the separating atomic product exerts a torque on the molecular fragment AB^*. This torque will obviously be enhanced when photoexcitation causes a change in the equilibrium bond angle and in these instances, at least, the contribution to $\underset{\sim}{j}_{fragment}$ from the rotation of the parent molecule may safely be neglected. Since the fluorescent emission from AB^* will be preferentially directed along its transition moment $\underset{\sim}{\mu}_{em}$, the anisotropic spatial distribution of the product diatomic rotors arising in the photofragmentation of ABC^* will reveal itself as polarised fluorescence.

Two possibilities can arise when we come to consider the alternative general case, where the molecule ABC has a linear ground state:

(i) If the excited state ABC^* prepared by photon absorption is linear too (a linear→linear transition) the resulting photofragments will tend to separate along the ABC internuclear axis. The dynamics of such a dissociation process will cause little torque between the recoiling fragments; consequently the rotational angular momentum of the parent molecule cannot be ignored. We

shall see in more detail later that in these circumstances, angular momentum conservation requires the mapping $\underset{\sim}{J}_{parent} \rightarrow \underset{\sim}{j}_{fragment}$ though this requirement must necessarily be relaxed in, for example, near threshold dissociations where the constraint of overall energy conservation must also be satisfied.

(ii) Where photoexcitation leads to population of a non-linear excited state (linear → bent transition) the molecular transition moment must lie either in, or perpendicular to, the plane of the bent excited state ABC^*. As before, linearly polarised irradiation will selectively excite those molecules for which the product $|\underset{\sim}{\mu}.\underset{\sim}{\varepsilon}|^2$ is a maximum, as a result of which the photoexcited ABC^* molecules will tend to bend into planes that are respectively parallel or perpendicular to the $\underset{\sim}{\varepsilon}$ vector of the incident beam. Provided that the linear → bent geometry change in the photoexcitation develops sufficient torque that $\underset{\sim}{j}$ fragment >> $\underset{\sim}{J}_{parent}$ this situation is equivalent to that encountered previously following excitation from a non-linear ground state. Any spatial anisotropy in the ensemble of photoexcited parent molecules ABC^* will manifest itself as an anisotropic distribution of $\underset{\sim}{j}_{fragment}$ orientations. Thus for either a linear → linear or a linear → bent transition the spatial distribution of $\underset{\sim}{j}_{fragment}$ is anisotropic and the subsequent AB^* fluorescence will be polarised. As with the photofragment angular distributions discussed earlier, measurement of the degree of polarisation can provide information about the symmetry of the photoexcited state and its lifetime with respect to dissociation.

The extent to which fluorescence is polarised is traditionally represented by the degree of polarisation, p, defined as:

$$p = \frac{I_{\parallel} - I_{\perp}}{I_{\parallel} + I_{\perp}}$$

where $I_{\parallel}$ and $I_{\perp}$ are respectively the intensity of fluorescence measured through an analyser aligned parallel, or perpendicular, to the $\underset{\sim}{\varepsilon}$-vector of the linearly polarised photolysis beam. The degree of polarisation may also

be expressed in terms of the average angle γ between the electric dipole transition moment of the parent molecule ABC (approximated by a hertzian dipole oscillator with the same directionality, $\underset{\sim}{\mu}_{abs}$) and that of the electronically excited fragment AB^* (again approximated by a dipole oscillator, $\underset{\sim}{\mu}_{em}$) through the relationship:

$$p = \frac{3\cos^2\gamma - 1}{\cos^2\gamma + 3}$$

Clearly it is necessary to consider the average value of $\cos^2\gamma$ in order to apply this equation. This has been done [35] for a range of possible situations in the photodissociation of triatomic molecules. Table 2 lists the values for $\cos^2\gamma$, and hence p, determined for various cases of parallel and perpendicular photoexcitations in the parent molecule ABC (e.g. $\underset{\sim}{\mu}_{abs}$ parallel or perpendicular to the triatomic plane for bent → bent and linear → bent transitions or, in the case of linear → linear transitions, $\underset{\sim}{\mu}_{abs}$ parallel or perpendicular to $\underset{\sim}{J}_{parent}$) and for $\underset{\sim}{\mu}_{em}$ parallel or perpendicular to $\underset{\sim}{j}_{fragment}$.

A number of factors can cause the experimentally observed degree of photofragment fluorescence polarisation to be substantially less than these theoretical values. For example, in those cases where AB^* radiates via a perpendicular electronic transition (e.g. $^1\Sigma - {}^1\Pi$) table 2 reveals that the polarised fluroescence from P and R branch transitions will show the opposite sign to that from Q branch transitions. When individual rotational lines in the emission spectrum are not resolved the measured degree of polarisation will obviously be much reduced. Similarly it may not be possible to specifically photoselect only P and R, or Q, branch features in the excitation of linear → linear parent molecular transitions; the reduced degree of polarisation displayed by the resulting photofragment fluorescence will reflect this reduced anisotropy in the photoexcitation stage. Obviously the interpretation of experimentally derived degrees of polarisation becomes even more complex in situations where photon absorption prepares more than one

excited state. In deriving the theoretical values for p it is assumed that the photoexcited molecule fragments directly, i.e. it has no time to rotate before dissociating, and that the AB^* fragment undergoes no collisions during its radiative lifetime; predissociations can be expected to show a reduced degree of polarisation |36|.

Before returning to the main theme of this section - the VUV photodissociation of HCN and DCN - consider, as a particularly clear and illustrative example, the collisionless photodissociation of $HgBr_2$ using linearly polarised 193 nm radiation. The visible HgBr ($B^2\Sigma^+ \rightarrow X^2\Sigma^+$) fluorescence from the resulting HgBr(B) photofragments (τ_{rad} = 23.7 ns) is found to be linearly polarised, p = 11.9 ± 1.5% |37|. For this sixteen electron species Walsh's rules |15| predict a linear ground state and that the lower lying excited states are bent. This measured degree of polarisation, combined with the knowledge that the fluorescent emission involves a parallel (Σ-Σ) transition enables use of the data of table 2 to deduce that $\underset{\sim}{\mu}_{abs}$ lies in the molecular plane of $HgBr_2$. That the observed p is so close to the theoretical value (p = $^1/_7$) confirms the direct nature of the dissociation; assuming $D_{\infty h}$ symmetry for the ground state and C_{2v} symmetry for the excited state the dissociative transition may be identified as $^1B_2(^1\Sigma_u^+) \leftarrow {}^1\Sigma_g^+(^1A_1)$.

The polarisation of the CN(B → X) fluorescence resulting from photodissociation of HCN and DCN in the wavelength region 130-150 nm has been measured following excitation by an unpolarised, parallel beam of light |32|. Under these circumstances a reduced degree of polarisation

$$p' = \frac{p}{2-p}$$

is to be expected |35|. Results for DCN are displayed in figure 12. All of the main features of the respective PFES of HCN and DCN show positive polarisation. Since the CN(B → X) transition moment is directed parallel to the internuclear axis, reference to table 2 demonstrates that this observation is wholly consistent with the spectroscopic assignment of A'

symmetry for the excited state of the parent molecule. That the maximum degrees of polarisation observed even at the shorter wavelengths ($p' \sim 0.04$, $p \sim 0.08$) are less than the classically permitted maximum value ($p = 1/7$) may be attributed to some molecular rotation during the excited state lifetime with respect to predissociation [32]. We shall see more powerful demonstrations of the utility of polarised photofluorescence excitation spectroscopy when considering the VUV photodissociation of the cyanogen halides in the next section.

Measurements of the internal energy disposal in the fragmentation channel

$$H(D)CN + h\upsilon \rightarrow H(D) + CN(B^2\Sigma^+)$$

following excitation at the various monochromatic wavelengths provided by readily available atomic resonance lamps have also been used to derive some insight into the dynamics of this dissociation [38]. Armed with knowledge of the appropriate Franck-Condon factors and rotational line strengths, product vibrational and rotational state population distributions may readily be obtained through analysis of the wavelength resolved spontaneous CN(B→X) photofragment fluorescence under collision-free conditions. For the available excitation wavelengths energy conservation requires that the atomic H or D product be formed in its ground electronic state; thus, provided that the energetic threshold for the dissociation is known, completion of the detailed energy balance will yield the relative translational energy of the recoiling fragments.

Much theoretical effort has been devoted to modelling product state distributions arising in photodissociations of this kind, with a view to identifying the more important features of the potential energy surface over which the dissociation proceeds. The more recent models recognise the likely importance of each of the following effects on the eventual product state distributions:

(i) the Franck-Condon factors for the intrafragment, structural rearrangement of the molecular framework during transfer onto the final dissociative surface

(ii) interfragment final state interactions, where the impulsive recoil of the separating dissociation products affects the final translational, vibrational and rotational state distributions, and

(iii) the constraints imposed by the necessity to simultaneously conserve both the total energy and angular momentum of the photodissociating system; these last constraints reveal themselves most clearly through their influence on the form of the product rotational state distributions.

Historically, models for vibrational energy disposal in photodissociations have ranged widely in both the level of approximation introduced in formulating the problem and the mathematical sophistication employed in solving it. Simons and Tasker [25] were the first to present a so-called 'global' model that incorporated both intrafragment (i) and interfragment (ii) contributions to the ultimate vibrational energy disposal. For mathematical simplicity they presumed (as have most subsequent theoretical models [26]) the retention of linearity during the fragmentation and that the reaction coordinate for the dissociation process evolves from one of the molecule's normal modes. As applied to the predissociation of HCN the correct normal modes are approximated by the localised H-C and C-N bond vibrations. An estimate for the C-N stretching vibrational frequency in the photoexcited state can be gleaned from the absorption and photofragment fluorescence excitation spectra discussed earlier in which a progression involving excitation of one quantum of ν_3' was identified (ν_3'-1800 cm^{-1}). Since this is significantly less than the vibrational frequency of the product diatomic CN(B) fragment (ν = 2164 cm^{-1}) the Franck-Condon factors for this substantial intramolecular rearrangement during the predissociation can be expected to make a major contribution to the eventual vibrational energy disposal. In the absence of detailed information regarding the form of the potential energy surface involved, the interfragment recoil is presumed to occur under a potential that is exponentially repulsive along

the dissociation coordinate (r_{C-H}) and attractive along the C-N stretching coordinate (approximated by a simple harmonic oscillator function for CN(B)). The importance, or otherwise, of final state interactions upon the ultimate vibrational energy disposal is then determined principally by the steepness of the repulsive potential along the dissociation coordinate. |25,28|.

Fig.13 shows that the vibrational state distributions in the CN(B) fragments produced in the VUV photodissociation of HCN and DCN at 130.4 nm, and at two slightly shorter wavelengths, can be reproduced more than adequately by this relatively simple model. The appeal of this approximate model is that the two adjustable parameters involved may be envisaged as having a certain, at least qualitative, physical significance. The best theoretical 'fit' to each of the experimental vibrational distributions involves a considerable change in Δr_{C-N} and hence in the C-N oscillation frequency during the radiationless transfer from the photoexcited state (in accord with experimental observation for the $\tilde{C}^1A'$ state at least) and a large value for the range parameter L in the expression $V_o \exp(-r_{C-H}/L)$ used to describe the shape of the repulsive potential along the dissociation coordinate. Such a value is consistent with a gently repulsive potential between the separating fragments, and indicates that final state interactions make only a minor contribution to the eventual product vibrational excitation.

The more rigorous quantum mechanical models can, in principle at least, utilise a more correct normal mode description and the full, unseparated bound-free overlap integral |25| for the photodissociating molecule. Despite the added levels of mathematical complexity however, any solution to the problem must remain, at best, semi-quantitative in the absence of quite precise spectroscopic data for the predissociating state. Thus the continuing appeal of the relatively simple models which, when sensibly applied, should be adequate for identifying the dominant influence upon the ultimate vibrational energy disposal in molecular photofragmentations. In the case of HCN and DCN illustrated here, geometry changes within the triatomic molecule during the predis-

sociation largely govern the eventual product vibrational state distributions; a light H or D atom recoiling on a gently repulsive potential energy surface is unable to exert a significant impulsive contribution to the vibrating diatomic.

The comparatively minor effect of final state interactions in this particular dissociation is further demonstrated by the form of the CN(B) fragment's rotational energy disposal. Reference to fig.14 reveals that the rotational state distributions in the CN(B) photofragments produced in the VUV photodissociation of HCN at 147.0 nm and 141.1 nm and of DCN at 141.1nm closely map the room temperature thermal distribution over rotational states in the parent HCN and DCN molecules. No detailed model for rotational energy disposal in photofragmentation is required to account for this result. These photolysis wavelengths are close to the energetic threshold for this dissociation channel and thus the light, separating H and D atoms exert little impulse on the relatively heavy CN fragment as it recoils away. Conservation of angular momentum then requires that the rotational angular momentum of the parent molecules be carried over into the CN fragment rotation, precisely the behaviour observed |38|. In this particular instance it is clear that angular momentum conservation is the dominant influence on the rotational energy disposal. Excitation of HCN at 147.0 nm and 141.1 nm respectively excites the (0,3,0) and (0,6,0) bending vibronic levels of the $\tilde{C}^1A'$ state; neither the change in the excess available energy nor the level of bending mode excitation affect the resulting fragment rotational energy partitioning. At still shorter wavelengths however the excess energy becomes such that a gradual increase in the level of fragment rotational excitation is observed |39|.

Thus it should be clear that the results summarised in this section provide considerable insight into the VUV photodissociation dynamics of HCN. In contrast to the previously considered near UV dissociation of ICN, the structured absorption spectrum possessed by HCN in this wavelength region

allows spectroscopy to make an important contribution to our overall understanding of this predissociative process. Whilst it remains true that most of the detailed results relate to only one fragmentation channel - which in itself represents only about 5% of the total dissociation at any wavelength - the properties of an H or D atom, especially their light mass and their lack of low-lying excited electronic states, are such that a relatively clear picture of many of the more important dynamical features of the HCN fragmentation may be discerned.

VUV photodissociation of the cyanogen halides

As a final detailed case study we shall consider some selected aspects of the much studied VUV photodissociation of ICN, BrCN and ClCN. The VUV absorption spectra of these three molecules have been reviewed in some detail |8,40|, and a recent reassignment of the first two Rydberg features in the ClCN spectrum has been offered |41|. In view of the problems outlined whilst attempting to interpret the near UV absorption spectrum of ICN it should come as no surprise to learn that, if anything, the spectral complexity increases to shorter wavelengths. These three molecules display qualitatively similar spectra, though the corresponding features in each spectrum shift to shorter wavelengths as the mass of the associated halogen atom decreases. A representative spectrum (for BrCN) is shown in fig.15. At energies above the $\tilde{A}$-continuum, each molecule reveals a second region of continuous absorption - the $\tilde{\alpha}$-continuum. At still shorter wavelengths relatively sharp banded features appear superimposed upon a weak continuous absorption. In this section we shall concentrate on the photofragmentation dynamics of these three molecules following dissociation from their respective $\tilde{\alpha}$-continua and from wavelengths in the region of their first two Rydberg states, labelled $\tilde{B}$ and $\tilde{C}$.

There is now reasonable agreement that components of the intravalence $2\pi^3\pi$, $^1\Delta$ state contribute to the $\tilde{\alpha}$-continuum |8|. This conclusion has been reached through comparisons with the absorption spectra of other isovalent

molecules |8,42|, through analysis of photofragment fluorescence excitation spectra |19| and on the basis of correlation arguments |8|. The structured $\tilde{B}$ and $\tilde{C}$ systems are assigned to the first members of the $\ldots 2\pi^4$, $X^1\Sigma^+ \rightarrow \ldots 2\pi^3\sigma(ns)^{1,3}\Pi$ Rydberg series |8,40,43|; under $\Omega_c\omega$ coupling these terms correlate with the $(\frac{1}{2},\frac{1}{2})_1$ and $(3/_2,1/_2)_1$ states respectively as shown in fig.16. Quantum yield measurements, photofragment fluorescence excitation spectra and photofragment fluorescence polarisation measurements for this spectral region have been reported for all three molecules |40|. Fig.17 displays part of the CN(B→X) and CN(A→X) PFES resulting from BrCN photodissociation, along with measurements of the CN(B) fluorescence polarisation as a function of excitation wavelength. This latter data provides a dramatic illustration of the power of the polarised photofluorescence excitation spectroscopic technique, since it is readily apparent that the 'degree of polarisation' spectrum mirror images the CN(B→X) PFES. This observation may be interpreted as follows. Direct dissociation from the underlying continuum generates positively polarised CN(B→X) fluorescence consistent with photoexcitation into linear $\Sigma^+(0^+)$ or bent A' states of the parent molecule (see table 2) since the fragment emission arises via a parallel transition. The degree of polarisation is observed to fall and even become negative following excitation at wavelengths resonant with the structured vibronic features associated with the predissociated Rydberg states. This too is consistent with the spectroscopic assignment of these Rydberg features; a $^{1,3}\Pi(1) \leftarrow {}^1\Sigma^+(0^+)$ promotion has perpendicular character and is thus expected to generate negatively polarised CN(B→X) fluorescence, the precise magnitude of which may of course be reduced by parent molecular rotation during the predissociation lifetime. The actual value of p' measured at each wavelength therefore reflects the relative contributions from the Rydberg state predissociation and direct dissociation from the underlying intravalence continuum to the total CN(B) dissociation yield.

A number of detailed studies of internal energy disposal in the CN(B) photofragments produced in the VUV photodissociation of the cyanogen halides have been reported [39,44,45]. Whilst again it should be remembered that, in these molecules and at these wavelengths, the initial state selection due to photon absorption at any particular wavelength is not as well-defined as one would ideally wish, that no definitive measure of the wavelength dependence of the branching into the two spin-orbit states of the halogen atoms in these dissociations are available and that only about 5% of the total fragmentation is ever probed by monitoring just the CN(B→X) emission, data on the collision-free rotational and vibrational state distributions in these photofragments nevertheless still represent some of the most complete and detailed information against which to gauge models for photodissociation dynamics.

By way of illustration consider the wavelength resolved CN(B→X) photofragment emission spectra displayed in fig.18. This clearly shows that the CN(B) fragment rotational state distributions arising from the direct dissociation of ICN, BrCN and ClCN within their respective $\tilde{\alpha}$-continuum absorptions vary markedly despite the fact that the excitation wavelengths were selected so that in each case a similar total excess energy is available for partitioning within the internal and relative translational product degrees of freedom. In each case the major fraction of the available energy must be taken up in the form of relative translation of the separating products, since less than 10% appears as CN vibration and a relatively constant proportion (15-20%) goes into fragment rotation. However, whilst the vibrational state distributions from these three dissociations show little dependence on the mass of the departing halogen atom [45] the distribution of the rotational energy amongst the various rotational states in the CN fragment does depend critically on the parent molecule. The most populated states in the $CN(B)_{v=0}$ products from the 174.4 nm photodissociation of ICN are those with low N', though the population distribution shows a long 'tail' extending to the highest

energetically accessible N' states. The maximum in the rotational state population distributions shift progressively to higher N' in the order ICN < BrCN < ClCN; the detailed forms of the vibrational and rotational state distributions in the $CN(B)_{v'=0}$ fragments produced through photodissociation of these molecules at 174.4 nm, 158.0 nm and 147.0 nm respectively are shown in fig.19.

As a second illustrative example, fig.20 displays the collision-free wavelength resolved CN(B→X) fluorescence spectra obtained following photodissociation of BrCN at 149.4 nm (an atomic nitrogen resonance line) and 147.0 nm (a xenon emission line). Despite the fact that the available energy provided by photons at these two wavelengths differ by only ~1000 cm^{-1}, it is clear that photodissociation at the shorter wavelength gives rise to much more internally excited CN(B) fragments: most dramatic is the observation that the fraction of the total available energy partitioned into CN(B) vibration doubles to ~22% |39|. Certain rotational lines in the $CN(B)_{v'=0}$ level show anomalous intensity in the latter spectrum. A fuller analysis has revealed that these perturbed lines arise through accidental resonances with rotational levels in the v' = 10 level of the first excited $A^2\Pi_i$ state of CN |46,47|. Their appearance in the fluorescence spectrum of the CN(B) fragments from the 147.0nm photodissociation of BrCN indicates that CN(A) fragments produced in this particular dissociation carry a high level of vibrational excitation too, populating vibrational states up to v' = 10 at least.

In order to account for the marked variations apparent within these two sets of detailed observations it is necessary to consider further the dynamics of the dissociation processes giving rise to these products. This requires a far more elaborate theoretical model than that which was previously shown to provide an adequate description for vibrational energy disposal in the photodissociation of HCN and DCN. To this end Freed and coworkers |26,28,29,48|

have developed a three-dimensional fully quantum mechanical theory for the photodissociation of triatomic molecules that includes use of the correct normal modes of the initial bound state, lifts the constraint that dissociation necessarily proceeds collinearly and properly describes both the bending vibrations in the initial bound electronic state and the rotational motions on both the initial bound and final repulsive potential energy surfaces. The model therefore allows consideration of the influence of angular momentum, and its conservation, on the dissociation - clearly this is essential for any discussion of the resulting photofragment rotational distributions. The approach necessarily leads to multidimensional bound-continuum Franck-Condon integrals which, though strictly non-separable, can be approximated by a product of one dimensional integrals for mathematical convenience.

In the context of this particular discussion we are principally interested in a physical visualisation of the relative contributions made by the various components of the overall multidimensional overlap integral to the ultimate energy disposal. It is therefore illustrative to consider the multidimensional bound-free Franck-Condon factors as products of a one dimensional 'rotation-bending' term $|G|^2$ and a two-dimensional 'vibration-translation' term $|F_{EL}|^2$, i.e. the overall transition probability Γ for transfer from an initial bound state $|i\rangle$ to repulsive state $|f\rangle$ is given by a convolution of the form:

$$\Gamma_{i\to f} = \langle f|i\rangle^2 \propto |G|^2 . |F_{EL}|^2$$

These integrals contain respectively the constraints of angular momentum conservation and energy conservation; their forms have been studied independently [26,28,29,48]. If, for example, we consider the effect of the rotation-bending term alone on the fragment rotational state distribution arising in a strictly collinear photodissociation of a triatomic molecule, its form is such that the angular momentum initially present as parent molecular rotation J would be efficiently channelled into fragment rotation j. This accords

with intuition: the very small impact parameter associated with a collinear dissociation process cannot be expected to give rise to significant orbital angular momentum $\underset{\sim}{L}$. However, for the more general case in which there is at the instant of fragmentation some (small) displacement in the orientation of the diatomic fragment axis as compared with that of the equilibrium triatomic molecular axis in the initially bound state, Morse and Freed |29| have demonstrated that these 'dynamic axis switching' effects can substantially modify the partitioning of the parent rotational angular momentum $\underset{\sim}{J}$ into fragment rotation $\underset{\sim}{j}$ and relative orbital angular momentum of the atom about the diatom. Clearly these effects will be most noticeable when the departing atom is heavy, see fig.21. Thus, whilst the CN(B) fragment distributions from the photodissociation of HCN and DCN |38| described in the previous section accurately reflect the mapping $\underset{\sim}{J}_{parent} \rightarrow \underset{\sim}{j}_{fragment}$, the CN(B) rotational distribution produced through ICN photodissociation in its $\tilde{\alpha}$-continuum |39| and the CN(X) distributions arising in the 266 nm photodissociation of ICN from its $\tilde{A}$-continuum |21-23| peak at very low rotational quantum numbers. Further complications may arise when fragmentation occurs from excited bending vibrational modes of the parent molecule |28,29| since nodes in the bending wavefunction are carried over as undulatory structure in the fragment rotational state distributions, as shown in fig.21.

Since the initial photoabsorption event is likely to select parent molecules in a range of J states it is likely that most, if not all, of the predicted fine structure in these rotational state population distributions derived solely from consideration of the $|G|^2$ integrals in the multidimensional Franck-Condon factors will be washed out in any experimentally obtained spectrum by the effects of thermal averaging. Furthermore, we now have to consider the effects of the vibration-translational term $|F_{EL}|^2$ which contains the constraint of energy conservation and therefore depends implicitly on $\underset{\sim}{J}$ and $\underset{\sim}{j}$. |26|. Its likely influence is most easily visualised in the case

of a near threshold dissociation where the restricted available energy may reduce severely the probability of populating the higher energy rotational states in the diatomic fragment. More generally its role in determining the ultimate rotational energy disposal has been portrayed qualitatively in terms of the overlap along a dissociation coordinate Q_1 of an effective one-dimensional oscillator (a theoretical construct which carries properties of both the bound triatomic initial state and the bound diatomic fragment vibration) and a repulsive potential surface as shown in fig.22. |26,28|. Consider first the situation where the absorbed photon carries insufficient energy, E_{avl}, for the translational continuum wavefunction, $\psi_{cont}(Q_1)$, to overlap maximally with the effective oscillator wavefunction, $\psi_{eff}(Q_1)$ (fig. 22a). Any partitioning of the available energy into internal excitation of the molecular fragment will reduce the energy released into translation and cause $\psi_{cont}(Q_1)$ to shift even further from the region of strong overlap. Fig.22b demonstrates the converse situation where it is desirable for a substantial fraction of the energy carried by a shorter wavelength exciting photon to be channelled into fragment vibrational and rotational excitation in order to lower the continuum translational wavefunction and thereby maximise the bound-free overlap.

In the absence of quite detailed information about the final repulsive potential energy surface the effect of final state interactions on the ultimate rotational energy disposal is difficult to predict in any detail. Nevertheless it should be clear that the preceding summary of the major contributory terms to the appropriate multidimensional Franck-Condon factors for transfer from the initial bound state to the final repulsive state can provide qualitative explanations for the form of the various product energy disposals displayed in figures 18 and 20. For example, the dramatic change in the pattern of energy disposal in the photodissociation of BrCN when the excitation wavelength is reduced from 149.4 nm to 147.0 nm can be rationalised in terms of the

very different character of the respective initial states. Reference to the CN(B→X) PFES and polarisation data shown in fig.17 reveals that photon absorption at 149.4 nm excites predominantly the dissociative continuum (and, indeed, the observed energy disposal closely parallels that found following excitation at longer wavelengths in the $\tilde{\alpha}$-continuum) whilst excitation at the shorter wavelength leads to significant population of the predissociated (0,0,1) vibronic level of the $\tilde{B}(^3\Pi)$ $(^3/_2, {}^1/_2)_1$ state for which a reduced Br-CN bond length has been discerned |40,43|. Thus, in the simple description of fig.22, the disposition of the bound and free potential curves representing the two situations will be very different and dissimilar energy partitioning might well be expected.

Several factors would have to be clarified before it would become possible to present an unequivocal interpretation of the various CN(B) rotational state population distributions obtained in the direct dissociation of these cyanogen halides from their $\tilde{\alpha}$-continua |39,44,45|. Qualitatively we have seen how these various distributions might arise but, without a more complete knowledge of the photoselected state or states, their geometry, and the contribution to the overall CN(B) yield arising from photodissociation of that fraction of the thermal distribution of parent molecules in which the ν_2'' bending vibrational mode is excited, any more detailed discussion must remain speculative.

Conclusions

These three case studies have served to demonstrate many of the currently available avenues of approach to the study of molecular photodissociation processes in the vacuum ultraviolet. The most detailed information concerning the nature of the potential energy surfaces through which any given dissociation proceeds is contained in the rotational energy disposal. However, we have seen (especially in the last section) that a very high degree of initial

state selection and characterisation is necessary before it is possible to extract that information with any certainty. In this concluding section therefore we shall highlight two possible solutions to the problem of adequate state selection, and also outline other likely directions of advance.

Theory |29| predicts, as shown in fig.21, that in triatomic photodissociations yielding heavy atomic fragments the resulting population distribution over rotational states in the diatomic fragment is essentially independent of the initial parent molecular rotational angular momentum, $\underset{\sim}{J}$. For lighter triatomic molecules this will not be so, and the observed photofragment rotational state distribution will represent a superposition of different distributions over $\underset{\sim}{j}$ arising from the dissociation of parent molecules photoselected from a thermally determined range of $\underset{\sim}{J}$ states. This thermal averaging effect can be alleviated by supersonic nozzle expansion of the parent molecule seeded in an excess of inert carrier gas (e.g. He or Ar). The use of supersonic molecular beams thus offers the possibility of studying the photodissociation process in parent molecules with very little internal energy and $J \sim 0$, thereby providing a far more rigorous test of the quantitative value of the current theories. Preliminary results have appeared for the 193 nm photodissociation of H_2S |49,50| and BrCN |49|. In both instances it was necessary to use LIF in order to probe the respective diatomic fragment internal state distributions. Potential problems associated with collisional population redistribution amongst the photofragment quantum states prior to LIF probing have been demonstrated |49| and may account for the markedly different rotational energy disposals reported for the $SH(X)_{v''=0}$ fragments in the H_2S photodissociations |49,50|. More detailed and carefully controlled experiments along these lines can be anticipated in the near future.

The detail revealed in the time-of-flight spectra of photodissociation

products also benefits from the greatly reduced, and more precisely defined, internal energy of molecules in a beam created by supersonic expansion. Fig. 23 shows the centre of mass translational energy distribution of O_2 fragments produced through photodissociation of a supersonic molecular beam of O_3 at 266 nm |51| which clearly reveals the extent of $O(^1D)$ and $O(^3P)$ formation, as well as fully resolved vibrational state populations in the $O_2(^1\Delta_g)$ product. The precise energy of the $O_2(^1\Delta_g)_{v=0}$ peak even allows estimation of the fraction of the available energy channelled into diatomic rotational excitation. Much of the historical confusion concerning the relative importance of the various possible product channels in the near UV photodissociation of ICN (see earlier) might never have arisen had energy resolved data of this quality been obtainable seven years ago.

Weakly predissociated systems provide an alternative route to the problem of well defined state selection, since they exhibit absorption spectra that may be sufficiently well resolved to identify the initial predissociating vibrational (or even rovibrational) state. A preliminary report of the visible photofragmentation of CF_3NO via predissociation from specific vibronic levels of its first excited singlet state has appeared |52|; somewhat disappointingly, the internal state distribution of the NO fragment was found to depend only on the available energy and not on which vibrational mode of the parent molecule was initially excited by the photon absorption. In view of the preceding discussions of rotational energy disposal in the photofragmentation of light triatomic molecules, studies of predissociation from selected parent molecular J levels should prove more rewarding. Reference to fig.1 indicates that there are VUV wavelengths at which H_2O should be amenable to such experimental investigation. As intense, dedicated synchrotron sources become more commonplace and readily available for VUV absorption measurements it will be rather surprising if other molecules are not found similarly to possess Rydberg states whose lifetime with respect to dissociation is sufficient for

rotational structure to be identified spectroscopically. Indeed, rotational structure displaying what appears to be instrument limited linewidths ($<1 cm^{-1}$) has been observed very recently for the $\pi_g 3p\Pi_u\ ^3\Sigma_u^- - \tilde{X}^1\Sigma_g^+$ Rydberg transition in CO_2 at 110.6 nm |53|.

New techniques continue to find application in studies of molecular photodissociation dynamics. Photofragment laser induced fluorescence excited by a sufficiently narrow band dye laser will show Doppler limited spectral linewidths, from which translational velocity |54,55| and, in principle at least, even angular |55| distributions may be derived as a function of the product internal quantum state. Multiphoton ionisation (MPI) |56| and time resolved measurement of the infrared chemiluminescence from vibrationally excited ground state species |57,58| have both found use as detection methods for the primary products of photodissociation processes, both are in some respects complementary to LIF as detection techniques in that they may be applied to non-fluorescent species, e.g. the methyl radical |57-60|. Unfortunately, progress towards what must be the most important requirement of all for those studying VUV photodissociation processes - namely readily available, intense, narrow bandwidth, tunable sources of VUV radiation - has been somewhat less spectacular. However the increasing availability of pulsed synchrotron radiation, the demonstration of photochemically useful tunable VUV intensities through third harmonic generation of relatively narrow band dye laser radiation in the rare gases Kr and Xe |61|, and the prospects for tunable multiphoton excitation into the VUV offered by the more recent high power excimer or Nd-YAG pumped dye laser systems should ensure maintainance of the current intense level of activity in this field.

References

1. K. Watanabe and M. Zelikoff, J. Opt. Soc. Amer. 43, 753, (1958)

2. J.W.C. Johns, Can. J. Phys., 41, 209, (1963)

3. P.M. Johnson, Acc. Chem. Res. 13, 20, (1980)

4. P.M. Johnson and C.E. Otis, "Molecular Multiphoton Ionisation with Ionisation Detection", Ann. Rev. Phys. Chem. 32, 139, (1981)

5. J.H. Glownia, S.J. Riley, S.D. Colson and G.C. Nieman, J. Chem. Phys. 72, 5998, (1980); 73, 4296, (1980)

6. M.B. Robin, "Higher Excited States of Polyatomic Molecules" Vols. 1 and 2, Academic Press, N.Y., (1974)

7. H. Okabe, "Photochemistry of Small Molecules", Wiley, N.Y., (1978)

8. M.N.R. Ashfold, M.T. Macpherson and J.P. Simons, "Photochemistry and Spectroscopy of Simple Polyatomic Molecules in the Vacuum Ultraviolet" in "Topics in Current Chemistry", Springer-Verlag, Berlin, 86, 1, (1979).

9. R.N. Zare, Mol. Photochem. 4, 1, (1972)

10. R. Bersohn, Israel J. Chem. 11, 675, (1973)

11. J.P. Simons, "The Dynamics of Photodissociation" in "Gas Kinetics and Energy Transfer", R.S.C. Spec. Per. Rep., (eds. P.G. Ashmore and R.J. Donovan), 2, 58, (1977)

12. W.M. Gelbart, "Photodissociation Dynamics of Polyatomic Molecules", Ann. Rev. Phys. Chem. 28, 323, (1977).

13. S.R. Leone, "Photofragment Dynamics", in "Dynamics of the Excited State" (ed. K.P. Lawley), Adv. Chem. Phys. 50, 255, (1982)

14. J. A. Myer and J.A.R. Samson, J. Chem. Phys. 52, 266, (1970)

15. A.D. Walsh, J. Chem. Soc., 2266, (1953)

16. K.R. Wilson "Photogragment Spectroscopy of Dissociative Excited States" in "Excited State Chemistry" (ed. J.N. Pitts Jr.), Gordon & Breach, N.Y., (1970)

17. J.H. Ling and K.R. Wilson, J. Chem. Phys. 63, 101, (1975)

18. S.-C. Yang and R. Bersohn, J. Chem. Phys. 61, 4400, (1974)

19. G.A. West and M.J. Berry, Chem. Phys. Lett. 56, 423, (1978)

20. W.M. Pitts and A.P. Baronavski, Chem. Phys. Lett. 71, 395, (1980)

21. A.P. Baronavski and J.R. McDonald, Chem. Phys. Lett. 45, 172, (1977)

22. W. Krieger, J. Hager and J. Pfab, Chem. Phys. Lett. 85, 69, (1982)

23. A.P. Baronavski, Chem. Phys. 66, 217, (1982)

24. M.J. Sabety-Dzvonik and R.J. Cody, J. Chem. Phys. 66, 125, (1977)

25. J.P. Simons and P.W. Tasker, Mol. Phys. 26, 1267, (1973); 27, 1691 (1974)

26. Y.B. Band and K.F. Freed, "Product Energy Distributions in the Dissociation of Polyatomic Molecules", in Excited States (ed. E.C. Lim), Academic, N.Y., 3, 110, (1977)

27. J.A. Beswick and J. Jortner, Chem. Phys. 24, 1, (1977)

28. M.D. Morse, K.F. Freed and Y.B. Band, J. Chem. Phys. 70, 3604, 3620, (1979)

29. M.D. Morse and K.F. Freed, J. Chem. Phys. 74, 4395, (1981)

30. G. Herzberg, "Molecular Spectra and Molecular Structure", Vol. III "Electronic Spectra and Electronic Structure of Polyatomic Molecules", Van Nostrand Reinhold, Princeton, New Jersey, (1966)

31. G.A. West, Ph.D. Thesis, University of Wisconsin (1975)

32. M.T. Macpherson and J.P. Simons, J. Chem. Soc. Faraday II, 74, 1965, (1978).

33. D.T. Chuljian and J. Simons, J. Amer. Chem. Soc. 104, 646, (1982)

34. G.A. Chamberlain and J.P. Simons, Chem. Phys. Lett. 32, 355, (1975), J. Chem. Soc. Faraday II, 71, 2043, (1975)

35. M.T. Macpherson, J. P. Simons and R.N. Zare, Mol. Phys. 38, 2049, (1979)

36. G.W. Loge and R.N. Zare, Mol. Phys. 43, 1419, (1981)

37. J. Husain, J.R. Wiesenfeld and R.N. Zare, J. Chem. Phys. 72, 2479, (1980)

38. M.N.R. Ashfold, M.T. Macpherson and J.P. Simons, Chem. Phys. Lett. 55, 84, (1978)

39. M.N.R. Ashfold and J.P. Simons, J. Chem. Soc. Faraday II, 74, 280, (1978)

40. M.T. Macpherson and J.P. Simons, J. Chem. Soc. Faraday II, 75, 1572 (1979)

41. S.P. McGlynn, W.S. Felps and G.L. Findley, Chem. Phys. Lett. 78, 89, (1981)

42. J.W. Rabalais, J.M. McDonald, V. Scherr and S.P. McGlynn, Chem. Rev. 71, 73, (1971)

43. G.W. King and A.W. Richardson, J. Mol. Spect. 21, 339, 353, (1966)

44. M.N.R. Ashfold and J.P. Simons, J. Chem. Soc. Faraday II, 73, 858, (1977)

45. M.N.R. Ashfold, A.J. Georgiou, A.M. Quinton and J.P. Simons, J. Chem. Soc. Faraday II, 77, 259, (1981)

46. M.N.R. Ashfold and J.P. Simons, Chem. Phys. Lett. 47, 65, (1977)

47. S.R. Long and J.P. Reilly, J. Phys. Chem. 86, 56, (1982)

48. M.D. Morse and K.F. Freed, Chem. Phys. Lett. 74, 49, (1980)

49. M. Heaven, T.A. Miller and V.E. Bondybey, Chem. Phys. Lett. 84, 1, (1981)

50. W.G. Hawkins and P.L. Houston, J. Chem. Phys. 76, 729, (1982)

51. R.K. Sparks, L.R. Carlson, K. Shobatake, M.L. Kowalczyk, and Y.T. Lee, J. Chem. Phys. 72, 1401, (1980)

52. R.W. Jones, R.D. Bower and P.L. Houston, J. Chem. Phys. 76, 3339, (1982)

53. C. Cossart-Magos, S. Leach, M. Eidelsberg, F. Launay and F. Rostas, (to be published)

54. H. Zacharias, M. Geilhaupt, K. Meier and K.H. Welge, J. Chem. Phys. 74, 218, (1981)

55. E.J. Murphy, J.H. Brophy and J.L. Kinsey, J. Chem. Phys. 74, 331, (1981)

56. G. Radhakrishnan, D. Ng and R.C. Estler, Chem. Phys. Lett. 84, 260, (1981)

57. S.L. Baughcum and S.R. Leone, J. Chem. Phys. 72, 6531, (1980)

58. H.W. Hermann and S.R. Leone, J. Chem. Phys., 76, 4759, 4766 (1982)

59. T.G. DiGiuseppe, J.W. Hudgens and M.C. Lin, Chem. Phys. Lett. 82, 267, (1981); J. Phys. Chem. 86, 36, (1982)

60. J. Danon, H. Zacharias, H. Rottke and K.H. Welge, J. Chem. Phys. 76, 2399, (1982)

61. J.C. Miller, R.N. Compton and C.D. Cooper, J. Chem. Phys. 76, 3967, (1982)

Table 1

$\pi^3\pi$ excited state symmetries for linear and bent geometries of ICN

Point Group	Molecular Term		
$C_{\infty v}$ (linear)	Δ	Σ^+	Σ^-
C_s (bent)	A' A''	A'	A''

Table 2. Calculated degrees of polarisation, p, of the fluorescent photofragments, (AB)*, produced through photodissociation of triatomic parent molecules ABC by a beam of linearly polarised light.

Case	ABC transition	(AB)* transition	γ	$\cos^2\gamma$	p
		Non-linear parent molecule or linear→bent transition.			
I	$\underset{\sim}{\mu}_{abs}$ in (ABC)* plane	$\parallel$-type; $\underset{\sim}{\mu}_{em} \perp \underset{\sim}{j}$	45°	½	1/7
IIa	$\underset{\sim}{\mu}_{abs}$ in (ABC)* plane	$\perp$-type $\underset{\sim}{\mu}_{em} \parallel \underset{\sim}{j}$ (Q)	90°	0	-1/3
IIb		$\underset{\sim}{\mu}_{em} \perp \underset{\sim}{j}$ (P,R)	45°	½	1/7
III	$\underset{\sim}{\mu}_{abs}$ (ABC)* plane	$\parallel$-type; $\underset{\sim}{\mu}_{em} \perp \underset{\sim}{j}$	90°	0	-1/3
IVa	$\underset{\sim}{\mu}_{abs}$ (ABC)* plane	$\perp$-type; $\underset{\sim}{\mu}_{em}$ $\underset{\sim}{j}$ (Q)	0°	1	½
IVb		$\underset{\sim}{\mu}_{em}$ $\underset{\sim}{j}$ (P,R)	90°	0	-1/3
		Linear → linear transition			
V	$\parallel$-type; $\underset{\sim}{\mu}_{abs} \perp \underset{\sim}{J}$	$\parallel$-type, $\underset{\sim}{\mu}_{em} \perp \underset{\sim}{j}$	45°	½	1/7
VIa	$\parallel$-type; $\underset{\sim}{\mu}_{abs} \perp \underset{\sim}{J}$	$\perp$-type; $\underset{\sim}{\mu}_{em} \parallel \underset{\sim}{j}$ (Q)	90°	0	-1/3
VIb		$\underset{\sim}{\mu}_{em} \perp \underset{\sim}{j}$ (P,R)	45°	½	1/7
VIIa	$\perp$-type; $\underset{\sim}{\mu}_{abs} \parallel \underset{\sim}{J}$ (Q)	$\parallel$-type; $\underset{\sim}{\mu}_{em} \perp \underset{\sim}{j}$	90°	0	-1/3
VIIb	$\underset{\sim}{\mu}_{abs} \perp \underset{\sim}{J}$ (PR)		45°	½	1/7
VIIIa	$\perp$-type; $\underset{\sim}{\mu}_{abs} \parallel \underset{\sim}{J}$ (Q)	$\perp$-type; $\underset{\sim}{\mu}_{em} \parallel \underset{\sim}{j}$ (Q)	0°	1	½
VIIIb	$\underset{\sim}{\mu}_{abs} \perp \underset{\sim}{J}$ (P,R)		90°	0	-1/3
IXa	$\perp$-type; $\underset{\sim}{\mu}_{abs} \parallel \underset{\sim}{J}$ (Q)	$\perp$-type $\underset{\sim}{\mu}_{em} \perp \underset{\sim}{j}$ (P,R)	45°	½	1/7
IXb	$\underset{\sim}{\mu}_{abs} \perp \underset{\sim}{J}$ (P,R)				

Figure Captions

Fig. 1 Vacuum ultraviolet absorption spectrum of H_2O (after ref.1) together with an illustration of the resolved rotational structure associated with the 0-0 band of the $\tilde{C}\ ^1B_1 \leftarrow \tilde{X}$ transition around 124 nm (after ref.2).

Fig.2 Near ultraviolet absorption of ICN (after ref.14).

Fig.3 Schematic correlation between (Λ,S) and (Ω_c,ω) coupling for a $\pi^3\pi$ configuration; energy differences not to scale.

Fig.4 Time of flight distributions of (a) CN and (b) I fragments (detected at a laboratory recoil angle of 15^o) in the 266 nm photodissociation of ICN. The early time $\downarrow E_{int}$ peak corresponds to fragments with lower internal energy, the later $\downarrow E_{int}$ peak to fragments carrying a higher level of internal excitation (after ref.17)

Fig.5 Angular distribution of the recoiling CN fragments produced in the 266 nm photodissociation of ICN. The fragmentation channels yielding high ($\downarrow E_{int}$) and low ($\downarrow E_{int}$) internal energy products both exhibit laboratory angular distributions peaking around $\theta_{lab} = 0^o$. (after ref.17).

Fig.6 Total internal and centre of mass translational energy distributions for photofragments produced in the photodissociation of ICN at 266 nm. Arrows in the upper part of the figure represent calculated peak positions if the I and CN fragments were formed in particular electronic and vibrational states (after ref.17).

Fig.7 Wavelength dependence for the production of $I(^2P_{\frac{1}{2}})$ in the photodissociation of ICN(Ã). Solid points and curve represent the ICN absorption spectrum. Open circles joined by dashed curve show the product $\Phi_{I^*}.\epsilon_{ICN}$. Also shown is the resulting 'difference' spectrum $\epsilon_{ICN} - \Phi_{I^*}.\epsilon_{ICN}$ (after ref.20).

Fig.8 Laser Induced Fluorescence spectrum of CN(X) fragments produced in the photodissociation of ICN at 266 nm under collision-free conditions (upper spectrum) and collisionally relaxed by the presence of excess argon (lower spectrum). The wavelength variation of the probing dye laser intensity is plotted below each spectrum (after ref.22).

Fig.9 Vacuum ultraviolet absorption spectrum of HCN in the wavelength range 130-155 nm (after refs. 31 and 32).

Fig.10 Walsh diagram for an HAB molecule (after ref.15).

Fig.11 Photofragment excitation spectra of (a) CN(A) and (b) CN(B) from HCN. The spectral resolutions employed were 0.8 nm and 0.04 nm respectively, contributing to the very different apparent vibronic linewidths; the relative fluorescence signals are not scaled with respect to one another (after refs. 31 and 32).

Fig.12 DCN absorption spectrum (a), CN(B) photofragment fluorescence excitation spectrum (b) and CN(B→X) fluorescence polarisation measurements (c) as a function of vacuum ultraviolet wavelength in the range 130-150 nm. Only the one peak marked with an asterisk is significantly enhanced by the small amount of HCN impurity present in the sample. To aid the eye, the solid line (—) in (c) joins points corresponding to the $(0,\nu_2',0)$ progression, dashed line (---) points corresponding to the $(1,\nu_2',0)$ progression

Fig.13 Relative vibrational state populations in the $CN(B)_{v'}$ fragments produced in the collision-free photodissociation of HCN (•) and DCN(○) at three wavelengths. Modelled distributions for HCN (solid line) and DCN (dashed line) are included for comparison (after ref.38)

Fig.14 Relative rotational state population distributions in the $CN(B)_{v'=0}$ fragments produced in the collision-free photodissociation of (a) HCN at 147.0 nm (•) and 141.1 nm (○) and (b) DCN at 141.1 nm. The solid curves show the thermal population distribution over rotational states in the ground electronic states of the respective parent molecules at 298K (after ref. 38).

Fig.15 Vacuum ultraviolet absorption spectrum of BrCN (after ref.31)

Fig.16 Schematic correlation between (Λ,S) and (Ω_c,ω) coupling for a $\pi^3\sigma$ configuration; energy differences not to scale.

Fig.17 Photofragment excitation spectra of (a) CN(A) and (b) CN(B) from BrCN, along with (c) polarisation measurements for the total CN(B→X) fluorescence. Spectral resolutions employed respectively (a) 0.35 nm, (b) 0.20 nm. (after refs. 40 and 45)

Fig.18 Wavelength resolved CN(B→X) fluorescence produced through photodissociation of the three cyanogen halides in their respective $\tilde{\alpha}$-continua: (a) ClCN at 147.0 nm (E_{avl} = 7240 cm^{-1}), (b) BrCN at 158.0 nm and 163.4 nm (E_{avl} = 7110 cm^{-1} and 5020 cm^{-1} respectively), and (c) ICN at 174.4 nm (E_{avl} = 6450 cm^{-1}). Resolution of each spectrum ~0.01 nm (after refs. 39 and 44)

Fig.19 Collision-free vibrational and rotational state populations in the CN(B) fragments produced through vacuum ultraviolet photodissociation of (a) ClCN at 147.0 nm, (b) BrCN at 158.0 nm and 163.4 nm and (c) ICN at 174.4 nm (after refs. 39 and 44).

Fig.20 Wavelength resolved CN(B→X) fluorescence produced through photodissociation of BrCN at (a) 149.4 nm (E_{avl} = 10760 cm^{-1}) and (b) 147.0 nm (E_{avl} = 11850 cm^{-1}). (after ref. 39)

Fig.21 Calculated rotational state population distributions in CN fragments produced in the photodissociation of ICN:

(a) as predicted by the direct mapping $\underset{\sim}{J}$(ICN)→ $\underset{\sim}{j}$(CN) at 298K

(b) allowing for the effects of dynamic axis switching in the photofragmentation of ICN (0,0,0). Note that for molecules such as ICN, in which the departing atom is very heavy, the ultimate distribution in $\underset{\sim}{j}$ is largely independent of the initial parent angular momentum $\underset{\sim}{J}$; as $\underset{\sim}{J}$ increases angular momentum conservation is satisfied by a progressively more complete transfer of $\underset{\sim}{J}$ into orbital angular momentum $\underset{\sim}{L}$. (after ref. 29).

(c) as in (b) but for ICN in its excited bending vibrational state $(0,2^{o},0)$. (after ref.29),

(d) for comparison, experimentally derived rotational state population distributions for $CN(X)_{v''=0}$ fragments produced in ICN photodissociation at 266 nm (----) and for $CN(B)_{v'=0}$ fragments from ICN photodissociation at 174.4 nm (-·-·-) (after refs. 22 and 39).

Fig.22 Schematic representation of 'bound-free' overlap in molecular photodissociation: (a) overlap favours energy disposal into translational excitation, (b) overlap favours energy disposal into internal degrees of freedom (after refs. 26 and 28)

Fig.23 Centre of mass translational energy distribution of O_2 fragments produced in the 266 nm photodissociation of O_3, in which well resolved peaks corresponding to the formation of $O_2(^1\Delta_g)$ in v = 3,2,1 and 0 may be clearly discerned at the low translational energy end of the spectrum. (after ref.51)

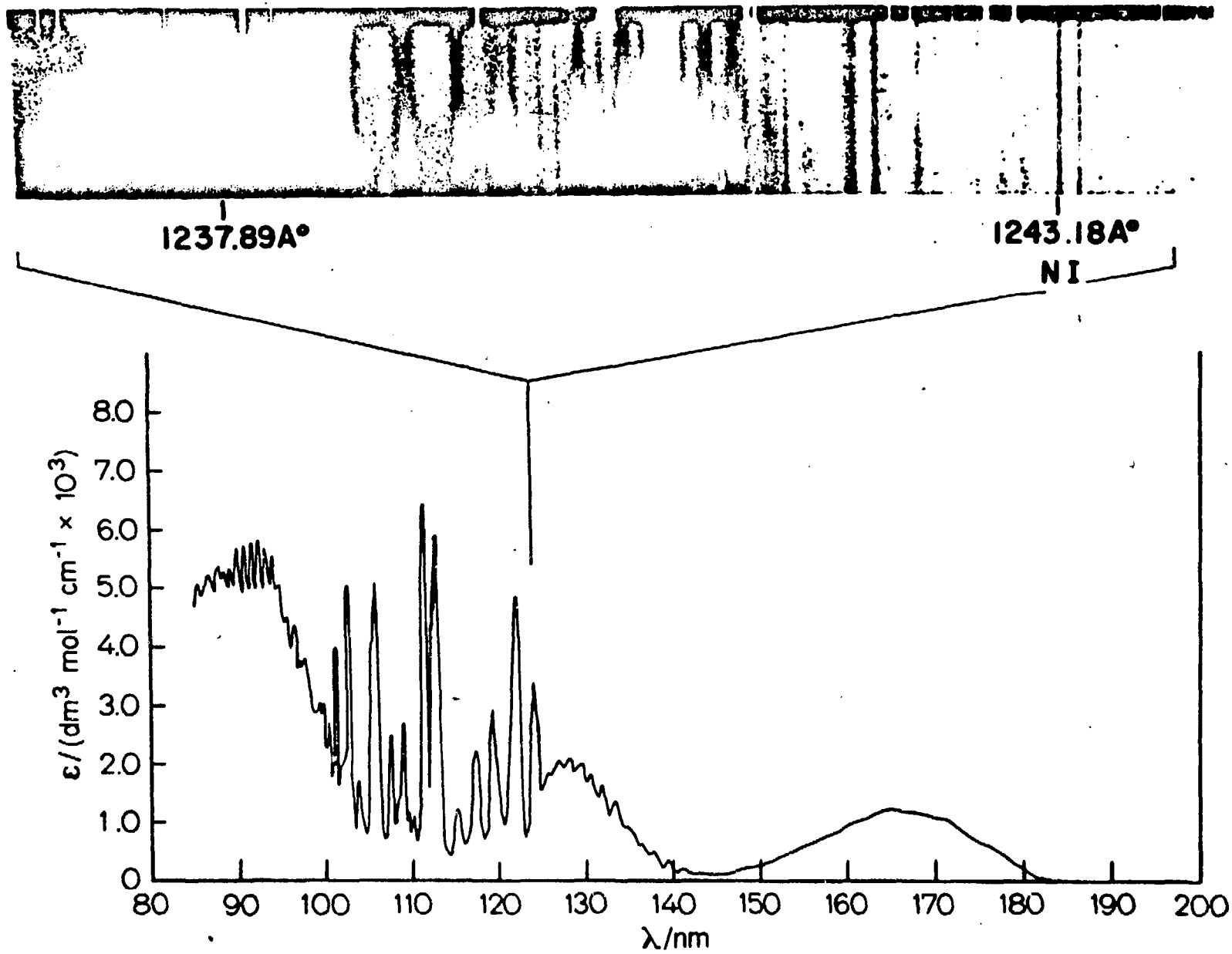
1237.89A°
1243.18A°
N I
8.0
7.0
6.0
5.0
4.0
3.0
2.0
1.0
0
ε/(dm³ mol⁻¹ cm⁻¹ × 10³)
80
90
100
110
120
130
140
150
160
170
180
190
200
λ/nm

Fig. 8.1

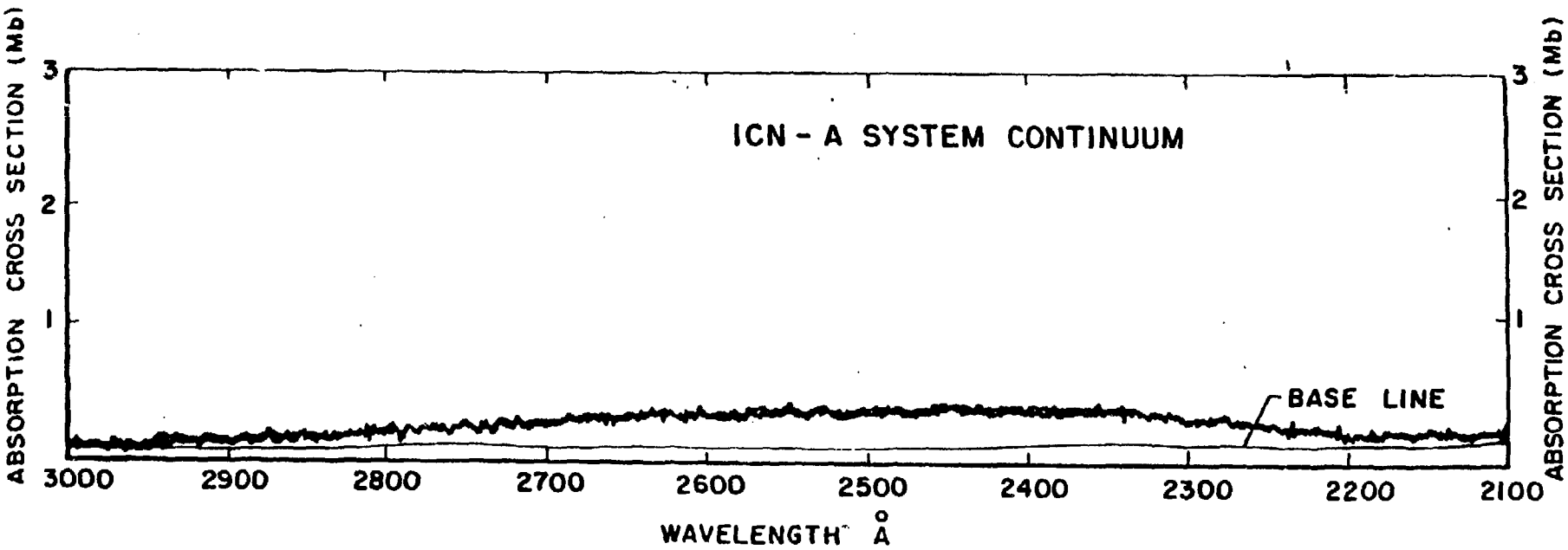
ICN - A SYSTEM CONTINUUM
BASE LINE
ABSORPTION CROSS SECTION (Mb)
ABSORPTION CROSS SECTION (Mb)
3
2
1
3000
2900
2800
2700
2600
2500
2400
2300
2200
2100
WAVELENGTH Å

Fig. 2.

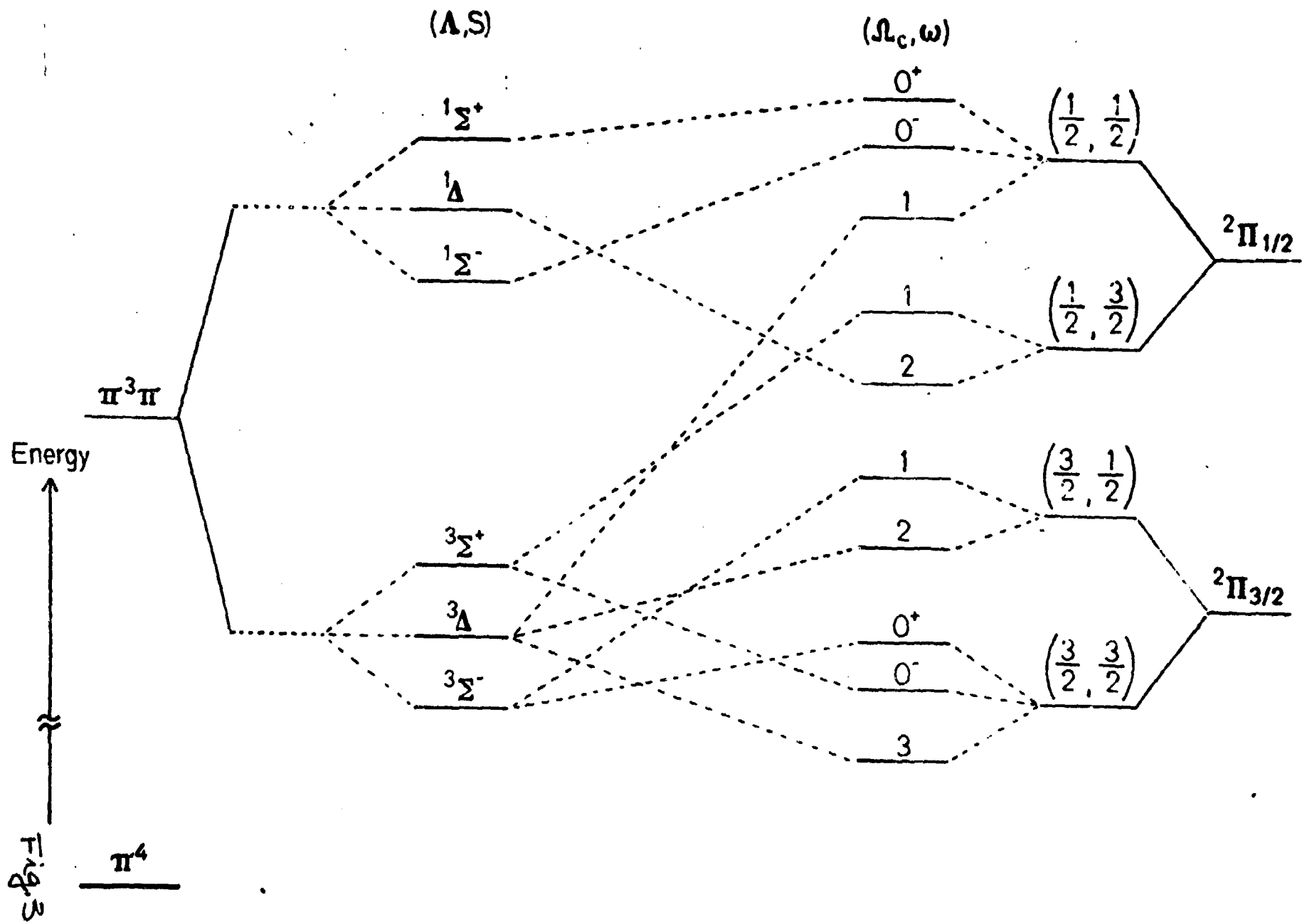
(Λ,S)
(Ω_c,ω)
Energy
π³π
π⁴
¹Σ⁺
¹Δ
¹Σ⁻
³Σ⁺
³Δ
³Σ⁻
0⁺
0⁻
1
1
2
1
2
0⁺
0⁻
3
(1/2, 1/2)
(1/2, 3/2)
(3/2, 1/2)
(3/2, 3/2)
²Π1/2
²Π3/2

Fig 3

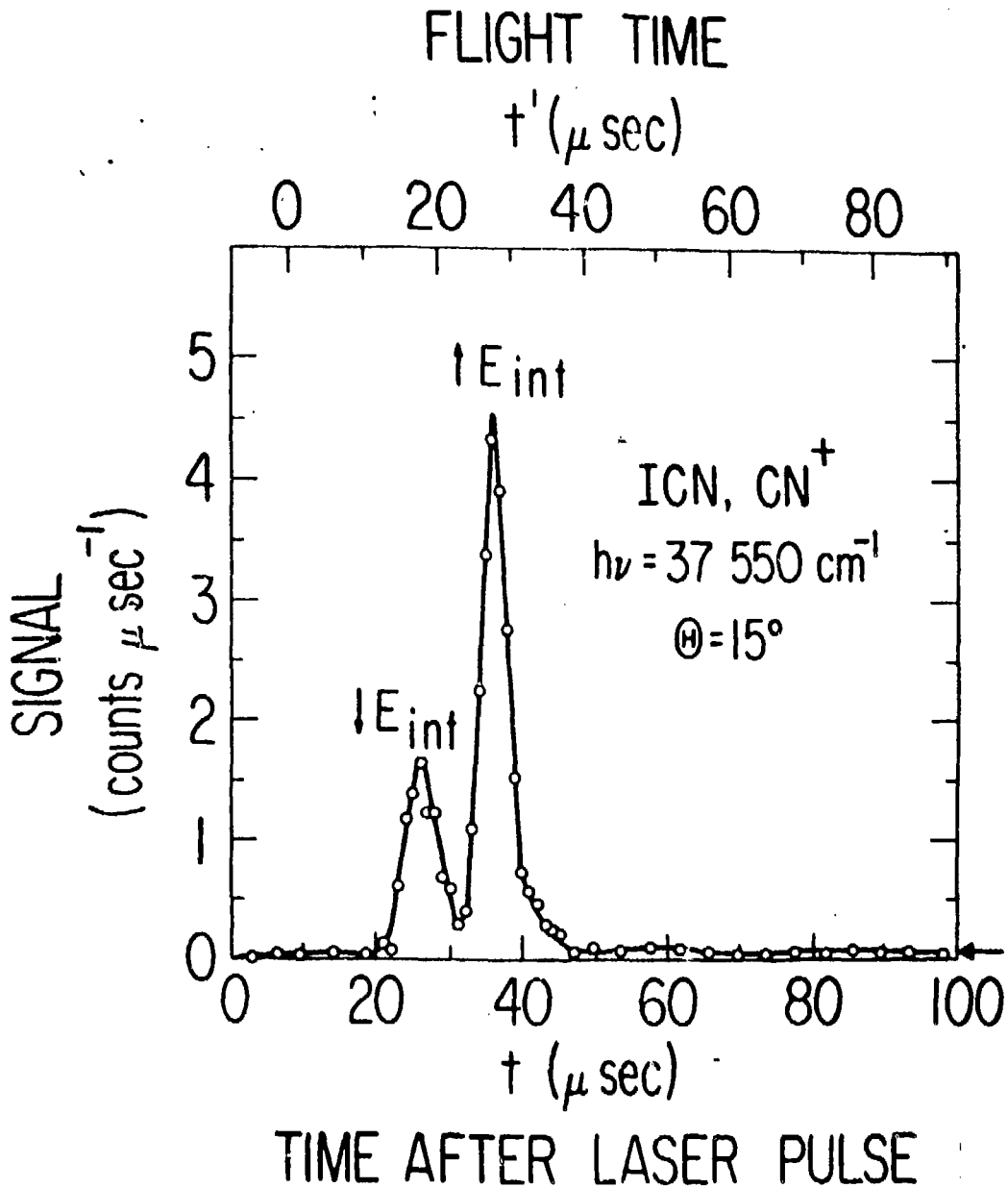
FLIGHT TIME
t'(μ sec)
0
20
40
60
80
5
4
3
2
1
0
SIGNAL
(counts μ sec⁻¹)
↓E int
↓E int
ICN, CN⁺
hν = 37 550 cm⁻¹
Θ = 15°
0
20
40
60
80
100
t (μ sec)
TIME AFTER LASER PULSE

Fig. 4(a)

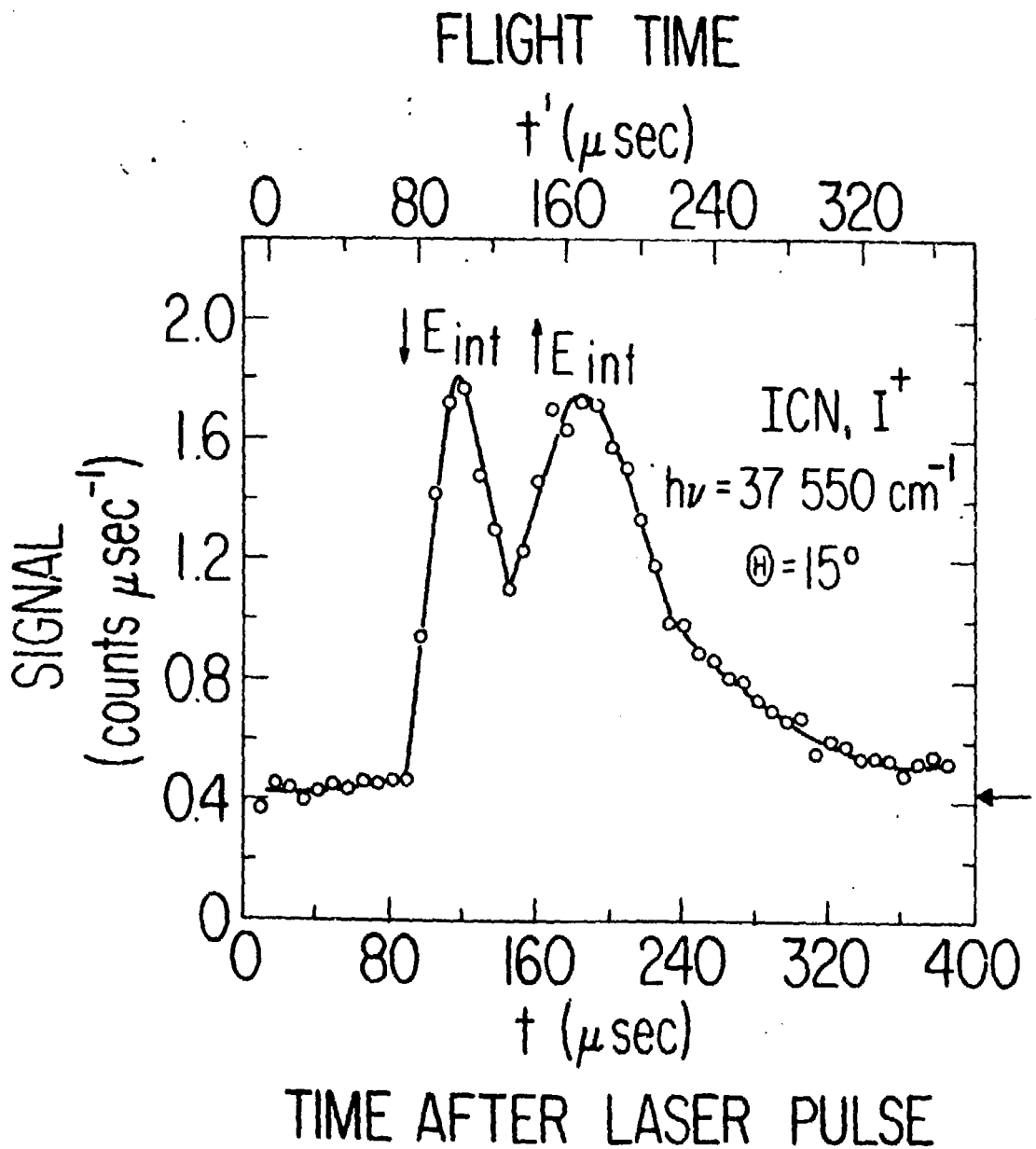
FLIGHT TIME
t' (μsec)
0
80
160
240
320
2.0
1.6
1.2
0.8
0.4
0
↓E int
↑E int
ICN, I+
hν = 37 550 cm-1
Θ = 15°
SIGNAL
(counts μsec-1)
0
80
160
240
320
400
t (μsec)
TIME AFTER LASER PULSE

Fig. 1(a)

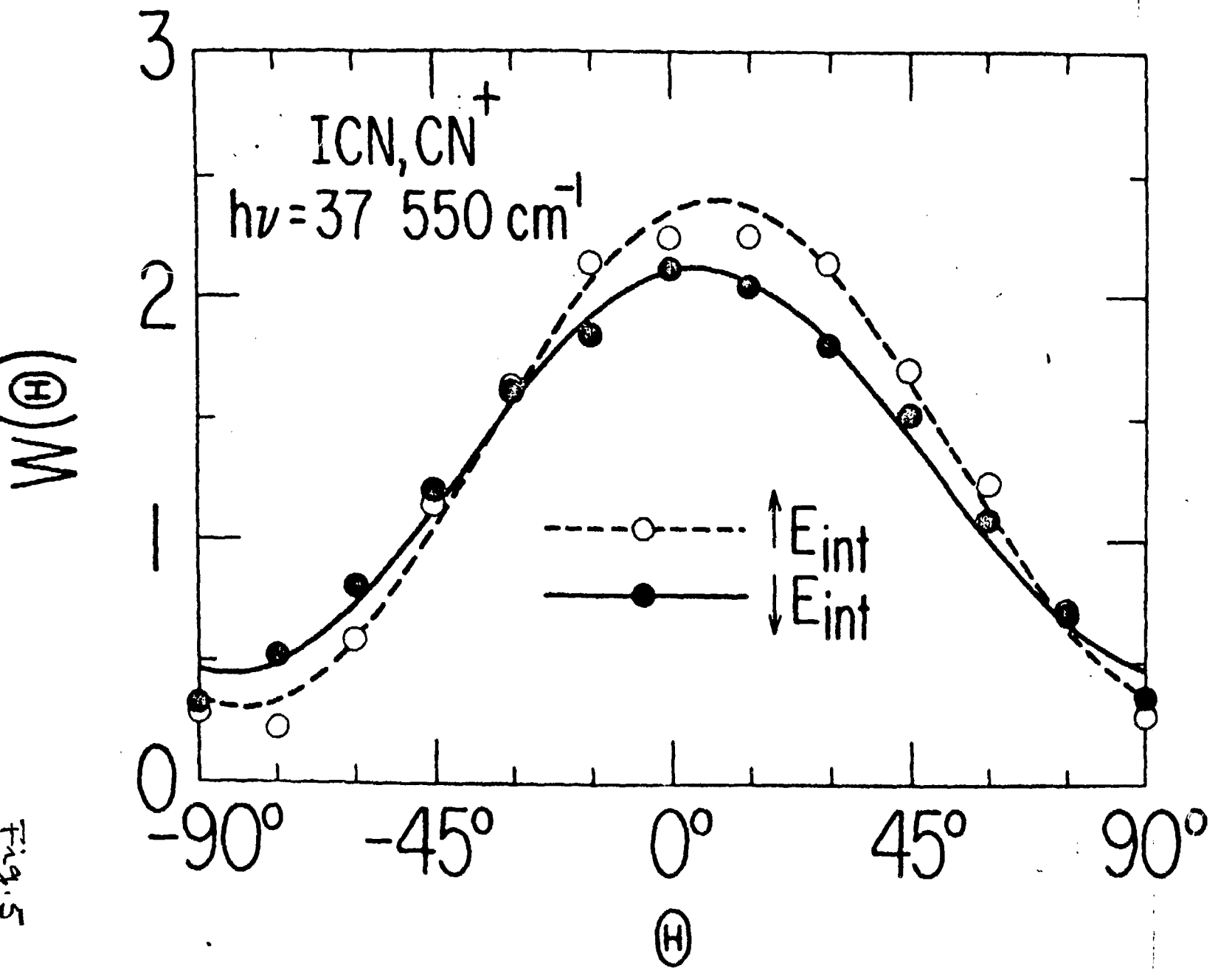
ICN, CN+
hν = 37 550 cm-1
W(Θ)
3
2
1
0
-90°
-45°
0°
45°
90°
Θ
↑Eint
↓Eint

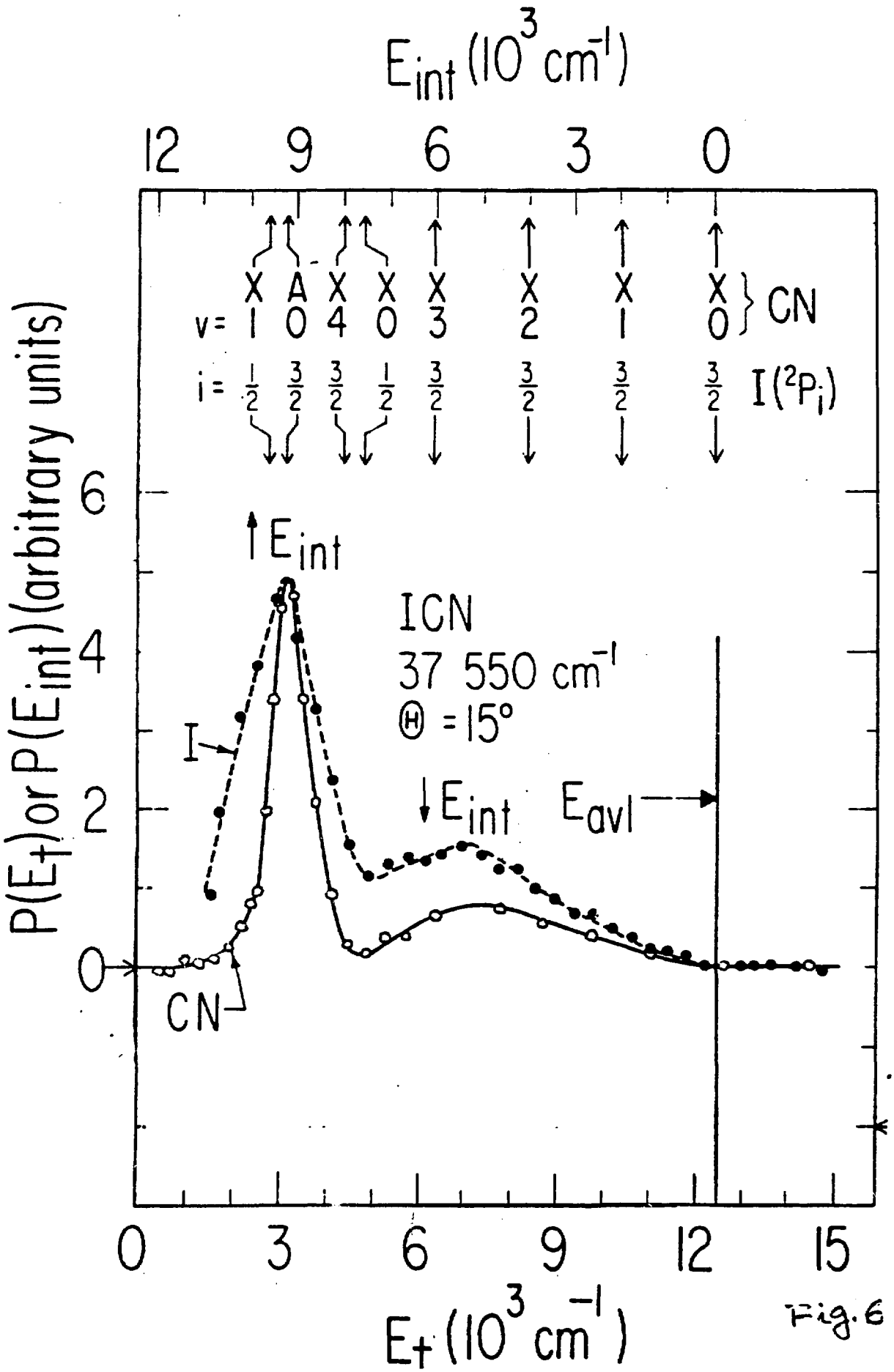
E_{int} (10^3 cm^{-1})
12
9
6
3
0
X A X X X X X X } CN
v= 1 0 4 0 3 2 1 0
i= 1/2 3/2 3/2 1/2 3/2 3/2 3/2 3/2 I(^2P_i)
E_{int}
ICN
37 550 cm^{-1}
Θ = 15°
I
E_{int}
E_{avl}
CN
$P(E_+)$ or $P(E_{int})$ (arbitrary units)
0
2
4
6
0
3
6
9
12
15
E_+ (10^3 cm^{-1})

Fig. 6

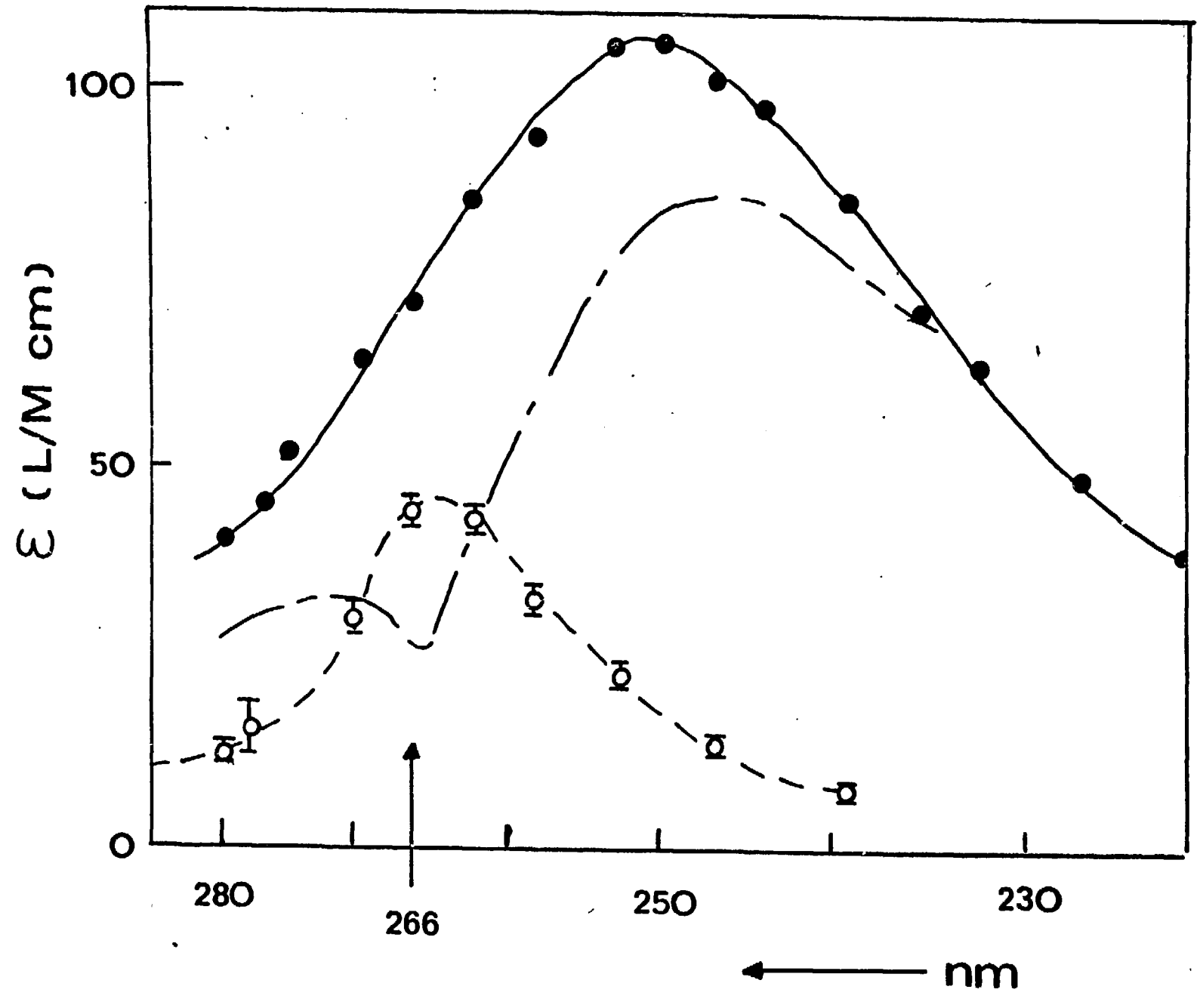

Fig. 7

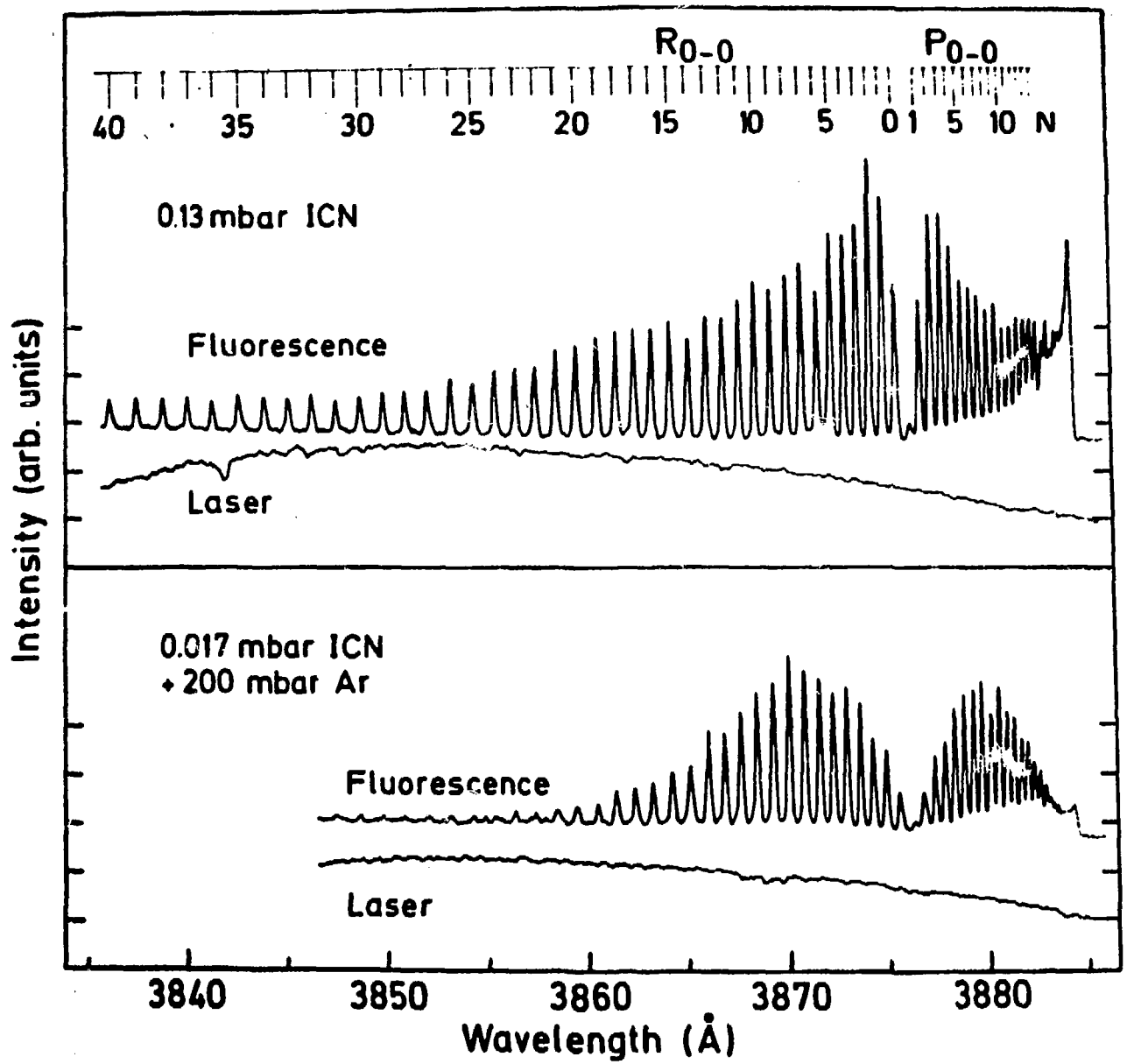
R_{0-0}
P_{0-0}
40 35 30 25 20 15 10 5 0 1 5 10 N
0.13 mbar ICN
Fluorescence
Laser
0.017 mbar ICN
+ 200 mbar Ar
Fluorescence
Laser
Intensity (arb. units)
3840 3850 3860 3870 3880
Wavelength (Å)

Fig. 8

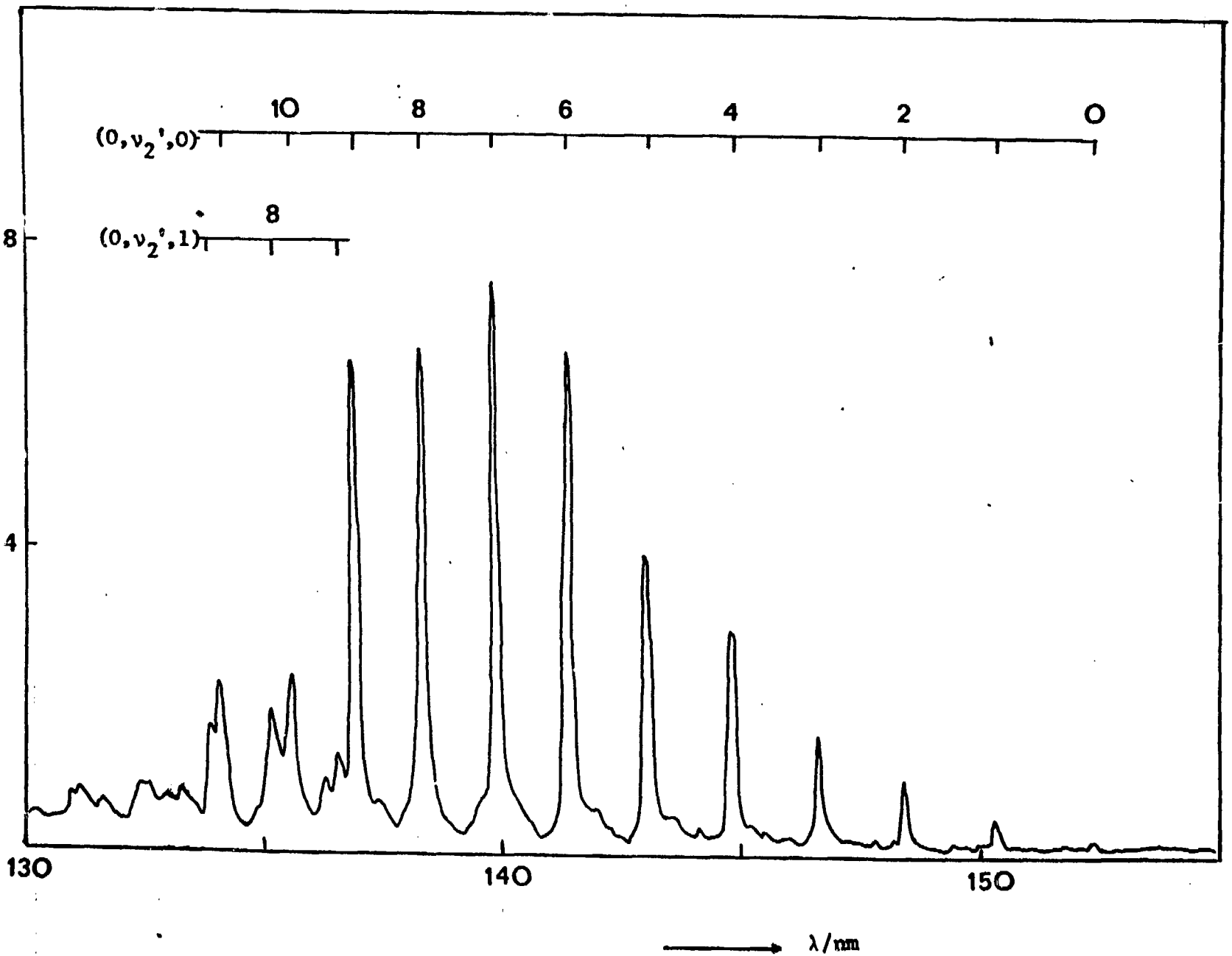
10
8
6
4
2
0
$(0,\nu_2',0)$
8
$(0,\nu_2',1)$
8
4
ε /dm^3 mol^{-1} cm^{-1} x 10^3
130
140
150
λ/nm

Fig. 9

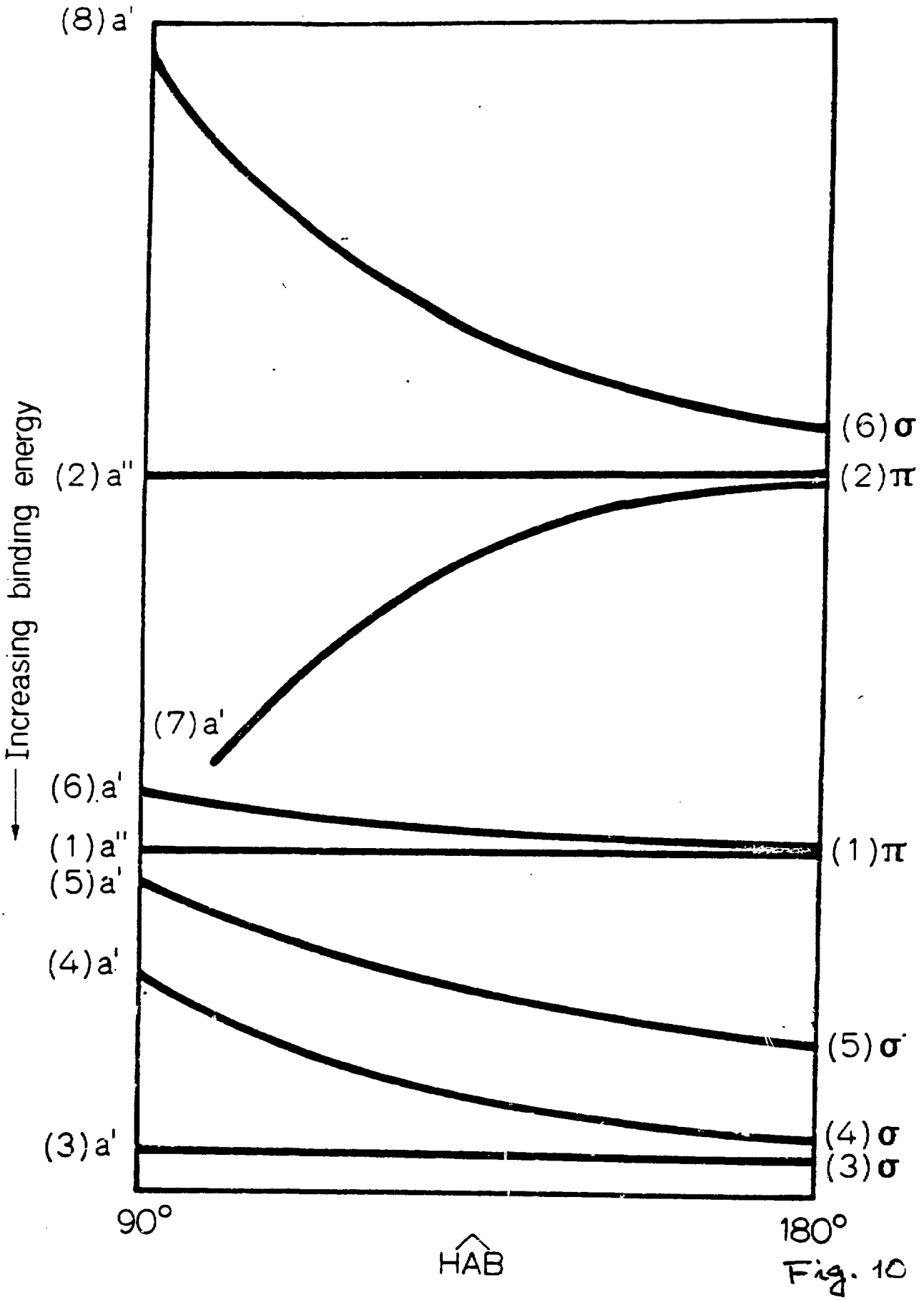
(8) a'
(6) σ
(2) a''
(2) π
(7) a'
(6) a'
(1) a''
(1) π
(5) a'
(4) a'
(5) σ
(4) σ
(3) a'
(3) σ
Increasing binding energy
90°
180°
HÂB

Fig. 10

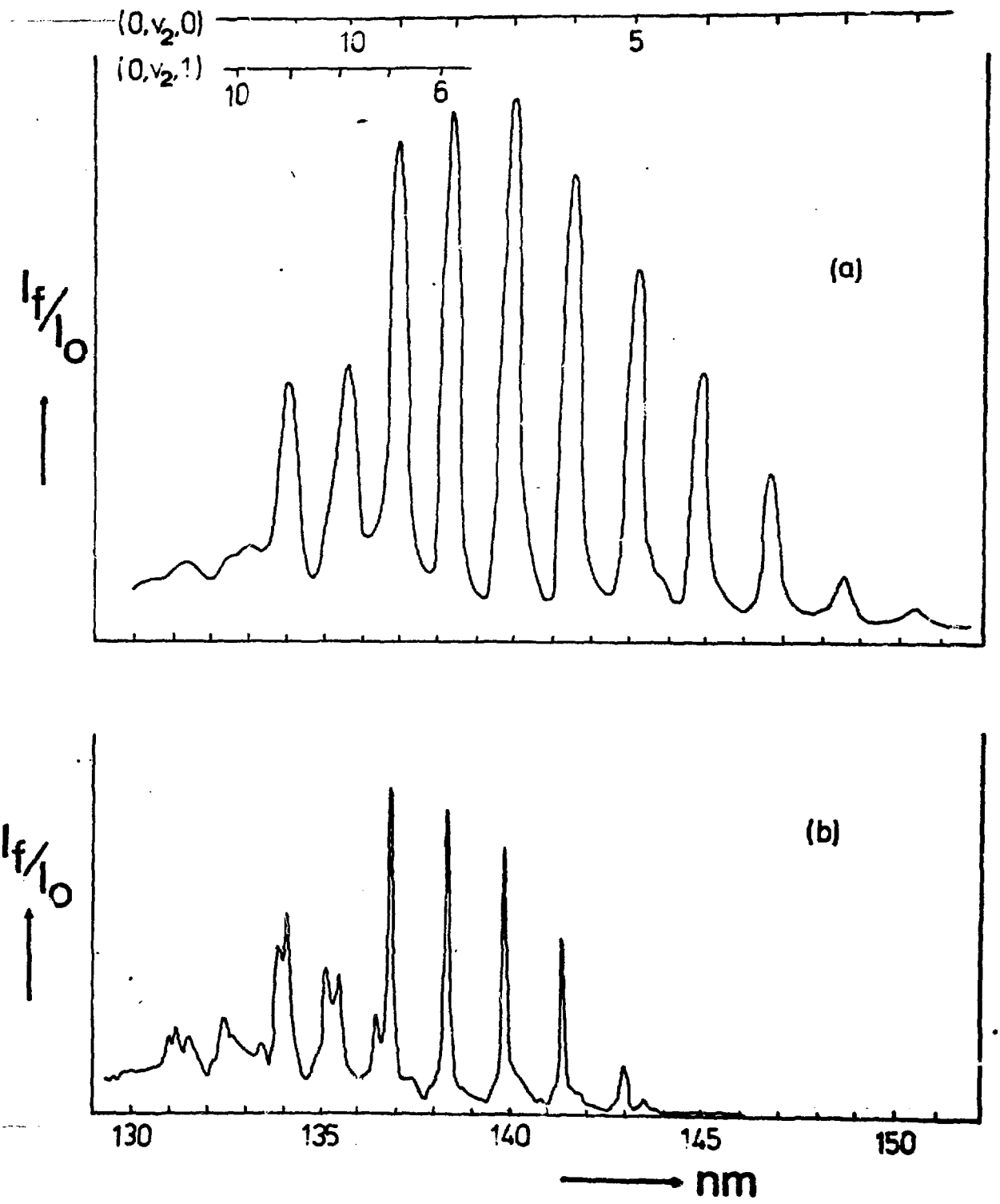

Fig. 11

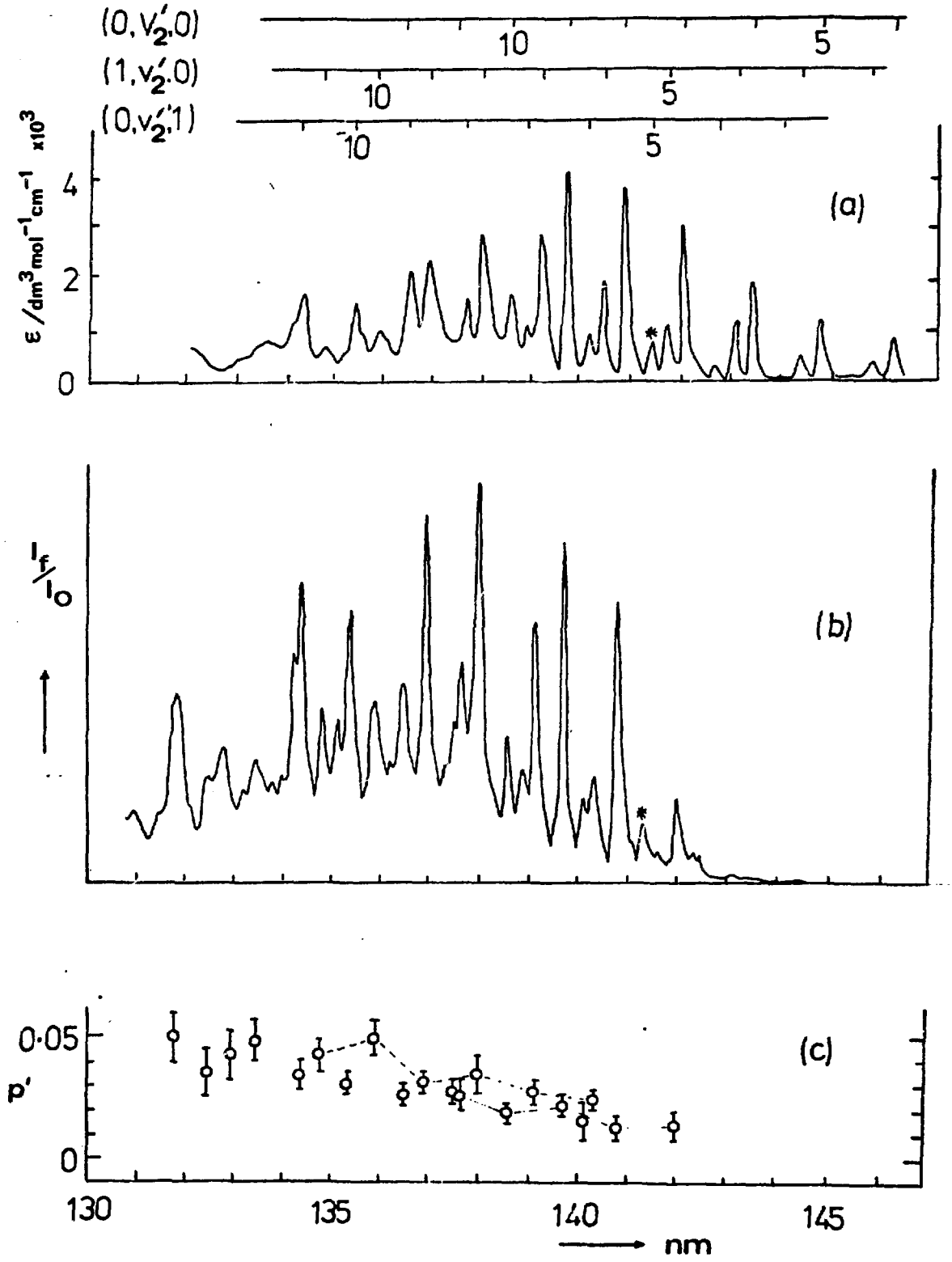
(0, v_2', 0)
(1, v_2', 0)
(0, v_2', 1)
10
5
10
5
10
5
ϵ /dm^{3}mol^{-1}cm^{-1} x10^3
4
2
0
(a)
I_f/I_0
(b)
p'
0·05
0
(c)
130
135
140
145
nm

Fig. 12

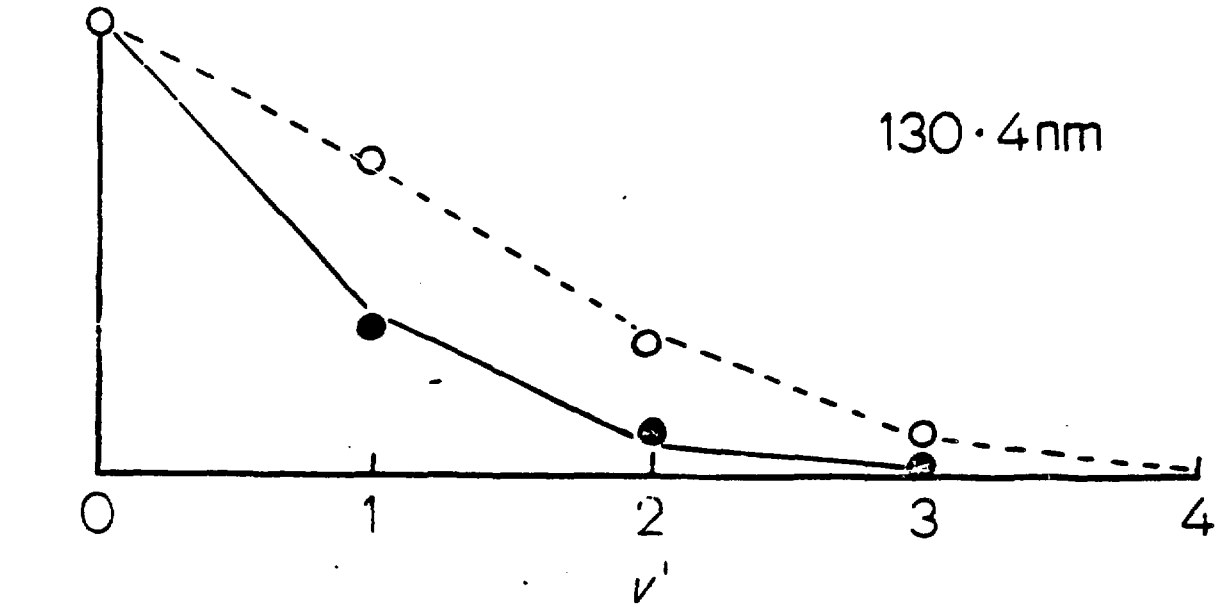

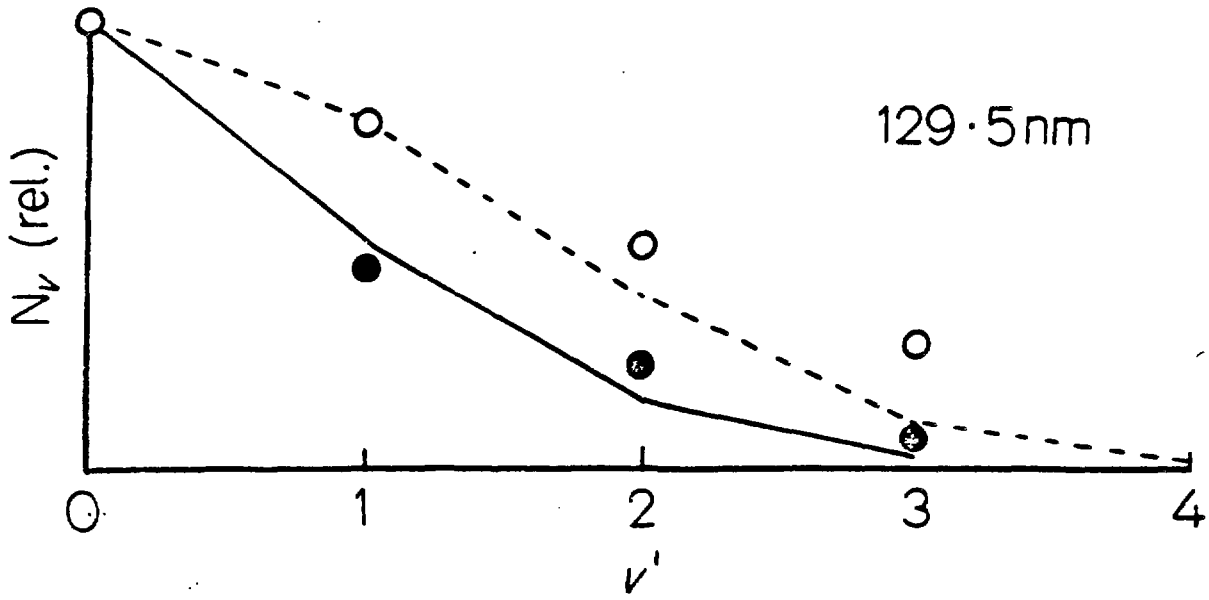

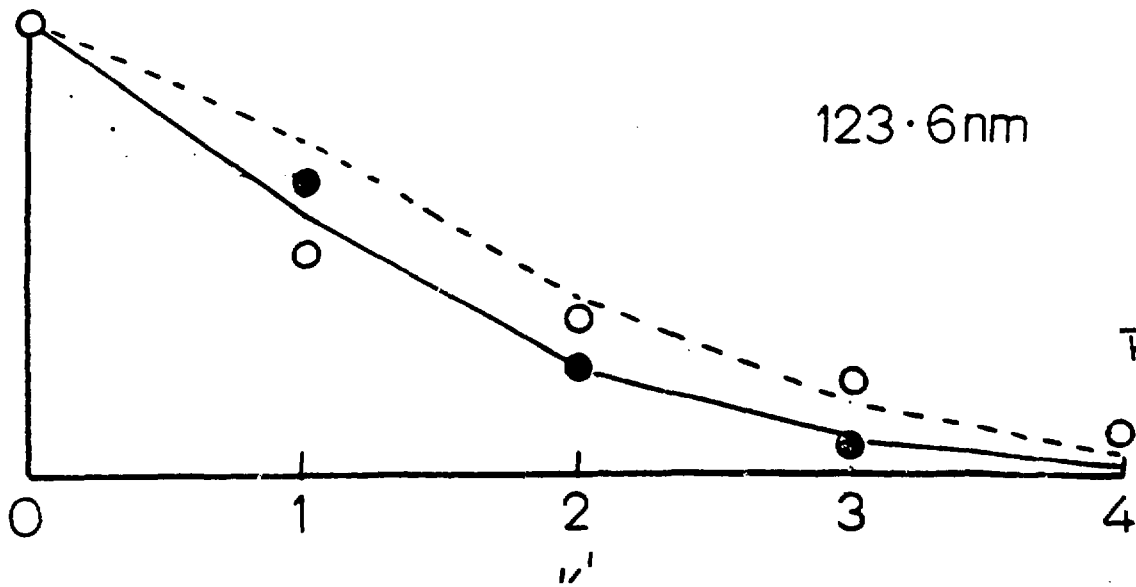

Fig.13

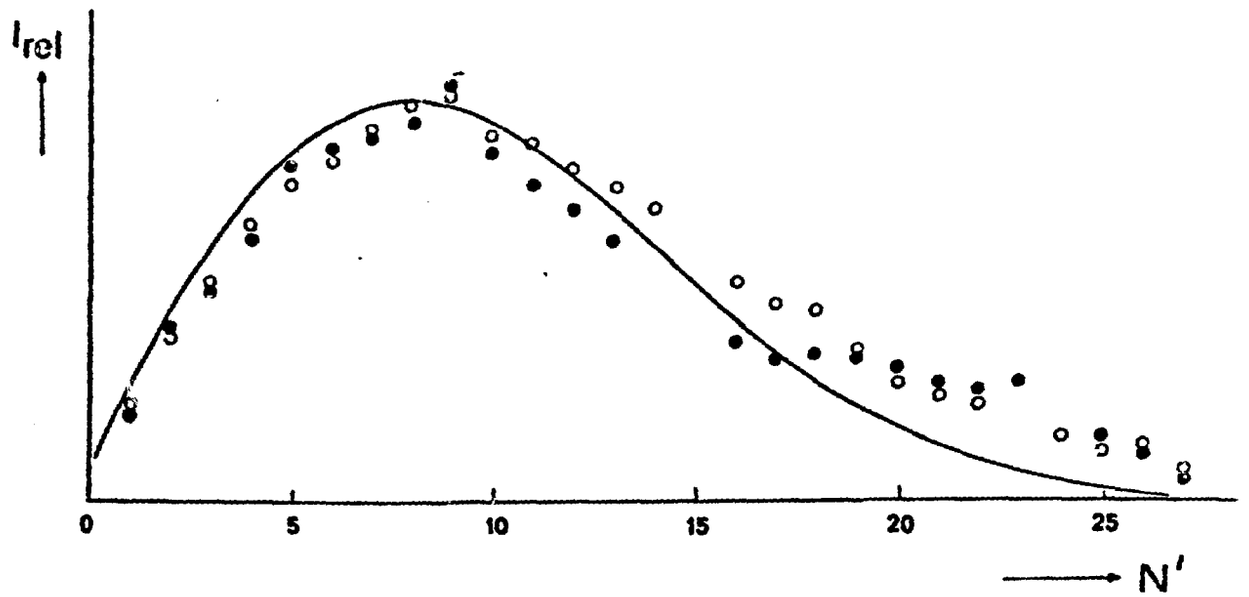

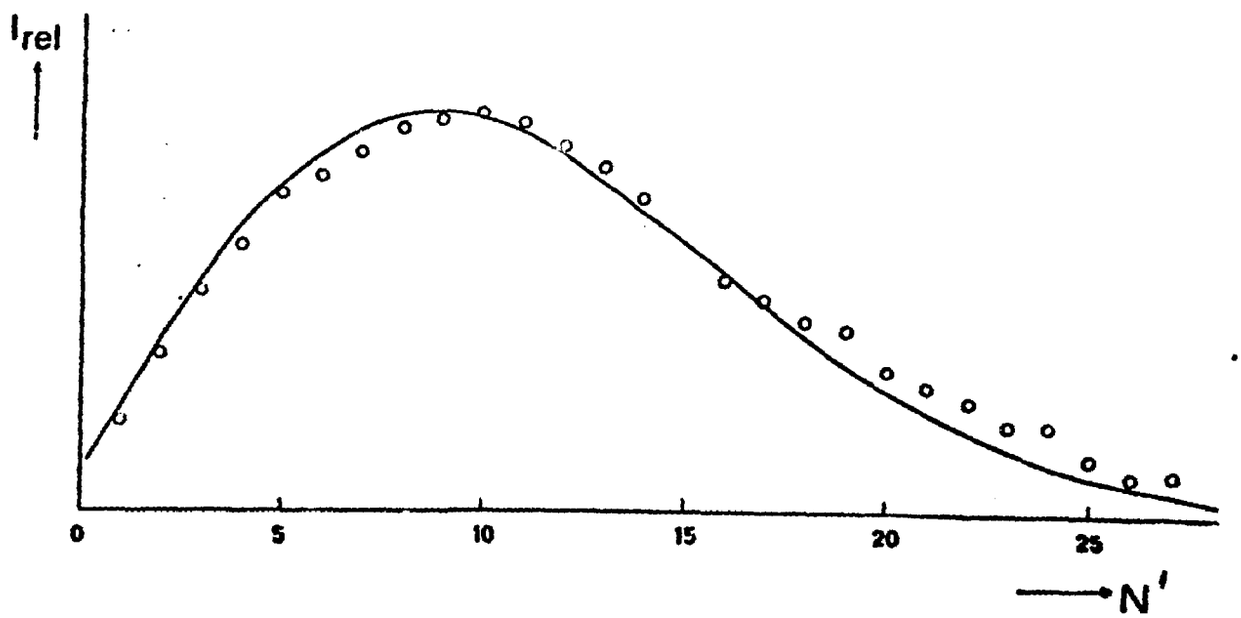

Fig. 14

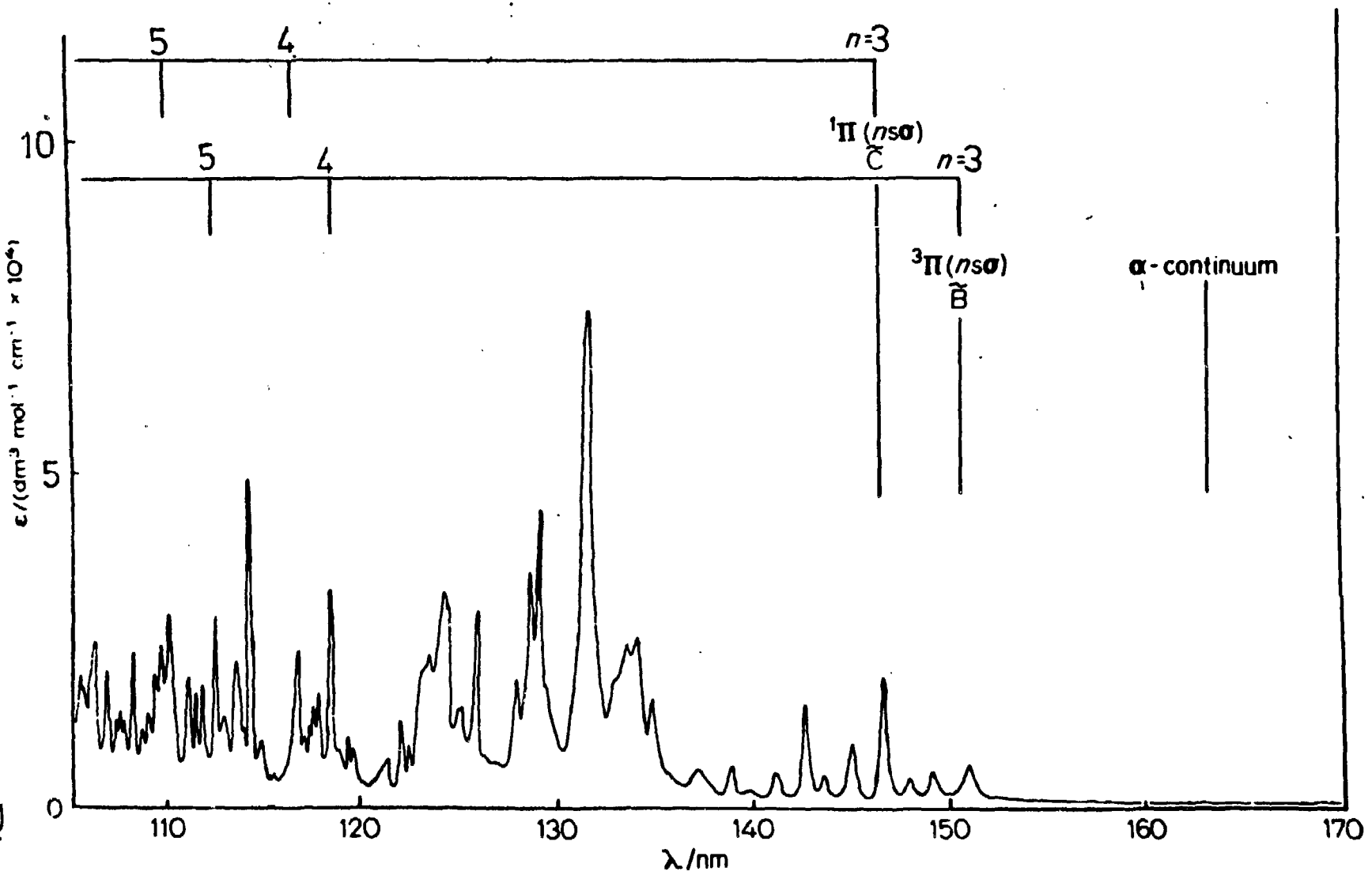
5
4
n=3
5
4
n=3
$^1\Pi$ ($ns\sigma$)
$\tilde{C}$
$^3\Pi$ ($ns\sigma$)
$\tilde{B}$
α - continuum
10
5
0
ε/(dm³ mol⁻¹ cm⁻¹ × 10⁴)
110
120
130
140
150
160
170
λ/nm

Fig. 8.15

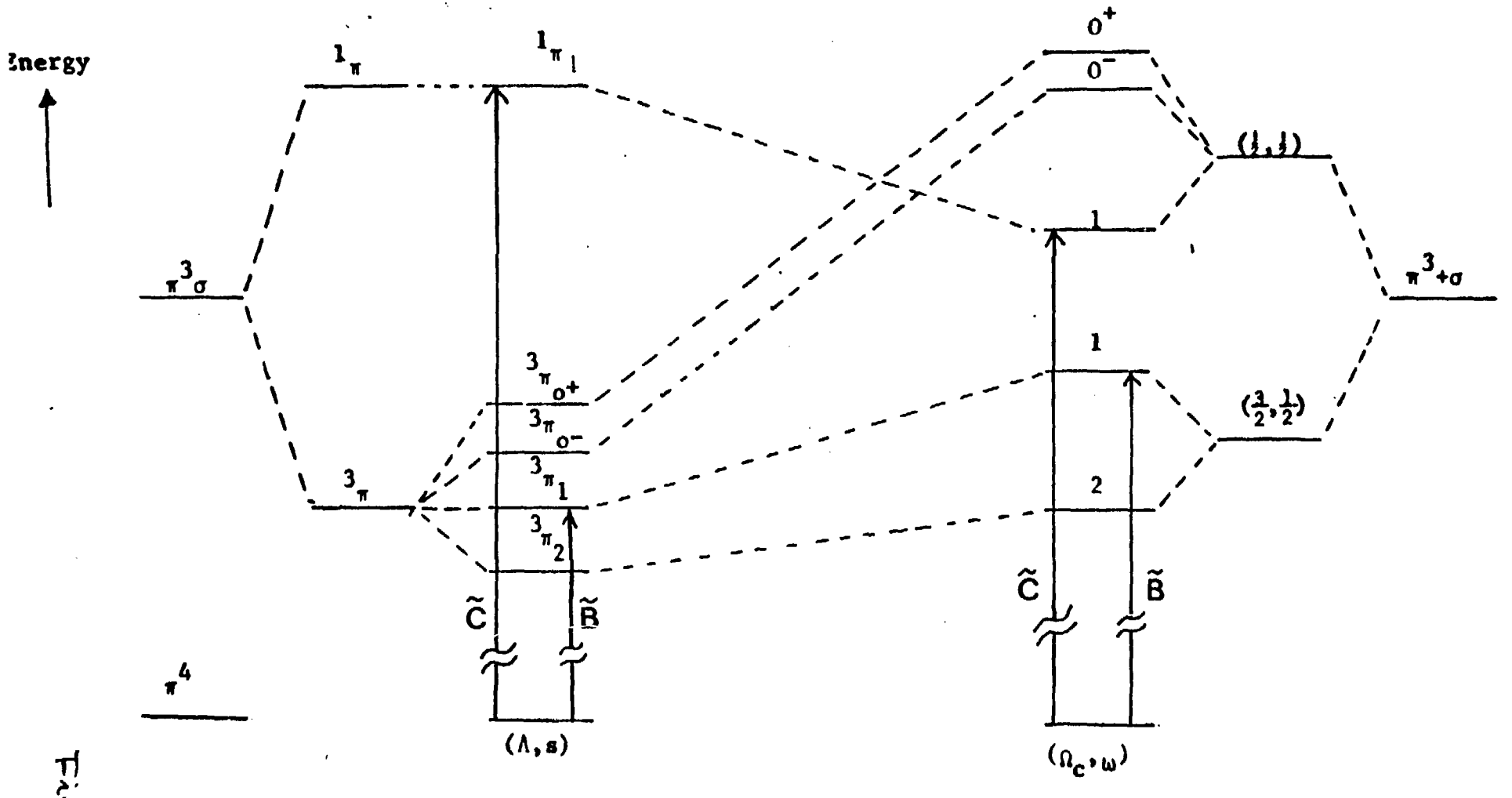
Energy
1_π
1_{π_1}
0^+
0^-
$(\frac{1}{2},\frac{1}{2})$
1
$\pi^3\sigma$
$\pi^3{}_{+\sigma}$
1
$3_{\pi_{0^+}}$
$3_{\pi_{0^-}}$
$(\frac{3}{2},\frac{1}{2})$
3_π
3_{π_1}
2
3_{π_2}
$\tilde{C}$
$\tilde{B}$
$\tilde{C}$
$\tilde{B}$
π^4
(Λ, s)
(Ω_c, ω)

Fig. 15

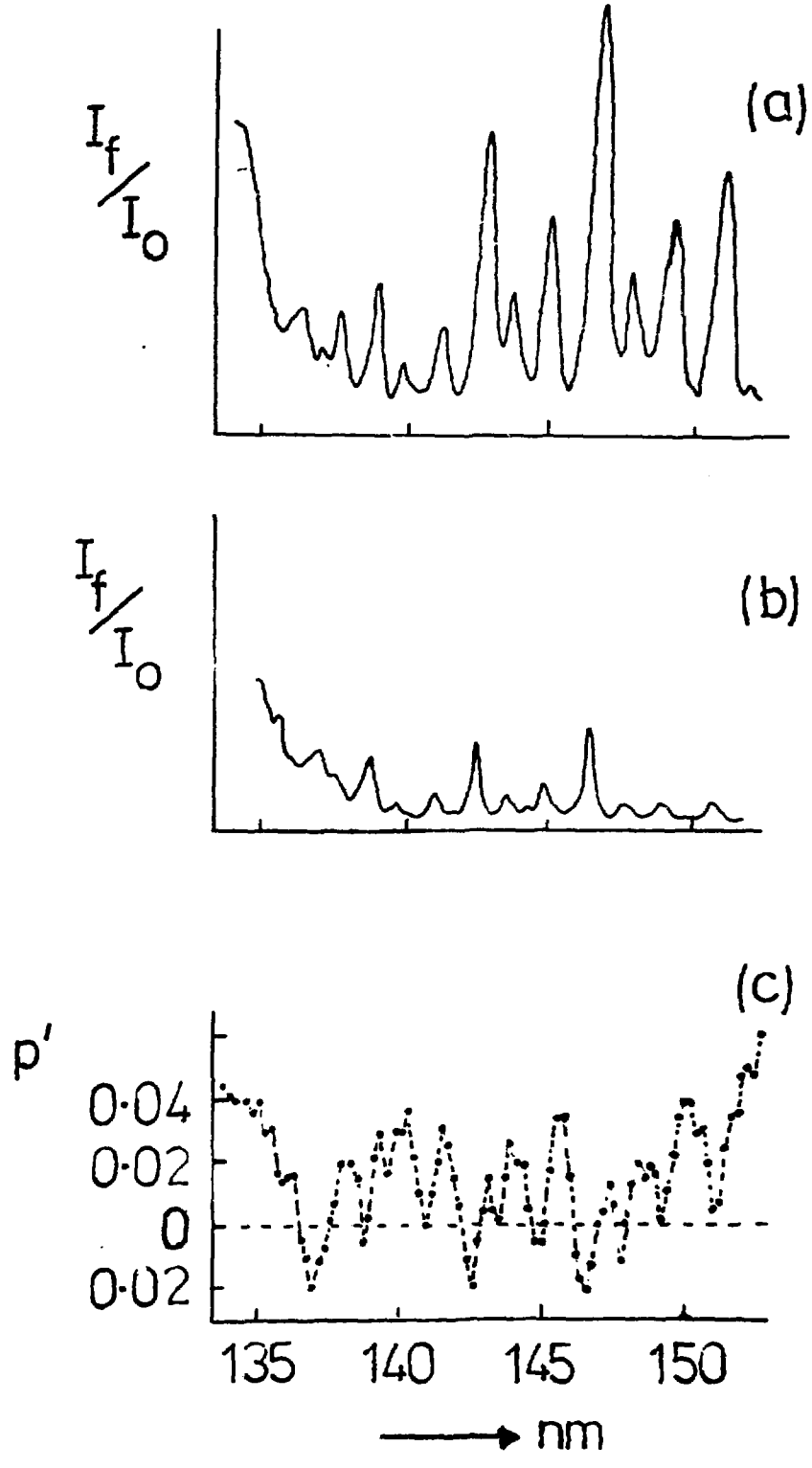

Fig.17

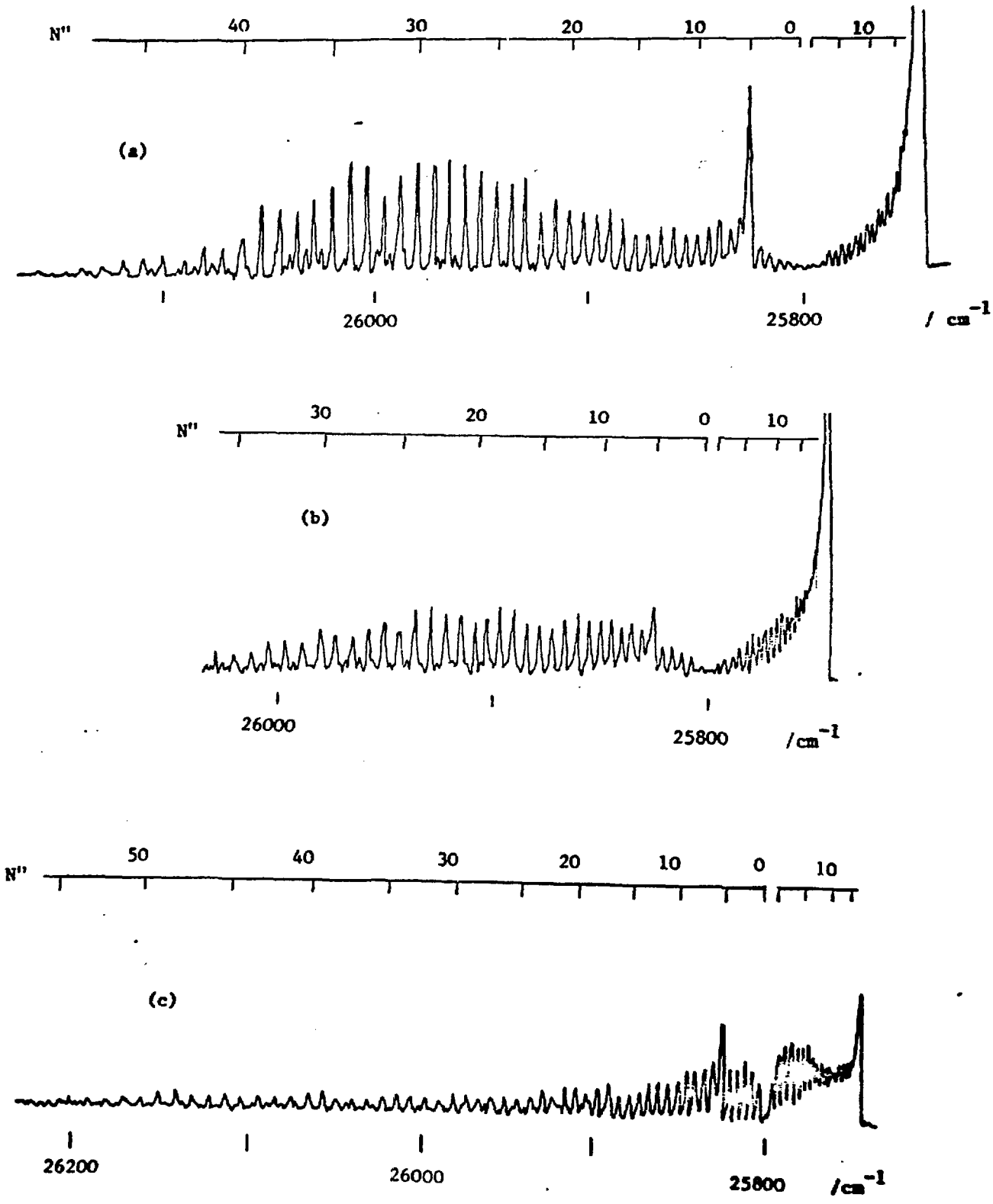
N''
40
30
20
10
0
10
(a)
26000
25800
/ cm^{-1}
N''
30
20
10
0
10
(b)
26000
25800
/cm^{-1}
N''
50
40
30
20
10
0
10
(c)
26200
26000
25800
/cm^{-1}

Fig.

Fig. 6.1

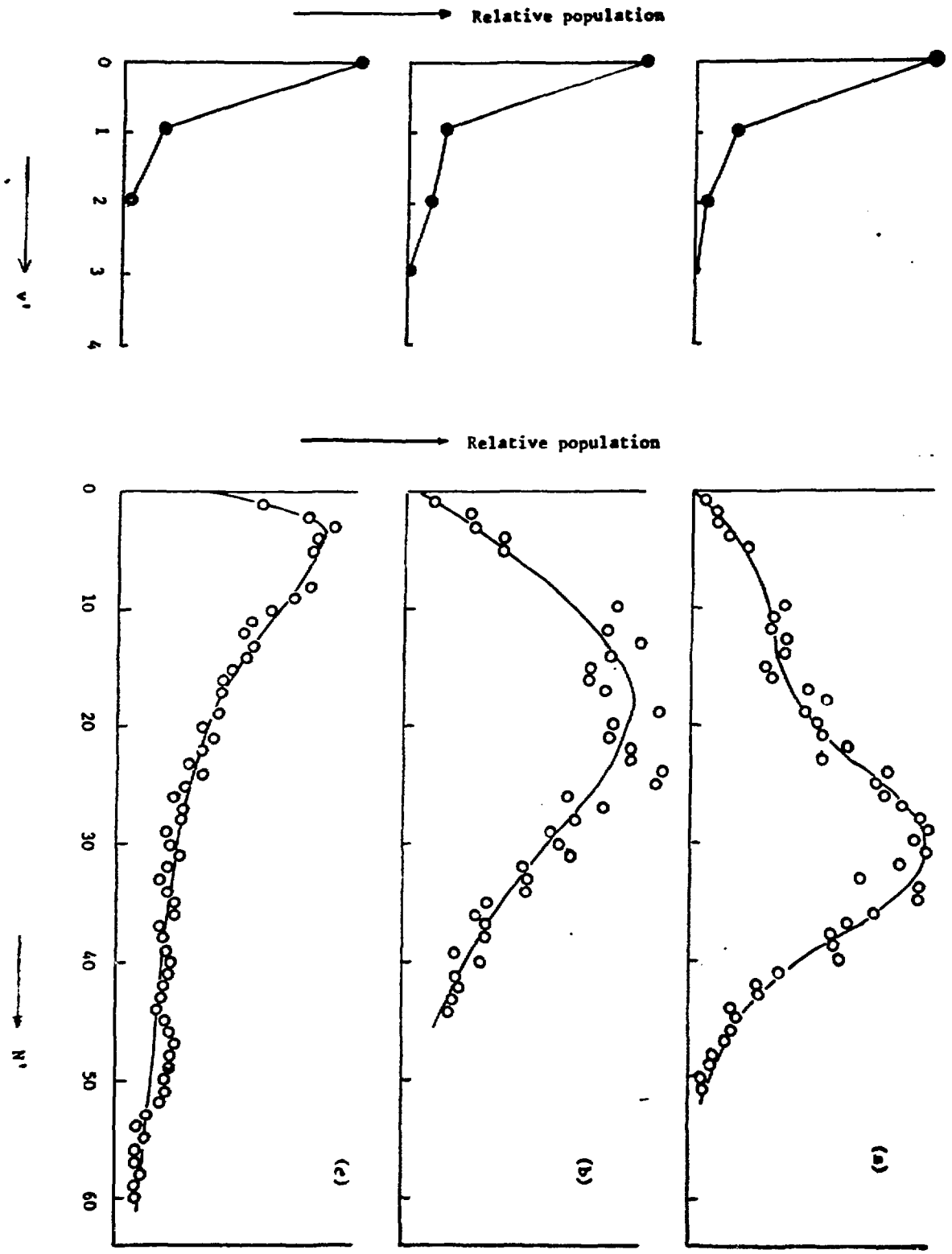
Relative population
0
1
2
3
4
N
Relative population
0
10
20
30
40
50
60
N
(c)
(b)
(a)

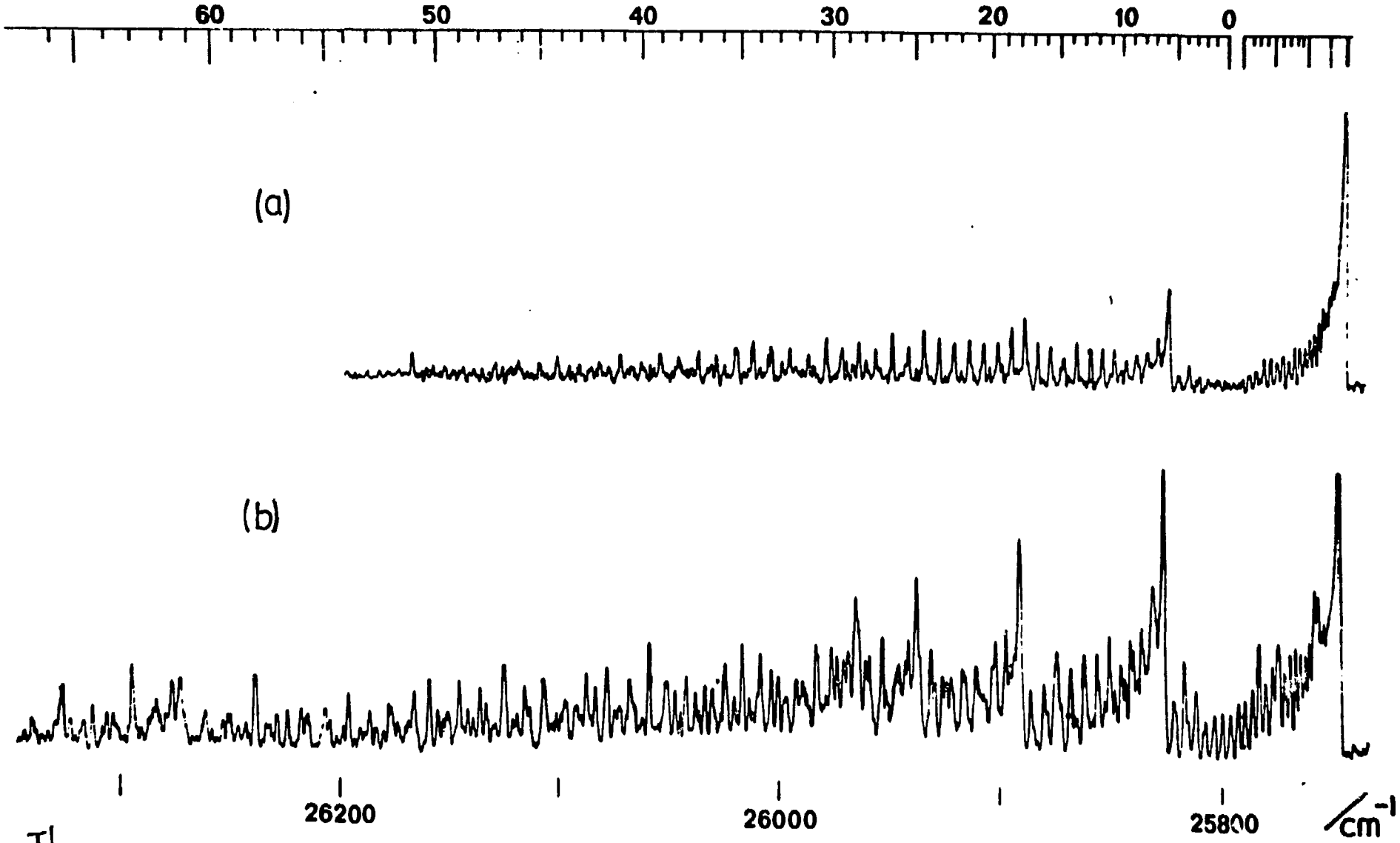

Fig. 1

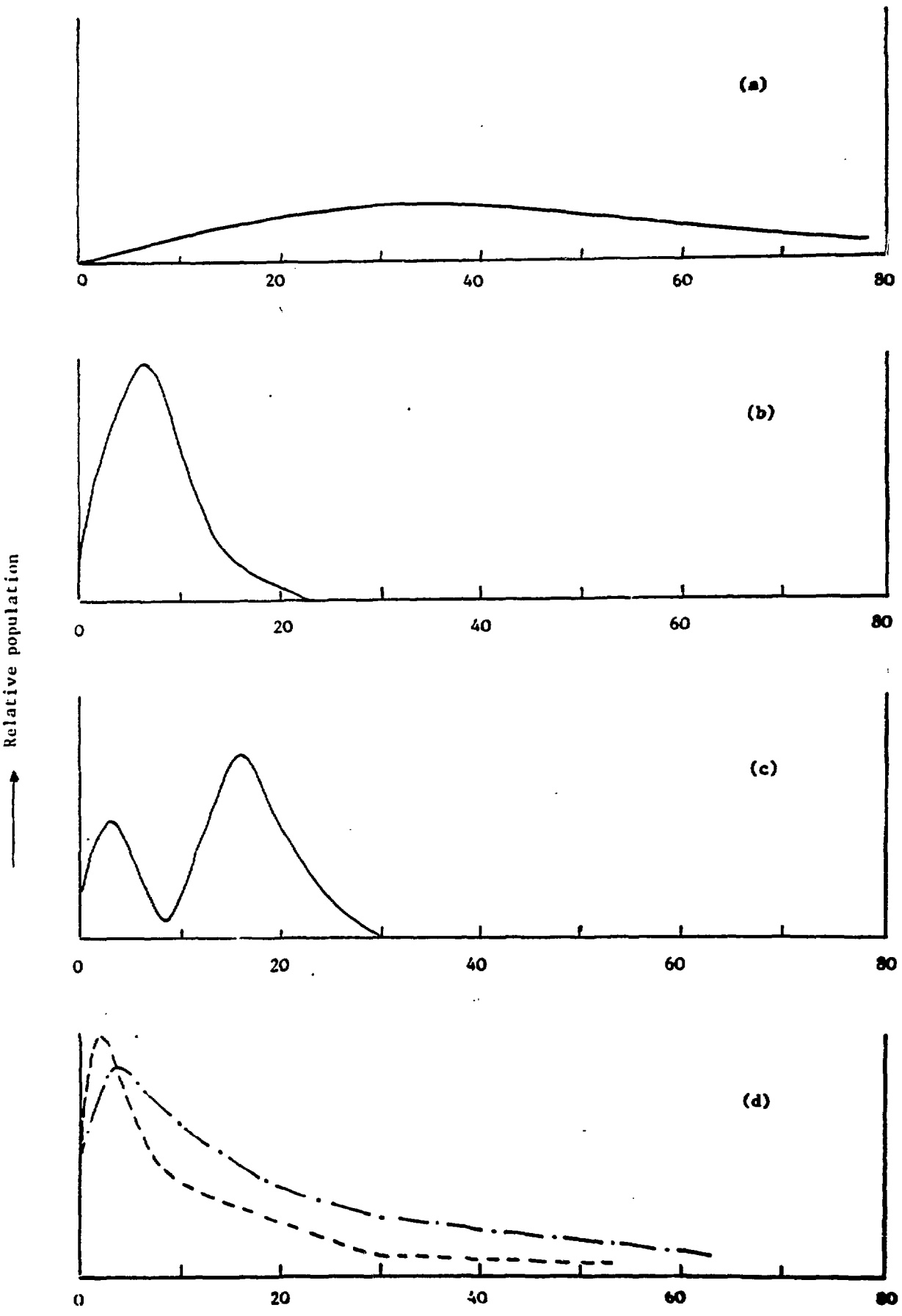
(a)
0
20
40
60
80
(b)
0
20
40
60
80
Relative population
(c)
0
20
40
60
80
(d)
0
20
40
60
80
Rotational Quantum Number

Fig. 21

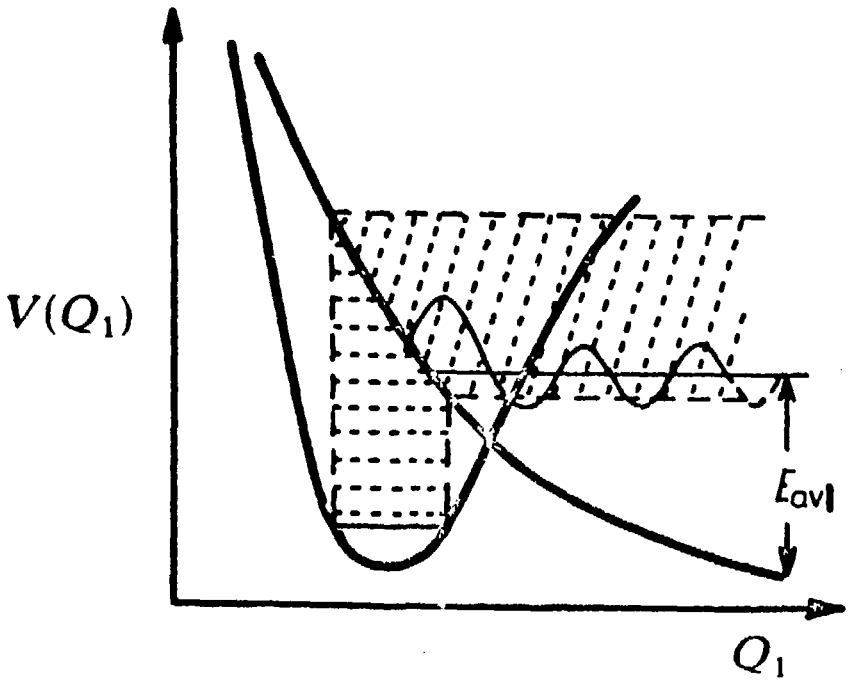

(a)

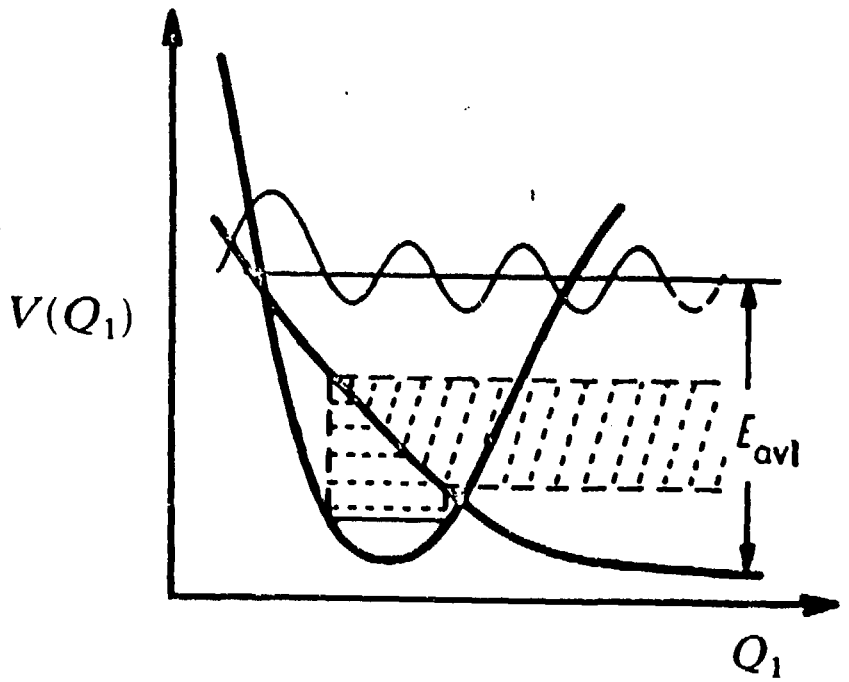

(b)

Fig. 2.

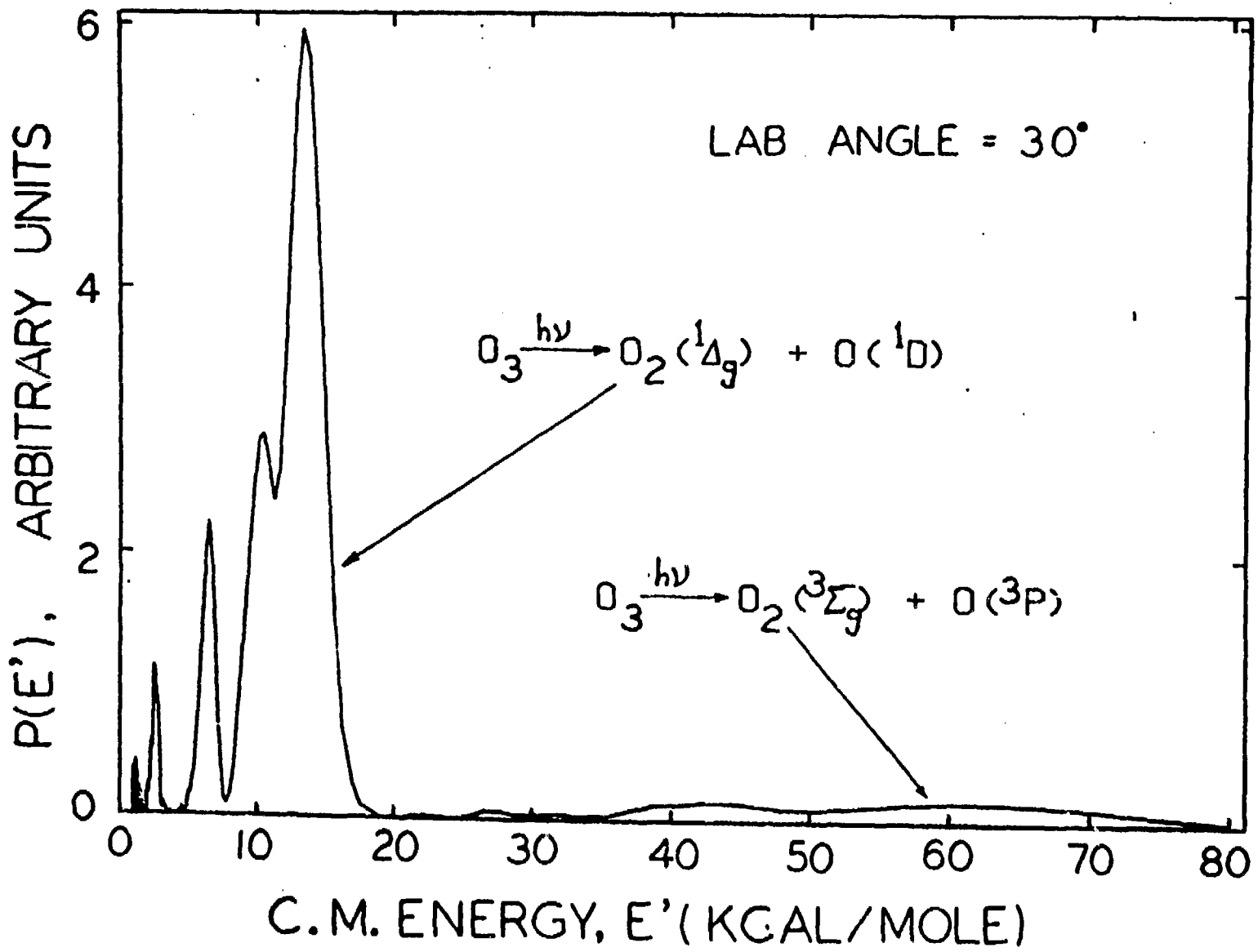
LAB ANGLE = 30°
$O_3 \xrightarrow{h\nu} O_2(^1\Delta_g) + O(^1D)$
$O_3 \xrightarrow{h\nu} O_2(^3\Sigma_g) + O(^3P)$
P(E'), ARBITRARY UNITS
C.M. ENERGY, E'(KCAL/MOLE)
0
2
4
6
0
10
20
30
40
50
60
70
80

Fig. 2

/ acceptance of this article, the
ublisher or recipient acknowledges
e U.S. Government's right to
tain a nonexclusive, royalty-free
ense in and to any copyright
vering the article.

PRODUCTION AND REACTIONS OF NEGATIVE IONS*

R. N. Compton

Chemical Physics Section, Health and Safety Research Division,
Oak Ridge National Laboratory, Oak Ridge, Tennessee 37830 U.S.A.

Introduction

Negative ions play important roles in many areas of photophysics and photochemistry. Negative ions can be produced directly by photodissociation of molecules through ion-pair production or indirectly via charge-exchange between photo-excited species and electronegative atoms or molecules. The most vivid illustration of the importance of negative ions in photophysics is to be found in the radiation emitted by the sun. The solar spectrum exhibits an intense absorption for wavelengths longer than 5000 Å. In 1939, Wildt[1] showed that H^- might exist in the solar atmosphere in sufficient concentrations to be the main source of opacity in the infrared region of the solar spectrum. In order to explain the absorption over the entire infrared region, it is necessary to take into account both photodetachment of H^- and the so-called free-free absorption in which an electron makes a transition between two continuum states in the field of an H atom.

In this review, we will discuss only negative ion properties and reactions in the gas phase. Negative ions in the condensed phase have been extensively studied by spectroscopic, electron spin resonance, and

---

*Research sponsored by the Office of Health and Environmental Research, U.S. Department of Energy under contract No. W-7405-eng-26 with the Union Carbide Corporation.

other techniques. Sanche[2] has recently suggested that shape resonances[3] which are formed by the capture of an incident electron by its centrifugal angular momentum barrier could form tight-binding π bands in organic insulators. Electronic motion within these bands could account for electrical conductivity in organic solids. Many organic dyes which are used in dye lasers probably fluoresce and lase between negative ion transitions. Although there have been no reports of a negative ion gas phase laser, there seems to be no reason why such a device would not be possible. Since most small (3 or 4 atom) negative ions do not possess bound excited states, such a laser would probably involve large organic anions and therefore might afford some moderate tuning capabilities.

We will also omit in this review studies of negative ions on surfaces, although this is an interesting area of research. It has recently been shown[4] that compound[3] states of O_2^- and N_2^- can play significant roles in the scattering of electrons from surfaces covered with O_2 and N_2.

Negative Ion Properties

The potential energy surface essentially defines the physical properties of a negative ion. Obtaining experimental and theoretical information on these surfaces has been an arduous task. There is accurate information on electron affinities, vibrational frequencies, and geometries for a number of small negative ions. In a few cases reasonably precise potential energy surfaces can be constructed.

The electron affinity (EA) of a molecule is defined as the difference in energy between the neutral molecule in its ground state, E^0, and the ion in its ground state E^- (i.e., $EA = E^0 - E^-$). Studies of electron

photodetachment or radiative attachment have provided values for atomic EAs with accuracies often less than 0.01 eV. The first accurate measurements of halogen EAs are credited by Berry and Reimann.[5] On the other hand, very few accurate determinations of molecular EAs have been made because of the complexity of molecular negative ions. In a few cases (notably NO and O_2) where photodetachment and photoelectron spectroscopy[6] have been applied, EAs are known with accuracies better than 0.01 eV. In cases where the EA is negative and a well-defined vibrational progression is observed, the resonance scattering technique[7] has provided adiabatic EAs with accuracies of about ±0.05 eV. In some cases, notably the studies of Brauman and co-workers[8] and Lineberger et al.,[9] accurate lower limits to EAs for complex molecules have been determined from photodetachment thresholds.

The determination of energy thresholds for the transfer of an electron between heavy particles and target molecules is often used to infer molecular EAs. For example, studies of reactions of the type $X^- + M \rightarrow X + M^-$ have provided accurate EAs (±0.2 eV) for many molecules.[10-15]

Helbing and Rothe[16] first employed the alkali collisional ionization technique to determine molecular EAs. This method involves the measurement of the energy threshold for the charge exchanging reaction between an alkali atom and a molecules, i.e., $A + M \rightarrow A^+ + M^-$. In one instance, the energy of the alkali ion was measured to infer the EA of CO_2.[17] A number of groups are actively employing the threshold collisional ionization technique for the purpose of determining molecular EAs (see the recent review by Baede).[18] This technique has proven especially useful for polyatomic molecules where other methods are not presently applicable. However, the method suffers from three major uncertainties:

(1) only lower limits to EAs are deduced, (2) the thresholds are sensitive to the target gas temperature, and (3) in some cases the actual threshold is difficult to determine because of weak signal or because of the nature of the cross section (or both). In cases where the target molecules are a gas at room temperature, the Doppler motion can have serious effects on the observed thresholds.

The flowing afterglow technique has provided a wealth of information on negative ion molecule reaction rates. The EAs of some molecules has also been bracketed by observing whether charge transfer does or does not proceed with the negative ions of known EA (see e.g., Refs. 19 and 20).

Electron affinity values which have been reported for atoms and small molecules (fewer than five atoms) range from $\sim$-2 to +4 eV. Figure 1 illustrates this with a plot of measured EAs for molecules made from atoms of the first (H) and second rows of the periodic table. The EA is plotted versus the number of valence electrons (total number of electrons minus the 2K shell electrons). Note that ions with 16 and 24 valence electrons are quite stable, reflecting the fact that greatest stability exists for "closed shells."

The EAs for these small molecules range from $\sim$-2 to +4 eV. There is evidence that the EAs of many larger hexafluoride molecules can possess EAs of up to 10 eV! The first evidence of these surprising molecular negative ion properties came from thermochemistry considerations. Bartlett[21] analyzed the oxidizing properties of the hexafluorides of the third transition metal series and found that the EAs increase in the order $WF_6 < ReF_6 < O_5F_6 < IrF_6 < PtF_6$ and EA (ReF_6) > 3.9 eV, EA (IrF_6) > 5.45 eV, and EA (PtF_6) > 6.75 eV.

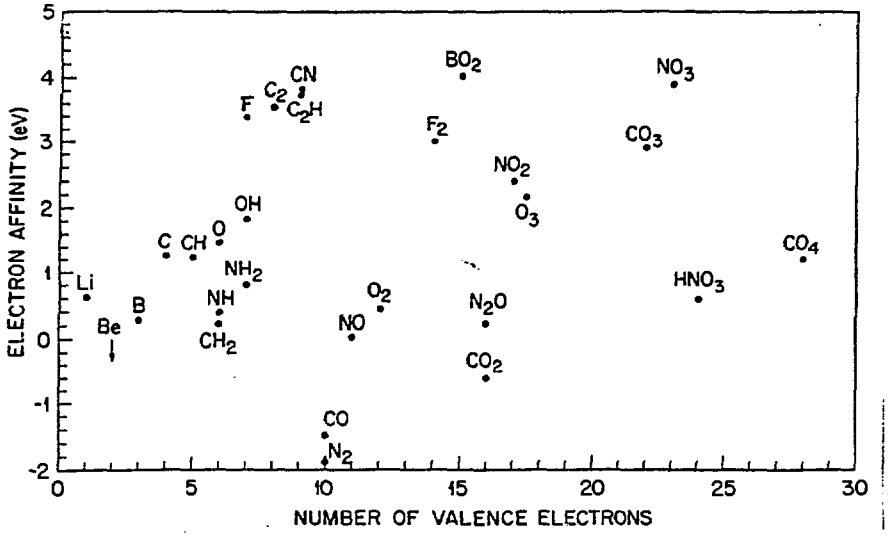

Fig. 1. Experimentally measured electron affinities for atoms and molecules made from atoms of the first (H) second row of the periodic table versus the number of valence electrons for the neutral. Notice that the values range from ∿-2 to +4 eV and abrupt changes occur at a completed shell.

The EAs increase ∿0.85 eV with unit increase in atomic number of the transition metal. More recent data of Barberi and Bartlett[22] give EA(PtF_6) = 9.3 eV. Bartlett's recent estimate of the EA(AuF_6) is 10 ± 0.5 eV (private communication)! Compton and Reinhardt[23] have studied the reaction Cs + $(AuF_5)_2$ → Cs^+ + AuF_6^- + AuF_4 and also find evidence for an EA > 9 eV for AuF_6.

Jensen and Miller have studied electron attachment and compound formation in flames and were able to deduce the following rather large molecular EAs: BO_2 (4.07),[24] WO_3 (3.64),[24] HWO_4 (4.35),[25] CrO_3 (4.04),[26] ReO_4 (4.45),[27] and $HMoO_4$ (4.25).[28] Although these EAs are not as large as those reported for some hexafluorides, they serve to illustrate that the EAs of many molecules can be larger than the accepted values for the halogen atoms.

Burgess et al.[29] have studied the thermochemistry of alkali metal hexafluoromolybdates and hexafluorotungstates to derive the standard enthalpies of formation of KWF_6, $RbWF_6$, $CsWF_6$, $KMoF_6$, $RbMoF_6$, and $CsMoF_6$. From these measurements, they estimate the gas phase EAs of WF_6 and MoF_6 to be 5.09 ± 0.05 and 5.36 ± 0.05 eV, respectively.

Charge-exchange reactions involving negative ions and hexafluorides and alkali atoms and hexafluorides have provided further evidence for very large EAs of many hexafluorides (see Ref. 30 and others cited therein).

Photoabsorption by Negative Ions

The interaction of electromagnetic radiation with negative ions is a large field of physics and chemistry. Recent review articles summarize most of the data[31-33] for the gas phase negative ions. There is an even larger set of data for negative ions in the condensed phase.

The cross section for photodetachment from an atomic negative ion is given by

$$\sigma_d = \frac{g_0 32\pi^4 m^2 e^2 v\nu}{g_i\ 3h\ c^3}\ |< \chi_i|\vec{r}|\chi_f >|^2$$

where ν is the light frequency $<\chi_i|\vec{r}|\chi_f>$ is the dipole matrix element and g_0 and g_i are the statistical weights of the ionic and neutral state. Photodetachment cross sections have been calculated from Eq. (1) for many atomic negative ions. The accuracy of the calculated cross sections is tested by applying known oscillator sum rules. The sum rule takes the form of an integral over the frequency and in the case where there are no bound excited states takes the form

$$\frac{e^2}{ha_o}\frac{mc}{\pi e^e}\int_{\nu_o}^{\infty}\frac{\sigma_d(\nu)}{\nu^5}\,d\nu = A_s$$

where A_s is a constant depending upon the wavefunction of the negative ion.

There are a few known examples of bound excited states of negative ions. Herzberg and Lagerquist[34] observed a well-developed band system in the range from 4800-6000 Å emitted from a high intensity flash discharge in methane which was not attributable to C_2 or C_2^+. Lineberger and Patterson[35] studied two-photon detachment of C_2^- and showed that the Herzberg-Lagerquist bands were due to $^2\Sigma_u^+ \rightarrow {}^2\Sigma_g^+$ transitions in C_2^-.

Autodetaching states of negative ions can have a large influence on photodetachment cross sections. Autodetaching states of neutral atoms have been extensively studied in optical absorption spectra. The famous Beutler lines in the rare gases (except He) are classic examples. Similarly autodetaching states can affect the continuum photodetachment cross sections. Many "window" type resonances are observed in the alkali negative ions both experimentally (see, e.g., Ref. 36) and theoretically.[37] One of the most interesting recent studies of the effects of shape resonances on photodetachment is the photodetachment of $He^-(1s2s2p)^4P°$ via the $He^-(1s2p^2)^4P^e$ shape resonance.[37] The $1s2p^2\ ^4P^e$ state of He^- gives rise to a very large ($\sim$24 $Å^2$) and narrow peak 10 meV above the $2^3P°$ threshold. Figure 2 gives the theoretical calculation[37] along with the recent experimental cross sections.[38,39]

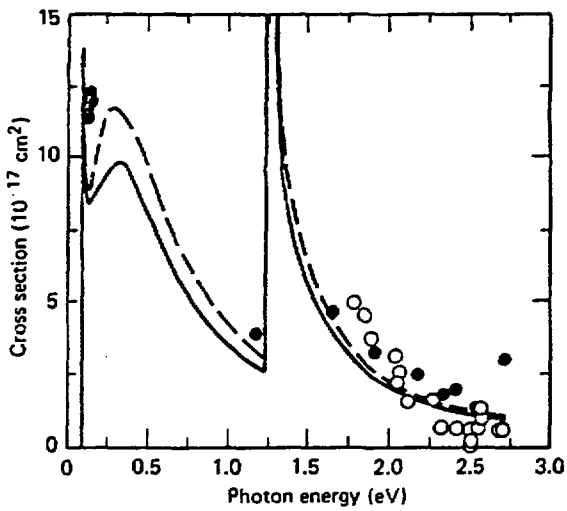

Fig. 2. Total absolute photodetachment cross section for He^- ($^4P°$); theory (Ref. 37), experiment (Refs. 38 and 39).

Perhaps one of the most exciting new discoveries in negative ion physics involves studies of Li^-. There are two excited states of Li^- which are bound relative to its parent excited neutral Li^- $1s2p^3\ ^5S°$ and Li^- $1s2s2p^2\ ^5P$.[40] The Li^- $^5S°$ state radiates to Li^- ^5P with a lifetime of 2.9 ns. Radiation at 3490 Å due to this transition has recently been identified in beam foil spectroscopy.

Recent studies of high-resolution photodetachment of polar anions[42] have revealed a series of very narrow, well-resolved resonances which are found just above the photodetachment thresholds for several negative ion species. The authors suggested the possibility that the resonant structures might be associated with bound excited dipole states of the molecular anions. These excited states although bound relative to the ground state neutral are so weakly bound that internal nuclear energy (rotation-vibration) allows for autodetachment. Garrett[43] found that

the dipole field of the species studied in Ref. 42 were exactly in the correct range (3 to 3.5 D) to yield one or two excited dipole states with binding energies so small that the bound excited states with some finite ro-vibrational energy would overlap with the continuum of one or more lower lying ro-vibrational levels.

Production of Negative Ions by Photon Reactions

The formation of ion-pairs by photon absorption, i.e.

$$h\nu + AB \rightarrow A^+ + B^-$$

is sometimes referred to as polar dissociation. This process can be particularly important in cases where the ion-pair limit lies below the ionization potential. The halogens I_2 and Br_2 are classic examples (e.g., the $I^+ + I^-$ limit is 0.49 eV below $I_2^+ + e$). In these cases large cross sections are observed below the ionization limit, however, once the photon energy approaches and exceeds the ionization limit the ion-pair cross section decreases dramatically. Figure 3 shows the experimental data of Morrison et al.[44]

It is interesting to consider the possibility of polar dissociation by photons for molecular clusters. For example, the threshold for the reaction

$$h\nu + (H_2O)_{12} \rightarrow (H_3O^+)(H_2O)_5 + OH^-(H_2O)_5$$

could be as low as $\sim$4 eV.

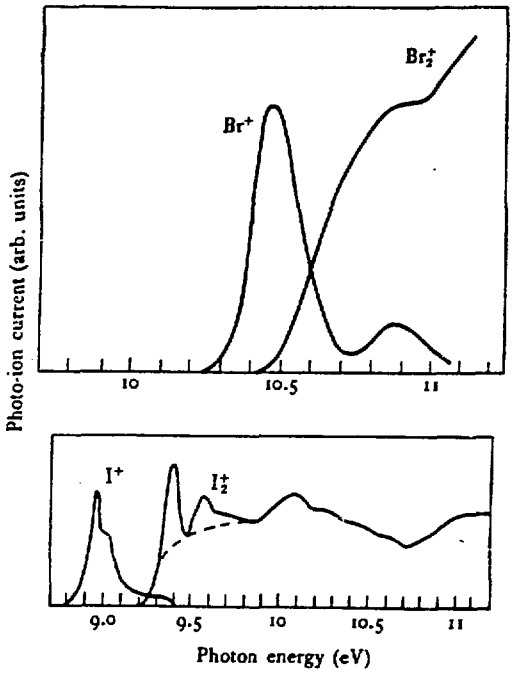

Fig. 3. Relative cross sections for $Br^+ + Br^-$ and Br_2^+ ($I^+ + I^-$ and I_2^-) produced from photon collision with Br_2 (I_2) as observed by Morrison et al.[44]

Collision of High Rydberg Atoms with Electron Attaching Molecules and the Possible Influence of Dipole Bound States

The Rydberg electron in a highly excited Rydberg state can be viewed as almost free and slow. That is, the excited electron and the ion core are sufficiently separated so that when a molecule collides with a Rydberg atom the molecule can be viewed as reacting with either the electron *or* ion core separately. Fermi[45] used data on ultra-low energy elastic electron scattering to analyze successfully the observed pressure shift of the high Rydberg series absorption spectra of an alkali metal atom perturbed by a foreign gas atom. Since Fermi's original contribution, there has been a considerable body of theoretical[46,47] and

experimental[48-50] evidence to suggest that the rate constant for transfer of a loosely bound Rydberg electron to a target molecule should be equal to the attachment rate for free electrons of the same energy. Perhaps the best experimental evidence for this equivalence comes from the unpublished data of Chupka.[51] Figure 4 displays the electron charge transfer rate from Rydberg excited Ar atoms to some hexafluoride molecules as measured by Chupka, versus the thermal electron attachment rate for the same hexafluorides as determined by Davis et al.[52] The solid line

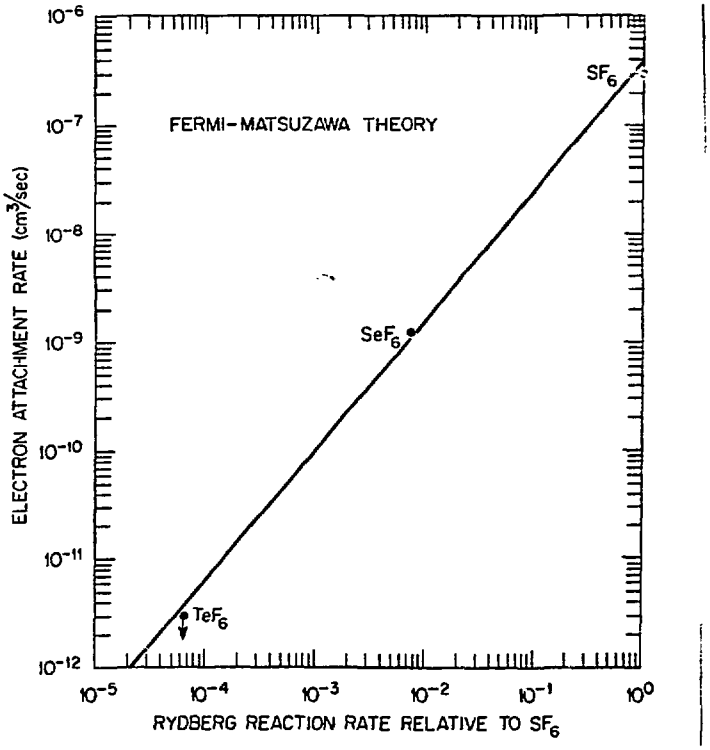

Fig. 4. Rydberg reaction rate leading to negative ions for various hexafluoride molecules relative to SF_6 as measured by W. A. Chupka (unpublished results) versus the thermal electron attachment rate as determined by Davis et al.[51] The Fermi-Matsuzawa[45,46] model predicts a straight line as shown.

through the data points is the Fermi-Matsuzawa prediction of equivalence between Rydberg reaction rates and slow electron attachment rates. The data not only confirms the Fermi-Matsuzawa model but the ions observed by Chupka are in fact identical to those found in slow electron attachment experiments (i.e., SF_6^-/SF_6, SeF_5^-/SeF_6, TeF_5^-/TeF_6).

The Rice University group of Stebbings, Dunning, and colleagues has presented some equally compelling evidence for the free-electron model. The thermal electron attachment rate for perfluoromethylcyclohexane (C_7F_{14}) is known to increase with electron energy.[52] Hildebrant et al.[53] have actually observed an analogous increase of the ionization rate with *decreasing* n when Xe atoms in high Rydberg states collide with C_7F_{14}. Thus, the equivalence of both the magnitude, energy dependence, and ion products for Rydberg charge exchange rates and thermal attachment rates seems to be well founded. We should hasten to point out, however, that the positive ion core of the Rydberg state can play a role in the collision other than simply bringing up the slow electron. For example, we know that thermal electrons attach to CH_3NO_2 to produce a short-lived $CH_3NO_2^-$ ion with a lifetime of less than 10^{-6} s. However, the $CH_3NO_2^-$ formed through Rydberg charge exchange is stable,[48] indicating that the recoiling positive ion relaxes vibrations initially excited in the negative ion. The very presence of the ion core can also make certain reactions possible which are apparently not available for slow electrons. For example, Chupka (unpublished results) has found that the reaction $Ar^{**} + HCl \rightarrow ArH^+ + Cl^-$ proceeds. Such a reaction would not be predicted from the model of free electron attachment since the thermal electron attachment rate to HCl is less than 3×10^{-12} cm^3/s and may well be

zero.[52] Thus, HCl is an example where the Rydberg core must play a critical role and, in fact, the reaction is only possible because of the $ArH^+ + Cl^-$ channel. But does the Rydberg electron transfer to HCl^- and then the Ar^+ core react to abstract a hydrogen atom? If so, we must postulate a potential energy surface for HCl^- that lies very close to the ground state. Such states have been postulated by Rohr and Linder[54] to explain their low-energy electron scattering data for the case of the hydrogen halides. The negative ion surface is believed to exist due to the dipole field of the molecule. Such negative ion states do not show up in limited basis set valence type calculations. However, the properties of the dipole field are such that we are assured of bound states if the dipole moment of a molecule is greater than ~2 Debye.[55,56] The dipole moment of HCl is only 1.08 Debye, less than the critical moment, but virtual states of the dipole field could provide a mechanism for electron transfer in the reaction

$$Ar^{**} + HCl \rightarrow Ar^+ \ldots HCl^- \rightarrow ArH^+ + Cl^- \quad .$$

Under this proposal the Fermi-Matsuzawa model would again apply. However, one could make an equally convincing argument that the Ar^+ core of Ar^{**} reacts with HCl to form ArH^+ and the Cl^- takes away the electron. Clearly, more experimental and perhaps theoretical work is necessary to solve this riddle.

There is a further example in which the thermal electron attachment rate does not approximate the Rydberg reaction rate. Namely, highly excited rare gas Rydberg atoms (excited by electron impact) react rapidly[57,48] with acetonitrile (CH_3CN) to produce CH_3CN^-, whereas the thermal energy

electron attachment rate constant for CH_3CN is $\leq 1.25 \times 10^{-14}$ cm^3/s. This, incidentially, is the lowest upper limit which has been placed on an electron attachment rate. Acetronitrile, like HCN, is a "closed shell" molecule, and the valence-type empty orbitals would be high in energy, and no valence-type bound states are expected. The dipole moment of CH_3CN is 3.92 Debye and well exceeds the minimum dipole moment required to form a bound state.[55,56] The dipole states are very fragile due to the low binding energy and would not survive the collisions inherent in an electron swarm experiment. Thus, it is not surprising that the attachment rate is unmeasurably small. We should mention that the Rydberg reaction rate estimated by Stockdale et al.[48] was not as large as that reported by Sugiura and Arakawa.[57] A possible explanation is that Stockdale et al.[48] did not detect all of the CH_3CN^- produced. In this connection, Odom and Hill (unpublished results) have reacted sodium high Rydberg states with CH_3CN and see *no* negative ions. They do observe a large cross section for collisional ionization producing a free electron. More experiments are definitely required to resolve the discrepancy. In resolving the discrepancy perhaps we will learn more about dipole states of the electron-molecule system.

The production and detection of dipole bound negative ion states offer a real challenge to experimentalists. The problem is to gently place the electron on the dipole and then detect the ion without ejecting the electron in the process of detection. Table I represents a list of molecules that are assured of weakly bound dipole states.[55,56] These compounds have vapor pressures that are suitable for use in mass spectrometer experiments. We have studied fast alkali collisions with each of these

Table I. Some Molecules With Dipole Moments Sufficiently Large to Permanently Bind an Electron

Molecule	Dipole Moment (Debye)
Cyanomethane H_3CCN (acetonitrile)	3.92
Formamide H_2NCOH	3.25
Nitromethane H_3CNO_2	3.46
Cyanamide H_2NCN	4.27
Dimethyl sulfoxide $(CH_3)_2SO$	3.96
Vinylene carbonate $C_3O_3H_2$	4.5

molecules and observe parent negative ions only in the case of nitromethane, which has a bound state due to an empty valence orbital (EA = 0.44 ± 0.2 eV).[58] In this case the dipole state should be considered as the excited state of $CH_3NO_2^-$.

Finally, we should mention that Matsuzawa[59] has suggested the use of high-Rydberg atoms to obtain information on electron-molecule resonance at ultra-low energies. Resonances in elastic electron molecule scattering would cause an oscillation in the n dependence of the pressure shift. As an example, if one could detect oscillations of 0.005 cm^{-1} in the pressure shift at low pressures where one can avoid multiple scattering effects, then the high-Rydberg atom could be used to detect resonances with widths of 10^{-3} eV.

References

1. R. Wildt, *Astrophys. J.* 89, 295 (1939).
2. L. Sanche, G. Bader, and L. Caron, *J. Chem. Phys.* 76, 4016 (1982).
3. G. J. Schulz, *Rev. Mod. Phys.* 45, 378 (1973).
4. L. Sanche and M. Michaud, *Phys. Rev. Lett.* 47, 1008 (1981); *Chem. Phys. Lett.* 84, 497 (1981).
5. R. S. Berry and C. W. Reimann, *J. Chem. Phys.* 38, 1540 (1963).
6. M. W. Siegel, R. J. Celotta, J. L. Hall, J. Levine, and R. A. Bennett, *Phys. Rev. A* 6, 607 (1972); R. J. Celotta, R. A. Bennett, J. L. Hall, M. W. Siegel, and J. Levine, *Phys. Rev. A* 6, 631 (1972).
7. L. Sanche and G. J. Schulz, *J. Chem. Phys.* 58, 479 (1973); I. Nenner and G. J. Schulz, *J. Chem. Phys.* 62, 1747 (1975).
8. J. H. Richardson, L. M. Stephenson, and J. I. Brauman, *J. Chem. Phys.* 59, 5068 (1973); *Chem. Phys. Lett.* 25, 321 (1974); *J. Am. Chem. Soc.* 97, 1160 (1975).
9. E. Herbst, T. A. Patterson, and W. C. Lineberger, *J. Chem. Phys.* 61, 1300 (1974).
10. W. A. Chupka, J. Berkowitz, and D. Gutman, *J. Chem. Phys.* 55, 2724 (1971).
11. J. Berkowitz, W. A. Chupka, and D. Gutman, *J. Chem. Phys.* 55, 2733 (1971).
12. C. Lifshitz, B. M. Hughes, and T. O. Tiernan, *Chem. Phys. Lett.* 7, 469 (1970).
13. T. O. Tiernam, B. M. Hughes, and C. Lifshitz, *J. Chem. Phys.* 55, 5692 (1971).

14. B. M. Hughes, C. Lifshitz, and T. O. Tiernan, *J. Chem. Phys.* 59, 3162 (1973).

15. C. Lifshitz, T. O. Tiernan, and B. M. Hughes, *J. Chem. Phys.* 59, 3182 (1973).

16. R.K.B. Helbing and E. W. Rothe, *J. Chem. Phys.* 51, 1607 (1969).

17. R. N. Compton, P. W. Reinhardt, and C. D. Cooper, *J. Chem. Phys.* 63, 3821 (1975).

18. A.P.M. Baede, *Adv. Chem. Phys.* 30, 463 (1975).

19. L. M. Babcock and G. E. Streit, *J. Chem. Phys.* 75, 3864 (1981).

20. E. E. Ferguson, D. B. Dunkin, and F. C. Feshenfeld, *J. Chem. Phys.* 57, 1459 (1972).

21. Neil Bartlett, *Angew. Chem. Int. Edit.* 7, 433 (1968).

22. P. Barberi and N. Bartlett (private communication).

23. R. N. Compton and P. W. Reinhardt, *J. Chem. Phys.* 72, 4€55 (1980).

24. D. E. Jensen, *Trans. Faraday Soc.* 65, 2123 (1969).

25. D. E. Jensen and W. J. Miller, *J. Chem. Phys.* 53, 3287 (1970).

26. W. J. Miller, *J. Chem. Phys.* 57, 2354 (1972).

27. R. K. Gould and W. J. Miller, *J. Chem. Phys.* 62, 644 (1975).

28. D. E. Jensen and W. J. Miller, *Thirteenth Symposium on Combustion, 363,* University of Utah, Salt Lake City, August 23-29, 1970.

29. J. Burgess, I. H. Haigh, R. D. Peacock, and P. Taylor, *J. Chem. Soc. (Dalton),* 1064 (1974).

30. R. N. Compton, P. W. Reinhardt, and C. D. Cooper, *J. Chem. Phys.* 68, 2023 (1978).

31. H.S.W. Massey, NEGATIVE IONS, Cambridge University Press, 3rd Ed. (1976).

32. B. M. Smirnow, NEGATIVE IONS, Translated by S. Chomet and Edited by H.S.W. Massey, McGraw-Hill (1982).

33. H. Hotop and W. C. Lineberger, *J. Chem. Phys. Ref. Data* 4, 539 (1975).

34. G. Herzberg and A. Lagerquist, *Can. J. Phys.* 46, 2363 (1968).

35. W. C. Lineberger and T. A. Patterson, *Chem. Phys. Lett.* 7, 469 (1970).

36. T. A. Patterson, H. Hotop, A. Kasdan, D. W. Norcross, and W. C. Lineberger, *Phys. Rev. Lett.* 32, 189 (1974).

37. D. L. Moores and D. W. Norcross, *Phys. Rev. A* 10, 1646 (1974); A. V. Hazi and K. Reed, *Phys. Rev. A* 24, 2269 (1981).

38. R. N. Compton, G. D. Alton, and D. J. Pegg, *J. Phys. B* 13, L651 (1980).

39. R. V. Hodges, M. J. Coggiola, and J. R. Peterson, *Phys. Rev. A* 23, 59 (1981).

40. C. F. Bunge, *Phys. Rev. Lett.* 44, 1450 (1980); *Phys. Rev. A* 22, 1 (1980).

41. S. Mannervik, G. Astner, and M. Kisielinski, *J. Phys. B* 13, L441 (1980); R. L. Brooks, J. E. Hardis, H. G. Berry, L. J. Curtis, K. T. Cheng, and W. Ray, *Phys. Rev. Lett.* 45, 1318 (1980); A. Denis and J. Desesquelles, *J. Physique* 42, L59 (1981).

42. A. H. Zimmerman and J. I. Brauman, *J. Chem. Phys.* 66, 5823 (1977); R. L. Jackson, A. H. Zimmerman, and J. I. Brauman, *J. Chem. Phys.* 71, 2088 (1979).

43. W. R. Garrett, *J. Chem. Phys.* 73, 5721 (1980).

44. J. D. Morrison, H. Hurzeler, M. G. Inghram, and H. E. Stanton, *J. Chem. Phys.* 33, 821 (1960).

45. E. Fermi, *Nuova Cim* 11, 157 (1934).

46. M. Matsuzawa, *J. Phys. Soc. (Japan)* 32, 1088 (1972).

47. M. Matsuzawa, *J. Phys. B* 8, 2114 (1975).

48. J.A.D. Stockdale, F. J. Davis, R. N. Compton, and C. E. Klots, *J. Chem. Phys.* 60, 4279 (1974).

49. W. P. West, G. W. Foltz, F. B. Dunning, C. T. Latimer, and R. F. Stebbings, *Phys. Rev. Lett.* 36, 854 (1976).

50. G. W. Foltz, G. J. Latimer, F. G. Hildebrant, F. G. Kellert, K. A. Smith, W. P. West, F. B. Dunning, and R. F. Stebbings, *J. Chem. Phys.* 67, 1352 (1977).

51. W. A. Chupka (unpublished results).

52. F. J. Davis, R. N. Compton, and D. R. Nelson, *J. Chem. Phys.* 59, 2324 (1973).

53. G. F. Hildebrant, F. G. Kellert, F. B. Dunning, K. S. Smith, and R. F. Stebbings, *J. Chem. Phys.* 68, 1349 (1978).

54. K. Rohr and F. Linder, *J. Phys. B* 9, 2521 (1976).

55. O. H. Crawford, *Mol. Phys.* 20, 585 (1971).

56. W. R. Garrett, *J. Chem. Phys.* 69, 2621 (1978).

57. T. Sugiura and A. Arakawa, *Proc. Int. Conf. Mass Spectrom.* University of Tokyo, Tokyo, p. 858 (1970).

58. R. N. Compton, P. W. Reinhardt, and C. D. Cooper, *J. Chem. Phys.* 68, 4360 (1978).

59. M. Matsuzawa, *J. Phys. B* 10, 1543 (1977).

SYSTEMATICS OF ELECTRONIC STRUCTURE IN RARE GAS VAN DER WAALS MOLECULES*

P. M. Dehmer and S. T. Pratt
Argonne National Laboratory, Argonne, Illinois 60439

ABSTRACT OF AN INVITED TALK TO BE PRESENTED AT THE
NATO ADVANCED STUDY INSTITUTE
ON
PHOTOPHYSICS AND PHOTOCHEMISTRY IN THE
VACUUM ULTRAVIOLET

Lake Geneva, Wisconsin
15-28 August 1982

---

*Work performed under the auspices of the U.S. Department of Energy and the Office of Naval Research.

The submitted manuscript has been authored by a contractor of the U. S. Government under contract No. W-31-109-ENG-38. Accordingly, the U. S. Government retains a nonexclusive, royalty-free license to publish or reproduce the published form of this contribution, or allow others to do so, for U. S. Government purposes.

It is well known that rare gas atoms repel each other except for van der Waals forces, which lead to weak molecular binding in all of the homonuclear and heteronuclear dimers except possibly He_2.[1] Removal of the outermost electron, which is antibonding in character, leads to a stable ground ionic state for all of the dimers. Several of the excited ionic states are bound as well, although, in general, the dissociation energies of the excited states are much smaller than those of the ground states. The addition of an electron in a Rydberg orbital to the ion in one of the bound states may result in a bound Rydberg state; however, little is known about the stable excited states of the neutral rare gas dimers except for those molecular states arising from the lowest atomic resonance transitions (i.e. the molecular excimer states). A notable exception is the detailed multichannel quantum defect theory analysis of the Rydberg states in He_2 which was presented recently by Ginter and Ginter.[2]

With this in mind, we have undertaken a systematic study of the photoionization spectra of the homonuclear (X_2) and heteronuclear (XY) rare gas dimers in order to better understand the nature of the bonding in the Rydberg states and the ions of these molecules. We have obtained results for Ar_2,[3,4] Kr_2,[5] Xe_2,[6] NeAr, NeKr, NeXe,[7] ArKr, ArXe, and KrXe.[8] The remaining dimer species (Ne_2 and the He-rare gas dimers) require a synchrotron light source and a more specialized supersonic molecular beam source capable of handling very high mass throughput.[9]

The photoionization spectrum of X_2 or XY consists of contributions both from direct ionization and from autoionization of Rydberg states of the neutral molecule. Since the Franck-Condon overlap between the ground state of the neutral molecule and the ground state of the ion is poor for several tenths of a

volt above the ionization threshold,[10,11] the photoionization spectrum in the region of the ionization threshold consists solely of autoionization structure. At shorter wavelengths, the autoionization structure appears superimposed on the direct ionization continuum. In the present work, we are concerned primarily with the molecular autoionization features and their relationship to the atomic Rydberg states.

The most significant advantage of photoionization mass spectrometry over photoabsorption for the study of the homonuclear and heteronuclear rare gas dimers is the ability of the former technique to discriminate against atomic structure through mass analysis of the product ions. In photoabsorption, the molecular structure is completely masked by the much more intense atomic structure near all of the optically allowed atomic Rydberg transitions.[12] This is not a serious problem near the low lying atomic Rydberg transitions, since the atomic structure is widely spaced; however, in the region between the atomic fine-structure thresholds, the atomic structure is not discrete, but rather is a true (albeit structured) continuum. Thus it is impossible to observe weak dimer structure superimposed on this very intense atomic continuum in photoabsorption studies. Furthermore the adiabatic ionization potential (and hence the dissociation energy of the ground state of the ion) can be determined from the present experiments, but not from the absorption spectrum, since the molecular Rydberg series converging to the ionization limit have not been analyzed.

The molecular spectra of the homonuclear and heteronuclear rare gas dimers show strong similarities to the corresponding atomic structure in the energy region between the atomic $^2P^o_{3/2}$ and $^2P^o_{1/2}$ fine structure thresholds. In the homonuclear dimers, molecular Rydberg series are observed that converge to the $C^2\Pi_{1/2u}$ and the $D^2\Sigma^+_{1/2g}$ states of the dimer ion. In the heteronuclear dimers,

the molecular Rydberg series converge to either the $B^2\Pi_{1/2}$ or $D^2\Sigma^+_{1/2}$ state of the ion, depending on whether the energy region corresponds to the region between the Y^+ or the X^+ fine-structure thresholds. This is a particularly simple region of the spectrum for most of the heteronuclear rare gas dimers, since all of the molecular Rydberg states converge to a single ionic limit. In addition, much of the molecular structure retains the characteristic Beutler-Fano profiles. Figure 1 shows the spectra of Xe, NeXe, ArXe, and Xe_2 in the energy region between the atomic Xe fine-structure thresholds and is a striking example of the progression from a spectrum that shows a strong resemblance to the atomic spectrum (NeXe) to a spectrum that shows only a modest resemblance to the atomic spectrum (Xe_2). Similar results are obtained for the Ar series and the Kr series. A simple analysis based on the values of the effective principal quantum numbers n^* and on the observed similarity between the atomic and molecular structure yields values of the vertical binding energies for both the Rydberg states and the ionic convergence limits.

In comparing the atomic and molecular spectra in the region between the atomic fine-structure thresholds one cannot help but note the similarity among them, and it is tempting to generalize this observation and conclude that molecular spectra of van der Waals molecules are merely weakly perturbed atomic spectra. However, in other regions of the spectra this similarity vanishes. Figure 2 shows a small region of the Ar_2, ArKr, and ArKe spectra near the Ar^* 4d and 6s dipole-allowed atomic transitions. The atomic Ar Rydberg states are also shown in the figure. There is little similarity in the atomic and molecular spectra in this wavelength region, indicating that it is an oversimplification to characterize the molecular spectra of these van der Waals dimers as perturbed atomic spectra.

In our presentation we will show the spectra of the rare gas dimers obtained at high wavelength resolution and will explore the trends in bond dissociation energies of the excited states and ionic convergence limits of these species. We also will discuss the extensions to heavier clusters and to molecular (rather than atomic) clusters.

REFERENCES

1. R. S. Mulliken, J. Chem. Phys. 52, 5170 (1970).
2. D. S. Ginter and M. L. Ginter, J. Mol. Spectrosc. 82, 152 (1980) and references therein.
3. P. M. Dehmer and E. D. Poliakoff, Chem. Phys. Lett. 77, 326 (1981).
4. P. M. Dehmer, J. Chem. Phys. 76, 1263 (1982).
5. S. T. Pratt and P. M. Dehmer, Chem. Phys. Lett. 87, 533 (1982).
6. P. M. Dehmer and S. T. Pratt, J. Chem. Phys. 75, 5265 (1981).
7. S. T. Pratt and P. M. Dehmer, J. Chem. Phys. 76, 3433 (1981).
8. P. M. Dehmer and S. T. Pratt, J. Chem. Phys. (submitted).
9. D. J. Trevor, Ph.D. thesis, University of California, Berkeley, 1980 presents results for Ne_2 obtained using a synchrotron light source. Experiments attempting to observe the photoionization spectrum of He_2 were inconclusive.
10. P. M. Dehmer and J. L. Dehmer, J. Chem. Phys. 68, 3462 (1978).
11. P. M. Dehmer and J. L. Dehmer, J. Chem. Phys. 69, 125 (1978).
12. See for example, Y. Tanaka and K. Yoshino, J. Chem. Phys. 53, 2012 (1970).

Figure 1. Relative photoionization cross sections for Xe, NeXe, ArXe, and Xe_2 in the energy region between the Xe fine-structure thresholds. The wavelength resolution was 0.45Å for Xe_2 and 0.28Å for the remaining systems.

Figure 2. Relative photoionization cross sections for Ar_2, ArKr, and ArXe in the region of the Ar^* 4d and 6s dipole-allowed atomic resonances, taken at a wavelength resolution of 0.15Å. The structure at the exact positions of the atomic Ar transitions is due to the associative ionization reaction $Ar^* + Ar(Kr, Xe) \rightarrow Ar_2^+ (ArKr^+, ArXe^+) + e^-$.

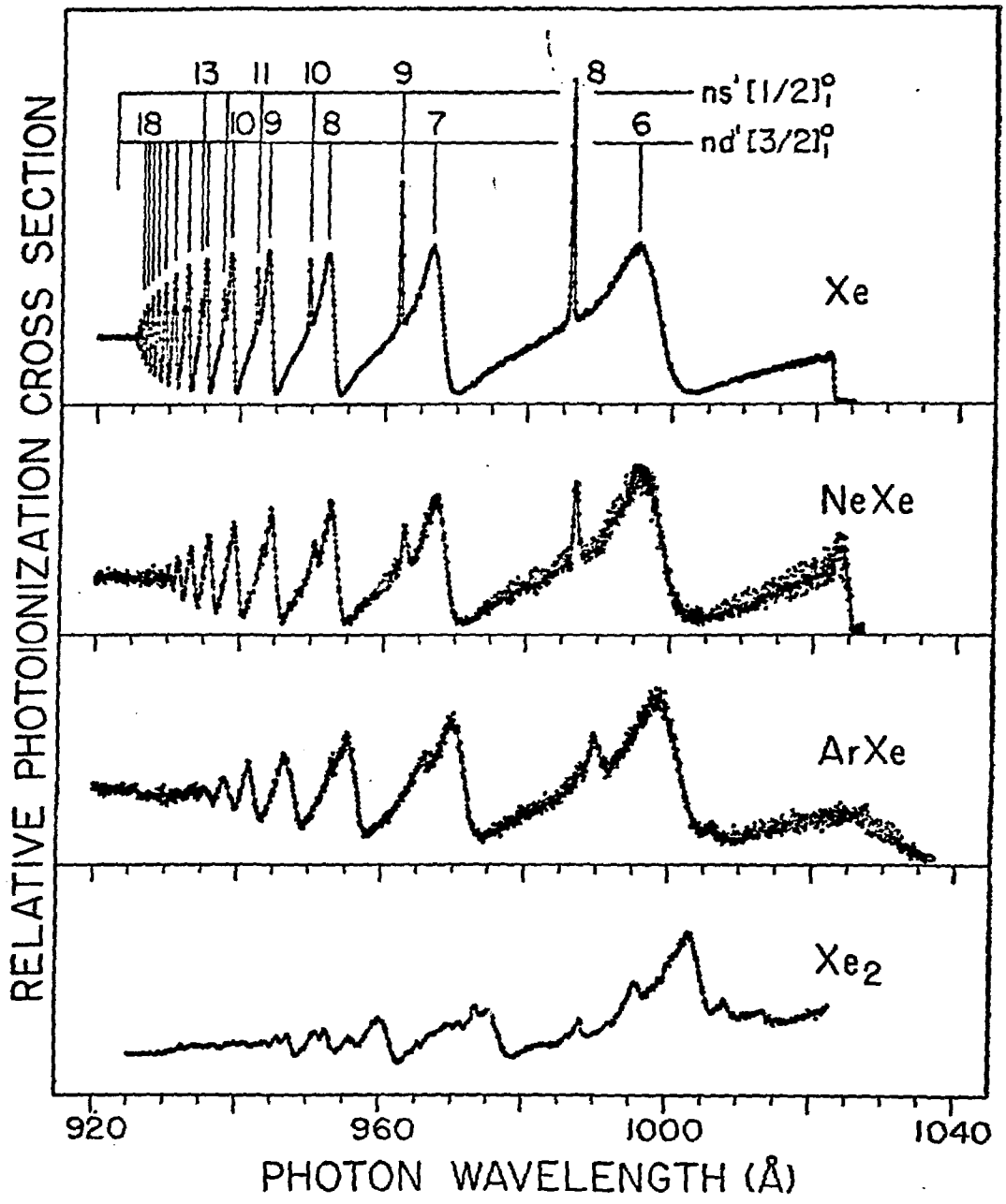
13
11
10
9
8
ns'[1/2]°1
18
10
9
8
7
6
nd'[3/2]°1
Xe
NeXe
ArXe
Xe2
RELATIVE PHOTOIONIZATION CROSS SECTION
920
960
1000
1040
PHOTON WAVELENGTH (Å)

FIGURE 1

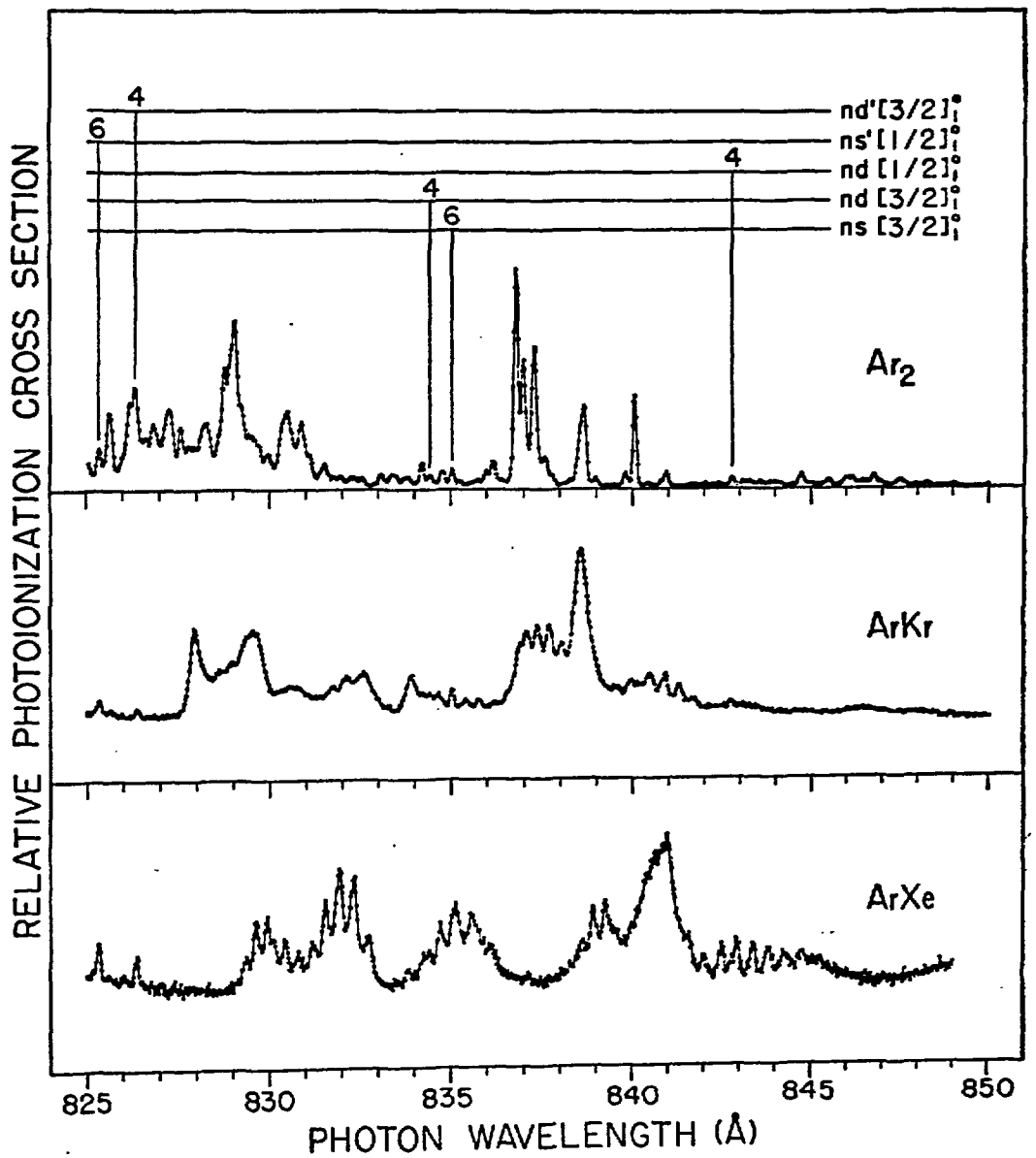
RELATIVE PHOTOIONIZATION CROSS SECTION
nd'[3/2]$_1^o$
ns'[1/2]$_1^o$
nd [1/2]$_1^o$
nd [3/2]$_1^o$
ns [3/2]$_1^o$
4
6
4
6
4
Ar_2
ArKr
ArXe
825
830
835
840
845
850
PHOTON WAVELENGTH (Å)

FIGURE 2

Multiphoton Spectroscopy and Photochemistry*

M. B. Robin

Bell Laboratories

Murray Hill, New Jersey 07974

ABSTRACT

A molecule struck by an intense laser pulse can undergo two general types of nonlinear photochemistry: ionization followed by fragmentation (Class A), or fragmentation followed by ionization (Class B). This classification scheme is applied toward an understanding of the MPI spectra and photochemistries of various Class A systems (acetaldehyde, dimethyl mercury, and tetramethyl silane), and Class B systems (chromium hexacarbonyl, the mercuric halides, tetramethyl tin and silicon tetrachloride). Additionally, we discuss the MPI of stannic chloride which shows Class A and Class B behavior simultaneously, and of methyl iodide, which is Class A in one spectral region, and Class B in another.

---

*This paper is a condensed version of one submitted to J. Phys. Chem.; "Nonlinear Photochemistry in Organic, Inorganic and Organometallic Systems", by A. Gedanken, M. B. Robin and N. A. Kuebler.

Multiphoton Spectroscopy and Photochemistry*

M. B. Robin

Bell Laboratories

Murray Hill, New Jersey 07974

INTRODUCTION

UV/visible laser multiphoton ionization (MPI) of polyatomic molecules in the gas phase is rapidly becoming a popular tool in the hands of the molecular spectroscopist. In this technique, the photocurrent flowing within a pulse-irradiated sample is monitored as the wavelength of the laser is scanned; photocurrent peaks arise whenever the absorption of an integral number of photons results in a resonance excitation in the target molecule [1]. A typical experimental setup for MPI spectroscopy is shown in Fig. 1. In the simplest experiment, 5 nsec pulses from a dye laser pumped at ca. 10 Hz are focused with a 15 cm lens to a 100 μ spot between a pair of flat-plate electrodes within the sample cell. With 50 μJ pulses from the dye laser, peak powers of ca. 100 MW/cm^2 are generated at the focus, and with a

*This paper is a condensed version of one submitted to J. Phys. Chem.; "Nonlinear Photochemistry in Organic, Inorganic and Organometallic Systems", by A. Gedanken, M. B. Robin and N. A. Kuebler.

bias of 200-800 V on the plates, DC currents of ca. 10^{-12} A can be read with an electrometer or picoammeter. Sample gas is typically at 1-50 Torr pressure in such static experiments.

How can a visible light pulse ionize a molecule having an ionization potential perhaps three times larger than the energy of one such photon? In general, at some unspecified frequency ν in the visible/UV, such a laser pulse will drive a molecule from the ground state Ψ_0 to ionization (Ψ_f) via a three-photon coherent absorption. This proceeds through virtual levels Ψ_j and Ψ_k with a rate proportional to

$$I^3 \left| \frac{\sum\sum \langle \Psi_0 | er | \Psi_j \rangle \langle \Psi_j | er | \Psi_k \rangle \langle \Psi_k | er | \Psi_f \rangle}{(\Delta E_{0j} - h\nu)(\Delta E_{0k} - 2h\nu)} \right|^2$$

where I is the instantaneous optical power and ΔE_{0j} is the energy separation between stationary levels 0 and j. The factor given above is readily generalized to the case of n-photon absorption.

If the laser frequency is scanned, eventually an m-photon resonance will be achieved, $\Delta E_{0m} - mh\nu$ goes to zero and the overall ionization rate then increases by several orders of magnitude. Thus, on scanning, an ionization spectrum results in which the peaks correspond to m-photon resonances in the absorbing system. The I^n dependence of the ionization rate, with n larger than m and typically 3 or 4, makes pulsed laser ionization the only practical mode, for

in this case I is 10^{27} photons/cm^2 sec, whereas for a CW source of the same bandwidth, I is only 10^{16} photons/cm^2 sec at best. The 10^{-7} duty cycle of the pulsed source is more than compensated by the far larger value of I and the extremely nonlinear dependence of the ionization rate on I.

The MPI technique can be used to several ends. In the hands of the molecular spectroscopist this simple technique has revealed many two-photon excitations in high-symmetry molecules which were otherwise unobservable in one-photon absorption spectra. Moreover, the technique uncovers resonances in the vacuum UV region (below 2000 Å) without the cumbersome vacuum UV hardware otherwise needed, and the symmetry of the resonance state occasionally can be deduced from the ratio of ionization currents produced using linearly and circularly polarized light. The high sensitivity and specificity of MPI spectroscopy suggests its use as an analytical tool [2], and indeed, single -molecule sensitivity has been claimed [3,4].

Another MPI facet of potential interest is that of multiphoton-driven photochemistry.

NONLINEAR PHOTOCHEMISTRY

In this paper, we describe the three most distinct types of nonlinear photochemical behavior, and then go on to illustrate them with MPI data on a number of organic, inorganic, and organometallic compounds. The three general

types of nonlinear photochemical behavior are shown schematically in Fig. 2 [5]. In this general scheme, we postulate that the first excitation step is a two-photon coherent absorption from the ground state (Grnd) to the resonance state (Res), via a virtual level (Virt) in the polyatomic molecule MXYZ. While the lifetime in the virtual level (ca. 10^{-15} sec) is too short to allow photochemical transformation, that in the resonance state is longer; if it is in the range 10^{-3} - 1 nsec (as compared with a laser pulse width of ca. 5 nsec), the molecule might readily decompose or rearrange within the duration of the laser pulse. Thus at the resonance state there is a branching into Class A and Class B systems, depending on whether the molecule absorbs one or more photons and ionizes, or fragments/rearranges before another photon can be absorbed.

The n-photon absorption rate between levels x and y is $I^n\sigma_{xy}$ where I is the optical power and σ_{xy} is the relevant cross section. In Class A systems, the one-photon absorption rate from the resonance state to a superexcited state SE, $I\sigma_{RSE}$, in the ionization continuum is much larger than the decomposition rate γ, so that the molecule is preferentially excited to the superexcited level and then relaxes to the parent ion $MXYZ^+$. At low laser powers (ca. 10^5 W/cm^2) often only $MXYZ^+$ is formed initially, and it does not further photofragment. However, in intense pulses with power of ca. 10^9 W/cm^2, $MXYZ^+$ may be further excited and fragmented, eventually forming M^+, X^+, etc. The general

course of Class A behavior is ionization followed by fragmentation, Fig. 2.

In a Class B system, the photochemical relaxation rate γ in the resonance state is much larger than $I\sigma_{RSE}$, and so the molecule fragments before another photon can be absorbed. If the molecular fragments are also multiphoton (or one-photon) resonant with the incident light and are no more photostable than the parent system, then they will continue to absorb and fragment until only atoms remain. These atoms, as typified by M in Fig. 2, then are multiphoton ionized via atomic resonance states.

While most materials investigated to date are either Class A or Class B, examples are also known of systems which are Class A in one spectral region, and Class B in another, and if γ is approximately equal to $I\sigma_{RSE}$, then mixed behavior can be expected as well. It may also happen that a parent molecule behaves as a Class B system to yield a polyatomic neutral fragment, which then behaves as a Class A system. Class C behavior has not been identified positively in a molecular system, being known in rare-gas atoms only. Note however, that even in sharp-line MPI spectra there always is observed an underlying continuum of ionization which in many cases appears to be nonresonant and therefore corresponds to Class C. Characteristics of the various Classes are listed in Table I.

In general, the Class A molecules are multiply-bonded

organics of low-atomic-weight atoms, i.e., acetaldehyde, benzene, butadiene, cyclopropane, etc. Class B on the other hand encompasses inorganic and organometallic compounds having one or more heavy-metal atoms, as in $Cr(CO)_6$, $Mn_2(CO)_{10}$, ferrocene, $SnCl_4$, etc. It is apparent that multiphoton excitation of inorganic and organometallic systems can be a clean source not only of metallic ions in the gas phase, but of ground and/or excited-state atoms as well.

TWO EXAMPLES

Let us now consider two examples which are already in the literature, but which illustrate many of the points listed in Table I. In the region between 3600 and 3700 Å there is a sharp two-photon resonance in acetaldehyde [6-8] terminating at the (n, 3s) Rydberg level; n -> 3s is a well-known one-photon transition in this molecule. These simple observations (Points 3, 6, and 10) firmly place acetaldehyde in Class A. In accord with this, the mass spectrum of acetaldehyde ionized at low laser power shows a preponderance of CH_3CHO^+ parent ion; however, with increasing laser power, this gives way to CH_3CO^+, CH_3^+, CH_2^+, etc. (Point 2). At low power, I, the ionization signal, S, obeys a power law of the form $S \propto I^n$ with n = 3, while three photons indeed are required to ionize acetaldehyde at the n -> 3s resonant wavelengths (Point 5). Acetaldehyde is the prototypical Class A system.

To elaborate somewhat on the situation in acetaldehyde, the first two photons are absorbed in a coherent excitation to (n, 3s) [probably with (n, π*) functioning as the virtual level], and a third photon then converts the (n, 3s) resonance state into the parent ion. This is called a (2+1) process. Absorption of a fourth photon by the parent ion at high optical power then leads to the photochemical production of the fragment ions CH_3CO^+ and HCO^+. The first of these fragments can absorb a fifth photon and dissociates to CH_4^+, CH_3^+, and CH_2^+. Among these, CH_4^+ can be further photolyzed to produce CH_3^+ and CH_2^+, while CH_2^+ can be photolyzed to yield CH^+. Each of the ionic species listed above is produced with its own characteristic power index. The total-ion power index as conventionally determined using an ionization cell is thus a complex average of these indices and has no meaning by itself, except at very low optical power where only the parent ion is formed.

When excited at 2485 Å, the acetaldehyde excitation is one-photon resonant with the smooth, continuous high-frequency wing of the n -> π* valence transition, and by Point 6, it then follows that the nonlinear photochemistry in this region will be Class B, as observed [9].

The MPI spectrum and photochemistry of $Cr(CO)_6$ in the 4000-5000 Å region [10-12] stand in strong contrast to those of acetaldehyde discussed above. The one-photon spectrum of $Cr(CO)_6$ is broad and continuous at all wavelengths shorter

than 3500 Å (Point 6), whereas the MPI resonances in this molecule are atomically sharp and plentiful. These resonances are found in the MPI spectra at identical wavelengths regardless of which Cr compound is irradiated (Point 3), and moreover, the MPI-driven mass spectrum of $Cr(CO)_6$ reveals only a single ion, i.e., Cr^+ (Point 2). This latter observation stands in strong contrast to the conventional situation in which the mass spectrum is generated by electron impact, for in this case over a dozen ions are observed, from $Cr(CO)_6^+$ to Cr^+ [13]. Kinetic-energy analysis of the MPI-ejected electrons shows that in $Cr(CO)_6$ they originate in the ground and excited states of the Cr atom (Point 8). Finally, at low power, a power index of 5-6 is observed, although only 3 photons are required to ionize $Cr(CO)_6$ itself (Point 5). Clearly $Cr(CO)_6$ in this region is exhibiting Class B behavior.

To summarize the situation in $Cr(CO)_6$, the first two photons are coherently absorbed to excite the molecule in the broad-band region. This results in immediate dissociation to $Cr(CO)_5$, which then absorbs another two photons [probably incoherently, i.e., (1+1)] and dissociates to produce Cr(I) in its ground and excited states. These molecular absorptions are most likely valence shell metal <-> ligand charge-transfer promotions. The Cr(I) atom then undergoes (2+1) excitations to form Cr^+. Though more than enough energy is supplied in this seven-photon excitation to form $Cr(CO)_6^+$, this ion is not observed.

OTHER SYSTEMS

The techniques and criteria described above for acetaldehyde and chromium hexacarbonyl have been applied to a large number of other organic, inorganic and organometallic systems. The results of some of these studies are summarized very briefly below.

Divalent Mercury

Divalent mercury systems are interesting because they show both Class A and Class B behavior. We have studied the MPI processes in HgY_2, where Y = CH_3, Cl, Br, and I. As already reported [14], the MPI spectrum of $Hg(CH_3)_2$ in the one-photon region 4000-3550 Å displays very sharp two-photon molecular resonance features, which place it in Class A by Point 3. In accord with this, the MPI mass spectrum of $Hg(CH_3)_2$ is rich in parent ion at low power (Point 2), the power index at low power is 3.0, Fig. 3 (Point 5), the one-photon absorption in the 2000-1800 Å region is sharp (Point 6), and no Hg atomic lines are seen in the MPI spectrum (Point 3). The two-photon excitation in question in $Hg(CH_3)_2$ involves the promotion of a Hg-C σ-bonding electron into a spin-orbit component of the 6pπ Rydberg orbital (Point 10). At low power in $Hg(CH_3)_2$, one has a straightforward (2+1) molecular ionization in a Class A system.

By contrast, in the mercury halides, the lowest one-photon excitation is to an A-state, in which a halogen

lone-pair electron is promoted into the Hg-X σ^* MO. This excitation is valence shell (Point 10) and is totally structureless in the one-photon spectrum (Point 6), thus leading one to expect Class B photochemical behavior. Indeed, the MPI spectra of the mercury halides are rich in Class B Hg-atom transitions (Point 3). Note however, that these originate at atomic levels between 37,645 and 54,069 cm^{-1} above the $^1S_0$ ground state of Hg(I); moreover, three-photon resonances in atomic mercury vapor are seen in just this spectral region, originating at the $^1S_0$ ground state [14], but these are not observed when $HgBr_2$ serves as the source of Hg(I). Thus the multiphoton dissociation of $HgBr_2$ in the 4300-3550 Å region yields only excited Hg(I) atoms. Many of the MPI lines originate at $^1P_1$ which is 54,069 cm^{-1} above the ground state [15]. Ionization of resonances originating at this state are then (1+1) processes.

Two-photon excitation of $HgBr_2$ using a fundamental wavelength in the vicinity of 4400 Å should populate the A state; X -> A is a transition with a continuous band shape. According to calculations by Wadt [16], the X -> A promotion is immediately followed by dissociation into two Br atoms and the Hg atom in its ground state. Thus Hg-atom MPI resonances resulting from A-band resonance and dissociation should originate at the $^1S_0$ ground state. This is contrary to our findings.

Note however, that Wadt's assignment of the A band

($^1\Sigma_g^+ \rightarrow {}^3\Pi_u$) is to that one state which is one-photon allowed of five predicted in this region. Our experiment involves a two-photon excitation however, which must be $^1\Sigma_g^+ \rightarrow {}^{1,3}\Pi_g$ (via an intermediate Π_u level); according to Wadt's calculation, these Π_g states relax to X atoms and the stable ground state of HgX. We presume then that the HgBr(X) next is promoted in a two-photon process to unbound levels which yield excited-state Hg atoms.

The strong contrast between the nonlinear photochemistries of $Hg(CH_3)_2$ and HgX_2 can be traced directly to the different orbital natures of the resonance states, and the chemistry that then flows from them. In the case of $Hg(CH_3)_2$, the resonance state is Rydberg and stable, whereas in HgX_2, it is valence shell and unstable (Point 10).

Tetravalent Tin

The large differences in the photochemistries of $Hg(CH_3)_2$ and HgX_2 led us to investigate a similar pair, $Sn(CH_3)_4$ and $SnCl_4$. The first one-photon electronic transition in $SnCl_4$ [17] is found centered at 2000 Å (50,000 cm^{-1}), with a perfectly smooth, symmetric vibronic profile. Compared to the $SnCl_4$ ionization potential of 97,500 cm^{-1}, the frequency of the 50,000 cm^{-1} band is far too low for it to be a Rydberg excitation, and consequently it has been assigned as valence shell [18]. It is most likely an A-band transition (chlorine 3p -> σ^*), similar to those in HgX_2 in the same region. According to Points 6 and 10, the MPI of

$SnCl_4$ should show Class B nonlinear photochemistry in the laser pulse.

The lowest band in the $Sn(CH_3)_4$ electronic spectrum has been described as a continuum extending from 2100 to 2600 Å [19]. Nothing else is known of this molecule's electronic spectrum. It would seem that on the basis of Point 6, $Sn(CH_3)_4$ is also Class B, in contrast to $Hg(CH_3)_2$.

The MPI resonances in $Sn(CH_3)_4$ consist of a very large number of lines, extending from 4100 Å down to 3587 Å. Many, but not all of these lines are assignable as two-photon resonances in the tin atom, originating at the $^3P_0$ ground state and at the $^3P_1$, $^3P_2$ and $^1D_2$ excited states. A large number of other equally sharp and prominent lines also are observed, but could not be assigned under any assumptions as either Sn(I) or Sn(II) transitions according to the levels listed in reference [15]. Though the two-photon region spanned by 4100 - 3587 Å in one photon is beyond the continuum absorption described for $Sn(CH_3)_4$, there is little doubt that we are exciting into a second dissociative continuum above it, and that this leads to Class B photochemistry in this molecule.

We have measured the power exponent for ionization of $Sn(CH_3)_4$ at 3805 Å, and find 5.5 ± 0.6 from the data at the lowest measurable powers. The difference between the measured power index of 5.5 and the anticipated value of 6.0 can

be attributed to the action of the AC Stark effect (Point 5). A power index of 5.5 is equivalent to 18 eV at 3805 Å, which clearly indicates that a large part of the overall photon energy (even at low optical power) is being used to break bonds in molecular species leading to ionic species.

The obvious production of Sn atoms in the laser photolysis of $Sn(CH_3)_4$, implies the presence as well of methyl-radical resonances in the MPI spectrum of this compound. As described in another paper [20], such methyl group two-photon resonances have been assigned to two broad features observed at 67,820 and 67,990 cm^{-1} in $Sn(CH_3)_4$.

MPI mass spectrometric measurements on $Sn(CH_3)_4$ are totally in line with the characteristics of Class B non-linear photochemistry. Thus we have excited several of the MPI resonance lines of $Sn(CH_3)_4$ within a TOF mass spectrometer and observed only Sn^+ at all optical powers, as expected for a Class B system (Point 2). In contrast, the ions $Sn(CH_3)^+_{4-x}$ are found in the electron impact mass spectrum of $Sn(CH_3)_4$, with x running from 0 to 4 [21].

A brief study of $SnCl_4$ quickly confirms our expectation that it will show Class B photochemistry. This expectation is based upon the continuous nature of its absorption bands (Point 6), the valence nature of its resonance state (Point 10), and upon its energy-level diagram, which looks much like that of $Sn(CH_3)_4$ with two fragmented configurations below the resonance state (Point 7). The MPI spectrum of

$SnCl_4$ shows all of the Sn(I) resonance lines observed for $Sn(CH_3)_4$ (Point 3). There are no chlorine-atom resonances in our spectral region. The ions resulting from 3550-Å irradiation of $SnCl_4$ within the mass spectrometer proved to be 80% Sn^+, 20% $SnCl^+$ and less than 1% $SnCl_2^+$. In the electron-impact (31 eV) mass spectrum of $SnCl_4$ [22], $SnCl_3^+$ is the major ion with all others at about 1/5 its intensity, while with an electron-impact energy equal to the ionization threshold, $SnCl_4^+$ is predominant.

Methyl Iodide

Methyl iodide is a hybrid system in the sense that it is clearly Class A in one spectral region, but Class B in another. This follows naturally from Points 6 and 10 in Table I, for the one-photon spectrum of methyl iodide in the region 3600-2100 Å is continuous, corresponding to an $\underline{n} \rightarrow \sigma^*$ A-band valence shell excitation, whereas the second excitation beginning at 1950 Å is an $\underline{n} \rightarrow 6s$ Rydberg transition which is quite sharply structured [23]. Thus resonance in the first of these should give Class B behavior while resonances in the second will behave as Class A.

Excitations which are one-photon resonant in the A-band of methyl iodide yield CH_3 and I fragments with near-unit quantum yield, with the I atoms in either the $^2P_{3/2}$ or $^2P_{1/2}$ state. Accordingly, when irradiated at wavelengths shorter than 3100 Å, MPI atomic resonances are observed to originate

from these two states of the iodine atom, as expected for Class B behavior. Resonance features are also observed for the methyl radical [20]. On the other hand, pumping at 4000-3300 Å sidesteps the $\underline{n} \rightarrow \sigma^*$ resonance, but two-photon excites the $\underline{n} \rightarrow$ 6s and $\underline{n} \rightarrow$ 6p molecular levels. Consequently, only the CH_3I^- molecular Rydberg resonances are observed [20,24]. The mass spectrum in this region shows a strong parent-ion peak (Point 2), together with I^+ and CH_3^+ which must come from photodissociation of the parent ion which is one-photon resonant in this wavelength region. Further, the thresholds for the production of CH_3^+ and I^+ from CH_3I^+ are exceeded by a one-photon absorption in the parent ion.

The Class A-to-Class B shift of nonlinear photochemistry displayed by methyl iodide is due to a change of resonance state on scanning though the UV/visible region, i.e., from $(5p,\sigma^*)$ valence shell to (5p,6s) Rydberg. A somewhat similar change is observed in NO_2 [25], where a shift from Class A to Class B behavior is encountered upon exceeding the disscoiation wavelength (4000 Å) of the valence excitation in the visible region.

ACKNOWLEDGEMENTS

I wish to acknowledge helpful conversations with A. Gedanken, N. A. Kuebler, G. J. Fisanick, William Wadt and T. Bowmer.

References

[1] P. M. Johnson, Accts. Chem. Research 13, 20 (1980).

[2] D. A. Lichtin, L. Zandee and R. B. Bernstein, in "Lasers and Chemical Analysis," G. M. Hieftje, F. E. Lytle and J. C. Travis, Eds., Humana Press, Clifton, N.J., 1980, p.1.

[3] C. Klimcak and J. Wessel, Appld. Phys. Lett. 37, 138 (1980).

[4] V. S. Antonov, V. S. Letokhov and A. N. Shibanov, Optics Commun. 38, 182 (19819.

[5] A. diagram of this sort also has been presented by V. S. Antonov and V. S. Letokhov, Appld. Phys. 24, 89 (1981).

[6] G. J. Fisnaick, T. S. Eichelberger, IV, B. A. Heath and M. B. Robin, J. Chem. Phys. 72, 5571 (1980).

[7] B. A. Heath, M. B. Robin, N. A. Kuebler, G. J. Fisanick, and T. S. Eichelberger, IV, J. Chem. Phys. 72, 5565 (1980).

[8] T. S. Eichelberger, IV, and G. J. Fisanick, J. Chem. Phys. 74, 5962 (1981).

[9] J. P. Riley and K. L. Kompa, Adv. Mass Spectrom. 8B, 1800 (1980).

[10] D. P. Gerrity, L. J. Rothberg, and V. Vaida, Chem. Phys. Lett. 74, 1 (1980).

[11] G. J. Fisanick, A. Gedanken, T. S. Eichelberger, IV, N. A. Kuebler, and M. B. Robin, J. Chem. Phys. 75, 5215 (1981).

[12] M. A. Duncan, T. G. Dietz, and R. E. Smalley, Chem. Phys. 44, 415 (1979).

[13] G. A. Junk and H. J. Svec, Z. Naturforsch. 23b, 1 (1968).

[14] A. Gedanken, M. B. Robin, and N. A. Kuebler, Inorg. Chem. 20, 3340 (1981).

[15] C. E. Moore, "Atomic Energy Levels," Vol. III. National Bureau of Standards Circular 467, 1958.

[16] W. R. Wadt, J. Chem. Phys. 72, 2469 (1980).

[17] W. R. Wadt, Appld. Phys. Lett. 34, 658 (1979).

[18] M. B. Robin, "Higher Excited States of Polyatomic Molecules," Vol. I, Academic Press, New York, 1974; Vol. II, Academic Press, New York, 1975.

[19] H. W. Thompson and J. W. Linnett, Proc. Roy. Soc. London 156A, 108 (1936).

[20] A. Gedanken and M. B. Robin, J. Chem. Phys. 76, 4798 (1982).

[21] J. J. de Ridder and G. Dijkstra, Recueil 86, 737 (1967).

[22] A. S. Buchanan, D. J. Knowles, and D. L. Swingler, J. Phys. Chem. 73, 4394 (1969).

[23] R. A. Boschi and D. R. Salahub, Mol. Phys. 24, 289 (1972).

[24] D. H. Parker, R. Pandolfi, P. R. Stannard, and M. A. El-Sayed, Chem. Phys. 45, 27 (1980).

[25] M. B. Robin, Appld. Optics 19, 3941 (1980).

Figure Captions

Fig. 1. Experimental setup for MPI spectroscopy. A, pump laser; B, dye laser; C, focusing lens; D, glass ionization cell with quartz windows; E, regulated voltage supply; F, electrometer; G, recorder.

Fig. 2. The three paths of photochemical behavior under multiphoton excitation. Vibrational structure in the resonance state may be either discrete (left-hand side, Class A behavior), or continuous (right-hand side, Class B behavior).

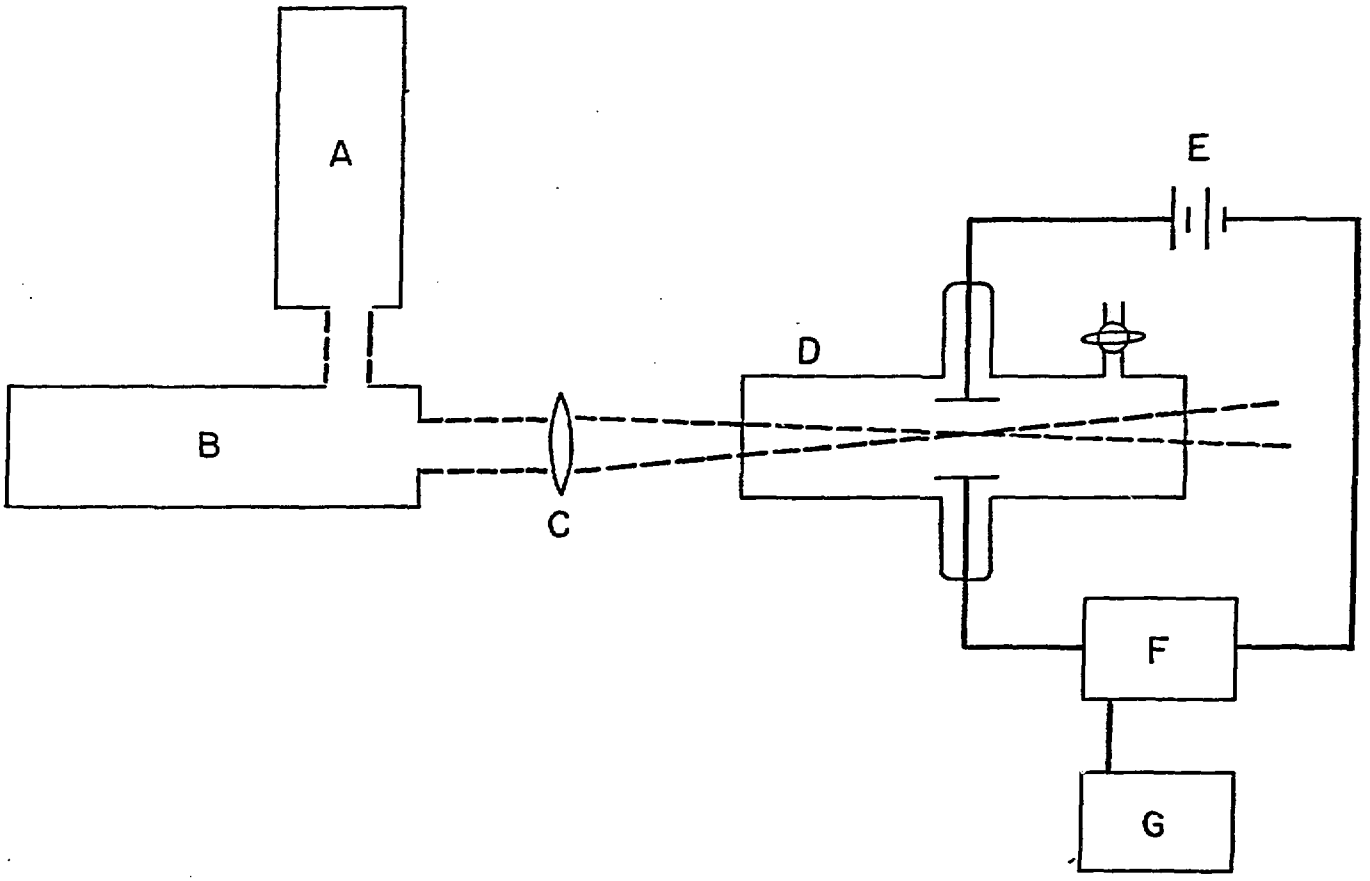

Fig. 1

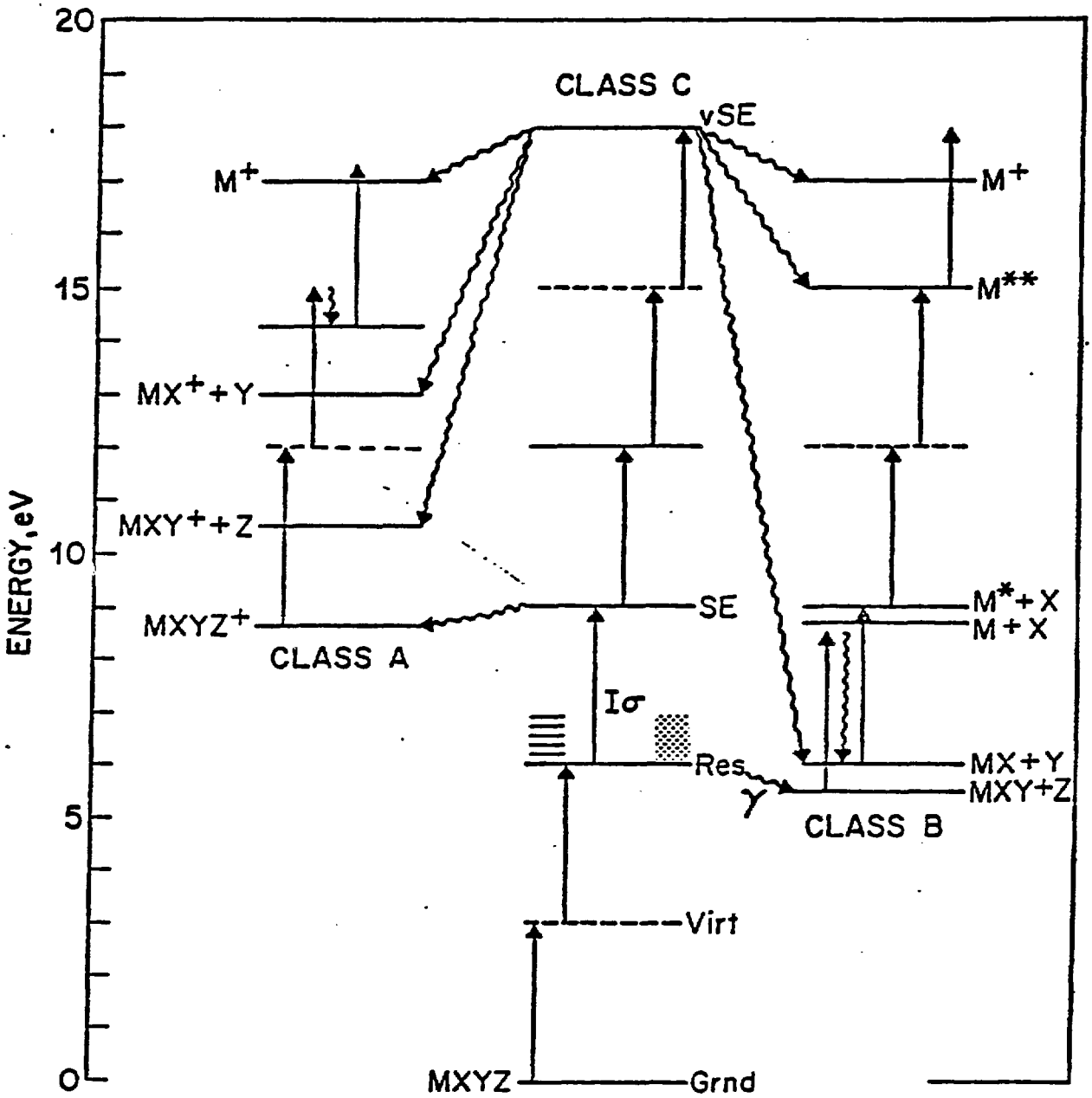
20
15
10
5
0
ENERGY, eV
CLASS C
vSE
M+
M+
M**
MX+ + Y
MXY+ + Z
MXYZ+
CLASS A
SE
M* + X
M + X
Iσ
Res
MX + Y
MXY+Z
γ
CLASS B
Virt
MXYZ
Grnd

Figure 2

Table I . Characteristics of Molecular Systems undergoing Multiphoton Ionization

Class A	Class B	Class C
1. System is ionized, then atomized	1. System is atomized, then ionized	1. System is atomized and ionized simultaneously
2. Produces $MXYz^+$ at low power, giving way to MXY^+, MX^+, and finally M^+ at high power	2. Produces only M^+ at all powers	2. Produces constant ratios of various ions at all powers
3. MPI shows molecular resonances characteristic of target molecule	3. MPI shows atomic resonances independent of target molecule	3. Shows no resonances
4. MPI resonances originate at ground state only	4. MPI resonances originate at ground and also at excited states	4. Shows no resonances
5. Low-power index = IP/hν	5. Low-power index >> IP/hν[a]	5. Power index >> IP/hν at all powers
6. One-photon spectrum to resonance state is discrete	6. One-photon spectrum to resonance state is continuous	6. One-photon spectrum is irrelevant
7. Total energy of the fragments lies above the resonance state	7. Total energy of the fragments lies below the resonance state	7. Total energy of the fragments lies below the final state
8. Ejected electron K. E. results from molecular ionization process; K. E. < hν	8. Ejected electron K. E. results from atomic ionization process; K. E. < hν	8. Ejected electron K. E. results from molecular ionization process; K. E. >> hν
9. At very high power, the course of ionization is unchanged	9. At very high power, Class B may become Class A[b]	9. Products independent of power
10. Molecular resonance always Rydberg	10. Molecular resonance valence shell, or infrequently Rydberg	10. Molecular resonances irrelevant

---

[a] The power index is larger by 1 in a Class B' system than it would be if the same system behaved as Class B.

[b] Class B' cannot be converted to Class A at high power.

MULTIPHOTON IONIZATION AND THIRD-HARMONIC GENERATION IN ATOMS AND MOLECULES*

John C. Miller and R. N. Compton

Chemical Physics Section, Health and Safety Research Division
Oak Ridge National Laboratory, Oak Ridge, Tennessee 37830 U.S.A.

Abstract

We will discuss recent experiments on multiphoton ionization and third-harmonic generation in rare gases and small molecules using focused laser power densities of 10^9 to 10^{11} W/cm^2. Also, some elementary experiments using vacuum ultraviolet light generated by frequency tripling in xenon and krypton will be described. These experiments include absorption and ionization studies using vacuum ultraviolet radiation as well as two-photon ionization using one vacuum ultraviolet photon and one laser photon.

Introduction

The recent invention and development of the pulsed, high-powered, tunable dye laser is allowing physicists and chemists to discover many new nonlinear optical effects in the interaction of electromagnetic radiation with gaseous atoms and molecules. The extreme intensity of such light sources allows one to study a multitude of multiphoton phenomena. Also, the fact that the source is tunable means that very high densities of excited state target species can be produced leading to collective excitation phenomena. For example, so-called "energy pooling" effects have been observed in alkali excitation studies.[1] It is now possible to perform experiments in which the laser field alters a chemical reaction or makes the reaction energetically possible. These studies fall under the general heading of "Collisions in the Field of a Laser" and are in the early stages of development. There is some promise that one can study the transition state of a chemical reaction (i.e., the laser could take a "snapshot" of the fleeting transition state).

The use of tunable dye lasers to produce resonantly enhanced multiphoton ionization (REMPI) provides a powerful new method for investigating atomic and molecular energy levels. Recent reviews[2,3] and a paper[4] contain references to work in this rapidly growing field of spectroscopy. The method is particularly useful in discovering and characterizing certain optically forbidden transitions. For example, new electronic states have been observed in iodine,[5] benzene,[6] and ammonia[7] using the REMPI technique. The method is particularly well suited for studying Rydberg transitions in molecules and is experimentally easier than the traditional use of far ultraviolet radiation in conventional spectroscopy. In addition, the use of two or more tunable dye lasers to produce sequential REMPI spectra has significant advantages in signal intensity, spectral simplification, and the ability to probe different Franck-Condon regions of a molecule.[8] In the case where two resonant states are excited the technique carries the nomeclature optical-optical double resonance (OODR).

The addition of mass spectroscopy to studies of multiphoton ionization (MPI) of polyatomic molecules has shown that considerable fragmentation can accompany ionization. In particular, REMPI of benzene can lead to extensive fragmentation, with C^+ being the dominant ion, while little or no parent ion is observed.[4,9,10] Although at least six photons are energetically required to produce C^+ from C_6H_6, the reported power indices range from 2 to 3.5.* The degree of fragmentation is independent of wavelength for benzene; however, for other polyatomics (pyrrole and furan)[10] the degree of fragmentation is highly dependent upon the wavelength (resonant intermediate state). In some regions of the spectrum the parent ion dominates.

Two mechanisms have been invoked to rationalize the production of small fragment ions from benzene and other molecules. In the first, multiple absorption of photons via neutral valence, Rydberg, and autoionizing states leads to superexcited states which subsequently autoionize and dissociate to produce the observed fragmentation. The second mechanism assumes that the parent ion is initially produced by MPI, and then absorbs further photons to reach dissociative or predissociative ionic states. Evidence that fragmentation occurs via absorption in the parent ion for benzene comes from the two-laser experiments of Beosl et al.[9] and the nonresonant MPI photoelectron spectra of Meek et al.[11] as well as the Oak Ridge National Laboratory (ORNL) experiments to be discussed below. Conversely,

*Research sponsored by the Office of Health and Environmental Research, U.S. Department of Energy under contract W-7405-eng-26 with the Union Carbide Corporation.

By acceptance of this article, the publisher or recipient acknowledges the U.S. Government's right to retain a nonexclusive, royalty free license in and to any copyright covering the article.

two-laser experiments on azulene[11] indicate that fragmentation results from photoabsorption through autoionizing states. Several theoretical treatments of MPI fragmentation based upon statistical phase-space models have recently appeared.[13,14,15] Recent measurements of photoelectron and ion kinetic energy distributions at ORNL provide direct answers to the above questions and will be discussed below.

The interpretation of multiphoton studies in gases at high pressure (>1 torr) are complicated by the detection techniques, collisional effects, and the possibility of many body or collective phenomena. Payne, Garrett, and Baker[16] recently invoked a collective emission phenomenon to explain some very surprising experimental data in the five-photon ionization of gaseous xenon. In these experiments,[25] it was found that MPI and third-harmonic generation (THG) were competing processes and that THG could completely quench the MPI signal at pressures above 0.3 torr. More details will be given later.

Experimental

Our studies of MPI and THG have been performed at pressures above and below 10^{-3} torr in two different experimental arrangements. Figures 1 and 2 show the low- and high-pressure experiments, respectively. Two different lasers have been used in the studies described below: (1) nitrogen pumped dye laser [Molectron UV24 (1 MW) and DL400] and (2) excimer pumped dye laser [Lambda Physik EM6101 and FL2000]. In Fig. 1 the polarization of the laser beam is in the direction of the energy analyzer.

Low Pressure Results

The low-pressure experiment is used to study mass-resolved MPI spectroscopy and to determine the MPI photoelectron and photoion kinetic energy distributions. The ionic masses are determined by observing their time-of-flight up the stack of electrodes shown in Fig. 1. The ion and electron kinetic energies are determined with a 160° spherical sector energy analyzer. It is also possible to determine both mass spectra and kinetic energy simultaneously and to perform coincidence studies in which electron counts can trigger a multichannel analyzer to record the mass corresponding to that electron. Such studies are in progress. Resonantly enhanced multiphoton ionization photoelectron spectra (MPI-PES) have been recorded for Xe,[17] I_2,[18] NO,[19] NH_3,[20] H_2S,[21] CH_3I (unpublished) and C_6H_6.[18] Such a spectrum is shown for xenon in Fig. 3 in which the excimer pumped dye laser is tuned to the $6s[3/2]^o_{J=1}$ state. This data is of somewhat higher resolution but

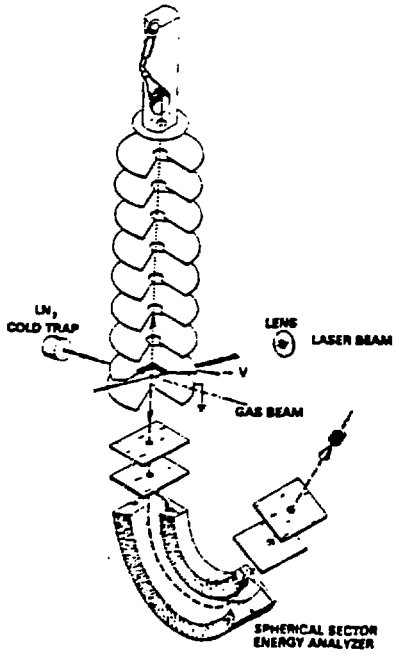

Fig. 1. Schematic diagram of the multiphoton ionization mass spectrometer and photoelectron energy analysis apparatus. (ORNL Dwg 79-14575)

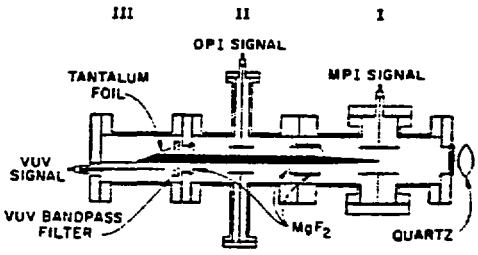

Fig. 2. Schematic diagram of the apparatus used for studies of one-photon absorption and ionization and of two-photon ionization using third-harmonic generation in rare gases. Chamber I is the frequency tripling cell, chamber II is the ionization or absorption cell, and chamber III is a vacuum ultraviolet light detector. Each chamber functions as a proportional counter for detecting electrons. See text for details. Chamber I also functions as a cell for conventional multiphoton ionization studies. (ORNL Dwg 81-10035)

qualitatively the same as that published earlier.[18] The higher resolution in this data is attributed to three factors: (1) lower operating pressure due to the higher power of the laser, (2) reduced RF noise on the analyzer itself, and (3) a digital data acquisition system which allows detection of a very low ion density in the focal region thus reducing the energy spread due to space charge. The interesting point to note for xenon is that MPI results in leaving Xe^+ in both possible fine-structure states despite the fact that enhancement occurs through $[5/2]J=1$ core excitation. MPI-PES contain a great deal of information about the resonant intermediate states as well as the pathways of ion fragmentation. In a recent study of NO,[20] where fragmentation did not occur, we showed that the distribution of NO^+ vibrational levels was determined primarily by the Franck-Condon factors connecting the resonant intermediate ($A^2\Sigma^+$ and $C^2\pi$) states and the $X^1\Sigma^+$ ionic state. Figure 4 shows the MPI-PES data for the case in which two photons are resonant with the v=1 level of the $A^2\Sigma^+$ state using the higher quality data from the excimer pumped dye laser. The intense peak at high energy corresponds to leaving the ion also in v=1 which is expected from Franck-Condon considerations (the $A^2\Sigma^+$ state is a Rydberg state converging upon the $X^1\Sigma^+$ ionic ground state). We also note weaker photoelectron peaks corresponding to leaving the ion in v=2,3,4 etc. The MPI-PES data for other vibrational levels of the A state show the same trend.

Without going into great detail, we attribute the zero energy peak to the fact that two additional photons are required to ionize the resonant intermediate state. Resonances or near resonances in the third-photon region can allow access to different autoionizing states than a direct two-photon ionization from the A state. In particular, vibrational autoionization (not possible from the A state) can lead to a single peak of slow electrons. The large zero energy peak is therefore attributed to vibrational autoionization from electronic states resulting from transitions involving the three-photon excited states. Zero-energy electrons are not observed when the laser is tuned to the $C^2\pi$ state since the third photon is capable of ionization.

Iodine, ammonia, and hydrogen sulfide are three simple systems which show intense fragment ions resulting from MPI. In each case, the photoelectron spectrum shows directly that the initial ionization step results in the formation of the parent ion, I_2^+, NH_3^+, and H_2S^+. The fragment ions must be produced from the further absorption of photons by the parent ion. Furthermore, in the case of I_2, we were able to measure the kinetic energy of the I^+ ion[19] which corresponded to the reaction $h\nu+I_2^+ \rightarrow I^+ + I$.

For the larger polyatomics the ion kinetic energies could not provide direct evidence for this model. However, in the case of NH_3 it was possible to show that the extensive fragmentation was due to photon absorption into the first excited state of NH_3^+ which is dissociative. This is shown in Fig. 5 where we have plotted the percent of fragment ions as a function of excess internal energy above the ground state of the ion. The data points represent fragment percentages for up to eight vibrational levels of five different electronic intermediate states. The energy onset for fragmentation corresponds exactly with the onset of the first excited state of NH_3^+ as shown in the one-photon photoelectron spectrum. The photoelectron spectra of the two larger molecules studied at ORNL, CH_3I and benzene, also show that fragmentation follows creation of the parent ion. A major

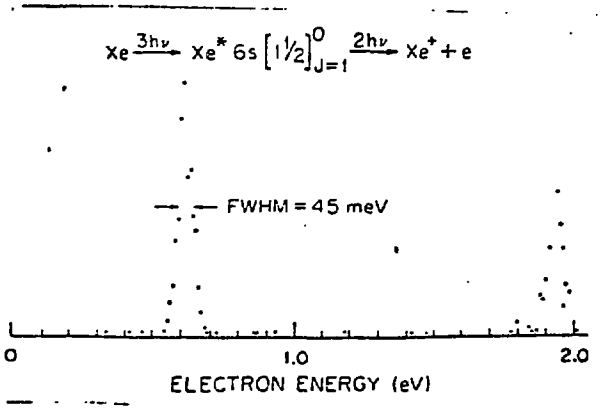

Fig. 3. Three-photon resonant, five-photon ionization photoelectron spectrum of xenon. The two peaks correspond to leaving the Xe^+ in the $^2P_{3/2}$, $^2P_{1/2}$ final states. (ORNL Dwg. 81-23083)

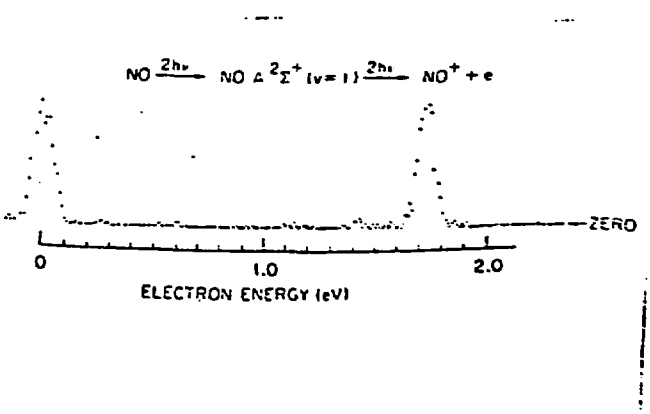

Fig. 4. Resonantly enhanced multiphoton ionization photoelectron spectrum for four-photon ionization resonant with the v=1 vibrational level of the $A^2\Sigma^+$ state of NO. (ORNL Dwg. 81-23084)

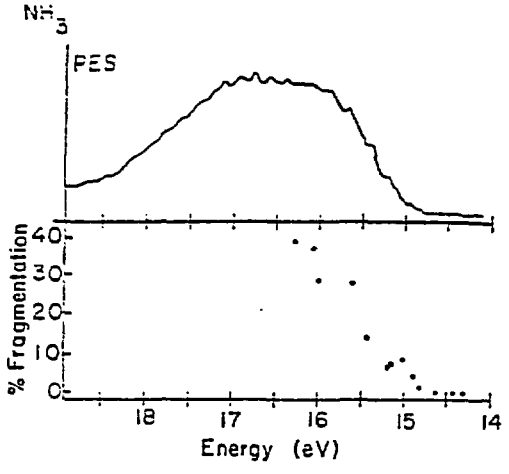

Fig. 5. The photoelectron spectrum of the $(\ldots 1e^3 3a_1^2)\,^2E \leftarrow (\ldots 1e^4 3a_1^2)\,^1A_1$ transition ($NH_3^+ \tilde{A} \leftarrow \tilde{X}$) of ammonia (upper panel), and the extent of fragmentation following multiphoton ionization for fixed laser power (lower panel). The percent fragmentation is plotted vs five times the incident photon energy so that the two energy scales coincide. [Adapted from M. J. Weiss and G. M. Lawrence, J. Chem. Phys. 53, 214 (1970).]

conclusion of our MPI-PES studies is that in every case studied thus far the fragmentation is due to absorption in the ionic manifold. No evidence for absorption in the autoionization manifold has been observed in any molecule but NO where a minor ionization pathway involves absorption of one photon from an autoionizing state. The detailed physics of the ionic photodissociation processes is still under investigation.

High Pressure Results

Multiphoton ionization studies at high pressures can lead to new and interesting effects, some of which were mentioned in the introduction. We will discuss below our studies of high-pressure MPI in light of possible effects of THG in the rare gases Ar, Kr, and Xe. Aron and Johnson[22] reported the first REMPI spectrum of xenon at pressures ranging from 1 to 100 torr. They noted the complete absence of any ionization signal when tuning through the $6s[3/2]^0_{J=1}$ three-photon-allowed intermediate state. At low pressure (10^{-6} torr), we found that MPI through the 6s state was very intense and dominated the spectrum.[18] In a later publication,[23] we further showed that for a laser beam focused by a 3.8 cm lens to a power density of $\sim 5 \times 10^9$ W/cm^2, the ionization signal produced via the 6s state rapidly disappeared at pressures above ~0.3 torr. Third-harmonic generated light in the direction of the pump beam was detected as the ionization disappeared. The excitation lineshape of both the MPI and THG signals were similar and were found to shift and broaden asymmetrically to shorter wavelength as the pressure was increased. Although the intensities of the ionization and third-harmonic light is entirely relative, the dramatic decrease of ionization with increase in THG suggested that the two processes were interfering or in "competition." The THG light is expected in any negatively dispersing medium and the excitation lineshape is expected to shift to shorter wavelengths as the pressure increases due to phase matching considerations. For wavelengths far off resonance, the normal theory for THG involving the nonlinear susceptibility (X_3) applies. The broadening and shifting of the MPI lineshape along with the quenching of the MPI signal are not easily rationalized in terms of our present understanding of such phenomena. In a recent theoretical study of these results, Payne et al.[16] found it necessary to include terms involving the coherent, collective excitation of xenon atoms. These terms result in greatly enhanced THG near odd-photon resonances with concomitant, very rapid depletion of the resonant population.

Multiphoton ionization and third-harmonic generation near the $6s'[1/2]_{J=1}$ resonance in xenon shows similar behavior to that of the $6s[3/2]_{J=1}$ state discussed above. Differences in the two sets of data are shown for pressures from 0.5 to 25 torr in Fig. 6 and at higher pressures (50 to 310 torr) in Fig. 7. The ionization signal is seen to broaden and shift at low pressures similar to that near the $6s[3/2]_{J=1}$ region. The ionization signal does not disappear however. Also molecular effects (Xe_2) are seen in the high pressure data (Fig. 7). It is important to note that only four photons are required to ionize xenon in this wavelength region and this may account for the fact that the nonresonant ionization signal does not disappear.

The ionization signal which is observed to broaden and shift in both the wavelength regions near the 6s and 6s' resonant intermediate states can be ascribed to MPI using one third-harmonic photon plus two- or one-laser photons, respectively. The fact that both the MPI and THG signal have identical lineshapes at low pressures strongly supports this hypothesis. However, it does not explain the absence of signal at the resonance line position. This would require some other quenching mechanism.

At the present time, new experiments using the higher power of the excimer laser are underway to test the above models of MPI at high pressure. Such experiments will include unfocused laser MPI, polarization experiments, focal length dependences, and two-color laser experiments.

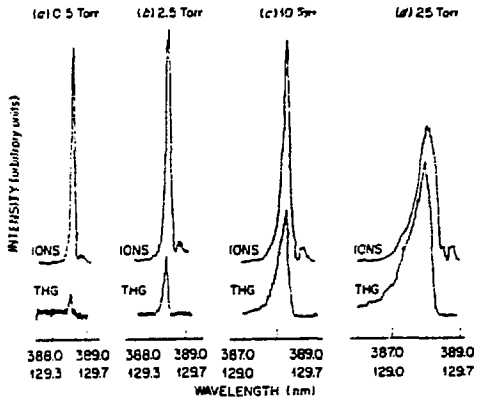

Fig. 6. The multiphoton ionization spectra and third-harmonic generation lineshapes near the 6s' resonance in xenon recorded at various pressures from 0.5 to 25 torr. The upper wavelength scale corresponds to the laser and the lower scale to the third-harmonic generation (one-third of the laser wavelength). (ORNL Dwg 81-18464)

Studies Using Third-Harmonic Light

The third-harmonic light generated in the experiments described above is sufficiently intense to be useful in spectroscopic studies of gaseous species in the near vacuum ultraviolet (VUV) region (100-200 nm). The 200-100 nm spectral region is especially important as the ionization potential (IP) of most atoms lies between 6.2 and 12.4 eV. Although the spectroscopy of the lowest-lying states of most atoms and molecules is studied in the visible and near UV regions, most Rydberg states lie in the VUV. Due to the difficulty of obtaining and using VUV light, photoionization and Rydberg absorption studies have not been as frequent or as detailed as corresponding studies in the visible and near UV.

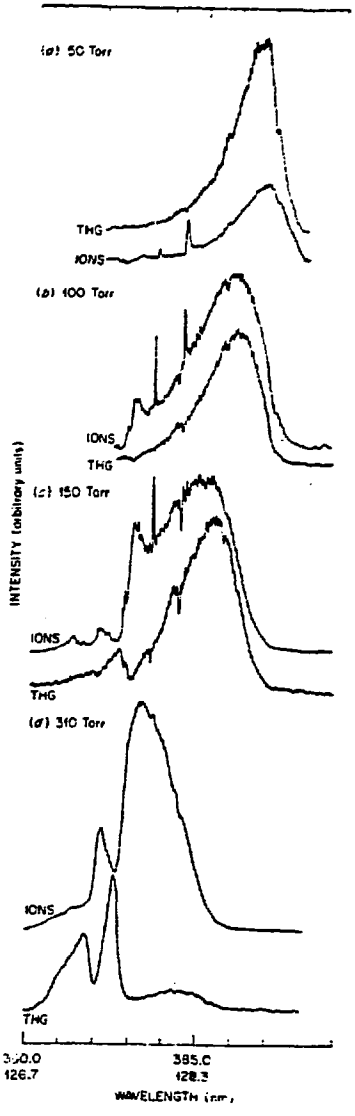

Fig. 7. The multiphoton ionization spectra and third-harmonic generation lineshapes near the 6s' resonance in xenon recorded at various pressures from 50 to 310 torr. The upper wavelength scale corresponds to the laser and the lower scale to the third-harmonic generation (one-third of the laser wavelength). (ORNL Dwg 81-18463)

The traditional source of tunable photons in the VUV region has been the rare gas or hydrogen discharge lamp coupled with a vacuum monochromator. More recently, synchrotron sources have provided relatively more intense, continuum VUV light which also requires a monochromator for high resolution. Currently, there is intense interest in developing laser-based sources of VUV light. The aim is to extend to this region the unique laser properties such as high intensity, very narrow bandwidth, spatial and temporal coherence, and short pulse times. These factors along with the extensive tunability of dye lasers have already revolutionized the fields of atomic and molecular structure, spectroscopy, and photophysics.

The range of tunable laser sources has been extended through the near UV by exploiting the nonlinear response of certain crystals to frequency double or triple visible dye laser radiation. Spectroscopic studies from 217-360 nm are now routine.

Further extension of tunable coherent light sources into the VUV, however, poses considerable problems as frequency conversion crystals become opaque in this region. For THG into the VUV, the rare gases have most often been used as the nonlinear medium.[23-40] These studies of THG in krypton and xenon have characterized the properties of the nonlinear process, mostly with the aim of producing a bright source at the Lyman α and β lines for

hydrogen detection schemes.[27,28,31,32,35,36] In addition, fifth- and seventh-order frequency conversion has been reported in helium and neon at much shorter wavelength.[41] Also, several excimer laser lines have been tripled in the rare gases.[33,34,37] These studies have demonstrated tunable THG in xenon in the range of 140.3-146.9 nm and 125.0-129.6 nm in krypton and 120.3-123.6 nm and 110.0-116.5 nm with conversion efficiencies of 10^{-5}-10^{-6} and fluxes in the range of 10^{7}-10^{10} photons/pulse.[25-40] The output power, linewidth, and tuning range are, of course, dependent on the properties of the laser supplying the fundamental frequencies.

In contrast to the many studies involving generation of THG, there have been only a few involving the use of tunable VUV as a spectroscopic tool. Wallenstein et al.[32,39] have traced the Lyman-α absorption of H and D atoms and a fluorescence excitation band of CO using THG in krypton and argon generated with a Nd:Yag pumped dye laser system. Egger et al.[37] and Rothschild et al.[42,43] in an elegant series of experiments have performed very high resolution studies of H_2 and D_2 Rydberg states in the XUV near 83 nm. These experiments used xenon to triple the frequency of a high resolution KrF laser system. Zacharias et al.[44,45] have studied resonant two-photon ionization of H and D atoms and of CO in a mass spectrometer where the VUV photon was produced by THG in krypton using a Nd:Yag pumped dye laser. The ionizing photon was one of the harmonics of the pump laser.

The apparatus, shown in Fig. 2, is a further extension of a cell initially built for MPI studies[10,25] and previously modified for THG experiments. It consists of three separately evacuable chambers, each of which functions as a proportional counter. Electrons produced in such a counter are accelerated toward an electrode maintained at positive bias voltages (10-500 V) and undergo ionizing collisions with other gas molecules causing an electron avalanche. The amplification produced is proportional to the ratio of electric field to pressure (E/P). The gain is finally limited by dielectric breakdown. The first chamber (I) consists of a stainless steel Varian six-way cross connected to an ion pump and capable of baseline vacuums of 10^{-8} torr. The beam of a N_2 laser (Molectron UV-24) pumped dye laser (Molectron DL400) is focused in chamber I by a 3.8 cm focal length lens to a spot ≤20 μm, giving a power density of the order of 5×10^{9} W/cm^2. Krypton or xenon gas (Matheson, 99.995 and 99.9%, respectively) was used as the nonlinear medium and any electrons produced by MPI in the tripling gas were detected with the biased flat-plate electrode. Multiphoton ionization, resonant with various atomic levels of the rare gases, gives signals which are useful for coarse wavelength calibration[22,25,40] after accounting for a-c Stark shifts and pressure effects. For fine calibration a 1.26 m monochromator (Spex 1269) was used. The VUV light, produced by THG in the focal spot, is collimated with a MgF_2 lens (focal length = 4 cm) and passes through a MgF_2 window into the second chamber (II). This section is a stainless steel tube (3.8 cm ID; 7.6 cm long) with three side arms for two electrodes and a pump-out port. Again, any electrons resulting from one-photon ionization (OPI) and MPI are amplified in the sample gas and detected at the electrode. The VUV beam exits chamber II through an MgF_2 window and passes through a dielectric VUV bandpass filter (Acton Research) to remove the blue pump light. This filter could also be placed between chambers I and II when necessary. Although various filters were available, most experiments used a filter with 46% transmission peaked at 141.5 nm and a bandwidth (FWHM) of 55.0 nm (Acton 145-B) which passed ≲1% of the blue light. Chamber III is a VUV photon detector consisting of a 3.8 cm Varian nipple (8.5 cm long) containing a tantalum foil and a single flat-plate electrode. Photons whose energy exceeds the work function of tantalum (~4.1 eV) eject electrons which are detected in the proportional counter. Xenon at pressures of 300-500 mtorr is the counter gas. The whole system uses standard flanges with copper gaskets and is thus bakeable. Each chamber has a thermocouple vacuum gauge and in addition can be connected to a capacitance manometer (MKS Baratron) with a 1 torr or 1000 torr head for more precise pressure measurement. Signals from charge-sensitive preamplifiers connected to any two of the three chambers were averaged in a dual channel boxcar integrator (Princeton Applied Research, No. 162/165) and displayed on a dual-channel X-Y recorder and oscilloscope as a function of wavelength.

The absolute intensity of the third-harmonic light is on the order of 10^{7}-10^{8} photons/pulse depending on the wavelength.[31] The bandwidth of the THG will be at most one-third the bandwidth of the input laser (nominally ~0.1 Å). An additional factor of $\sqrt{3}$ reduction in width results from the I^3 dependence of the THG if a Gaussian pump beam is assumed. The expected bandwidth is thus 0.02 Å at 1470 Å (~0.9 cm^{-1}). Use of an etalon would reduce the laser bandwidth to 0.01 Å and that of the THG to 0.002 Å (0.09 cm^{-1}) at 1470 Å. This is on the order of the Doppler broadening of light molecules. Unfortunately, the insertion loss of the etalon used with Coumarin dyes reduced the present laser's output such that no THG was observed. Even smaller bandwidths can be obtained by injection-locking a pulsed laser with a single-mode CW dye laser.[37]

By monitoring the THG intensity in chamber III with a sample gas in chamber II, a VUV absorption spectrum can be obtained. Figure 8 shows an absorption spectrum of the $A^1\pi(v=3) - X^1\Sigma^+(v=0)$ band of CO which is a red degraded band whose head appears at 144.73 nm.

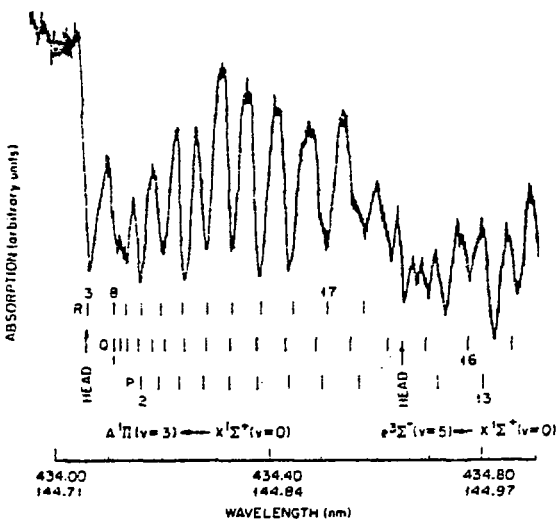

Fig. 8. A portion of the vacuum ultraviolet absorption spectrum of CO recorded using third-harmonic generation in xenon. The upper wavelength scale is the laser wavelength in air and the lower scale is the VUV wavelength corrected for the refractive index of air.
(ORNL Dwg 81-10037R2)

The upper wavelength scale is the laser wavelength in air while the lower number is the VUV wavelength corrected for vacuum. This band is partially overlapped by the $e^3\Sigma^-(v=5) \leftarrow X^1\Sigma^+(v=0)$ band at lower energies. Unfortunately, the spectrum does not show the full resolution of the system due to the mostly unresolved, closely spaced P,Q,R, triplet in each band. The Doppler width for CO at room temperature is 0.0034 Å. Thus, an etalon in the present laser would produce sub-Doppler resolution for CO as was observed by Hilbig and Wallenstein.[39] Absorption spectra also taken for I_2 and NO in this region, while complicated, were similar to published spectra. The NO absorption results are shown in Fig. 9 and will be discussed below.

Direct photoionization spectra of benzene, CH_3I, NO, and I_2 were studied in the Xe6s' and Kr5s wavelength regions. These spectra were easily obtained and were identical to previously reported spectra. Ionization thresholds for a number of molecules have been studied from which accurate IPs have been determined [e.g., iodobenzene (IP = $8.75^{+0.01}_{-0.04}$ eV) o-xylene (IP = $8.54^{+0.01}_{-0.04}$ eV)].

Third-harmonic generation results quite naturally in a colinear beam of VUV and blue light. Therefore, by removing the VUV bandpass filter separating chambers I and II (i.e., same configuration as Fig. 2) it is possible to study two-photon, two-color ionization experiments. Figure 9 displays the two-photon (one VUV plus one blue photon) ionization spectrum (upper trace) and one-photon (VUV) absorption spectrum (lower trace) of NO in the region of the $F^2\Delta(v=3) \leftarrow X^2\pi$ transition. The transitions involved are shown in Fig. 10. The two leading peaks of each bandhead represent the transitions from fine structure $^2\pi_{3/2,1/2}$ splitting of the ground state. An indication of the spectral simplification provided by this technique can be seen by comparing the sharp, rotationally resolved two-photon ionization spectrum with the absorption spectrum. Although there is one-to-one correspondence in some areas of the spectrum, in most regions the absorption spectrum is vastly more complicated. The success of these experiments points to the possibility of studying processes where the VUV photon is fixed to provide a state-selected Rydberg intermediate state and a second tunable dye laser used to excite higher autoionizing states of an atom or molecule like NO.

Acknowledgments

The authors are greatly indebted to Dr. A. D. Williamson whose initial work provided us with many of the tools necessary to carry out the studies described herein, and to Professor C. D. Cooper (University of Georgia) for his major contribution to the VUV experiments.

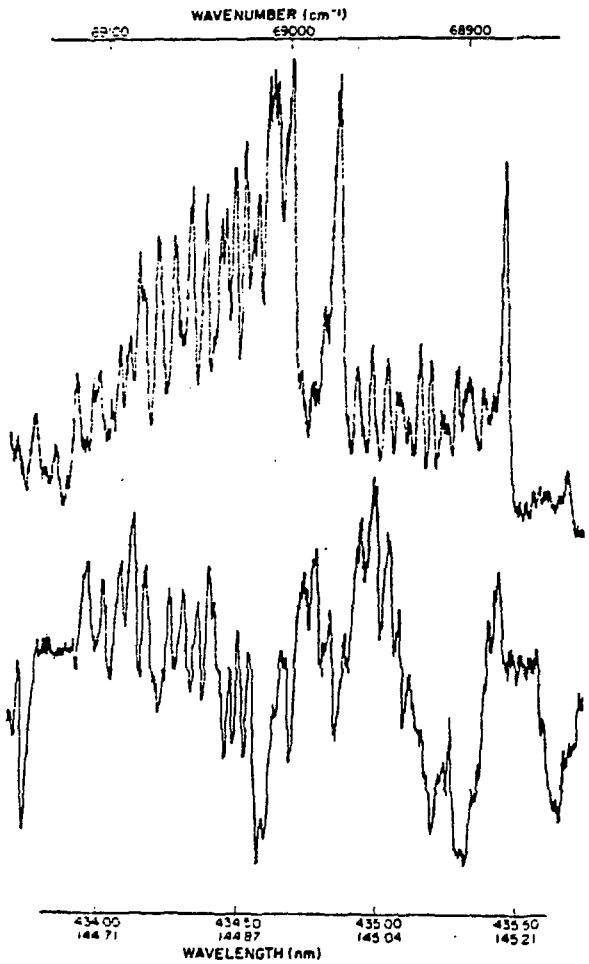

Fig. 9. The two-photon (one vacuum ultraviolet plus one blue) ionization spectrum (trace) and one-photon absorption spectrum (lower) of ^{14}NO in the region of the $F^2\Delta(v=5) \leftarrow X^2\pi_{3/2,1/2}$ transition. The upper wavelength scale and the wave number scale have been corrected for the refractive index of air.

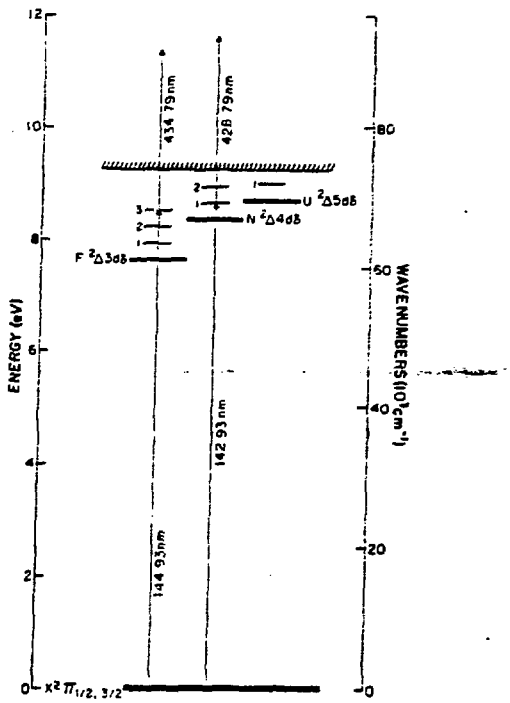

Fig. 10. The partial energy level diagram of NO showing the $F^2\Delta$ state and the two-photon transition responsible for the ionization signal shown in Fig. 9.

References

1. V. S. Kushawaha and J. J. Leventhal, Phys. Rev. 22, 2468 (1980); and references cited therein.
2. D. H. Parker, J. O. Berg, and M. A. El-Sayed, Advances in Laser Chemistry (A. H. Zewail, Ed.), Springer, Berlin (1978).
3. P. M. Johnson and C. E. Otis, Ann. Rev. Phys. Chem. 32, 139 (1981).
4. L. Zandee and R. B. Bernstein, J. Chem. Phys. 71, 1359 (1979).
5. G. Petty, C. Tai, and F. W. Dalby, Phys. Rev. Lett. 34, 1207 (1975); F. W. Dalby, G. Petty-Sil, M. H. Pryce, and C. Tai, Can. J. Phys. 55, 1033 (1977).
6. P. M. Johnson, J. Chem. Phys. 62, 4562 (1975).
7. G. C. Nieman and S. D. Colson, J. Chem. Phys. 68, 5656 (1978).
8. A. D. Williamson and R. N. Compton, Chem. Phys. Lett. 62, 295 (1979).
9. V. Beosl, H. J. Neusser, and E. W. Schlag, Z. Naturforsch. Teil A33, 1546 (1978); J. Chem. Phys. 72, 4527 (1980).
10. C. D. Cooper, A. D. Williamson, J. C. Miller, and R. N. Compton, J. Chem. Phys. 73, 1527 (1980).
11. J. T. Meek, R. K. Jones, and J. P. Reilly, J. Chem. Phys. 73, 3503 (1980).
12. D. M. Lubman, R. Naaman, and R. N. Zare, J. Chem. Phys. 72, 3034 (1980).
13. J. Silberstein and R. D. Levine, Chem. Phys. Lett. 74, 6 (1980).
14. F. Rebentrost, K. L. Kompa, and A. Ben-Shaul, Chem. Phys. Lett. 77, 394 (1981).
15. F. Rebentrost and A. Ben-Shaul, J. Chem. Phys. 74, 3255 (1981).
16. M. G. Payne, W. R. Garrett, and H. C. Baker, Chem. Phys. Lett. 75, 468 (1980).
17. R. N. Compton, J. C. Miller, A. E. Carter, and P. Kruit, Chem. Phys. Lett. 71, 87 (1980).
18. J. C. Miller and R. N. Compton, J. Chem. Phys. 75, 2021 (1981).
19. J. C. Miller and R. N. Compton, J. Chem. Phys. 75, 22 (1981).
20. J. H. Glownia, S. J. Riley, S. D. Colson, J. C. Miller, and R. N. Compton, submitted.
21. J. C. Miller, R. N. Compton, T. E. Carney, and T. Baer, submitted.
22. K. Aron and P. M. Johnson, J. Chem. Phys. 67, 5099 (1977).
23. J. C. Miller, R. N. Compton, M. G. Payne, and W. R. Garrett, Phys. Rev. Lett. 45, 114 (1980).
24. A. H. Kung, Appl. Phys. Lett. 25, 653 (1974).
25. A. H. Kung, J. F. Young, and S. E. Harris, Appl. Phys. Lett. 22, 301 (1973).
26. J. F. Ward and G.H.C. New, Phys. Rev. 183, 57 (1969).
27. R. Mahon, T. J. McIllrath, and D. W. Koopman, Appl. Phys. Lett. 33, 305 (1978).
28. R. Mahon, T. J. McIllrath, V. P. Myerscough, and D. W. Koopman, IEEE J. Quantum Electron. QE15, 444 (1979).
29. L. J. Zych and J. F. Young, IEEE J. Quantum Electron. QE14, 147 (1978).
30. D. Cotter, Opt. Lett. 4, 134 (1979).
31. D. Cotter, Opt. Comm. 31, 397 (1980).
32. R. Wallenstein, Opt. Comm. 33, 119 (1980).
33. J. Reintjes, Opt. Lett. 4, 242 (1980).
34. J. Reintjes, Opt. Lett. 5, 342 (1980).
35. R. Mahon and Y. M. Yiu, Opt. Lett. 5, 279 (1980).
36. H. Langer, H. Puell, and H. Röhr, Opt. Comm. 34, 137 (1980).
37. H. Egger, R. T. Hawkins, J. Bokor, H. Pummer, M. Rothschild, and C. K. Rhodes, Opt. Lett. 5, 282 (1980).
38. W. Zapka, D. Cotter, and V. Brackmann, Opt. Comm. 36, 79 (1981).
39. R. Hilbig and R. Wallenstein, IEEE Quantum Electron. QE17, 1566 (1981).
40. J. C. Miller, R. N. Compton, and C. D. Cooper, J. Chem. Phys. (in press).
41. J. Reintjes, C. Y. She, and R. C. Eckardt, IEEE Quantum Electron. QE14, 581 (1978).
42. M. Rothschild, H. Egger, R. T. Hawkins, H. Pummer, and C. K. Rhodes, Chem. Phys. Lett. 72, 404 (1980).
43. M. Rothschild, H. Egger, R. T. Hawkins, J. Bokor, H. Pummer, and C. K. Rhodes, Phys. Rev. A 23, 206 (1981).
44. H. Zacharias, H. Rottke, and K. W. Welge, Opt. Comm. 35, 185 (1980).
45. H. Zacharias, H. Rottke, J. Danon, and K. W. Welge, Opt. Comm. 37, 15 (1981).

1. Tunable Laser Sources in the VUV
2. Laser Spectroscopy and Photophysics in the VUV

Stephen C. Wallace
Departments of Chemistry and Physics
University of Toronto
Toronto
Ontario Canada M5S 1A1

Abstract

In 1970, the first report (R.T. Hodgson, Phys. Rev. Lett. 25, 494 (1970)) of the molecular hydrogen laser at 160 nm opened up a period of intense activity in the development of laser sources in the VUV spectral region. The term laser source is now taken to encompass both VUV lasers and also harmonic generation techniques starting with visible lasers. Moreover, although VUV lasers were the first to be developed, it is the more recent strides in using third-order harmonic generation schemes, which have led to intense, narrow-livewidth, and continuously tunable laser sources spanning the 100-200 nm region and suitable for spectrosopic studies. These are laboratory scale systems and hence are beginning to find a wide range of applications in chemistry and physics.

The first lecture will briefly review fixed frequency and tunable VUV lasers. Next, I will discuss the principles of non-linear optics, which are relevant to methods of harmonic generation into the VUV. This will include both

sum and difference frequency mixing, higher order non-linear processes and saturation effects. A comparison of different non-linear systems will be provided. Finally, there will be a brief discussion of recent progress in broad band XUV sources using laser-induced plasmas.

In the second lecture I will outline a number of recent examples of laser spectroscopy in the VUV. These are principally laser-induced fluorescence studies and include both measurement of photophysical properties of small molecules and the detection of nascent products (atomic and molecular species) in both photo-fragmentation and molecular beam scattering.

Elements of Quantum Defect Theory

C. H. Greene, K. T. Lu and A. R. P. Rau

This set of six lectures will aim at a pedagogic development of quantum defect theory starting with a background that only assumes a basic graduate level course in quantum mechanics. From the elementary starting point we will proceed to develop the theory in sufficient depth so as to give both an understanding of the analytical aspects of the theory and its practical usefulness for organizing the extensive spectrosopic data one may have for an atom or a molecule.

The term quantum defect theory was originally applied to an atomic system like an alkali atom. It is well known that highly excited Rydberg states of any atom form a Bohr-Rydberg sequence very similar to the prototype hydrogen spectrum except that the principal quantum number n is reduced by a constant μ, called the quantum defect. This observation points directly to the significant characteristic of such states, that the electron moves for the most part in a region of large radial distances where the potential is the hydrogenic Coulomb field due to the rest of the atom. Not only the energy values, but also other characteristics of such states, are therefore expressed in the same standard form as in hydrogen. All the effects stemming from the core region of a non-hydrogenic field can be described by a few parameters (like μ). These parameters are not sensitive to the asymptotic energy of the state because they reflect influences of a region where much stronger potential terms dominate. As a result, they are common to the entire set of Rydberg states and also extrapolate into

the continuum. Thereby a quantum defect analysis provides a powerful organizing method for treating at one time an entire set (infinite) of states.

Though quantum defect theory arose in the context of a long range Coulomb potential, the above arguments are clearly not confined to the specific character of the field that prevails at large distances. The advantages of treating similarly all the states in other problems where there are complicated short range interactions but a standard long range potential has led in recent years to the extension of quantum defect theory along these lines. In this set of lectures we begin in fact with simple cases like a one-dimensional square well or three-dimensional spherical wells that are familiar and canonical examples in quantum physics. The ideas of quantum defect theory are developed for these examples where there is no long range field. After these considerations, we apply the results to a concrete problem in atomic physics where in fact there is no residual long range field, namely, the photodetachment of a negative ion. This application also serves to introduce extensions of quantum defect theory to a case when there is more than one set of states, say two different series ("channels") which overlap in energy and, therefore, interact with each other. After this we turn to the case of a long range Coulomb field, first in the context of an alkali atom when there is only one series and later the generalization to a many-channel situation. The photoabsorption spectrum of a rare gas serves as the main illustration for this development of multi-channel quantum defect theory. This system is also taken up to illustrate the semi-empirical features of the theory. A large amount of data of a complicated atomic spectrum can be organized through a powerful graphical interpretation of quantum defect theory into a handful of parameters. These are then viewed either as providing starting values for calculating other atomic properties in, perhaps, other regions of the spectrum or as the set of physically significant quantities that should be the

target for explanation by theories which account for the complicated short range interactions.

An example drawn from molecular physics, the photoabsorption from the ground vibrational state of H_2 in the vicinity of the lower ro-vibrational states of H_2^+, is then considered in detail. Here again both experiment and theory have gone hand in hand to elaborate at great length a rather complicated spectrum. This involves an extension to the vibrational states of the molecule in which the quantum defect parameters become functions of the internuclear distance R. Finally this introduces yet another application of quantum defect theory, this time when highly excited vibrational states and the states of dissociation of the two atomic fragments of the molecule can be viewed in similar terms, with a motion in a standard long range field in R and the more complicated form of the inter-nuclear potential at smaller R. These extensions allow such complicated phenomena as dissociative recombination and predissociation to be treated within the quantum defect framework.

Molecular Photoionization Dynamics with Emphasis on Shape and Autoionizing Resonances*†

J. L. Dehmer
Argonne National Laboratory, Argonne, IL 60439

D. Dill
Department of Chemistry, Boston University, Boston, MA 02215

A. C. Parr
National Bureau of Standards, Washington, D.C. 20234

Shape and autoionizing resonances are key probes of molecular photoionization dynamics. Each has provided the means to gain a deeper physical insight into the mechanisms of excitation, resonant trapping of the photoelectron, and decay of the excited complex which occur during the photoionization process. Of particular interest in this context are the uniquely molecular aspects resulting from the anisotropic molecular field and the interplay among rovibronic modes. We will review the fundamental aspects of both types of resonant process and will discuss some current problems and prospects for future work from both experimental and theoretical points of view.

---

* Work supported in part by the U.S. Department of Energy, the Office of Naval Research, NATO Grant No. 1939, and National Science Foundation Grant CHE78-08707.

† Abstract of Lecture to be presented at the NATO Advanced Study Institute on Photophysics and Photochemistry in the Vacuum Ultraviolet, Lake Geneva, Wisconsin, 15-28 August 1982.

REGULAR AND IRREGULAR MOTION IN CLASSICAL AND QUANTUM SYSTEMS

Marko Robnik

Astronomische Institute
SFB 131 - Radioastronomie
Auf dem Hügel 71
D-5300 Bonn 1, F.R.G.

Extended Abstract

It is now widely known that simple, nonlinear, deterministic dynamical systems can exhibit chaotic motion, which is unpredictable even in principle. By simple we mean that the system has only a few degrees of freedom, say N = 2. By deterministic we mean that local laws of motion are perfectly known, described by some velocity vector field in phase space. The motion in time is obtained by finding the integral curves, i.e. by solving the ordinary differential equations so that the future and the past are completely determined by the initial state in phase space. The origin of chaotic motion lies in the instability of trajectories, which can separate exponentially as time goes on. The motion thus displays a sensitive dependence on initial conditions. Since the initial conditions can never be known with infinite precision, our predictions will be wrong eventually. In the course of time the system will possibly pass arbitrarily close to any point of phase space.

Regular motion on the other hand can arise when the motion is confined to some smooth submanifold of the phase space, and is periodic or quasi-periodic there. This can be the case when the system has some global smooth integrals of motion. The invariant submanifolds are then level sets of such constants of motion.

It is not necessary to stress the importance of the theory of nonlinear dynamical systems since we all know that a large part of physical processes can be modelled by them, and the applications go of course beyond the limits of physics, to the study of chemical reactions, evolution of populations in biological systems, nonlinear oscillations in electrical and mechanical engineering.

It is the subject of ergodic theory to study the behavior of dynamical systems for long times, their stability and structural stability, and the statistical properties of the motion. This involves also bifurcation and catastrophe theories. The dissipative systems are important for the study of turbulence, for example, while the study of Hamiltonian systems is of great importance for celestial mechanics (the whole theory developed more or less from the three-body problem), plasma physics, atomic systems, etc.. In the following we shall consider only the Hamiltonian systems. The first part of the paper deals with classical systems, the second one is devoted to quantum systems, and in the third part their interconnections are discussed, some examples are given and some open questions are formulated.

Part I

First the integrable systems are reviewed. Then the question of what happens to them under a perturbation is discussed, leading to the KAM-Theorem. The Poincaré mappings of a surface of section in phase space are introduced. They can be used to study the stability of a given system. Some general results on area preserving mappings are given, and the emphasis is put on the two basic facts implying the chaotic motion: hyperbolicity + transversality imply homoclinic oscillation, which is a prototype of irregular motion. The Birkhoff-Gustavson normal form of an Hamiltonian system can be very useful for constructing formal, i.e. approximate integrals of motion in the regular regions of phase space, where the existence of invariant tori is warranted by the KAM-Theorem. Finally, we discuss the ergodic and mixing systems and give the definition of the K-entropy.

Part II

The definitions of integrability and stochasticity in quantum systems are given. The problem of the explicit quantization of integrable and (non-integrable) irregular systems is considered (the tori quantization and the sum over closed classical trajectories). Then the statistical properties of energy spectra and their fine structure are studied. The application of the Birkhoff-Gustavson normal form in the semiclassical tori quantization is pointed out.

Part III

We discuss the problem of a quantum analogy of the KAM-Theorem, review some properties of the Wigner-Weyl mapping, and make some conjectures on this problem. We give also some specific examples, e.g. the quadratic Zeeman effect in hydrogen atom, where the correspondence between the classical and the quantum properties is sufficiently well known. This is illustrated also for various kinds of billiards.

Basic references

1. HELLEMANN, R.H.G., in Fundamental problems in statistical mechanics, 5, ed. E.G.D. Cohen, Amsterdam, North-Holland (1980) 165-233.
2. ARNOLD, V.I., Mathematical methods of classical mechanics, Nauka, Moscow (1974).
3. ARNOLD, V.I. and AVEZ, A., Ergodic problems of classical mechanics, New York Benjamin (1968).
4. SIEGEL, C.L. and MOSER, J.K., Lectures on celestial mechanics, Springer (1971).
5. BERRY, M.V., in Proc. July 1981 "Les Houches Summerschool" on Chaotic behavior of deterministic systems, ed. R.H.G. Helleman and G. Iooss, Amsterdam, North Holland (1982).
6. ZASLAVSKY, G.M., Phys. Rep. 80 (1981) 158-250.